Future frequency response requirements in low inertia grids

Submitted by

Samuel James Homan

for the degree of Doctor of Philosophy

The University of Sheffield

Department of Chemical and Biological Engineering

Centre for Doctoral Training in Energy Storage and its Applications

September 2021

Declaration

I hereby declare that this thesis is entirely of my own work and original in content and that all sources have been accurately reported and acknowledged. This document has not, in its entirety or in part, been submitted at any other institution to obtain an academic qualification. I am aware of the University of Sheffield's guidance on Unfair Means (www.sheffield.ac.uk/ssid/unfair-means).

Abstract

Electricity grids around the world are undergoing tremendous transitions due to the pressing need to decarbonise. Great strides have been made in Great Britain in recent years, *wind and solar penetration doubled between 2014 and 2019*, but there are concerns about the effect this transition will have on grid stability. Ancillary services are the tools that electricity system operators use to help maintain grid stability. One of these, frequency response, is a service with the goal of maintaining a stable grid frequency. Grid inertia is another important property of the grid, and the level of inertia is inversely proportional to the rate of change of frequency. Traditionally, frequency response and inertia have mostly been provided by large fossil-fuel power stations.

Given the situation outlined above, the aim of this thesis is to understand the frequency response requirements in low inertia grids, with a focus on the situation in Great Britain. From an analysis of historic grid data, I find that frequency volatility has increased in Great Britain in recent years and the underlying causes are likely high rates of change of demand and settlement period boundaries. The increasing penetration of renewables may have also contributed. Using the swing equation, I find that to secure the GB grid in the future, for all potential infeed losses, demand, and inertia scenarios, 1600 MW of frequency response capacity at a delay/ramp time of 0.5 s/0.5 s is needed. I find that in normal day-to-day operation, the frequency volatility does not drastically deteriorate until an inertia level around 20% of current levels (inertia from nuclear and demand only). At this low level, a significant portion of the frequency response capacity needs to be fast acting for successful mitigation. Low inertia has a much greater effect on frequency response requirements in a large infeed loss situation compared to normal day-to-day operation.

Acknowledgements

Firstly, I would like to thank my supervisor Dr Solomon Brown for his brilliant support and guidance throughout my PhD. His positive attitude during times when I was doubting myself really helped me through. I would also like to thank those at RWE Generation UK, especially Dave Hinchliffe and Jeff Hulance, for making my industrial placement enjoyable and rewarding.

I would like to thank the Energy Storage and Its Applications Centre for Doctoral Training (ESA CDT) for providing me with the opportunity to undertake this PhD. Additionally, I gratefully acknowledge the Engineering and Physical Sciences Research Council for funding the ESA CDT, via grant EP/L016818/1, and RWE Generation UK for their project sponsorship and support.

To Max "might do, might not" Yan, chief rabbit-hole engineer, and all the other Kroto office clowns - thanks for making the office a place of laughter and lively discussion. So much hard work and ingenuity is required in the next 30 years as humanity faces its greatest challenge, and I am confident that all of you will make a great contribution.

Lastly, I want to thank those closest to me. H, Rog, Dan, Pel, Wrik, Nat, and Rob, you are all amazing friends who have kept me sane and happy during the last four years. To Tom and Evie, the best siblings you could ask for, and to Mum and Dad, the two people I admire most in the world, there just is not enough space to thank you enough. And last but not least, special thanks goes to Kayleigh. Your unwavering support, fantastic company during our many hikes, and delicious cooking is greatly appreciated. We have had some wonderful times during the last four years and I cannot wait to have more, especially once we are both finished with our PhDs and this pandemic has blown over!

Contents

List of figures

List of tables

Glossary

Ancillary services	Services that help electricity system operators maintain and operate a stable electricity grid
Demand damping	The power input change of frequency sensitive demand units in response to a frequency deviation. An intrinsic self-stabilising property of the grid.
Frequency response	The power output/input change of generation/demand units in response to a frequency deviation. An example of an ancillary service.
Grid frequency	The nominal number of oscillations of alternating voltage and current transmitted from power stations to end users
Grid inertia	The total rotational kinetic energy stored in synchronously connected generation and demand units. In this thesis, the units used for grid inertia are volt ampere seconds (VA.s), which is equivalent to joules (J)
Large infeed loss	A rapid loss of generation of a large magnitude
National Grid ESO	The electricity system operator of Great Britain
Swing equation	A differential equation governing the relationship between grid frequency and power imbalances in the

grid

List of symbols

f	Grid frequency
f_{n}	Nominal grid frequency
E_{n}	Grid inertia
$E_{\mathrm{n,gen}}$	Grid inertia contribution from the generation side
$E_{\mathrm{n,dem}}$	Grid inertia contribution from the demand side
H	Inertia constant
S	Rated (apparent) power capacity
β	Capacity factor
u	Power factor
P_{m}	Mechanical power provided by a prime mover
P_{ns}	Power from non-synchronous generation
P_{d}	Electrical power demand
I	Power imbalance
k	Demand damping constant
D_{n}	Demand of the grid at $f = f_{\mathrm{n}}$
R	Power from frequency response

R_{cap}	Frequency response capacity
t_{d}	Frequency response delay time
t_{r}	Frequency response ramp time
f_{ss}	Frequency after the transient period is over after an imbalance
f_{nad}	Frequency nadir
L_{rf}	RoCoF limit
L_{ss}	Steady-state frequency limit
L_{nad}	Frequency nadir limit
A	$A = kD_{\mathrm{n}}f_{\mathrm{n}}/2$

Chapter 1

Introduction

1.1 General background

1.1.1 Electricity grids

The purpose of an electricity grid is to deliver electric power to consumers who are demanding it. The main physical components of any large-scale electricity grid are power stations (where electricity is generated), transformers (for stepping voltages up or down), high voltage transmission lines (for transporting the electricity long distances), lower voltage distribution lines (for transporting electricity from the high voltage transmission lines to consumers), and consumers (where electricity is used for industrial, commercial, and domestic purposes).

Electrical grids are split into two parts: transmission networks and distribution networks. The transmission network links large-scale power stations (often larger than 1000 MW), high voltage transmission lines, distribution networks, and a few large-scale consumers. Coal-fired, gas-fired, nuclear, and hydro are examples of generation types that are often connected to the transmission network. The distribution networks link smaller-scale power stations (distributed/embedded generation), lower voltage distribution lines, and most of the consumers of electricity. Solar generation is entirely connected to the distribution network, and a significant portion of wind generation is too. An outline of the traditional electricity grid is shown in Fig. 1.1. The overall operation and manage-

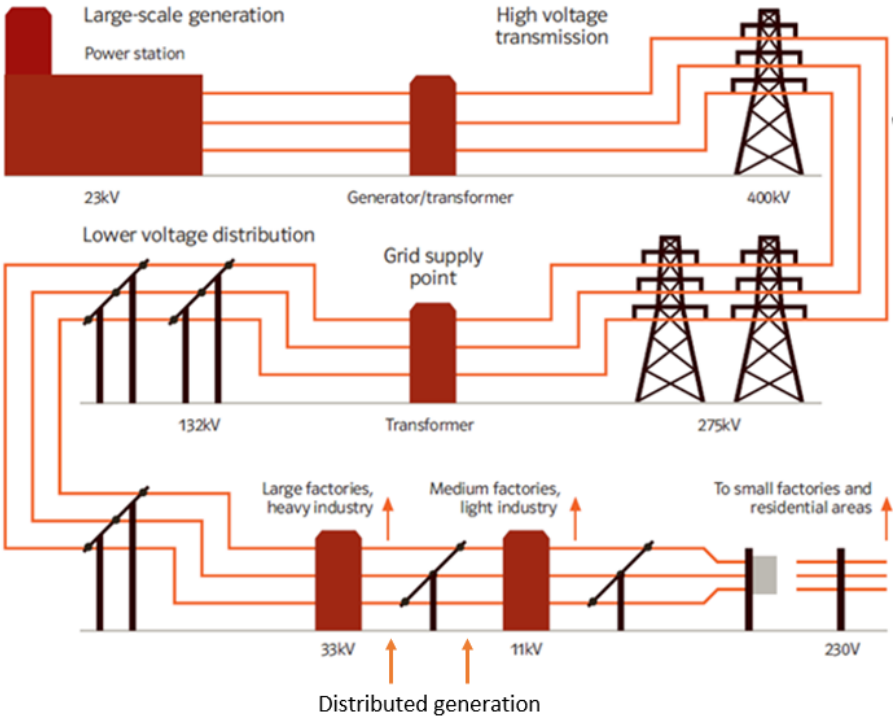

Figure 1.1: Outline of the traditional electricity grid (the flow of power is from top left to bottom right). Reproduced and adapted from Ref. [1].

ment of the whole electricity grid is the responsibility of the electricity system operator. The electricity system operator is responsible for keeping the grid stable and secure, and it manages the second-by-second balance of generation and demand of electricity. The electricity system operator in Great Britain (GB) is National Grid ESO.

In all types of electricity generation, the basic concept involves converting some initial form of energy (light, chemical, nuclear, etc) into electrical energy. The initial source of energy drives a prime mover (turbine, internal combustion engine, etc), which provides mechanical power to an electric generator. The electric generator converts mechanical power to electrical power via electromagnetic induction. Solar generation does not quite follow this path because electricity is generated in PV panels directly from light. Large-scale electricity grids run primarily on alternating current (AC) electricity, so generators must either generate AC electricity or use power electronics to convert DC to AC. Electricity generated at power stations passes through grid connection points and then begins its journey to the final consumer through the different components of the electricity grid

described above.

The Balancing Mechanism is a tool that the GB electricity system operator, National Grid ESO, uses to balance electricity supply and demand close to real time. Each day is split into 48 half-hour settlement periods. The electricity system operator forecasts demand in each of these settlement periods a long way in advance and the aim is for generation to match this through planning and trading via the electricity wholesale market. Gate closure occurs one hour before the settlement period starts, and at this point trading stops and generators and suppliers must submit information about their positions for the settlement period in question (this is called the final physical notification): power output, price for adjusting output, minimum and maximum possible output, and ramp rates. In the hour before the settlement period starts and during the settlement period, the electricity system operator sends instructions to Balancing Mechanism participants to either increase or decrease generation or demand to keep the system balanced in real time.

1.1.2 Transition to renewables

There are many different categories of electricity generation (some overlapping): conventional fossil fuel, thermal, low-carbon, renewable, and intermittent. Conventional fossil fuel generation has been around for a long time and makes use of one of the three fossil fuels: coal, natural gas, and oil. Thermal generation is any generation that involves converting heat energy to electrical energy. In the majority of power stations this is achieved by burning a fuel and using the heat to create steam, which is then driven through a steam turbine, and in turn this drives an electric generator. Gas-fired power stations make use of a gas turbine, where the working fluid is air instead of water. The exhaust heat from a gas turbine can be utilised in a heat recovery steam generator to drive a further cycle with a steam turbine. Power plants with this feature, combined-cycle gas turbines (CCGTs), are some of the most efficient thermal power plants in the world. Low-carbon generation produces significantly less CO_2 emissions than conventional fossil fuel generation but is not necessarily renewable. Renewable generation makes use of naturally occurring resources, which are replenished during a human lifetime. Intermittent generation has a low

capacity factor compared with conventional fossil fuel generation, is non-dispatchable, and dependent on the weather and other natural cycles (e.g. tides).

While conventional fossil fuel generation still accounts for over half of global electricity generation, it's contribution is falling. Across the world, renewable generation is increasing it's penetration, which is largely because of the global effort to combat climate change but also due to the falling costs of renewable generation. Global installed capacity of renewable generation has increased steadily since 2008 at an average rate of about 8% [2]. Decarbonising electrical grids is seen as low-hanging fruit compared to decarbonising heat and transport. In the UK, this change has been accelerated due to the UK Climate Change Act 2008 [3], which has committed the UK to reducing its carbon emissions by 80% by 2050 (compared to 1990 levels). The UK has recently set a more ambitious target of reaching net-zero emissions by 2050.

The rise of renewables is changing the structure of the GB grid. A lot of renewable generation is connected to the distribution network, and as a result the GB grid is becoming less centralised and more distributed. Due to decarbonisation and decentralisation, electrical grids of the future are likely to look a lot different to the traditional one in Fig. 1.1, where power is flowing one-way from large, centralised power stations to consumers. Instead, there is the strong likelihood of an increase in all of the following: local distributed generation, renewable generation, energy storage, interconnection between different national electricity grids, and intelligent communications between all the different players on the grid (the smart grid).

Below is a list of recent GB grid records, which illustrate the massive transition occurring (the source for all is National Grid ESO).

- In April 2017, the UK experienced its first coal free day since the industrial revolution
- From April to June 2020, the total coal-free period lasted 67 days
- On March 28th 2021, 88.4% of electricity generation was from low-carbon sources
- On May 21st 2021, maximum wind generation (17.8 GW) was experienced
- On April 20th 2020, maximum solar generation (9.7 GW) was experienced

1.1.3 Grid frequency

Electricity grids are synchronous, which means the whole grid is electrically tied together and operates at the same AC frequency throughout. An electricity grid that covers a large area (e.g. Great Britain) is a wide-area synchronous grid. The GB grid and the Continental European grid (which is transnational and serves most of continental Europe) are examples of wide-area synchronous grids. AC frequency is a key feature of electricity grids and is called the grid (or system) frequency. The nominal grid frequency for Great Britain, Europe, and most of the world is 50 Hz, but in North America it is 60 Hz. Generators connected to the grid are either synchronous or non-synchronous. Synchronous generators are electrically coupled to the grid, and their moving parts rotate synchronously with it at the grid frequency. Non-synchronous generators are electrically decoupled from the grid and are connected via power electronics, so their moving parts are not necessarily rotating at the grid frequency. In fact, they may not have moving parts at all (e.g. solar). Synchronous generation is largely fossil fuel based (apart from nuclear, biomass, and hydro) and non-synchronous generation is largely renewable (e.g. wind and solar).

In an electricity grid, the conservation of energy dictates that the total electrical power generated minus losses equals the total electrical power demand at all times. A key issue is the balance between mechanical power and electrical power within synchronous generators. If there is an imbalance, then the excess or lack of energy affects the rotational speed of the electric generator and causes the grid frequency to deviate from the nominal value. The grid frequency will increase or decrease depending on the nature of imbalance (this is explained in greater detail in the next section). It is the job of the electricity system operator to maintain grid stability and one of the key metrics of stability is having a steady grid frequency near the nominal value. If it deviates too far away from this, then unacceptable consequences can arise: equipment damage and failure, generator trips, and wide-scale blackouts. Fig. 1.2 shows the variation of grid frequency (at second resolution) on the GB grid for two hours at the start of 2018. During this time, the frequency varies by less than $\pm 0.3\%$ and has an average of 49.999 Hz.

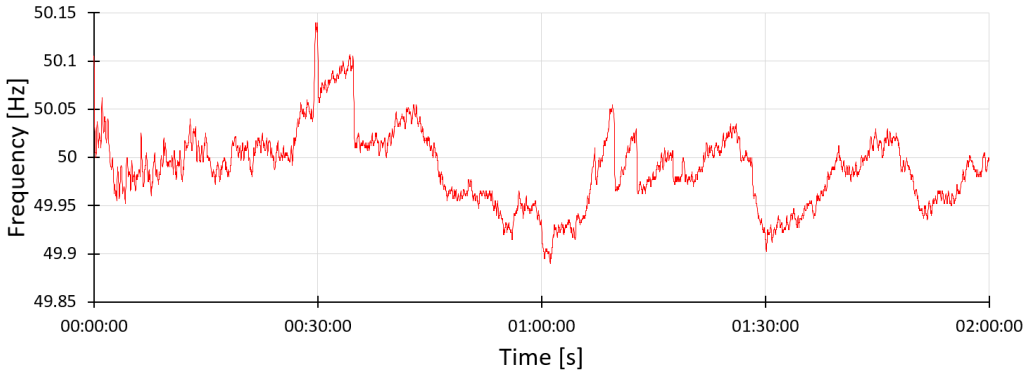

Figure 1.2: GB grid frequency for the first two hours of 01/01/2018 [4].

1.1.4 Grid inertia

Inertia is the resistance to a change in motion and is an inherent property of matter [5]. Generators often contain large rotating masses (fluids, turbines, and electric generators), which have a lot of rotational inertia. The rotational kinetic energy of a rotating mass is proportional to its inertia. The grid (or system) inertia is the term commonly given to the sum of the rotational kinetic energy of all the generators electrically coupled to the grid (which is not quite the same as the strict "physics" definition of inertia, but we will ignore that). Therefore, all online synchronous generators contribute to the grid inertia. Some non-synchronous generation, such as wind turbines, naturally have inertia but do not contribute to the grid inertia because they are electrically decoupled from the grid and connected via power electronics. Some non-synchronous generation does not contribute to grid inertia simply because of the fact that there are no moving parts involved (e.g. solar PV generation).

Synchronous generators of a different type and size will not have the same rotational kinetic energy and so contribute different amounts to the grid inertia. Grid inertia can fluctuate on a daily basis depending on the type of generation online and the system demand. For example, a day that starts with no wind/high demand but then ends with high wind/low demand would see a large swing in the grid inertia from high to low.

The connection between the grid frequency and power balance was briefly touched on in Section 1.1.3. To be more precise, the connection is between the grid frequency and

active power balance. The *reactive* power balance is closely related to grid voltages. Active and reactive power flows are fairly independent of each other in transmission networks [6] and can be treated separately. All mentions of power in this thesis refer to *active* power unless otherwise stated.

In a synchronous grid, all synchronous generators rotate at the grid frequency. If the sum of the mechanical power output of the prime movers (and the input into the electric generators) is equal to the sum of the electrical power output of the electric generators then the grid frequency remains constant. If there is an imbalance between mechanical power and electrical power, the rotational kinetic energy of the synchronous generators changes to satisfy the law of conservation of energy. When the mechanical power exceeds electrical power, the rotational kinetic energy increases resulting in a quickening of the rotation: grid frequency increases. When the mechanical power is less than the electrical power, the rotational kinetic energy decreases resulting in a slowing of the rotation: grid frequency decreases. As a result, imbalances between mechanical power and electrical power cause deviations in grid frequency from the nominal value. Hence, frequency is used as the primary control parameter by the electricity system operator to ensure that power is balanced on the grid.

The grid inertia, which is the sum of the rotational kinetic energy of all the generators electrically coupled to the grid, acts as a store of energy that is almost instantaneously released whenever there is a power mismatch (inertial response has been measured to peak after just 10 ms [7]). Fig. 1.3 shows a single synchronous generator where the electrical demand has suddenly increased from 1000 MW to 1034 MW. The mechanical input power is still 1000 MW at the moment of the demand step change and the shortfall in power comes from the rotational kinetic energy of the large masses involved. The release or capture of energy by the rotating masses results in a change of grid frequency, as described above. There is also another important point to make. The amount of grid inertia affects the rate of change of frequency (RoCoF). The higher the grid inertia, the less quickly the frequency of the machines (and hence the grid frequency) has to change when there is a power imbalance in order for energy to be conserved. RoCoF is proportional to the power

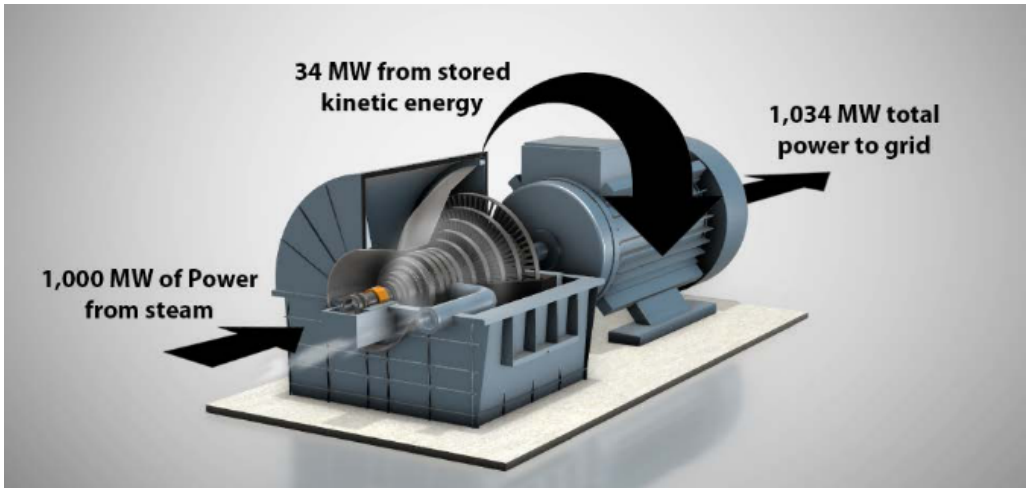

Figure 1.3: When the electrical demand of this synchronous generator suddenly increases, the inertia of the steam turbine and electric generator makes up the shortfall. Reproduced from Ref. [8].

imbalance but inversely proportional to the amount of grid inertia. Without sufficient levels of grid inertia, immediately after an incident, such as a system fault or sudden loss of generation (large infeed loss), the grid frequency would change unacceptably fast and also reach an unacceptable final level. Grid inertia is an inherent and fundamental way of providing stability in electrical grids. However, more is needed to achieve comprehensive stability. Grid inertia certainly helps to arrest the RoCoF in the few seconds after an incident, but it does not provide any assistance in bringing the grid frequency back to the nominal value. This is achieved through frequency response, which is explained in more detail in the next section.

1.1.5 Maintaining grid stability

The consequences of not adequately maintaining grid stability have the potential to be extremely severe. Two recent events, one in Great Britain and one in the USA, illustrate this. In August 2019, the simultaneous loss of multiple generation sources resulted in the largest frequency deviation seen in the grid for about a decade. A small percentage of demand was disconnected to protect the rest of the grid from widescale blackouts. However, despite the demand disconnection scheme working well and the recovery back to the nominal frequency happening quite shortly after the event, there were still severe

consequences. 1.1 million customers were without power for between 15 and 45 minutes including critical facilities such as Ipswich hospital and Newcastle Airport. Also, there was major disruption to the rail network due largely to 60 trains unexpectedly shutting down, half of which required a visit from a technician to restart. A far more serious incident occurred in Texas 2021. As a result of a winter storm, rolling blackouts turned into persistent days-long electrical outages affecting millions of Texans connected to the Electric Reliability Council of Texas (ERCOT) grid and leading to loss of life and billions of dollars of property damage [9].

To help maintain a stable and reliable grid, electricity system operators use ancillary services, and below is a (non-exhaustive) list of these services:

- Frequency response
- Reserve
- Voltage regulation
- Black start and system restoration

These ancillary services are mostly provided by generators connected to the grid. Some of the services are mandatory (depending on the generator size) and some are procured via competitive markets. In the month of September 2018, ancillary services cost National Grid ESO £33.93m (frequency response made up the highest proportion of the costs) [10].

Voltage regulation is the service that maintains a stable voltage across different parts of the grid and involves controlling the reactive power output of generators. It is distinct from frequency response services where, instead, active power output of generators is controlled. The black start and system restoration service is for when part of the grid has experienced a blackout. Black start is the starting of a power station with no external supplies of power (i.e. no assistance from the grid). The self-starting must come from auxiliary power generation onsite. A black start provider must self-start, re-energise the grid, and provide block loading of local demand. Generators Reserve is extra generation that is ready to come online when there is a generation shortage (e.g. after an unexpected

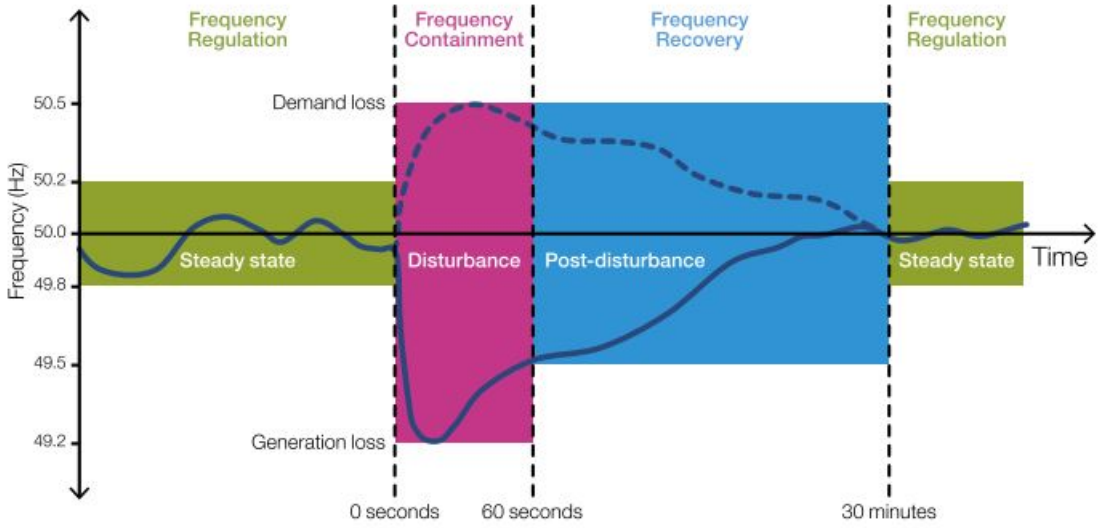

Figure 1.4: The different functions and timescales of frequency response. Reproduced from Ref. [11].

generator outage). Reserve is not the service that provides immediate response. That is the remit of frequency response.

Frequency response is the active power response of generation and demand units to grid frequency fluctuations. In previous sections it was explained that frequency fluctuations are caused by power imbalances in the grid. To counter frequency fluctuations, units providing frequency response vary their power output (or input) accordingly. When the frequency deviates below the nominal frequency, frequency responsive generation units output a little more power into the grid and vice versa. Fig. 1.4 shows the different functions and timescales of frequency response, termed by National Grid ESO as frequency regulation, frequency containment, and frequency recovery. The aim of frequency regulation is to keep the frequency as close to the nominal value as possible and reduce the standard deviation. The aim of frequency containment is to stop the frequency rise or fall after a large disturbance as soon as possible and to prevent the frequency crossing limits that would result in demand disconnection. The aim of frequency recovery, post-disturbance, is to return the frequency back to the nominal value.

There are four difficulties that wind and solar add to maintaining a stable frequency:

- No inertia offered

- Intermittent and non-dispatchable
- Stochastic (wind especially)
- Not ideal for providing frequency response

Recently, National Grid ESO proposed a new suite of frequency response services, which over the coming years will replace the current suite. This change has been prompted by growing concern that the current services are not fit for a future reduced inertia grid with a higher penetration of wind and solar. National Grid ESO has an ambition to run a zero-carbon grid, for short periods of time, by 2025 [12], and these new frequency response services are designed with this goal in mind and also designed to be technology neutral.

1.2 Thesis motivation

In the previous sections I explained the recent evolution of electricity grids around the world, the challenges this evolution is creating, and the various methods of maintaining grid stability that electricity system operator's have at their disposal. The huge importance of maintaining grid stability and the consequences of not being successful at this was also highlighted (i.e. blackouts). In Great Britain, the trajectory of the penetration of wind and solar and the decline of fossil fuel generation is almost certainly going to continue in the same direction. There were concerns that the stability of the GB grid would be compromised at levels of wind and solar penetration seen today. These have proven to be unfounded. However, the ambition to run a net-zero electricity grid as well as the strong likelihood of the electrification of lots of other consumption sectors (which could simultaneously help and hinder grid stability), ensures that these concerns have not gone away. It should be noted that although wind and solar generation cause some grid stability concerns, the effects of climate change could be far more devastating for the security and reliability of electricity grids.

The level of inertia in the GB grid is likely to continue to decline from current levels, which are much lower than the levels seen only five years previously. It is essential that there is a high level of understanding of what the future scenarios might require from grid

ancillary services, the gatekeepers of grid stability. Frequency response and grid inertia are inextricably linked since the level of inertia affects the frequency volatility and the job of frequency response is to keep frequency volatility as low as possible.

1.3 Thesis aim and research questions

The overall aim of this thesis is to understand the future frequency response requirements in low inertia grids. The emphasis of this thesis is on the situation in Great Britain, which sets the scope of the work. However, many similar sized grids in the world are undergoing comparable transitions in their power generation sector and the methods used in this thesis are applicable to these grids with adjustments to the input data.

The overall thesis aim was distilled into ten research questions, which are listed below. These research questions were generated from reviewing the literature in Chapter 2 and discussions with my industrial sponsors.

1. **What is the recent trend in grid parameters such as demand, generation, inertia, and frequency response holding volumes and what is their monthly and hourly variation?**

2. **What is the current state of frequency volatility and have there been significant changes in recent years?**

3. **What are the underlying drivers behind frequency volatility?**

4. **What are the future frequency response requirements of the GB grid, in terms of capacity and speed, to secure the grid against a large infeed loss in different inertia and demand scenarios?**

5. **With the constraint of maintaining acceptable frequency conditions after a large infeed loss, is there a simple mathematical relationship between the grid parameters (e.g. inertia and frequency response speed)?**

6. **Regarding the 9th August 2019 low frequency event, if the frequency response was faster or RoCoF relays were not triggered, could demand disconnection have been prevented?**

7. **Regarding the 9th August 2019 low frequency event, what effect would a different inertia, demand, and demand damping have had on the frequency profile?**

8. **How do frequency response characteristics (capacity and speed) affect normal day-to-day frequency volatility?**

9. **In which future scenarios does the normal day-to-day frequency volatility become unacceptable and what needs to change in frequency response provision to mitigate this?**

10. **What is the efficacy of the proposed new frequency response services compared with the existing frequency response services in a current and future scenarios?**

1.4 Research publications

The research publications produced during the course of this PhD are presented in Table 1.1. The table also shows the thesis chapter related to the published work. My contribution to the paper I was second author on, *A closed-loop analysis of grid scale battery systems providing frequency response and reserve services in a variable inertia grid*, was on the methodology and literature review.

Paper title	Journal	Publication date	Relevant chapters
A closed-loop analysis of grid scale battery systems providing frequency response and reserve services in a variable inertia grid [13]	Applied Energy	2019	Chapter 5
An analysis of frequency events in Great Britain [14]	Energy Reports	2020	Chapter 3
Current and future grid frequency volatility in Great Britain [15]	Applied Energy	2021	Chapters 3, 4, and 5.
The future of frequency response in Great Britain [16]	Energy Reports	2021	Chapter 5

Table 1.1: Research publications (bold font indicates first author) and the relevant thesis chapter.

1.5 Structure of the thesis

The structure of the rest of this thesis is as follows:

In **Chapter 2** I present a review of the literature on the swing equation, grid inertia estimation, low inertia, frequency response, the view of GB's electricity system operator on future grid stability, historic frequency data analysis, and blackouts. The gaps in previous work are summarised at the end of the chapter and this helped inform the research questions (stated in Section 1.3 and in the introduction to each results chapter).

In **Chapter 3** research questions 1 to 3 are the focus. I analyse GB grid data on generation and demand, grid inertia, frequency response, and grid frequency. I comment on patterns and trends in this data and look at correlations between different grid parameters. The work of this chapter is not only for the purpose of answering the first three research questions but also for providing values for certain parameters to be used in subsequent chapters (e.g. inertia).

In **Chapter 4** research questions 4 and 5 are the focus. I use a simplified model of frequency response to analytically solve the swing equation and derive constraints on certain grid parameters (inertia, frequency response capacity, and frequency response speed) that ensure that frequency requirements are met after a large infeed loss in current and

future scenarios.

In **Chapter 5** research questions 6 to 10 are the focus. I use three case studies to further my investigation into frequency response requirements. The three case studies are a real large infeed loss (9th August low frequency event in Great Britain), month-long (November 2018) frequency volatility in current and future inertia scenarios, and National Grid ESO's newly proposed frequency response services.

Chapter 6 concludes the thesis by summarising the work and discusses the implications of the key findings of the thesis in a wider context than the individual chapter conclusions. Also in this chapter are recommendations for future work.

Chapter 2

Literature review

2.1 Introduction

In this chapter I review the literature relevant to the studies undertaken in this thesis. Power system stability is a broad subject (see Fig. 2.1), but I only focus on frequency stability in this literature review and in my results chapters. Frequency stability can be considered separately from rotor-angle stability and voltage stability.

I start in Section 2.2 by introducing the swing equation, a key equation for this thesis, and the assumptions made within it. In Section 2.2.1 and Section 2.3 I review the parameter values used in the literature for some of the terms in the swing equation and also some of the methods behind the parameter value estimates. In Section 2.4, I introduce the challenges raised by low inertia in power grids, which was touched on in Chapter 1. In Section 2.5, I explain how frequency response works in Great Britain and in other grids around the world. I also describe how traditional frequency response is delivered and how it is commonly modelled in the literature. In Section 2.6, I review the literature that focuses on future frequency response requirements and this includes frequency response from alternative technologies. In a break from academic literature, I review the publications produced by National Grid ESO (relating to low inertia and frequency response) in Section 2.7. In Section 2.8 I review literature on historic frequency data analysis. In Section 2.9, I review recent grid blackouts and their consequences. In Section 2.10 I highlight

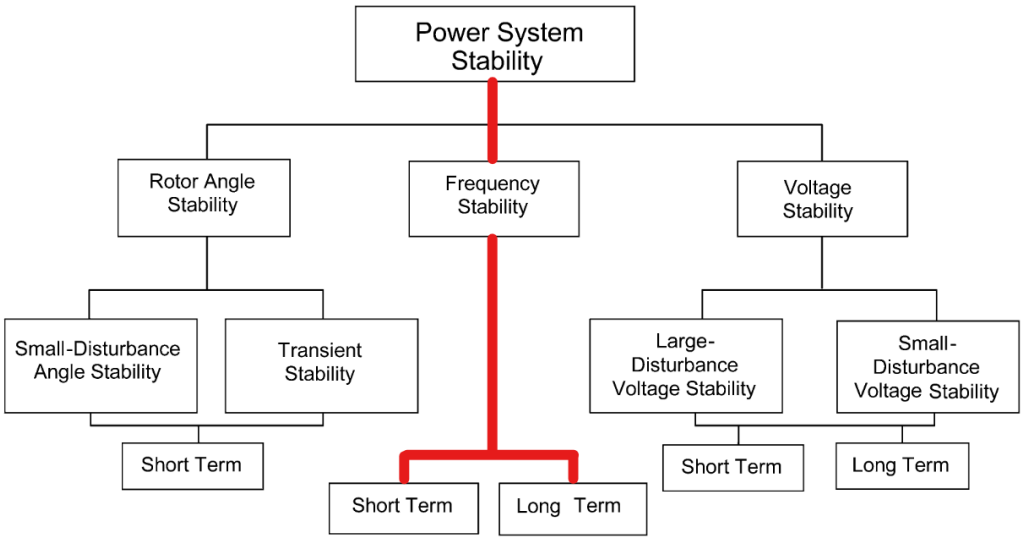

Figure 2.1: Classification of grid stability with the focus of this thesis in red. Adapted from Ref. [17].

the gaps in the literature that helped form the research questions stated in Section 1.3.

2.2 The swing equation

The swing equation (derivation in Appendix A) governs the relationship between the grid frequency and power imbalances of the grid [6, 18]:

$$\begin{aligned}\frac{\mathrm{d}f}{\mathrm{d}t} &= \frac{f_\mathrm{n}^2}{2E_\mathrm{n}f}\Delta P \\ &= \frac{f_\mathrm{n}^2}{2E_\mathrm{n}f}(P_\mathrm{m} + P_\mathrm{ns} - P_\mathrm{d}) \\ &= \frac{f_\mathrm{n}^2}{2E_\mathrm{n}f}(R + I - kD_\mathrm{n}\Delta f)\,. \end{aligned} \tag{2.1}$$

f is the frequency of the grid, f_n is the nominal frequency (50 Hz in Great Britain), and Δf is the frequency deviation ($\Delta f = f - f_\mathrm{n}$). E_n is the total rotational kinetic energy stored in the grid at f_n, which is the common definition of grid/system inertia and the definition we use throughout this thesis. We use units of volt ampere seconds (VA.s), which are equivalent to joules (J), for grid inertia. These are the most common units used for grid inertia in industry reports and academic literature. The inertia of an individual

generator (or the entire grid) can also be expressed as an inertia constant, H, with the units of seconds, which is defined as the ratio of the rotational kinetic energy stored at the nominal grid frequency to the rated capacity of the generator (see Appendix A). P_{m} is the sum of the mechanical input of all the synchronous generators, P_{ns} is the sum of all the non-synchronous generation, and P_{d} is the total electrical demand. R is the total frequency response of the grid, which can be positive or negative. I is the power imbalance of the grid and is positive when there is a demand loss and negative when there is a generation loss. Small imbalances result from continuous small fluctuations in demand or the variable output of intermittent generation whereas large imbalances are caused by unexpected generator trips, rapidly ramping interconnectors, and large demand swings. D_{n} is the demand of the grid at f_{n}. k is the demand damping constant, explained in more detail in Section 2.2.1. ΔP is the net power imbalance of the grid ($\Delta P = R + I - kD_{\mathrm{n}}\Delta f$).

From Eq. (2.1), we can see that the RoCoF is inversely proportional to the grid inertia and proportional to the power imbalance. It is also evident that the minimum or maximum frequency reached ($df/dt = 0$) after a large imbalance is determined by the frequency response, the size of the imbalance, the demand level, and the demand damping constant, not directly by the inertia.

The main assumption used in the derivation of Eq. (2.1) is the single infinite bus assumption, which is the same as the constant voltage approximation. This ignores the inter-machine oscillations and transmission system performance [6]. This approximation is valid for a highly meshed grid, in which all units can be assumed to be connected to the same grid bus [18]. In effect, all the individual generators are treated as one lumped generator and all the demand is treated as one lumped demand unit. The frequency, f, in Eq. (2.1) is more accurately the centre of inertia frequency [19].

The above assumptions means that Eq. (2.1) does not capture regional variations in grid frequency. Fig. 2.2 shows a frequency trace after a disturbance on the GB grid. In the first second after the disturbance, the frequency trace varied between regions. The variation depends on how close the measurements were taken to the source of the disturbance and the regional inertia level, since inertia is not uniformly spatially distributed [18, 20].

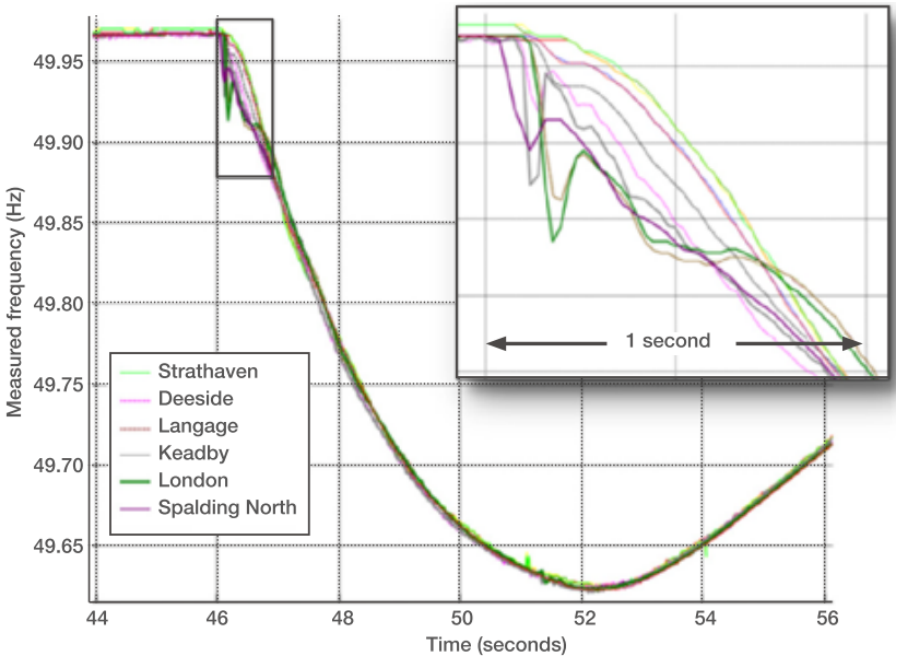

Figure 2.2: Regional variation in GB system frequency within the first second after a frequency event. Reproduced from Ref. [21].

After the first second, the regional frequency variations subside and the centre of inertia frequency becomes a good approximation for all areas of the grid. In this thesis, only the centre of inertia frequency will be considered, which is justified by the fact that the timescales of interest (starting at a few seconds) are much larger than the timescales of regional variations or high-order modes of vibration.

Another assumption used in the derivation of Eq. (2.1) is that there are no transmission losses in the grid, or rather that the transmission losses are not given their own separate term in the equation and are instead considered part of the demand.

2.2.1 Demand damping

Many loads on the grid have a power demand that is sensitive to the grid frequency (e.g. synchronous motors). Power demand increases slightly when the frequency is higher than the nominal value and decreases slightly when it is lower. This is referred to as demand damping (or load sensitivity) because it helps to stabilise the system e.g. demand on a system suddenly increases, which results in a frequency decrease, which then results in slightly less power demand on the demand side due to frequency dependent loads, which

reduces the impact of the initial sudden demand increase. This is a self-stabilising property of the grid and acts like instantaneous, inherent frequency response. It is one of the reasons why the frequency response requirement is not necessarily equal to the size of the loss of generation or demand. The higher the value of k, the demand damping constant, the greater this self-stabilising effect is. The contribution of demand damping to countering a generation loss that caused a frequency event in the GB grid in 2005 was estimated to be 36% [22]. The other 64% contribution came from frequency response from generators.

The relationship between frequency deviation and change in power demand (for frequency dependent loads) is often approximated as linear in the literature [18]. In reality, the relationship is likely to be different for different loads and more complicated. The total demand of the grid can be split into a frequency dependent part and a frequency independent part

$$P_{\mathrm{d}} = D_{\mathrm{n}} + kD_{\mathrm{n}}\Delta f\,, \tag{2.2}$$

where Δf is the frequency deviation ($\Delta f = f - f_{\mathrm{n}}$), D_{n} is the demand of the grid at f_{n}, and k is the demand damping constant and is a measure of how 'damped' the system is. The units for this parameter are %MW/Hz. Sometimes, in the literature, the units of k are given as Hz^{-1} or s. However, in this thesis, %MW/Hz is used because of its easy interpretation: if, as an example, a grid had a demand damping constant of $k = 2\,$%MW/Hz, then this means that for every 1 Hz deviation in frequency, the demand changes by 2%.

Pearmine *et al.* [22] highlight that accurately estimating the demand damping constant is important for electricity system operators when setting the appropriate amount of frequency response capacity. After a loss of generation event, when the frequency has settled to a steady-state value, the RoCoF is zero. Using Eq. (2.1), this means that

$$k = \frac{R + I}{D_{\mathrm{n}}\Delta f}\,. \tag{2.3}$$

Pearmine *et al.* [22] calculated the demand damping constant using Eq. (2.3) and data from 81 individual loss of generation events ($> 350\,$MW) that occurred in Great Britain

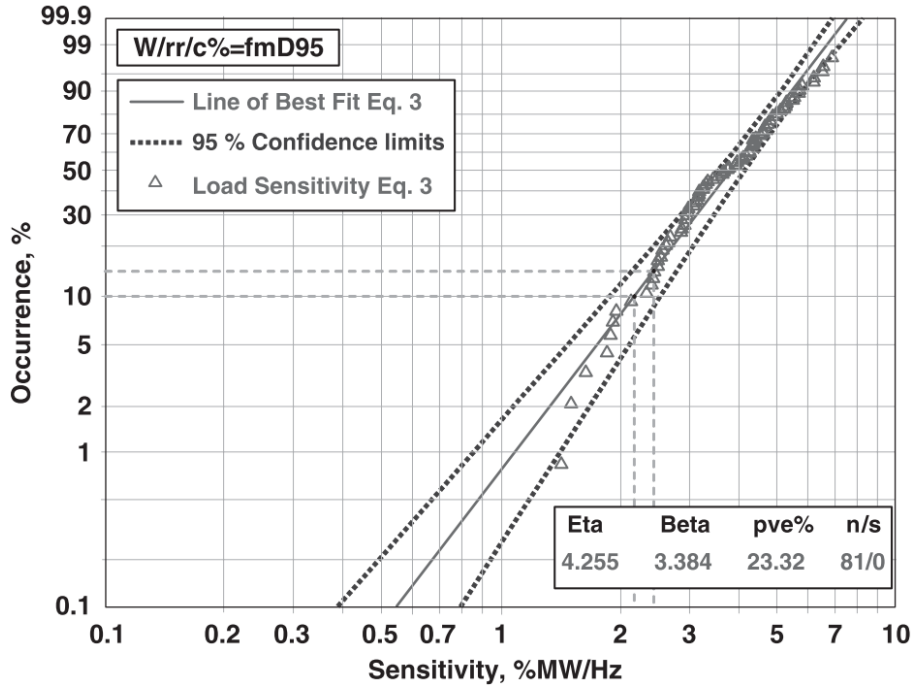

Figure 2.3: Distribution of the demand damping constant from the 81 GB frequency events considered in Ref. [22].

between April 2004 and June 2005. The data must have included at least the frequency, the size of the generation loss, the demand at the time of the loss, and the amount of frequency response from the generators. Their results, see Fig. 2.3, imply that in Great Britain a demand damping constant of 2 %MW/Hz is justified because 93% of the values calculated are higher. However, they suggest the possibility of considering an increase to 2.5 %MW/Hz, while still maintaining a high degree of security (since 2.45 %MW/Hz is the 15th percentile). This could imply savings of £22.6m on system balancing costs because slightly less frequency response holding volume would be required.

National Grid ESO currently use a value of 2.5 %MW/Hz [11] for the demand damping constant. Taylor *et al.* [23] use this value for Great Britain in their study on forecasting frequency-corrected demand (i.e. D_{n} rather than P_{d}) to support frequency control. This relationship is periodically reviewed as the demand background changes. Back in 1959, a report into the power/frequency characteristics of the British grid system estimated the value to be between 1 %MW/Hz and 2 %MW/Hz [24].

Outside of Great Britain, Kurth *et al.* [25] state that the demand damping constant

in the German region of the Continental European grid lies between 1.2 %MW/Hz and 2.2 %MW/Hz, and in a report by the European Network of Transmission System Operators for Electricity (ENTSO-E) into future system inertia in the Nordic grid [26], a value of 1.8 %MW/Hz was used in their modelling.

A big question is how will demand damping/load sensitivity change in the future? As the inertia of grids reduce due to higher penetrations of wind and solar, the importance of demand damping only increases. Frequency responsive load may reduce further in future as more power electronics are incorporated into electrical equipment [13], such as variable speed drives [27]. However, this could be counter-balanced by an increase in heat pump and air-conditioning units (as long as they are synchronously connected). In a recent study, Beláň *et al.* [28] measured the frequency characteristics of common home appliances. It was found that air conditioners and refrigerators add to the demand damping effect (i.e. these devices decrease their active power consumption with a negative change in frequency), high-pressure sodium and linear fluorescent lamps counteract the demand damping effect (i.e. these devices increase their active power consumption with a negative change in frequency), and LED lamps and incandescent lamps have no effect. In an older study by the IEEE Task Force on Load Representation for Dynamic Performance [29], a value of 2.6 %MW/Hz was determined for industrial loads, −0.3 %MW/Hz for aluminium refineries, 1.5 %MW/Hz for steel mills, 2.9 %MW/Hz for power station auxiliary plant, and 5.6 %MW/Hz for agricultural plants.

2.3 Grid inertia estimation

As the inertia of power grids decreases, accurate inertia estimates and forecasts are becoming increasingly important. They are also getting harder and more inaccurate due to increasing levels of embedded generation [30]. This section begins with an overview of some of the key papers on inertia estimation. After this, I summarise the different inertia estimation methods used across the literature (and industry). I then proceed to review some more literature and identify the methods used in the studies as well as any novelties.

Rearranging Eq. (2.1) gives us

$$E_{\mathrm{n}} = \frac{f_{\mathrm{n}}^2}{2f} \Delta P \left(\frac{\mathrm{d}f}{\mathrm{d}t} \right)^{-1}. \tag{2.4}$$

If all the terms on the right-hand side are known, then the inertia of the grid can be calculated. The power imbalance, ΔP, is the trickiest to obtain. Many of the studies I review below use the above equation to estimate inertia (along with other techniques).

Bian *et al.* [27] provide a method for quantifying the demand side inertia contribution based on past frequency deviation events. Their results show that the average inertia contribution from demand is 20% of total grid inertia in the GB grid and has an equivalent inertia constant of 1.75 s. In the paper, *demand* includes embedded generation. Here is an outline of their method, which can also be seen in Fig. 2.4. Their input data was 15 significant frequency events that occurred in the GB grid between April 2010 and August 2010 (data provided by National Grid at 100 ms resolution). The 15 events were caused by significant losses. The data included the power loss, initial frequency, and initial RoCoF. This information was used to calculate the total grid inertia, using the swing equation. The inertia contribution from the generation side was estimated by summing the product of inertia constants and active power output for each generation fuel type. As the authors note, this calculation underestimates the contribution from partially-loaded generators. The correct calculation is summing the product of inertia constants and rated capacities, see Eq. (A.17). However, data on the extent of partial-loading of each generator *is not available* whereas data on the power output of different generation fuel types *is available*. By subtracting the generation inertia estimate from the total grid inertia, the authors are left with the demand inertia plus another term representing the additional inertia contribution from the partially-loaded generators. These two unknowns were estimated using a least square fit method. For the 15 frequency events, the demand inertia varied between 17% and 25% (average of 20%) and the inertia contribution from partial-loading varied between 25% and 43% (average 30%) of the total generation contribution.

A phasor measurement unit is a device that can measure the magnitude and phase angle of voltage and current. High-precision time synchronisation (via GPS) allows the

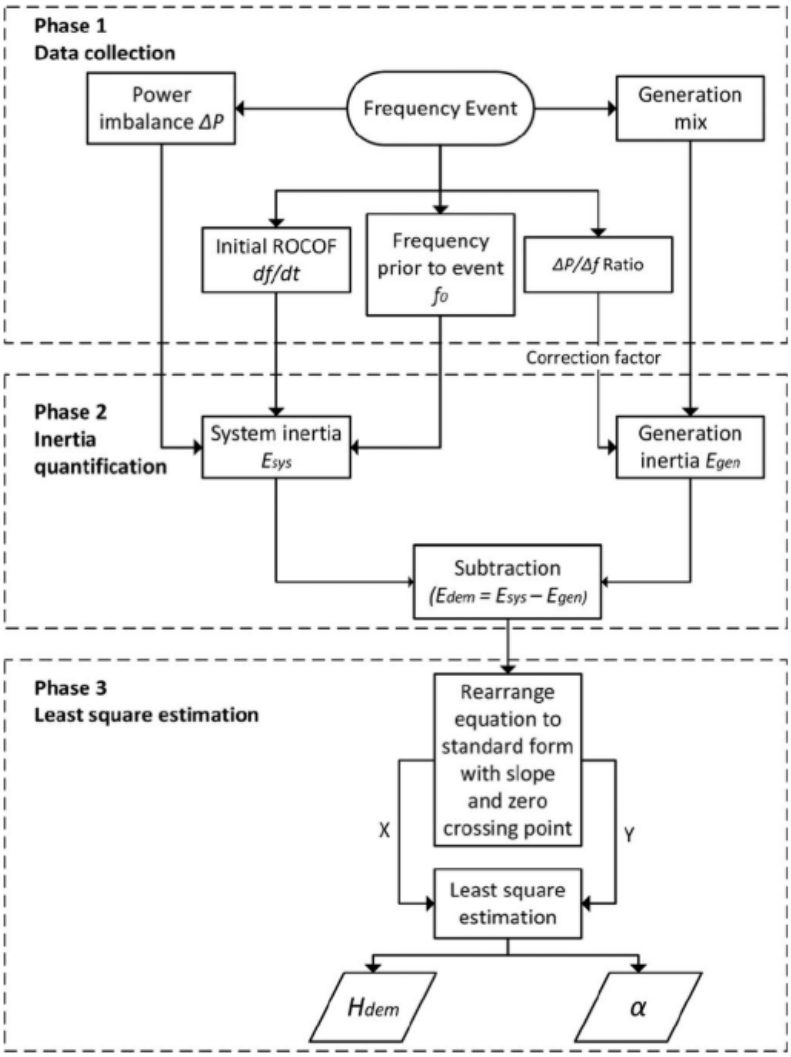

Figure 2.4: Methodology for quantifying demand side inertia from Bian *et al.* [27].

comparison of measured values from phasor measurement units in different locations, providing a detailed and accurate view of power quality across a wide geographic grid. Phasor measurement units can also measure the frequency, RoCoF, active power output of generators, and power flows on transmission lines with measurement rates of 30–60 per second. A time error of 1 µs corresponds to a phase angle error of 0.018 degrees at a frequency of 50 Hz. The change in grid frequency can be calculated by a phasor measurement unit by multiplying the change in phase angle by the measurement rate then dividing by 360 degrees. Therefore, a time error of 1 µs corresponds to a grid frequency error of 0.003 Hz at a measurement rate of 60 per second.

Ashton *et al.* [20] offer a procedure for estimating the total inertia of the GB grid using phasor measurement units and the swing equation. They divided the GB grid into regions of generation based on the constraint boundaries. The boundaries were determined following detailed analysis looking at circuit flows, voltages and generator stability risks following faults and the loss of circuits. A full dynamic model for the GB transmission system was simulated in DIgSILENT PowerFactory [31]. Seven loss-of-generation events were simulated. The GB grid in the model was split into regional areas and RoCoF measurements taken in each area. The power loss was estimated from the measurements using the swing equation and known quantities (inertia of each generator). The estimated power loss was compared to the actual power loss that was simulated. The more measurement nodes (spread in different regional areas), the more accurate the power loss estimation. This method was then used with 22 real frequency events. Power loss and inertia from generation was known for each event and phasor measurement units measured the RoCoF. The swing equation was used to calculate total system inertia. Ashton *et al.* [20] use a similar method to Bian *et al.* [27] to calculate the inertia contribution from embedded generation and demand, which they call *residual inertia*. They determine the percentage of residual inertia on the GB grid to be between 8% and 25%, with an average of 18.18%.

Tuttelberg *et al.* [32] provide a method of estimating the grid inertia from ambient frequency and active power signals measured by phasor measurement units. In other words, they calculate the inertia of the system during normal day-to-day operation (in the timescale of minutes or tens of minutes), not just during frequency disturbances as in Ref. [20, 27]. The main hurdle to overcome with estimating inertia during normal day-to-day operation is distinguishing the effect of inertia on the frequency from the effect of frequency control. The authors circumvent this by using a dynamic model of frequency control to separate the two. The efficacy of the method was demonstrated using real measurements from the Icelandic power system, containing 30 phasor measurement units. However, the method did prove unsuccessful in some cases.

GridMetrix®, developed by Reactive Technologies, is a technology that directly measures grid inertia in real-time. A small power change ($< 10\,\mathrm{MW}$) is used to create a tiny

frequency alteration ($\sim 0.0005\,\mathrm{Hz}$). These small power and frequency changes are used to continuously accurately measure grid inertia from both the generation and demand side. The measurement units are distributed around the grid in different locations, so they can also measure regional variations in inertia. Reactive Technologies and National Grid partnered on Project SIM to demonstrate the efficacy of GridMetrix® using "blind measurements" (Reactive Technologies had no knowledge of National Grid ESO's own estimated inertia values). Fig. 2.5 shows GB grid inertia measurement over the 2017 early May bank holiday weekend. In the figure are National Grid ESO's two inertia estimates. One of them (purple line) includes embedded generation and demand contributions. The blue line is the measurement from Reactive Technologies' GridMetrix® based on a 2.4 MW modulation signal [30]. National Grid ESO's total inertia estimate was sometimes too conservative, but also sometimes overly optimistic (yellow regions) and therefore hiding potential risks to the system. The conclusions from Project SIM were that Reactive Technologies had successfully measured grid inertia directly - a world first [33]. Following this success, Reactive Technologies and National Grid ESO signed an agreement that will see the implementation and continuous use of the GridMetrix® inertia measurement service across the GB grid to help National Grid ESO fulfil its 2025 zero carbon goals [34]. These are the main potential benefits of moving from inertia estimates to direct measurements: increased ability to integrate renewable generation and reduce curtailment, decreased procurement of surplus reserve services (thereby saving on costs), and lowering the risk of blackouts.

In summary, the methods used for estimating/calculating the grid inertia are:

- **Method A: Summing the inertia contribution from individual generators or generation types**. This method depends on the accuracy of the inertia constants assigned to each generator or generation type. This is the only method available if there is no access to detailed data on past frequency events.

- **Method B: Post-mortem analysis of past frequency events**. This involves using historic frequency incidents and the swing equation. The method works best for events where there has been a single, sudden loss of generation so the event start

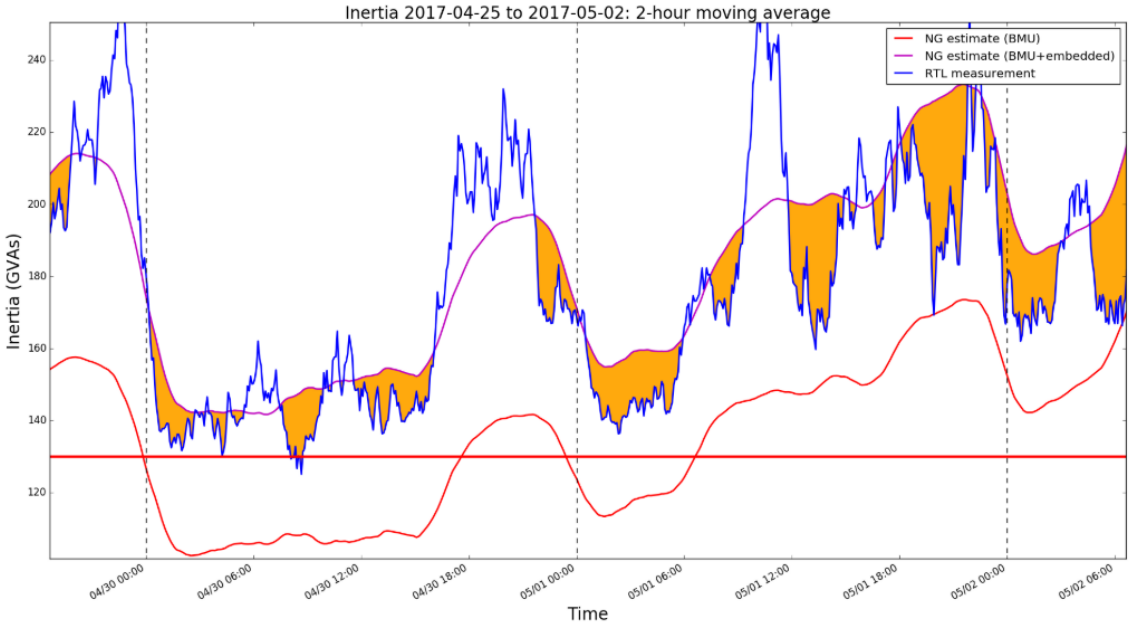

Figure 2.5: GB grid inertia measurement over the 2017 early May bank holiday weekend. Blue line: GridMetrix® measurement. Red line: National Grid ESO's estimate of inertia contribution from balancing mechanism units. Purple line: National Grid ESO's estimate of total inertia (including embedded generation and demand contribution). Reproduced from Ref. [35].

is clear and the subsequent dynamics of the frequency can be easily modelled by the swing equation.

- **Method C: Continuous real-time estimates of inertia based on small perturbations in frequency**. This involves many different techniques, and going into each one in detail is beyond the scope of this review, but examples include Refs. [36, 37] and Ref. [38] where regional inertia estimates were calculated for the GB grid using phasor measurement units bounding an area of the transmission system such that total net power flow into the area was known.

Method B cannot be used to estimate the real-time inertia in a grid. Real-time estimates using *method A* are possible, but often data on generation output is given as the average output over a time interval, so the estimate is not strictly real-time. *Method C*, which is a broad category that includes a lot of different methods, is the only way to truly achieve real-time inertia estimates and it is the commercialised approach [34, 39].

Method A was used on the ERCOT system [40] as a way of forecasting inertia. The future scheduling of the generators was used to predict inertia levels three hours ahead of time. The method was mostly successful but tended to underestimate inertia during low price periods. By returning to the description given in the start of this section, we can see that Bian *et al.* [27] utilise both *method A* and *method B* to obtain an estimate for the contribution to inertia from demand.

Inoue *et al.* [41] were the first to introduce the approach for inertia estimation that combines the swing equation with processed phasor measurement unit measurements of the frequency and the known size of the power loss to estimate the total system inertia (*Method B*). Chassin *et al.* [42] use this method to estimate the inertia of the Western Electricity Coordination Council system and find it to be linear with demand: $H = 62.2 \times 10^{-6} D_{\mathrm{n}} + 6.83\,\mathrm{s}$. Zografos *et al.* [43] improve on previous studies using *Method B* by including frequency response and voltage dependent characteristics of the load in the modelling of the power imbalance. By solving a system of linear equations, this allows the authors to estimate both the inertia and power imbalance.

As mentioned in the method summaries above, one of the issues with *method B* is not having data available on the size of the loss that caused the frequency event. Ref. [43] may have found a workaround, but the problem gets complicated further when there are sequential losses, which can occur as a consequence of the initial loss (e.g. embedded generation loss due to RoCoF tripping). Determining the frequency event start, where RoCoF is measured, is also difficult. A recently suggested technique in the literature estimates the frequency event start based on the second derivative of the RoCoF [44].

2.4 Low inertia

Eq. (2.1) tells us why low inertia is such a concern for frequency volatility. Power imbalances between generation and demand create frequency deviations, and the rate of change of frequency for a given power imbalance is inversely proportional to the amount of grid inertia. In a zero inertia grid, the link between power imbalances and frequency deviations would not so simply be governed by the natural physics of the machines in the system. The

power converters connecting generation and demand would need to independently form a grid voltage and frequency and maintain this voltage and frequency without an explicit communications network [8]. It should be noted that achieving a 100% renewable grid does not necessarily imply a 100% non-synchronous grid because some forms of renewable generation are synchronously connected, such as hydro. However, it does mean that a converter connected dominate grid is likely [45].

In August 2017, the European Commission passed a regulation [46] for electricity system operators to address the decreasing levels of inertia. The regulation (Commission Regulation (EU) 2017/1485 of 2 August 2017: establishing a guideline on electricity transmission system operation) places an obligation on all electricity system operators to determine if minimum inertia is a concern. This is something that system operators in many parts of Europe were already considering. In three reports between 2015 and 2017, the Nordic system operators highlight how higher volumes of converter connected renewable generation, the phasing out of nuclear, and high imports through high voltage DC connections are reducing the inertia on the Nordic grid [26, 47, 48]. In 2011, the electricity system operators of the Irish grid (EirGrid and SONI) embarked upon a programme [49] to ensure the secure operation of the Irish power system with increasing levels of variable non-synchronous renewable generation. One of the main aims of the programme was to increase the maximum system non-synchronous penetration level from 50% to 75% to achieve the 40% renewable energy share targets by 2020. The maximum system non-synchronous penetration level was raised to 65% in November 2017 due to works undertaken by the DS3 programme. Reaching penetration levels above 75% are deemed extremely difficult due to low inertia causing stability concerns.

Johnson *et al.* [50] focus on the impact that high renewable energy penetrations have on grid inertia levels using a region-specific and disaggregated unit commitment and dispatch model for the ERCOT grid. Several future renewable penetration scenarios were analysed while the grid inertia was constrained to always be above 100 GVA.s. Their results showed that the Texas grid could reach relatively high penetrations (30% compared to 18% in 2017). However, retiring nuclear plants and private-use networks (large combined heat

and power plants deployed at industrial facilities) did lead to some unstable inertia levels. Due to the constraint on the inertia to be above 100 GVA.s, multiple coal and gas CCGT plants were dispatched at part-load to maintain the inertia. In a following publication, Johnson *et al.* [51] use the same unit commitment and dispatch model to investigate far more ambitious renewable penetration scenarios. When the critical inertia limit was reduced from 100 GVA.s to 80 GVA.s to represent changes in grid operation, no critical inertia hours were observed for renewable penetration levels up to 93%. Many pathways for reducing the number of critical inertia hours were investigated: price signals to procure inertia contributions, grid-scale operational changes to reduce the critical inertia limit (e.g. reducing the size of the largest infeed loss), plant retirements, and fast frequency response. It was found that reducing the size of the largest infeed loss reduced critical inertia hours more than fast frequency response.

An increase in the percentage of converter connected generation on a power grid results in a decrease in the percentage of synchronous generation. So, this results in a decrease in inertia from the generation side. It was mentioned in Section 2.2.1 how an increase in variable speed drives on the demand side will reduced the demand damping effect. It also has the unfortunate effect of reducing the inertia contribution of these demand units [27, 52] as well. All in all, traditional providers of inertia are reducing in number so grids of the future will have to adapt to, and manage, low inertia as a high priority. Below is a list of adaption and management measures for low inertia [19, 52]:

- Decrease the size of the largest infeed loss
- Change grid regulations
  - Change the RoCoF relay protection limits
  - Change frequency limit for demand disconnection
- Maintain a minimum inertia level
  - Operate multiple synchronous generators at part-load
  - Create an inertia market and incentivise generators with high inertia

  - Limit the amount of converter connected generation

- New frequency/inertia response
  - Fast frequency response/synthetic inertia
  - Synchronous condensers (also fits in the above category)

Mehigan *et al.* [53] investigate the impact of renewables in the European power system on system inertia. They demonstrate that minimum inertia levels may be useful in the transition to higher penetration levels but will ultimately impede emissions reduction goals if not replaced in a timely manner. It is inevitable that grid regulations will have to be adapted and faster frequency response services will have to come online if 100% renewable and stable grids are to exist.

2.4.1 Synthetic inertia

The definition of synthetic inertia is not consistent in the literature. For starters, synthetic inertia goes by many names: virtual inertia [54], digital inertia [7], and emulated inertia [55]. Often, synthetic inertia is the term given to describe fast frequency response from converter connected technologies such as energy storage, solar PV, and wind [56]. However, Eriksson *et al.* [57], in their paper investigating synthetic inertia and fast frequency response from wind power control, clearly distinguish between the two by defining synthetic inertial response as being proportional to RoCoF and fast frequency response as being proportional to frequency deviations. The authors conclude that both synthetic inertia and fast frequency response can improve the frequency nadir after a large infeed loss. However, only fast frequency response is able to improve normal day-to-day operation frequency quality.

In my opinion, the term *synthetic inertia* should probably be retired and replaced with *fast frequency response* (but clearly distinguishing when this response is proportional to the RoCoF). Fast frequency response and inertia from synchronous generators are very different physical phenomena. By definition, the inertia of synchronous generators acts instantaneously when the frequency deviates because the inertia is part of the reason why

the frequency deviates. Fast frequency response cannot act instantaneously like inertia, so will never be able to affect the very initial RoCoF when a disturbance occurs on a grid. However, if the RoCoF measurement of interest is one that is measured over a time period of 500 ms, for example, then frequency response with a shorter delay time than this *would* lower the measured value and therefore would produce an effect similar to having an increased amount of inertia. In this specific case, I argue that the description of the situation should be "the fast frequency response has *acted like* synthetic inertia".

2.4.2 Synchronous condensers

A synchronous condenser, also called a synchronous compensator, is a synchronous machine operating without a prime mover. It is essentially a synchronous motor/generator with no load, the shaft is not connected to anything and spins freely. Synchronous condensers can support grid voltage by providing reactive power and can add additional inertia to the grid [58]. Synchronous condensers can also be used to support a black start [59]. The field of a synchronous condenser is controlled by a voltage regulator, which can switch the machine from a reactive power generating device to a reactive power absorbing device depending on the system voltage needs. Typical reactive power ratings for synchronous condensers connected to the grid are in the range of 20 to 200 MVAr [60]. Synchronous condensers have played an important role in maintaining voltage stability in power systems for more than 50 years [61,62], whereas the attention on their inertia contribution is a more recent research interest.

Nguyen *et al.* [63] demonstrate that synchronous condensers can improve the frequency conditions of a future Western Danish power system with high wind penetration. The modelled synchronous condenser allows the frequency to reach a nadir after a 200 MW load loss rather than the frequency collapsing to unacceptable levels. However, it was unclear from the paper what size the synchronous condenser was. In a later paper by the same author [64], the combination of synchronous condensers and synthetic inertia from wind power plants for frequency stability are analysed. The synchronous condenser model includes a real automatic voltage regulator system that is interfaced with the simulations

through hardware-in-the-loop. A simplified Western Danish power system is simulated in a real-time digital simulator to demonstrate the effectiveness of the strategies. The three synchronous condensers in the simulation had a size range of 150 to 242 MVAr and an inertia constant range of 2 to 2.5 s. It was found that the synchronous condenser provided mainly the inertial response (improving RoCoF) and the synthetic inertia from wind plants acted like extremely fast frequency response and improved the maximum frequency deviation.

Nedd *et al.* investigate the use of synchronous condensers in the GB grid to counter challenges presented by increasing renewable penetration and associated low inertia [65,66]. From the swing equation, it is suggested that 5 GVA of synchronous condensers with an inertia constant of 2 s could increase the loss of infeed tolerance (based on the 0.125 $\mathrm{Hz\,s^{-1}}$ RoCoF limit) from 375 MW to 425 MW at a very low grid inertia of 75 GVA.s. This ignores the effect of demand damping. The theoretical analysis is confirmed by using a single-bus representative GB transmission network model.

In 2017, SP Energy Networks won financing from National Grid ESO's Network Innovation Competition to develop a hybrid synchronous condenser solution (synchronous condenser with a static compensator). This became known as Project Phoenix [67], with the aim to develop a 140 MVA device and connect it to a 275 kV substation in Neilston, Scotland. The trial of the device went live in late 2020 [68].

2.5 Frequency response

2.5.1 Frequency response in Great Britain

In Great Britain before 2016, there were traditionally three main types of frequency response: primary, secondary, and high. These services still exist today in the GB grid. Primary frequency response acts when the frequency deviates past the deadband below 50 Hz. The frequency deadband is a range of frequencies where there is no frequency response. In Great Britain it is ~ 0.015 Hz. Primary response must respond with 2 s and be at full output at 10 s and sustained for 30 s. High frequency response must have the

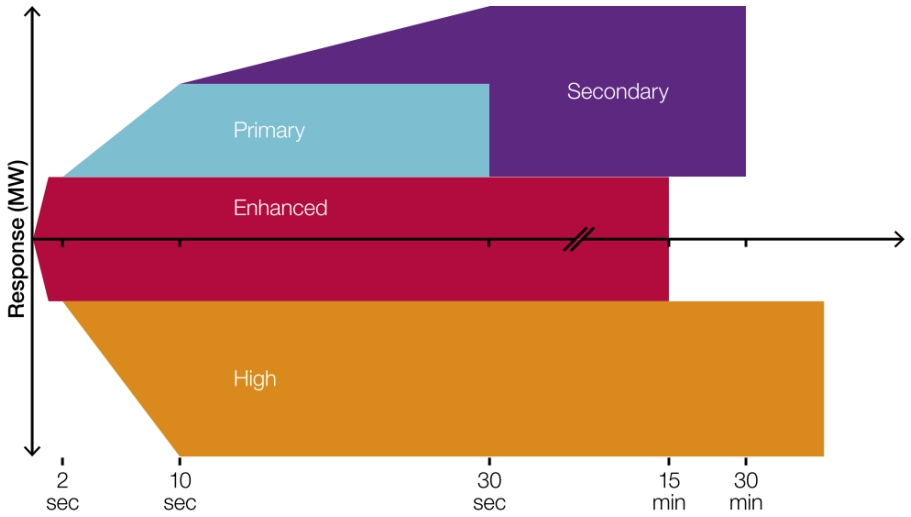

Figure 2.6: Frequency response services in Great Britain in 2019. Reproduced from Ref. [11].

same response speed as primary but also is required to act indefinitely. Referring back to Fig. 1.4, these two frequency response services are the main ones involved in the frequency containment phase. Secondary frequency response acts when the frequency is below 50 Hz and must respond fully within 30 s and sustained for 30 min. Referring back to Fig. 1.4, secondary frequency response (and high above 50 Hz) is the main service involved with frequency recovery after a large infeed loss. All three of these traditional forms of frequency response are shown in Fig. 2.6.

In July 2016, National Grid ESO tendered for a newly designed frequency response service: Enhanced Frequency Response (EFR). As can be seen in Fig. 2.6, a provider of EFR must offer symmetrical response and fully respond within 1 s and sustain delivery for 15 min [69]. This was a significant increase in response speed compared to the traditional primary, secondary, and high services. The aim of EFR was (and still is) to improve the management of grid frequency pre-fault i.e. normal operation, but the service also offers assistance post-fault. There were eight tenders that were accepted giving 201 MW of EFR at a total cost of £65m [70]. Every successful tender was a battery energy storage system.

In 2019, National Grid ESO published a report [71] that introduced four potential new frequency response services, which could replace the traditional primary, secondary, and high services in the future. More detail on these new services is given in Section 2.7.1.

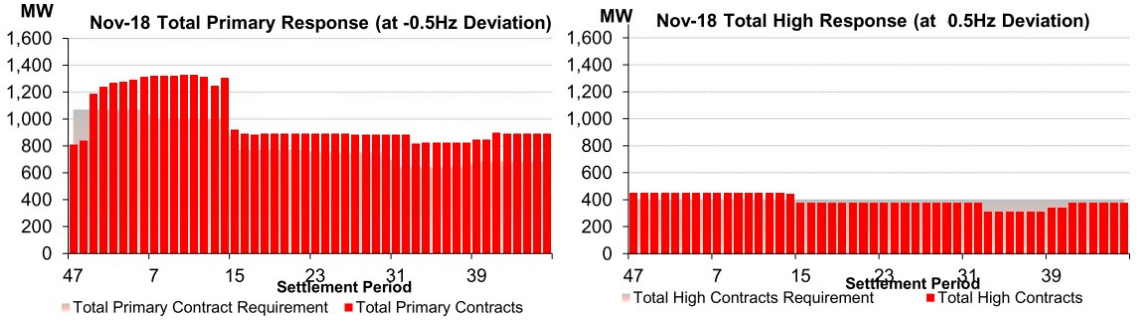

Figure 2.7: Primary and high frequency response requirement (in grey) in Great Britain in November 2018 and the contracts to meet the requirement (in red). Reproduced from Ref. [74].

National Grid ESO forecasts the amount of response capacity it needs for each frequency response service and acquires this capacity though mandatory arrangements (mandatory frequency response) and a commerical market (firm frequency response). Fig. 2.7 shows the primary and high frequency response requirement in Great Britain in November 2018 and the contracts to meet the requirement. The requirement is determined based on system modelling conducted by National Grid ESO, with one of the main factors being the size of the largest potential infeed loss [72]. The primary response requirement in November 2018 was between 1000 MW and 700 MW throughout the day, 200 MW of this was fulfilled by EFR. The high response requirement in November 2018 was 400 MW throughout the day, 200 MW of this was fulfilled by EFR.

Again, taking the month of November 2018 as an example, the total spent to balance the system for the month was £111.04m [73], which was charged to generators and suppliers through the Balancing Services Use of System charge. £45.62m (40%) of this was spent on ancillary services, which include black start, frequency response, constraint management, reserve, etc. Breaking it down further, frequency response cost £12m, and was between £10m and £12m for each month between April and November 2018.

2.5.2 Frequency response in other grids

Three recent reviews of international grid codes by Luo *et al.* [75], Roberts [76], and Meng *et al.* [77] have been used here to summarise the differences and similarities between frequency response in Great Britain and frequency response in other grids around the

Region	Maximum deadband	Response time requirement	Minimum duration
Great Britain	0.015 Hz	Full activation by 10 s	30 s
Ireland	0.015 Hz	Full activation by 2–10 s	30 s
Finland	0.1 Hz	50% by 5 s and full activation by 30 s	2 min
Italy	0.01 Hz or 0.02 Hz	50% by 15 s and full activation by 30 s	15 min
New Zealand	No deadband	Full activation by 6 s	60 s
Texas, USA	0.034 Hz or 0.017 Hz	Full activation by 14–16 s	30 s

Table 2.1: Comparison of different frequency response parameters in different regions around the world [75–77].

world.

Table 2.1 shows a comparison of different frequency response parameters in different regions around the world. Fast response is more important in grids with a higher penetration of non-synchronous generation, which is why the GB, Ireland, and New Zealand grids have a faster response requirement. New Zealand and Ireland also have quite small grids in terms of total demand compared to the Nordic synchronous system, the Continental European system, and the Texas ERCOT system. In New Zealand, there is no requirement on the deadband because the frequency response is procured solely through the market, and this gives generators more flexibility [77].

EFR and Dynamic Containment are two examples of new frequency response service in Great Britain. Other grids around the world are also introducing new services. In Australia there are two fast frequency response services (FFR 1 and 2), with a required response speed of 0.5–1 s and a duration of 6 s. In PJM, part of the Eastern interconnection in the USA, a new service called RegD [78] requires a response within 2 s and created a surge in grid-scale battery storage connections to the grid.

The amount of frequency response capacity held in different grids around the world is largely determined the same way across all of them: by securing the grid against the

potential largest loss that grid could suffer. ±3000 MW of primary reserve is held on the Continental European grid, which is equal in size to the two largest generating facilities connected to the same bus bar [76]. In New Zealand, the largest imbalance may result from the tripping of the interconnector between the North and South island or the largest potential infeed loss.

2.5.3 Frequency response mechanism and modelling

Frequency response has traditionally been provided for by large synchronous generators. The mechanism for this response capability will briefly be explained. As explained in Section 1.1 and shown in Fig. 1.3, if the power demand of a synchronous generator changes, the difference in power is provided or absorbed first by the rotational kinetic energy of the large rotational masses involved. This either speeds up the rotation (grid frequency increase) or slows it down (grid frequency decrease). Historically, a spinning flyball governor (see Fig. 2.8), connected to the generator shaft, was used to convert this change in rotational speed to a change in throttle valve opening and ultimately to a change in mechanical input power into the generator. Nowadays, the flyball governors have largely been replaced by electronic sensors that rapidly measure frequency and send signals to control the throttle valve [8]. The deadband of the governor determines the range of frequency deviation where the governor action does not activate. The speed droop of a governor is the ratio of the percentage change in frequency to the percentage change in generator power output. The speed droop is always positive and it set to 3–5% in Great Britain [79].

Back in 2005, Lalor *et al.* [81] found that as the number and proportion of base-loaded CCGTs increases on the Irish grid, the frequency control becomes more challenging. Generators in frequency response mode, i.e. ready to offer frequency response at any moment, must be somewhat part-loaded. Wyman-Pain *et al.* [82] investigate the cost of part-loading different generator types for frequency response. Above a 75% part-loading level the cost is fairly flat for coal and CCGT plants. For nuclear, there is a sharp increase in cost below 90% indicating its unsuitability for part-loading. Part-loaded generators recoup their costs by receiving payments for providing frequency response to the grid.

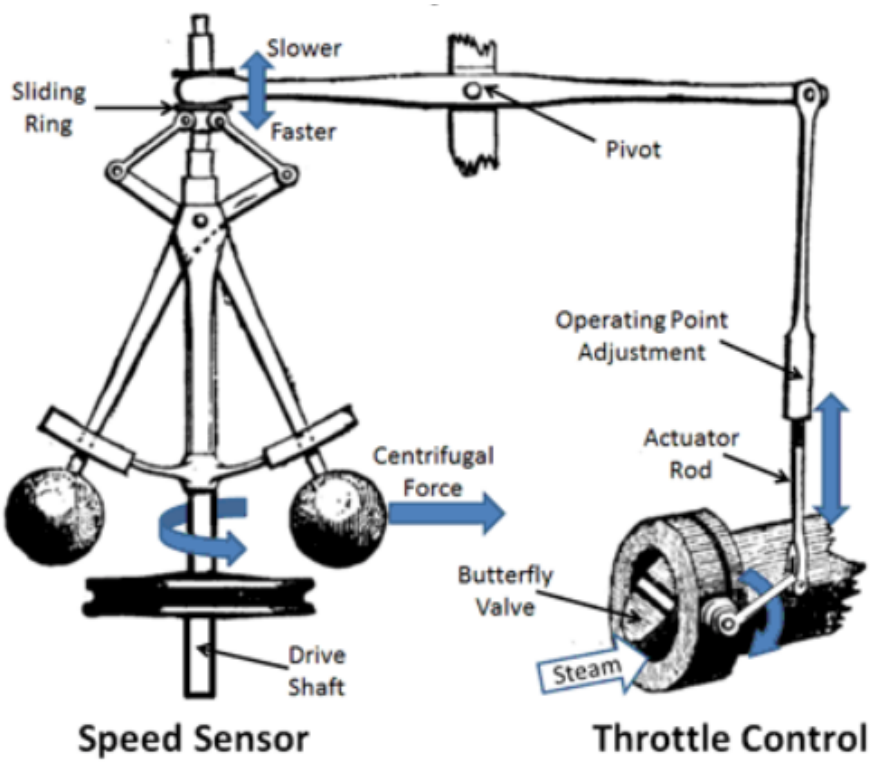

Figure 2.8: Flyball governor. When the frequency drops, the balls move in which opens the throttle. With the throttle opening further, more steam (or water in a hydroelectric plant) can flow through and increase the mechanical power. The opposite effect occurs when the frequency rises. Reproduced from Ref. [80].

There are different ways that frequency response has been modelled in the literature. Primary frequency response can be approximated as a linear ramp after a delay and this allows the swing equation, Eq. (2.1), to be solved analytically [79, 83].

In many studies, the frequency response of synchronous generators is modelled as a control system with transfer functions for the governor and turbine response. Fig. 2.9 gives a simple example of one of these control system block diagrams. The frequency output is multiplied by the speed droop and this signal then passes through the governor and turbine transfer functions $1/(1 + sT_g)$ and $1/(1 + sT_t)$, respectively. This determines the time evolution of the frequency response power output in the model. The signal after these transfer functions is then summed with the change in load on the grid, which then feeds into the swing equation to determine the next frequency signal.

Frequency response models are also commonly tested in power system simulators, an

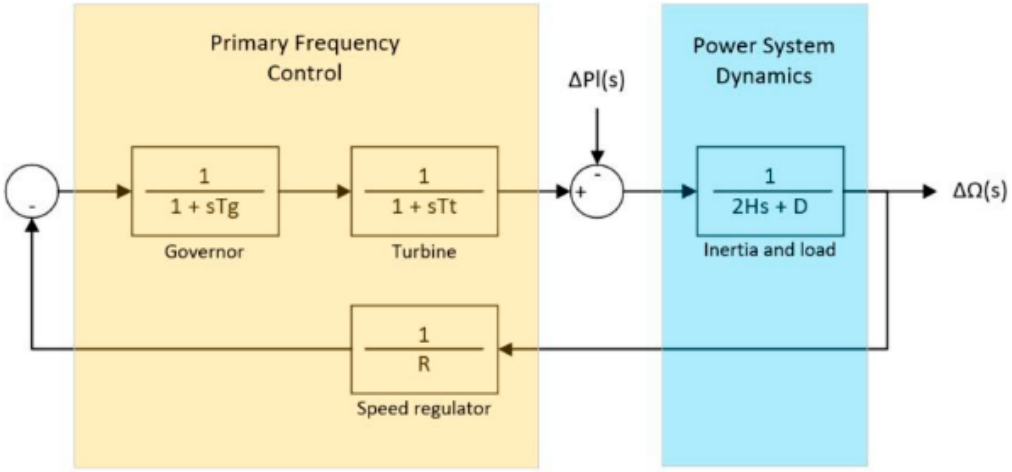

Figure 2.9: Block diagram of a simple model of the frequency response control system. Reproduced from Ref. [28].

example of which is DigSILENT PowerFactory [31]. PowerFactory is a leading power system analysis software application for use in analysing generation, transmission, distribution, and industrial systems. Ashton *et al.* [20] use a full dynamic model of the GB power system in their grid inertia estimation study, but Brogan *et al.* [84] adapt a standard IEEE 39 Bus System. The IEEE Bus Systems are widely used in the research community for testing new ideas and concepts. The IEEE 39 Bus System is a 10 generator system that represents the New England power system, developed in Ref. [85]. Note, the IEEE Bus Systems have multiple buses, which more closely matches reality, compared to the single infinite bus assumption of the swing equation (Section 2.2).

Hardware-in-the-loop is a technique used for testing controller software. A controller is connected to a test system that simulates reality. The controller can then respond to virtual stimuli from the software representing the real system. Greenwood *et al.* [86] use hardware-in-the-loop to evaluate the performance of energy storage systems delivering the EFR service. They connected a battery emulator and a laboratory 415 kV busbar with power system simulation software.

2.6 Future frequency response requirements

Previous discussions in this literature review have highlighted how improving frequency response is one of the main solutions to mitigate low inertia. Here we review the literature concerning future frequency response requirements in power systems. The first part of this review focuses on the GB grid. In Section 2.6.1, I review studies into frequency response provision from non-traditional technologies (traditional being thermal power plants).

Vogler-Finck *et al.* [79] use the swing equation and some simplified models of frequency response to investigate the frequency response requirements of the GB grid at different demand levels and wind penetration after a large infeed loss. Primary frequency response is modelled as a linear ramp to a target response with the target reached after 10 s. Secondary frequency response is also modelled as a linear ramp (after 30 s) and the amount of secondary frequency response in the model is enough to bring the steady-state frequency to 49.5 Hz within 60 s. Fast frequency response in the model rapidly increases within 0.2 s and then exponentially decays with a time constant of 5 s after primary frequency response has reached a maximum. The target response of fast frequency response is determined by the maximum RoCoF (fitting the definition of synthetic inertia given in Section 2.4.1). Fig. 2.10 shows the results for two scenarios: one with 500 MW of fast frequency response, and one without. The primary frequency response shown is just enough to prevent the frequency breaching 49.5 Hz after a large infeed loss of magnitude 1320 MW. The results show that a dramatic increase in primary frequency response capacity is required at low demand levels and high wind penetration, but this is reduced substantially by fast frequency response acting like synthetic inertia. The study does not address extremely low inertia scenarios because there is always 10 GW of $H = 4$ s baseload generation in the simulations and the frequency responsive generation has an inertia constant of 6 s.

Nedd *et al.* [87] use a single-bus model of the GB grid, developed in DigSILENT PowerFactory [31], for their system studies. The study applies the following assumptions: demand set at 20 GW, an inertia constant of 1.83 s is used for demand and embedded generation, the demand damping constant is 2.5 %MW/Hz, primary frequency response is

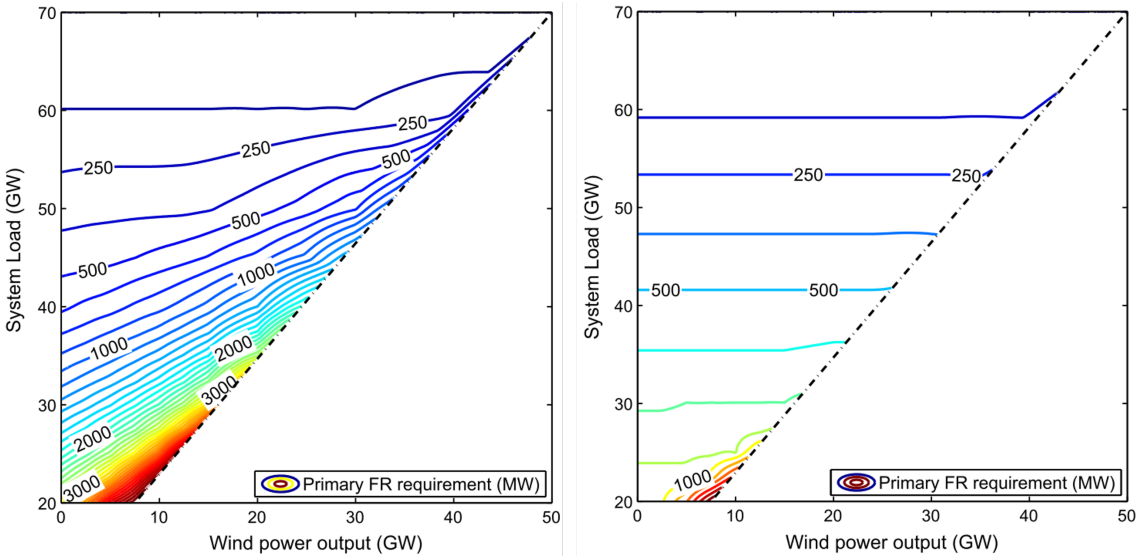

Figure 2.10: Variations of primary frequency response requirements with different load and wind output. On the right is the scenario in which there is 500 MW of fast frequency response, and on the left is the scenario without fast frequency response. Reproduced from Ref. [79].

provided by generators at 75% part-loading, the generation is obtained from National Grid ESO's Gone Green scenario and the generation is dispatched in the order of nuclear, gas (if the inertia target is not yet achieved), and then non-synchronous generation. The study looked at the success of different combinations of frequency response provision (primary, EFR, and dynamic containment) at containing a large infeed loss in the GB grid. Dynamic containment is a new frequency response service, which is explained more in Section 2.7.1. For the response provision to be deemed successful, the frequency must stay within $\pm 0.5\,\mathrm{Hz}$ and the RoCoF within $0.125\,\mathrm{Hz\,s^{-1}}$ in one case, and within $0.5\,\mathrm{Hz\,s^{-1}}$ in another. At low inertia and low demand, it was found that the RoCoF limit of $0.125\,\mathrm{Hz\,s^{-1}}$ can only be managed by curtailing the largest infeed loss from $\sim 1\,\mathrm{GW}$ to around 650 MW. Once the RoCoF limit is changed to $0.5\,\mathrm{Hz\,s^{-1}}$, containing large infeed losses becomes more of an issue of adequacy of frequency response (speed and capacity). The paper did not report on the actual value of capacity or speed of the frequency response required to secure the GB grid.

Forkasiewicz *et al.* [88] investigate the effectiveness of primary frequency response ramp rates using the swing equation. Again, the authors study the case of a large infeed loss

(1000 MW) with a response capacity of 1000 MW. The response is considered a failure if the frequency drops below 49.5 Hz. The inertia value was randomly chosen from a normal distribution of inertias (representing the GB grid). It was found that the failure rate drops from 94% at a 10 s ramp rate to 9% at a 4 s ramp rate. The authors ignore demand damping in their modelling.

Hong *et al.* [89] also investigate the characteristics (delay and ramp time) of fast frequency response on the effectiveness of frequency control after a large infeed loss. They find that delays up to 1 s are not significant, but the ramp rate of the response is, which is why resources such as energy storage, demand-side response, and interconnectors are more suited to the provision of fast frequency response services. Conventional, large synchronous generators cannot ramp quick enough.

Rapizza *et al.* [90] calculate the optimal amounts of synthetic inertia and fast frequency response (taking into account the cost of each service) to maintain frequency stability. The non-linear optimisation procedure was tested on an annual scenario for the power system of Sardinia. The optimal quantities of the two services were calculated at each hour by assuming a maximum generation (100% of the hours) or demand loss (60% of the hours). The most critical situation found was for a demand loss because the frequency limits were stricter in this direction.

Wall *et al.* [91] nicely summarise the requirements of future frequency response (which they term *smart frequency control*). It must be faster to limit the magnitude of the frequency deviation, more adaptive to accommodate daily/seasonal variation in inertia, and more regional in nature to accommodate the regional variation in inertia.

The studies I have gone into detail about above all determine frequency response requirements after a large infeed loss to keep the frequency within acceptable limits. Below is a review of two studies that look at the long-term effect of grid parameters on the grid frequency.

Power systems can be modelled using stochastic differential equations, and the Ornstein–Uhlenbeck process is often the one used [92]. The Ornstein–Uhlenbeck process is similar to the random walk process (a stochastic process in which the change in the ran-

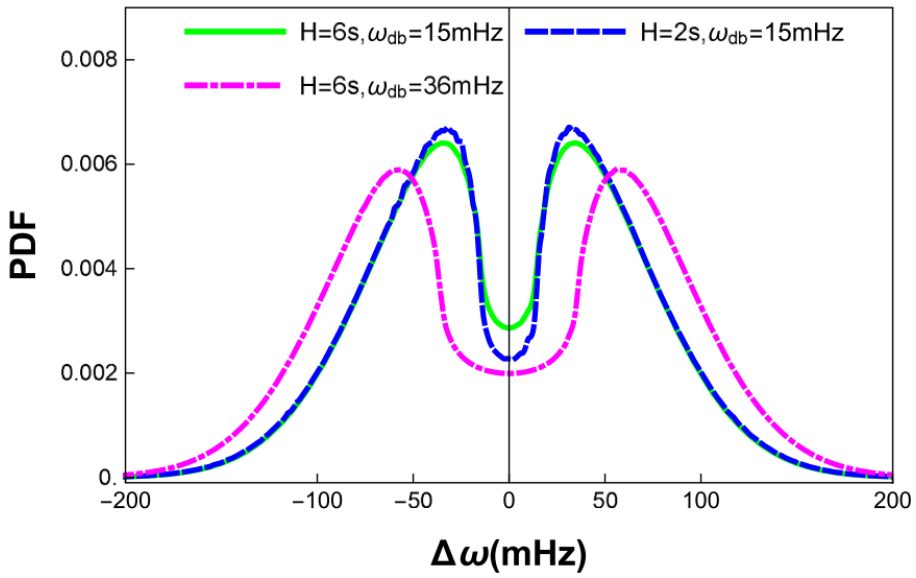

Figure 2.11: Effect of deadband width and grid inertia (given as an inertia constant) on frequency deviations probability density function. Reproduced from Ref. [95].

dom variable is uncorrelated with past changes) but with the tendency of the stochastic behaviour of the system state to remain somewhat close to the long-term mean [93]. The time evolution of the probability density function of a system governed by the Ornstein–Uhlenbeck process can be described by the Fokker-Planck equation, a partial differential equation [94]. Solving this Fokker-Planck equation thereby returns the probability to observe the system in a certain state at a certain time.

Vorobev *et al.* [95] derive and solve a Fokker-Planck equation for the frequency probability density function. This allows them to establish the influence of grid parameters on the long-term frequency distribution. They show that grid inertia has little effect on the frequency distribution, see Fig. 2.11, making synthetic inertia services insufficient for keeping frequency close to nominal under ambient load fluctuations. This contrasts with the important role inertia plays when analysing the frequency dynamics after a large infeed loss. The authors also demonstrate the effect of governor deadbands: a narrower deadband could reduce the standard deviation of frequency deviations without significantly increasing generator wear-and-tear.

del Giudice *et al.* [96] conduct a similar study to Ref. [95]. They use a simplified model of a power system with a stochastic load. The authors agree with the assessment

of Ref. [95] that grid inertia only plays a marginal role in the frequency distribution. The authors note that if the inertia of a power system decreases, frequency deviations can still be kept small if the demand damping constant is adequately large. They suggest that the demand damping effect could be increased by exploiting thermostatically controlled loads (e.g. refrigerators, air conditioners, heat pumps, etc).

2.6.1 Frequency response from alternative technologies

Frequency response is no longer just the domain of synchronous generators. There are many alternative technologies that have been studied in the literature and, recently, provided active service on real electricity grids (e.g. batteries performing the EFR service in Great Britain [70]). Examples of alternative technologies include batteries, solar PV, wind, and demand-side response. In the vast majority of cases, these technologies are converter connected to the grid. They do not have inherent inertia to offer the grid, but can perhaps counter this negative stability aspect by providing the grid with very fast frequency response, much faster than a traditional synchronous generator [8].

Batteries are so attractive for frequency response because of their ability to deliver power extremely quickly, with ramp rates as low as 40 ms being demonstrated [97]. By studying faults on the Irish power system, it was found that 360 MW of batteries could ramp up to the same amount of power after 0.1 s as the inertial response of 3000 MW of synchronous generators [7, 98]. Brogan *et al.* [84] investigate the effect of response from batteries on the frequency nadir and RoCoF on a simulated power system model (representing the Irish grid) after a loss of generation event. The power capacity of the battery system, delay time, and time taken to ramp to full power (ramp time) were varied. To model the Irish power system, a standard IEEE 39 bus system was calibrated in DIgSILENT PowerFactory [31] by tweaking parameters to reflect observed behaviour measured by phasor measurement units at generation sites on the Irish system during a real under-frequency event. With the model calibrated and tuned to match the Irish power system, a battery system was added into the system and simulations run with a loss of generation of 430 MW (10.5% of total load) and battery parameters varied: power

(0 MW to 500 MW), delay time (0.01 s to 6 s), and ramp time (0.01 s to 10 s). The battery is modelled with only a delay and then a linear ramp in power: this means that the study is actually technologically agnostic and the results and conclusions apply to technologies with a response similar in characteristics. For a battery to have a significant effect on frequency nadir it is important that the sum of delay time and ramp time is less than the time taken to reach the frequency nadir. It was found that a combined delay and ramp time under 0.5 s provided almost 100% of the maximum potential reduction of frequency nadir. This study shows that to improve RoCoF, delay times less than 0.25 s and ramp times less than 0.75 s are needed. The authors note how sensitive the results are to the method for measuring RoCoF. The definition they use is the median of the instantaneous RoCoF values in moving 0.5 s windows.

High electric vehicle uptake could dramatically increase electricity demand in the future. Managing this increase in demand and possible constraint issues is seen as a huge challenge for National Grid ESO and distribution network operators [99]. However, each electric vehicle contains a battery, which also brings the possibility of using the country's electric vehicle fleet as a huge frequency response asset. There have been a number of studies investigating the potential of electric vehicles to perform frequency response in Great Britain [100–102]. In each one a simplified GB power system model was used, based on the swing equation. The studies conclude that electric vehicles can provide a significant contribution to primary frequency response capacity, but the effectiveness of this contribution depends on the type of charging strategy. Smart charging can help increase the availability of electric vehicles to be able to deliver response throughout the day. The effectiveness of electric vehicles in providing grid stability has also been studied for smaller, isolated systems [103]. In Ref. [103], the electric vehicles were modelled with a droop response and a synthetic inertia response (proportional to RoCoF [57]). It was found that the droop response was more effective but more energy was discharged from the battery.

Domestic heating is a huge source of carbon emissions in the UK, and heat pumps are an option being pursued to facilitate decarbonisation [104]. The aim is for 600,000 heat

pump installations per year by 2028 [105]. This will increase the electricity demand in the future, similar to the situation with high electric vehicle uptake. Muhssin *et al.* [106] investigate dynamic frequency response from controlled domestic heat pumps. Case studies were carried out by combining a representative model of the aggregated heat pumps to a 36-bus model of the GB grid. The heat pumps respond to simulated large infeed losses by reducing their power demand. 3.8 million heat pumps offering frequency response improved the frequency drop by 0.78 Hz after a 1724 MW loss. The total heat pump demand dropped by 1000 MW during the event, which is 0.26 kW per heat pump ($\sim$ 3% of a domestic heat pump power rating). Other areas of demand that could be utilised for demand-side response include smart buildings [107], bitumen tanks [108], data centres [109], and commercial food refrigeration systems [110]. All of these are examples of loads that have a high overall electricity demand, but also have the ability to spread this demand and can occasionally reduce or increase their demand to support the grid.

Wind turbines have kinetic energy stored in the rotating blades, shaft and generator. In a fixed speed wind turbine (connected by an induction generator), this inertia can support the grid [111]. The inertia constant mostly ranges from $H = 2\,\mathrm{s}$ to $H = 6\,\mathrm{s}$ [112] for wind turbines with a rated power over 1 MW. In other words, the ratio of rotational kinetic energy to rated power in $> 1\,\mathrm{MW}$ wind turbines mostly ranges between 2 and 6. However, most modern wind turbines in power systems are variable speed wind turbines and these are connected to the grid via power electronics [113]. Normally, the controllers of variable speed wind turbines endeavour to keep the turbine at its optimal speed, so it is producing maximum power. However, additional controllers have been proposed in the literature that allow the wind turbine to provide inertial and frequency response [114,115]. Providing inertial and frequency response requires wind turbines to not be operating at their maximum power output (de-loading), but there are various de-loading strategies that could keep this to below 10% [116].

Frequency response from solar PV can be provided by operating the plant at less than full output so there is headroom (i.e. de-loading). The Californian system operator conducted a demonstration project on a large solar PV power plant to test its ability to

provide ancillary services [117] and found it could successfully deliver a wide range such as frequency response, load following, and voltage support. However, providing these services reduces the capacity factor of the plant.

2.7 The view of Great Britain's electricity system operator

In Section 2.7.1 we review literature authored by National Grid ESO focussing on low inertia and frequency response, and in Section 2.7.2 we review the modification of loss of mains protection settings.

2.7.1 Low inertia and frequency response

National Grid ESO started publishing their system operability framework (SOF) in 2014 to provide a holistic view on the impact of decarbonisation and decentralisation on grid stability, using the National Grid ESO Future Energy Scenarios. In the year that the first SOF was published, a change was made to the Distribution Code that required embedded generators to modify their RoCoF loss of mains protection settings. This was to avoid spurious tripping, which is more likely in a system with reduced inertia. Modelling work in SOF 2014 [118] predicts that the previous RoCoF relay setting of $0.125\,\mathrm{Hz\,s^{-1}}$ would be breached around 90% of the time after the maximum infeed loss by 2025 (in the scenarios representing significant decarbonisation). For a RoCoF relay setting of $1\,\mathrm{Hz\,s^{-1}}$, it was predicted that in 2025 there would be tolerance 100% of the time for an infeed loss $< 1162\,\mathrm{MW}$ (again, for decarbonisation scenarios). SOF 2014 also mentions that rapid frequency response is considered likely necessary in the future.

The Future Energy Scenarios considered in the 2015 and 2016 SOF were Consumer Power, Gone Green, No Progression, and Slow Progression. Consumer Power is a scenario in which prosperity is high and new technologies are prevalent, but decarbonisation is less of a priority. Gone Green is a scenario in which prosperity and innovation are high, and decarbonisation is a high priority. Slow progression is a scenario where economic conditions result in some progress towards decarbonisation but at a slower pace than society would like. No progression is a scenario where society is focused on short-term

goals and affordability rather than decarbonisation.

Frequency response requirements were assessed in the 2015 edition of the SOF [119]. Studies were performed at five year intervals for each of the four future energy scenarios from 2015 to 2035. Fig. 2.12 shows the amount of traditional frequency response required to keep the grid frequency within statutory limits (± 0.5 Hz) after a maximum infeed loss at minimum summer demand levels (both demand and maximum loss change with scenario and year). Traditional frequency response refers to response deliverable between 2 and 10 s following the infeed loss (i.e. the type of response provided by traditional synchronous generators). The white crosses on the graph refer to scenarios where it is not possible to achieve the volume of frequency response needed from the predicted generation mix on the system. Alternative providers of response, such as energy storage, would need to make up the shortfall. The response requirement increases with time in all scenarios. The first big jump in requirement occurs in the Gone Green scenario in 2025 due to the increase in the size of the maximum infeed loss before the other scenarios. By 2030, in all scenarios, the amount of frequency response required is three to four times higher than current levels. The SOF 2015 report predicts that in two scenarios (Gone Green and Consumer Power), no frequency response will be provided for by synchronous generators during the summer minimum demand level. Many options to mitigate the challenge of securing the system during the summer minimum were discussed:

- Synchronous compensators. These could be retrofitted to decommissioned generators or introduced as stand-alone devices.
- Operating thermal generators at lower output thereby increasing the inertia of the system
- Incentivise wind and solar to run part-loaded to offer frequency response
- Distribution System Operators (DSOs) with the ability to control the frequency response of embedded generation
- Synchronous energy storage (e.g. compressed-air energy storage) could provide frequency response and inertia to the system

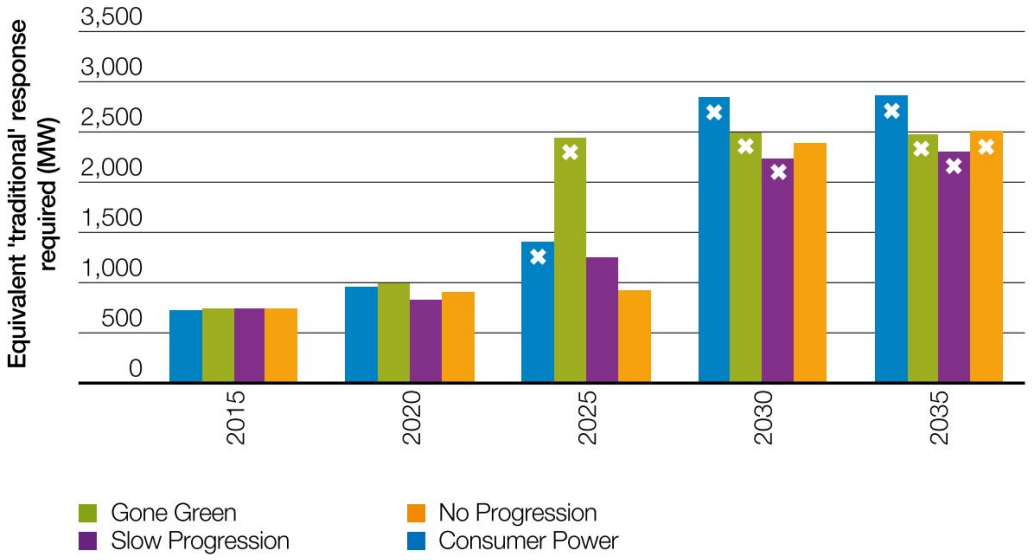

Figure 2.12: Capacity of traditional frequency response required to keep the grid frequency within statutory limits after a maximum infeed loss (with demand at summer minimum level) for different future energy scenarios. Reproduced from Ref. [119].

- Flywheels and batteries could provide fast frequency response
- Demand-side flexibility (e.g. EVs)

The discussion about frequency response requirements and reducing grid inertia continued in the SOF of 2016 [11]. Fig. 2.13 shows how the distribution of grid inertia changes across all future energy scenarios from 2016/17 to 2025/26. In the Consumer Power, Gone Green, and Slow Progression scenarios, the distribution peaks below 100 GVA.s in 2025/26. In 2016/17 the peak is roughly 210 GVA.s. Across all scenarios, it was predicted that the inertia would still spend some time above 250 GVA.s in 2025/26 but much less time than in 2016/17. The shifting to the left of the distributions is due to the predicted increase in non-synchronous generation. The 2016 SOF report recommended a systematic review of the primary, secondary, and high frequency response services due to their barriers to entry and lack of rapid response. It also highlighted the importance of continuous dynamic response as part of the total response requirement to reduce frequency volatility.

By 2017 it was clear that the role of the electricity system operator was becoming more challenging and there was a general view that National Grid ESO's balancing services were too complicated and involved too much overlap. In 2017, National Grid ESO published the

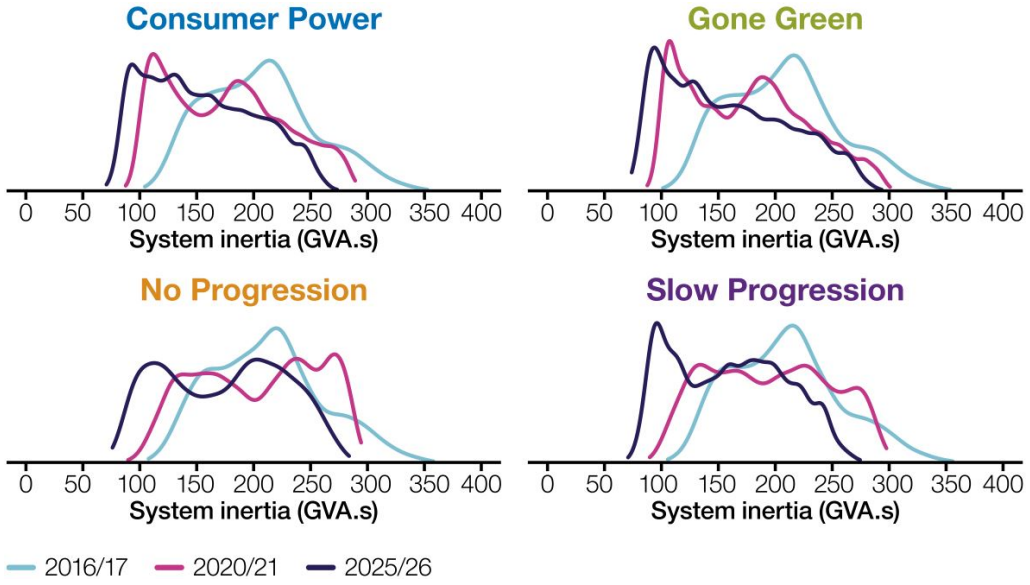

Figure 2.13: Annual distributions of grid inertia by future energy scenario. Reproduced from Ref. [11].

System Needs and Product Strategy (SNaPS) document [120], which was the first of the *Future of Balancing Services* initiative. SNaPS gave the National Grid ESO's overview of the system needs in the near future and explained the various routes the electricity system operator could take to simplify and evolve the current balancing services to deal with the needs. The report also asked for engagement and ideas from industry and academia. Following a consultation period, National Grid ESO published the Product Roadmap for Frequency Response and Reserve in December 2017 [121]. The Product Roadmap outlined the ESO's plan to introduce a set of faster-acting frequency response services and their commitment to lowering barriers to entry.

Following on from SNaPS and the Product Roadmap for Frequency Response and Reserve, National Grid ESO published a report [71] in 2019 that detailed the exact characteristics of the proposed new frequency response services they had designed. The services were designed based on system requirements and supporting technology neutrality. Four new services were designed: Dynamic Regulation, Dynamic Moderation, Dynamic Containment, and Static Containment. Dynamic Regulation and Moderation are symmetric pre-fault services and Dynamic Containment and Static Containment are asymmetrical post-fault services. Dynamic Containment was the first service to launch in October

2020 [122] and has already assisted the grid with containing frequency dips.

The electricity grid in GB has made great progress in decarbonising in the last few years. However, for the UK to meet carbon emissions targets, much more work needs to be done. National Grid ESO recognise this and published a report [12] about their ambition to be able to safely and securely operate a zero carbon grid by 2025 whenever there is sufficient renewable generation on-line and available to meet the national demand. It is expected that by 2025, there will be times when the total demand for electricity is met through renewable generation only. Having enough renewable capacity is not the main concern, it is the challenges to grid stability that are. Currently, National Grid ESO still need to schedule conventional generation and curtail renewable generation to maintain grid stability. Low inertia and frequency response are listed in the report as key challenges that need to be addressed. Some of the actions outlined in the report were:

- Finish changing RoCoF and vector shift loss of mains protection settings (see Section 2.7.2)
- Hold reserve and frequency response on wind and solar generation sources
- Increase the deployment of storage technologies, which are enhancing the frequency response markets
- Develop the full technical definition of the services necessary to provide inertia (possible inertia market)

Following on from the *Zero Carbon Operation 2025* document, National Grid ESO published a report on operating a low inertia system [123]. The report has two sections: current system inertia management and future system inertia management. National Grid ESO explain how the largest current inertia challenge is still ensuring that the maximum infeed loss does not trigger RoCoF relays used for loss of mains protection. This is managed by limiting the maximum infeed loss (by reducing the output of units above the maximum infeed loss limit) or increasing inertia (by bringing additional synchronous generation on-line). Fig. 2.14 illustrates the cost of reducing the maximum infeed loss on the grid compared to the cost of increasing inertia. The amount of inertia on the grid determines

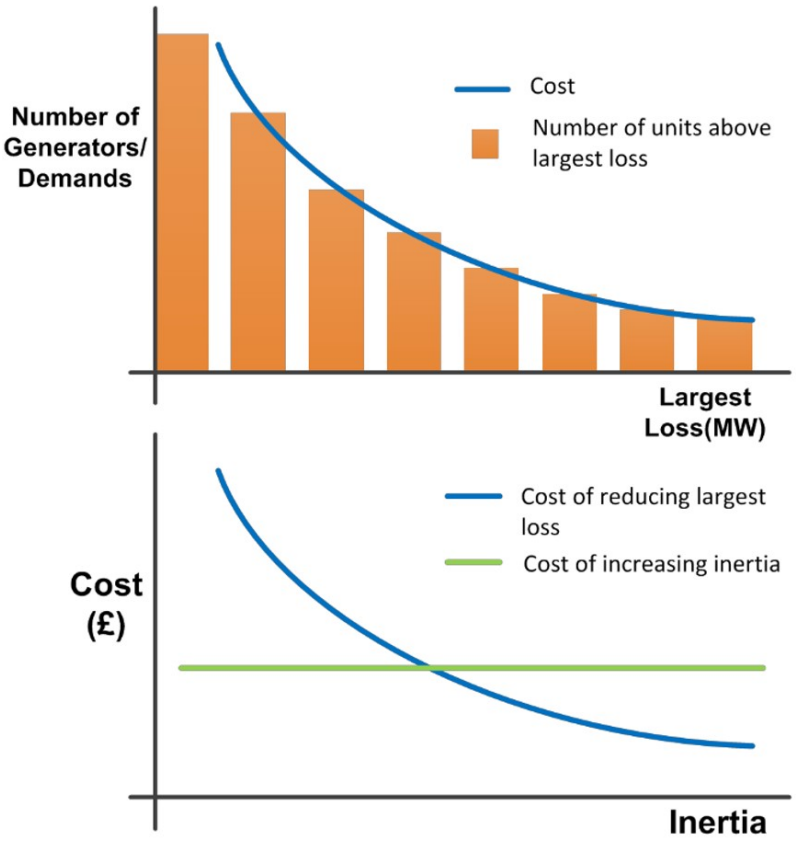

Figure 2.14: The cost of reducing the largest loss on the grid compared to the cost of increasing inertia. Reproduced from Ref. [123].

the maximum infeed loss limit. Once the maximum infeed loss is known, National Grid ESO can determine the number of units that need to have their output reduced to below this limit. The lower the inertia, the more units that need to have their output reduced, so the cost for this action increases. National Grid ESO assume the cost of increasing inertia is fairly constant. After the inertia levels reduce to a certain point, it becomes more economic to increase inertia than manage the maximum infeed loss. This is why an inertia market is being considered in the future. RoCoF relays settings are being modified across the grid (see Section 2.7.2) and over time will no longer feature as part of the largest inertia challenge. These future challenges are expected to be large and rapid frequency deviations and a reduction in other stability parameters such as short circuit level. To tackle the first of these challenges, the new frequency response services mentioned above need to be rolled out and their capability tested.

2.7.2 Modification of loss of mains protection settings

Loss of mains protection is used to detect a loss of mains supply and to prevent power islanding. Power islanding can occur when a part of the distribution network loses connection with the rest of the electricity grid but stays energised because embedded generation in the island continues to supply the demand in the affected area. The power island operates in isolation from the rest of the electricity grid. Power islands cause problems for a number of reasons. The voltage and frequency of the power island cannot be easily controlled and is likely to be a lot more volatile, presenting a risk of damage to connected equipment on the generation and demand side. Also, the power island may become unearthed and pose an electric shock risk to workers trying to fix the problem. To protect machines and personnel in the event of power islanding, loss of mains protection systems disconnect the embedded generators from the area of the network where the island has formed. As a result, the power island is quickly de-energised and ceases to be a power island.

There are two main types of loss of mains protection in GB embedded generation: RoCoF and vector shift. RoCoF loss of mains protection works by measuring the RoCoF and using RoCoF relays to disconnect the generator when the RoCoF is higher than a set value. Vector shift loss of mains protection works by detecting sudden changes in the voltage angle. Both vector shift and RoCoF loss of mains protection use the fact that conditions in a power island are far less stable than in the larger electricity grid. Generation and demand are less likely to be well balanced, so high RoCoF and sudden changes in voltage angle are expected. One of the most dangerous situations is the unlikely situation that generation is very well matched with demand in a power island and loss of mains remains undetected for a period of time.

Before 2014, as set out in the Distribution Code and Engineering Recommendation G59, the minimum setting for detecting loss of mains via RoCoF was $0.125\,\mathrm{Hz\,s^{-1}}$. This meant that the RoCoF relays of embedded generation with this minimum setting would trip the generator offline when a RoCoF greater than $0.125\,\mathrm{Hz\,s^{-1}}$ was measured. In 2014, a change was made to the Distribution Code and Engineering Recommendation G59:

RoCoF loss of mains protection settings must be modified, for generation sites with a registered capacity of 5 MW or greater, to 1 Hz s^{-1} and the RoCoF must be continuously measured in excess of the required setting for 500 ms before the trip relays activate [124]. In other words, the RoCoF loss of mains protection settings needed desensitising. The change was recommended in a 2014 National Grid ESO report [125] on frequency changes during large disturbances and their impact on the total system. Fig. 2.15 illustrates the desirable and undesirable operation of loss of mains protection.

The reason for this change is that grid inertia levels were expected to reduce significantly from 2014 onwards because the penetration of renewables was expected to increase so that the UK could meet its carbon targets. RoCoF is inversely proportional to the inertia on the system, so the concern was that the RoCoF would be high enough to activate RoCoF relays on connected embedded generators if there was a large infeed loss elsewhere on the system. The RoCoF relay would then disconnect the generators even though they were not part of a power island. At high levels of embedded generation, this spurious tripping of generators could add significant extra losses to the system on top of the original large infeed loss and exacerbate the situation. This is precisely what happened during the 9th August frequency event, discussed in more detail below and in Section 5.3. Another reason is that the proportion of embedded generation was expected to increase from 2014 onwards. Both these expectations, higher penetration of renewables and higher proportion of embedded generation, have come to pass (see Section 3.2).

In the 2014 National Grid ESO report [125] on frequency changes during large disturbances and their impact on the total system, results of an analysis into potential RoCoF after large infeed losses were presented. Fig. 2.16 shows the predicted average system RoCoF after a loss of 1320 MW or 1800 MW in two different demand conditions. The magnitude of the two losses refer to the maximum potential large infeed loss risk at the time and in the near future, respectively. The 100 ms and 500 ms refer to the length of time the RoCoF is averaged over, starting at the instant of the infeed loss. The average RoCoF decreases as measuring time length increases because the maximum RoCoF occurs at the very instant of the infeed loss and decreases in magnitude thereafter. Average

RoCoF was predicted based on the assumption that the generation mix would travel on a "Gone Green" trajectory from 2014 to 2020. Also, the results shown in Fig. 2.16 are for a high wind and high imports scenario (i.e. low inertia). The predicted RoCoF values shown are all above the $0.125\,\mathrm{Hz\,s^{-1}}$ setting, which gave a strong reason to recommend the desensitising of RoCoF loss of mains protection settings. The report also acknowledges that the RoCoF could be even higher than the results in Fig. 2.16 suggest due to the analysis not including a conceivable reduction in demand inertia and demand damping (both contribute to reducing the RoCoF after a large infeed loss).

The RoCoF loss of mains protection setting modification was predicted to result in balancing services savings of £33m by the end of the fifth year after implementation [125]. This is due to the fact that National Grid ESO has to manage the largest potential RoCoF on the grid every second of the day based on the inertia levels and size of largest loss. The actions National Grid ESO takes are either to pay for additional generators to run (these must be of a type which can limit the RoCoF) or to limit the size of the infeed loss the system can be exposed to by reducing generator or interconnector output (or demand as the case may be). With the RoCoF relays set at $1\,\mathrm{Hz\,s^{-1}}$ instead of $0.125\,\mathrm{Hz\,s^{-1}}$, the largest potential RoCoF can be greater before balancing actions are necessary. In effect, this reduces the number and duration of balancing actions caused by RoCoF risk. The modification was also predicted to help decrease greenhouse gas emissions in the electricity sector by reducing the number and duration of the occasions where additional fossil fuelled plant have to be run to provide inertia to the total system [125].

It was estimated that a maximum of 178 existing generation sites (totalling 3045 MW capacity) would need to make changes to comply with the modification of the Distribution Code and Engineering Recommendation G59 [125]. The time given to generators to implement the changes was two years [124]. Between 2017 and 2019, further modifications to the Distribution Code [126–128] disallowed vector shift as a form of loss of mains protection due to the risk of spurious tripping and stipulated that *all* embedded generators are required to update their RoCoF relay settings to $1\,\mathrm{Hz\,s^{-1}}$ (measured over 500 ms), not just generators $> 5\,\mathrm{MW}$ as required in 2014. September 2022 is the compliance deadline.

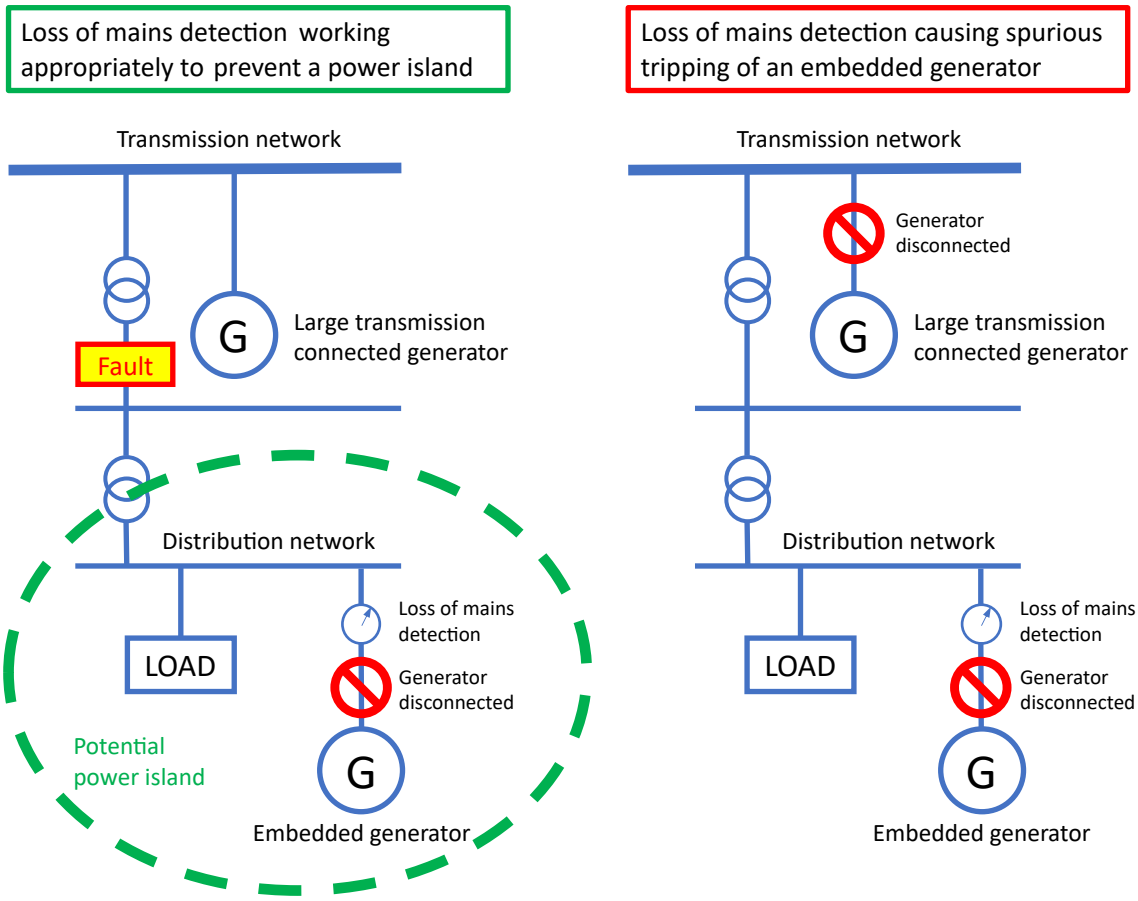

Figure 2.15: A desirable and undesirable case of the operation of loss of mains protection. On the left, a fault has occurred on the network and an isolated power island forms with a likely volatile frequency and voltage angle. The embedded generator's loss of mains protection detects a loss of mains (via vector shift or RoCoF) and trips the generator offline, preventing the power island from existing any longer. On the right, a large infeed loss is caused by the tripping of a large transmission connected generator, which results in a sudden decrease of the grid frequency. The embedded generator's loss of mains protection detects this change and trips the generator offline, even though there is no power island. The spurious tripping further increases the infeed loss of the grid, exacerbating the situation.

Year	Demand	RoCoF Hzs^{-1}			
		1320 MW loss		1800 MW loss	
		100ms	500ms	100ms	500ms
2014	20 GW	-0.26	-0.26	-0.36	-0.36
	35 GW	-0.14	-0.13	-0.19	-0.18
2016	20 GW	-0.27	-0.27	-0.38	-0.37
	35 GW	-0.14	-0.14	-0.20	-0.19
2018	20 GW	-0.33	-0.32	-0.47	-0.45
	35 GW	-0.17	-0.17	-0.24	-0.24
2020	20 GW	-0.42	-0.40	-0.57	-0.56
	35 GW	-0.21	-0.20	-0.29	-0.28

Figure 2.16: Predicted average system RoCoF after a large infeed loss in a high wind/high imports scenario. Reproduced from Ref. [125].

The Accelerated Loss of Mains Change Programme, a joint initiative led by National Grid ESO and the Energy Networks Association, has been set up to encourage generators to make the necessary changes to their RoCoF loss of mains protection settings. The programme's latest progress report [129] in January 2021 indicates that 80% of identified capacity (equating to approximately 20 GW) still requires work to be done to be compliant. This implies that there is still currently a risk of RoCoF relays exacerbating a large infeed loss situation.

On the 9th August 2019, a simultaneous loss of a wind farm and a steam turbine at a CCGT power station caused the grid frequency to suddenly drop from 50 Hz [130]. Almost instantaneously after the initial loss, the sudden drop caused some embedded generation on vector shift loss of mains protection to also trip offline, taking the total loss to 1131 MW. The demand at the time of the incident was roughly 35 GW and the grid inertia roughly 217 GVA.s. The demand and size of loss were very similar to an entry in Fig. 2.16 in which the predicted RoCoF was $0.20\,\mathrm{Hz\,s^{-1}}$ (average over 500 ms). The measured RoCoF during the 9th August event (measured over 500 ms) was $0.235\,\mathrm{Hz\,s^{-1}}$, slightly higher than predicted. A lot of embedded generation still had RoCoF relays with a $0.125\,\mathrm{Hz\,s^{-1}}$ setting, so the $0.235\,\mathrm{Hz\,s^{-1}}$ measured RoCoF caused 430 MW of embedded generation to trip offline 0.5 s after the initial loss. This brought the total imbalance to 1561 MW and a resulted in a frequency nadir of 48.790 Hz. Further losses (unrelated to RoCoF relays) resulted in the frequency reaching such a low level that demand had to be disconnected. This large frequency event made clear the importance of having less sensitive RoCoF relays.

2.8 Historic frequency data analysis

In this section we review literature on historic frequency data analysis. The frequency of the grid contains a lot of information about the state of the system. The net power imbalance of the system, which can be caused by numerous processes, displays itself through the dynamics of the grid frequency as explained in Section 1.1.3. Consequently, analysing historic frequency data reveals a lot about the underlying patterns that occur within grids

and potential causes of instability.

In Section 2.8.1, we review literature that investigated the deterministic and stochastic properties of day-to-day grid frequency data. In Section 2.8.2, we review literature that focussed on analysing the times when the frequency deviated outside certain limits, termed *frequency events*.

2.8.1 Deterministic and stochastic properties

Weissbach *et al.* [131] highlight the fact that large, unintended frequency deviations occur mainly at the change of the hour in the European grid. This is attributed to trading actions in electricity markets. Frequency deviations from trading actions cause slower frequency deviations but often larger amplitudes than regular power generation losses. In the paper, examples are given of past frequency deviations in the European grid accompanied by potential causes due to trading. Fig. 2.17 shows one such example. On 21st December 2006 at 21:00, a $-0.12\,\mathrm{Hz}$ deviation occurred on the European grid. With a network frequency characteristic of $26.1\,\mathrm{GW\,Hz^{-1}}$, the maximum absolute power deficit that caused the frequency drop can be estimated: $26.1\,\mathrm{GW\,Hz^{-1}} \times 0.12\,\mathrm{Hz} = 3.1\,\mathrm{GW}$. A possible cause was two power generation areas having different ramps to their new stepwise power target values. Area I quickly ramps down in 3 min (perhaps due to pumped storage pumping switching on rapidly). However, area II takes 10 min longer to ramp up (perhaps due to slow thermal plants). As a result, their is a maximum power deficit of 3.1 GW, which causes the frequency to fall. Primary control must be utilised to compensate the trading imbalances. This places a higher than necessary stress on the plants that provide this service. The authors suggest improvements to the electricity market structure to reduce the impact of trading on frequency deviations and primary control plants. They suggest that stepwise power target changes should be replaced by rampwise changes.

In a later study [132], Weissbach *et al.* build on the study discussed above. Again, the focus is on the influence of electricity market trading on frequency deviations. They advance their investigations by looking at a daily load profile instead of just one trading boundary at constant load. Fig. 2.18 shows the correlation between the frequency profile

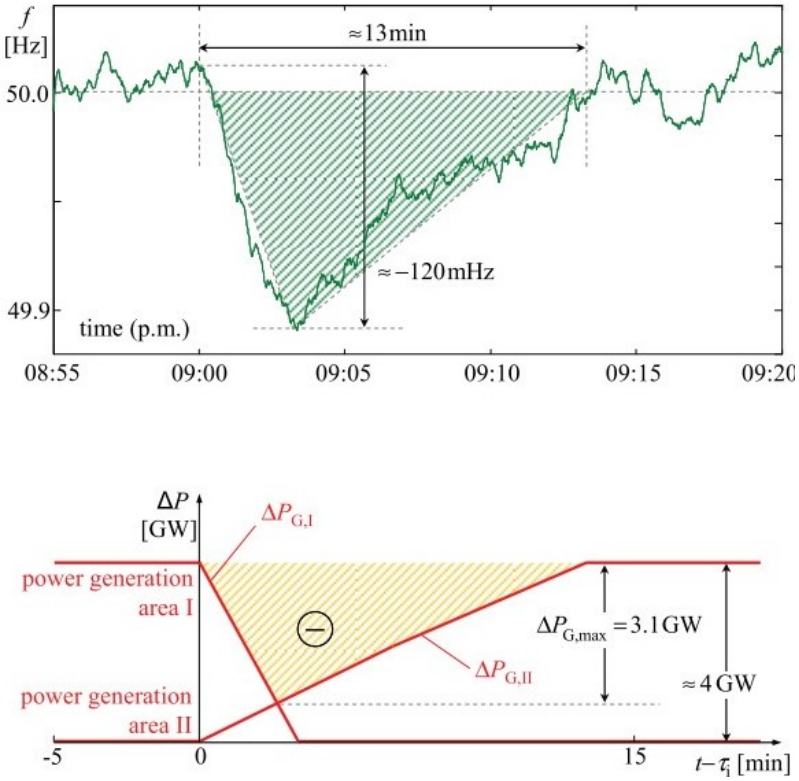

Figure 2.17: European grid frequency measurement 21st December 2006 at 21:00 (top). The potential cause: stepwise power target value changes of 4 GW between two power generation areas I and II that ramp to their target at different speeds (bottom). Reproduced from Ref. [131].

over a day (average over six winter months) and load gradients. Positive load gradients correspond to frequency deviations upwards, and negative load gradients correspond to frequency deviations downwards. For both directions, the magnitude of the frequency deviations directly depend on the corresponding load gradients. This applies for the whole course of the day. The authors use a simple dynamic model of the Continental European grid to illustrate that a system with 100% schedule-based generation (no load-following) would experience large frequency deviations of maximum magnitude 0.4 Hz. Actual measurements of the frequency profile over a day (average over six winter months) show that deviations have a lower maximum magnitude: 0.08 Hz. The authors reproduce this in simulations with a 20% weighting assigned to schedule-based generation and 80% to load-following. The authors reiterate their suggested improvements to the electricity market structure to reduce the impact of trading on frequency deviations and primary

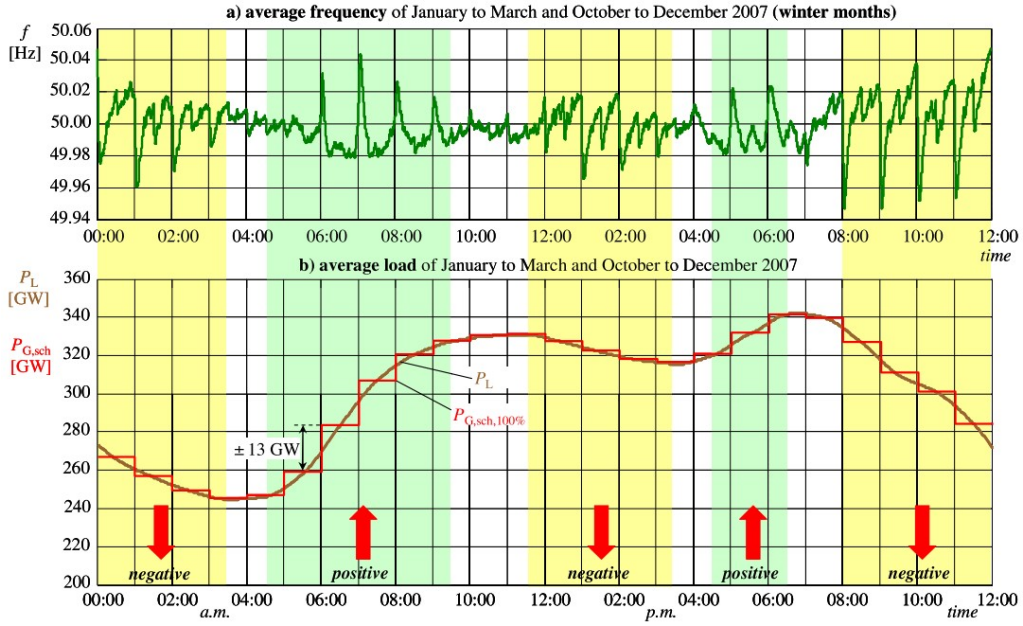

Figure 2.18: Average daily European grid frequency (top) and load profile (bottom) for the winter months in 2007. Reproduced from Ref. [132].

control plants made in [131]: a move from stepwise to rampwise power target changes.

Schäfer *et al.* [133] conducted a statistical analysis of the frequency distributions of various power grids: Continental European, Nordic, Mallorcan, Japanese, GB, and Eastern Interconnection. They determine that all the distributions have a non-Gaussian nature. Continental European, Nordic, Mallorcan, and Japanese grids have heavier tails than Gaussian (kurtosis > 3). This implies that large deviations are more frequent than predicted from a Gaussian. The GB and Eastern Interconnection grids are asymmetric with a positive skewness. Lévy-stable and q-Gaussian distributions were found to be the best fitting distributions. They point to two different microscopic mechanisms underlying the frequency dynamics: q-Gaussians arise when the power fluctuations are Gaussian on short timescales, but with a variance or mean changing on longer timescales. In contrast, Lévy-stable distributions arise when the underlying power fluctuations are heavy tailed or skewed themselves. Analysing the autocorrelation of the frequency data revealed that after an initial exponential decay of the autocorrelation, there were pronounced autocorrelation peaks every 15 min in the Continental European grid and every 30 min in the GB grid (see Fig. 2.19). These are due to trading actions in electricity markets as explained

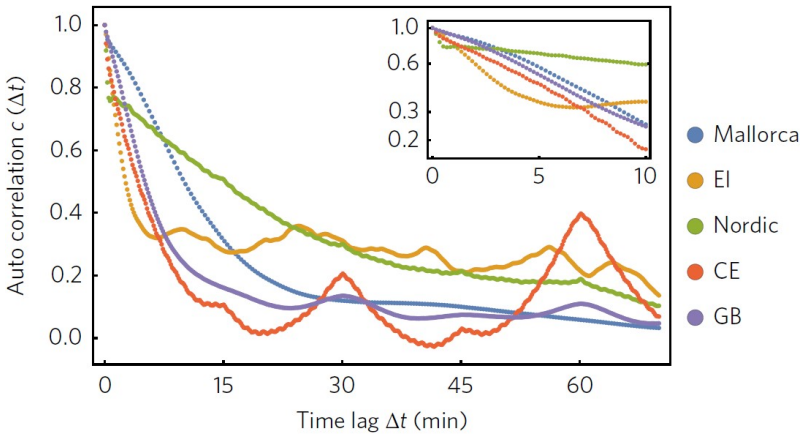

Figure 2.19: Autocorrelation of frequency data as a function of time lag Δt. Datasets are from 2015 and all year for Continental European, GB, Mallorca, and Nordic grid and one day for Eastern Interconnection. Reproduced from Ref. [133].

in Refs. [131, 132]. All of the grids studied had an autocorrelation decay time of the same order of magnitude (200 s–550 s), which is not surprising given the synchronous machines in these regions do not differ substantially.

Schäfer *et al.* [134] add to their previous study by investigating the impact of trading on grid frequency fluctuations and whether this impact has changed over time. They analyse Continental European grid data from 2011 and 2017. The data for both years was aggregated into one hour blocks and analysed on a minute-by-minute basis. Fig. 2.20 shows the number of large frequency deviations ($|\Delta f| > 0.1$ Hz) each minute. Large deviations were more likely in 2011 when there were fewer short (15 min) trading intervals compared to 2017. This suggests that shorter trading intervals are beneficial to frequency volatility. More large deviations occur near the start of the hour than at any other time in both 2011 and 2017. As in their previous paper [133], the authors emphasise how the Continental European frequency distribution is best characterised by Lévy-stable or q-Gaussian distributions due to the heavy tails. The paper then asks the question whether trading significantly impacts the width and the heavy tails of the frequency distribution. They answer this by comparing two frequency distributions from 2017 data: one is the aggregation of frequency data either side of a trading boundary every 15 min (*trading*) and the other is the aggregation of the rest of the data (*non-trading*). The *trading* distribution has a higher kurtosis than the *non-trading* distribution (4.8 compared with 3.8) and

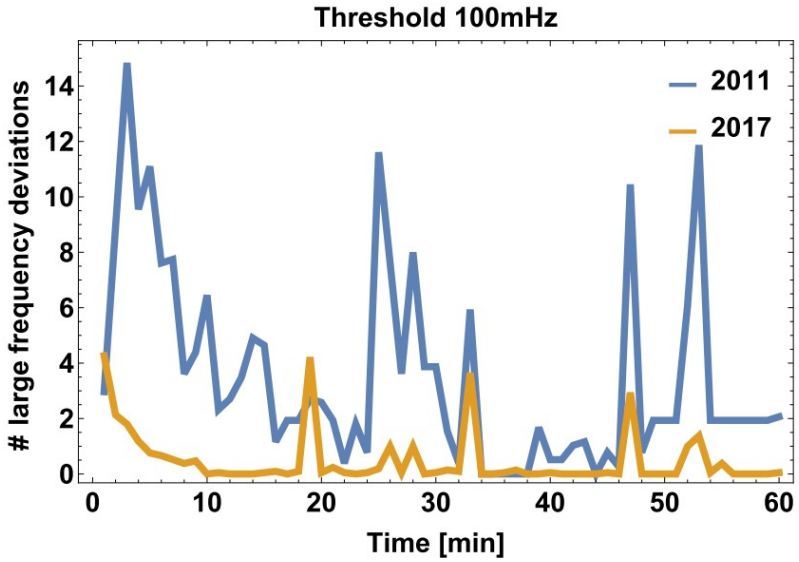

Figure 2.20: Number of large frequency deviations on the Continental European grid in 2011 and 2017 each minute of the hour. Reproduced from Ref. [134].

displays heavier tails. In contrast the standard deviation between the data sets differs by less than 10%.

Anvari *et al.* [135] go further than [133, 134] by investigating the stochastic properties of historic frequency data from GB (2016) and Continental Europe (2015 and 2017). They performed different tests to determine whether the data is stationary or non-stationary (time-independent), linear or non-linear (i.e. is there time symmetry in the data), and Markovian (i.e. do future states only depend on the current states or do they have a memory). To test whether the data is stationary or non-stationary, the authors analysed the power spectrum of the data, which can be seen for GB in Fig. 2.21. The sharp peaks at 1/4, 1/2, 1, 12, and 24 h in both the GB and Continental Europe spectra emphasise the existence of periodicity on different timescales and shows the non-stationary nature of the data on these timescales. The spectrum amplitude decreases past 24 h with no sharp peaks, which suggests grid frequency is stationary at longer timescales. Clearly, electricity market trading actions and daily cycles leave an imprint on the spectrum of grid frequency, but other natural cycles, such as the weekday-weekend pattern and seasonal cycles, do not. The authors conclude that both GB and Continental Europe frequency is approximately linear, with small non-linearities more pronounced in Continental Europe

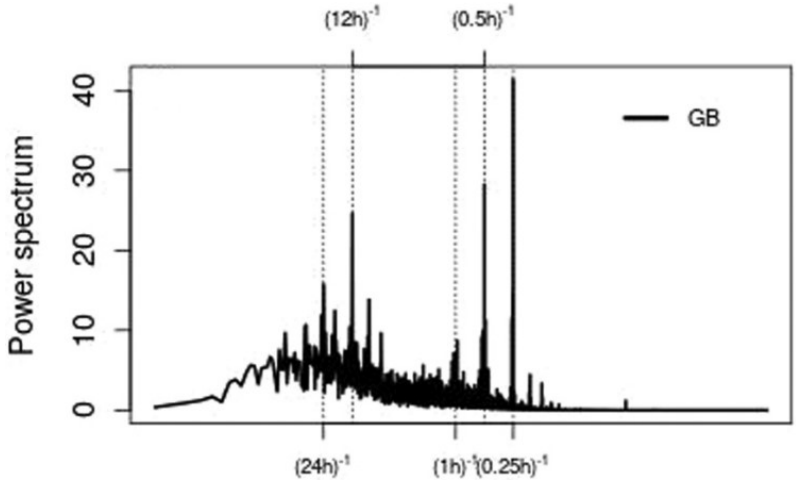

Figure 2.21: Power spectrum of 2016 GB frequency data. The spectrum exhibits sharp peaks at the labelled period lengths. Reproduced from Ref. [135].

(possibly due to the greater effect trading has in Continental Europe, see Fig. 2.19). A Chapman-Kolmogorov test was used to determine that the frequency data from both grids is mostly Markovian.

2.8.2 Frequency events

As already mentioned, Schäfer *et al.* [134] looked at where frequency events occur within the hour in the Continental European grid (see Fig. 2.20) for two different years. More events were recorded at the start of the hour than at any other time. This analysis was specifically for understanding trading influences on the Continental European grid frequency. The rest of the literature in this section focusses on other grids in the world and with a wider range of focus than just trading influences.

Folgueras *et al.* [136] used frequency data collected at National Renewable Energy Laboratory's Wind Technology Centre during an approximate two year period (Aug 2014–Jun 2016) to analyse extreme low frequency events caused by a generation loss. The data was validated with information provided by the North American Electric Reliability Council (NERC). NERC also provided the magnitude of generation loss that caused the frequency event. 67 events were recorded, but only 44 events were used in linear regression analysis because the rest did not have generation loss data. A positive correlation ($r = 0.89$) was found between grid inertia and event duration. The results also suggest a correlation

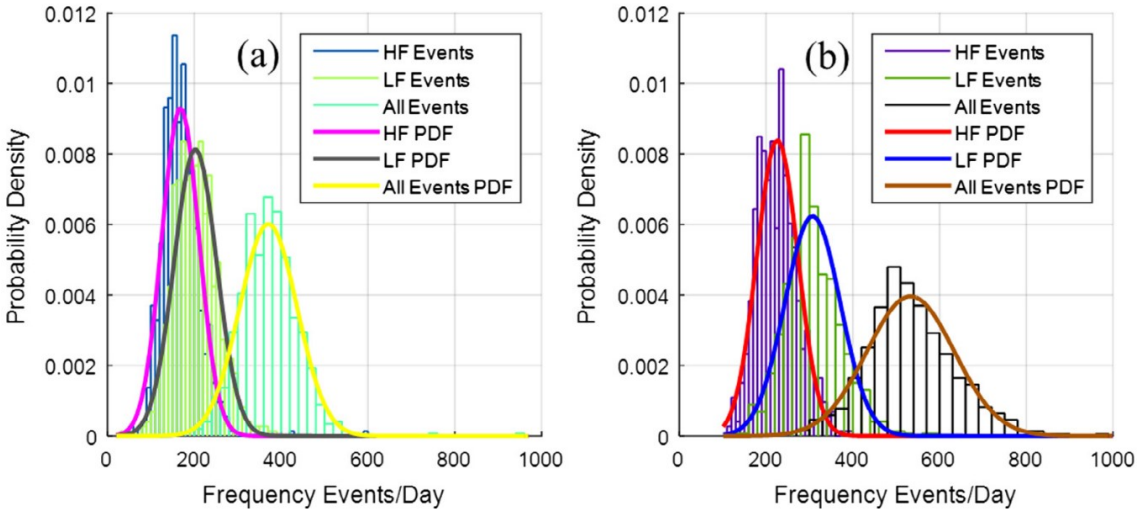

Figure 2.22: Histograms and probability distributions of frequency events per day for (a) the EFR wide service and (b) the EFR narrow service. Reproduced from Ref. [86].

between extreme events and seasonality. More events occur in the off-peak spring and autumn months compared to the summer and winter. The explanation the authors offer is that plant operators take advantage of off-peak months to conduct maintenance, and as a result there are fewer generators online. This lowers the grid inertia making it more susceptible to large frequency deviations if a generation loss event occurs.

Greenwood *et al.* [86] also analysed historic GB frequency data from 2014–2015 in the context of a paper discussing the EFR service, which was new at the time the paper was published. At the time, the proposed EFR service was split into two types: a narrow service (± 0.015 Hz deadband) and a wide service (± 0.05 Hz deadband). When the frequency goes outside of these deadbands the authors define this as a frequency event. This is important because it determines how often the service provider has to exchange power with the grid. Fig. 2.22 shows the distribution of the number of narrow and wide events per day for high, low, and all events. The average number of events per day for the wide service is 370, for the narrow service it is 530. For both services, low events were more common than high events. There are hundreds of events per day but the majority of events are very short in duration. Only 0.26% of wide events lasted 15 min or longer, the maximum mandated EFR delivery duration, compared with 3.09% of narrow events.

Wyman-Pain *et al.* [137] analysed historic GB frequency data, from 2014–2016, to find

the time spent outside of operational limits ($> \pm 0.2$ Hz from 50 Hz) and the number of times the limit is breached (frequency events). They point out that no deviations beyond statutory limits (49.5 Hz and 50.5 Hz) occurred in the three year time period, but there were 370 events in 2014, 252 events in 2015, and 345 events in 2016 where the frequency went outside of the operational limits. 594 of these events were high events (> 50.2 Hz) and 373 were low events (< 49.8 Hz). Frequency events are more likely to occur in winter weekday evenings (periods of high demand). High events are focussed in the evenings whereas low events are less focussed. Time spent outside limits follows a similar trend although more peaks occur also in mornings. The authors suggest that the correlation of increased frequency volatility and high demand is in part due to the increased number of generators and demand units connected to the grid, increasing the likelihood of there being an unexpected failure. The authors also take a look at the frequency response holding volume in the same time period. Frequency response holding volume decreases steadily from early 2014 to July 2016, but this does not correspond to a period of increased number of events. They claim that lower levels of frequency response holding volume during Winter 2014/15 and Spring 2016 contributed to an increase in frequency events. However, the evidence for this is not strong.

It is interesting to compare Wyman-Pain *et al.*'s historic GB frequency data analysis [137] and Greenwood *et al.*'s [86]. When the frequency event definition is $> \pm 0.2$ Hz [137], there are more high events than low events. The opposite is true when the event definition is narrowed to $> \pm 0.05$ Hz or $> \pm 0.015$ Hz [86]. Also, there was roughly one $> \pm 0.2$ Hz event per day compared to hundreds per day when using the narrower event definitions.

Within an all-Ireland (Northern Ireland and Republic of Ireland) transmission system performance report [138] is a graph of the number of large low frequency events that occurred on the system in an eight year period (see Fig. 2.23). The grid is much smaller than the Continental European and GB grids, so large frequency excursions are more likely due to lower demand and lower grid inertia. The recent trend is a substantial decrease in the number of large low frequency events.

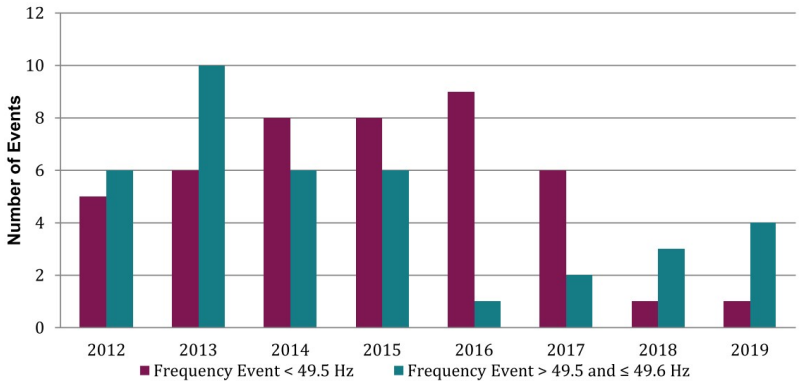

Figure 2.23: Number of large low frequency deviations on the Irish grid each year. Reproduced from Ref. [138].

2.8.3 Summary of historic frequency data analysis

- Trading actions have a significant effect of the grid frequency. The mismatch between scheduled stepwise power (in the electricity market) and a continuous load curve causes regular large frequency fluctuations. These deviations occur at regular intervals based on the trading period.
- Multiple grids have non-Gaussian frequency distributions. Some are skewed (e.g. GB) and some are heavy-tailed (e.g. Continental Europe). Trading actions contribute to heavy-tails in a distribution.
- Frequency events in GB typically occur during periods of higher demand (e.g. winter weekday evenings)

2.9 Grid blackouts

It was mentioned in Section 1.1.5 that the consequences of not adequately maintaining grid stability have the potential to be extremely severe. One of these consequences is a blackout. A blackout is the loss of electrical power to the end user, also called a power outage. The underlying cause of these events are varied and include unexpected weather events, poor planning and risk management, equipment failure, and falling trees. This underlying cause often creates a mismatch between generation and demand and the frequency of the grid deviates away from the nominal value. If demand is greater than generation and the

frequency deviates too low, then some areas of demand are automatically disconnected (load-shedding) to try to restore the balance. This results in localised blackouts and is what occurred in Great Britain on August 9th 2019. These areas of demand can then be reconnected fairly straightforwardly once the electricity system operator has got the situation back under control. If there is not enough generation to meet demand for a long period of time, the electricity system operator will rotate the areas being switched off. These are termed *rolling blackouts*, and are a common feature of the South African grid run by ESKOM [139].

An extreme scenario is when there is a widescale blackout across the whole power system, or large areas of it. A full grid blackout has never occurred in Great Britain, although the hurricane of 1987 did leave Kent and Surrey disconnected [140]. Recovery from a widescale blackout requires generators that are capable of black-starting the grid. Black start, also known as self-start, is the starting of a power station with no external supplies of power (i.e. no assistance from the grid). Once the grid is reenergised, demand can be added sequentially in a process called block-loading. The black start service is traditionally provided by large transmission connected generators, which have been started with the help of their auxiliary generation (e.g. diesel gensets).

Table 2.2 gives a non-exhaustive list of major blackouts in the world and their consequences. It is clear that the risk of blackouts and their consequences are faced by power systems all over the world. After the 2003 blackouts that occurred in North America and Europe, an expert panel concluded that grid reliability standards were not adequate and gave a series of general policy recommendations, including the recommendation that more investment should be going into system reliability [141]. Unfortunately, one of the main reasons for the 2021 winter blackout in Texas was the failure to sufficiently winterise its electricity and gas networks [9], suggesting that stricter enforcement of reliability standards is needed.

The economic cost of a blackout is severe, with the value of lost load estimated to be £16 940 MWh^{-1} in Great Britain [152]. 931 MW of demand was disconnected for roughly half an hour during the August 2019 event in Great Britain [130], which means 416 MWh

Country	Year	Load loss [GW]	Economic loss	People affected [millions]	Duration [hours]	Ref.
Iran	2003	~ 7	Not available	22	8	[142, 143]
USA and Canada	2003	61.8	$ 6.4 billion	50	16–72 (USA), up to 192 (Canada)	[142, 144, 145]
Italy	2003	24	£ 120 million	~ 56	Up to ~ 18	[142, 145]
Russia	2005	~ 3.5	$ 1–2 billion	4	~ 4	[146]
Western Europe	2006	~ 14	Not available	15	~ 2	[145, 147]
Great Britain	2008	~ 1.5	Not available	Not available	~ 0.5	[148]
USA and Mexico	2011	4.3	~$ 100 million	> 5	~ 11	[146]
India	2012	~ 48	Not available	670	2–8	[143, 149]
Turkey	2015	32.2	Not available	70	> 7	[143]
Australia	2017	~ 1	Not available	0.85	3	[150]
Great Britain	2019	2	Not available	1.1	0.5	[130]
Texas	2021	30	$ 130 billion	10	Up to 100	[9]

Table 2.2: Recent large-scale blackouts in the world and their consequences. Adapted from Ref. [151].

was lost. Using the value of loss load figure above, we can estimate that the blackout cost roughly £7m. RWE, Hornsea 1 Ltd, Eastern Power Networks plc, and South Eastern Power Networks plc agreed to pay an aggregate of £10.5m for their respective roles in causing the disruption [153].

2.10 Conclusions

The effect of low inertia on the frequency dynamics after a large infeed loss has received a fair amount of attention in the literature. However, another practical concern, the effect on normal day-to-day frequency volatility, has been given far less attention. There have been

a couple of studies [95, 96] that have investigated this using the Fokker-Planck equation, but there is certainly a gap for more work in this area, especially in understanding how frequency response can mitigate.

There have also been a few recent developments in the GB grid that have not been well studied. The RoCoF relay limits are in the process of changing from $0.125\,\mathrm{Hz\,s^{-1}}$ to $1\,\mathrm{Hz\,s^{-1}}$, which means that the speed of frequency response is likely to become the limiting factor in the future, rather than the RoCoF. Solving the swing equation analytically to establish a simple relationship between minimum inertia and frequency response speed is not something I have come across in the literature. The August 2019 frequency event was the first significant frequency disturbance in over a decade in Great Britain and gives a great opportunity to validate parameter assumptions. The newly proposed frequency response services have not been well reported on in the literature due to their young age, but it is essential that they are well understood.

In terms of studying historical frequency data, what is missing from the literature is a more recent study analysing the potential impact of higher renewables penetration and decreased grid inertia on frequency distribution and frequency events.

These gaps identified in the literature informed the research questions listed in Section 1.3, which I will address in the following three results chapters.

Chapter 3

Historic grid data analysis

3.1 Introduction

A lot of changes have occurred in the last five years on the GB grid and other grids around the world as they strive to decarbonise. Detailed analysis of grid data is necessary to acquire a greater understanding of how an electricity grid is evolving.

In Section 2.8, we reviewed the literature on the subject of historic frequency data analysis. While trading actions were shown to have an impact on frequency distributions and cause frequency deviations, it was less clear what impact other grid parameters and processes (e.g. inertia) have. To fill this gap in knowledge and to further existing work, this chapter addresses the following research questions:

- **What is the recent trend in grid parameters such as demand, generation, inertia, and frequency response holding volumes and what is their monthly and hourly variation?**
- **What is the current state of frequency volatility and have there been significant changes in recent years?**
- **What are the underlying drivers behind frequency volatility?**

I address the first question by collating and processing grid data obtained from various sources to get a clear picture of recent trends and monthly and hourly variations

in demand, generation, inertia, and frequency response holding volumes. I address the second question by performing an analysis on six years of 1 s resolution GB frequency data (2014–2019). I primarily focus on two metrics for frequency volatility: number of frequency events and standard deviation. The third question is addressed by comparing the recent trends and monthly and hourly variations in the grid parameters (demand etc) and frequency volatility. I look for correlations and then determine whether we think this implies causation.

The rest of the chapter is outlined as follows. In Section 3.2 the data collection and processing method for generation and demand data is outlined. The recent trends and monthly and hourly variation are then presented. The same structure applies in Section 3.3 and Section 3.4 for grid inertia and frequency response, respectively. The results of the comprehensive GB frequency data analysis are given in Section 3.5. Section 3.6 links all the sections together and uses information from them all to answer the third research question above. Section 3.7 concludes the chapter and includes a list of highlights of the results.

3.2 Generation and demand

3.2.1 Data collection and processing

The transmission system demand of the grid is the sum of transmission connected generation and interconnector imports. The underlying demand of the grid is the sum of transmission connected generation, embedded generation, and net flow of power coming in from interconnectors (imports minus exports), with the power used during pumped storage (PS) pumping subtracted. The underlying demand is the sum of the electricity demand of all domestic, commercial, and industrial users. The relationship between underlying demand and transmission system demand is given below:

$$UD = TSD + \text{embedded gen} - \text{interconnector exports} - \text{PS pumping}\,, \tag{3.1}$$

where UD is underlying demand and TSD is transmission system demand.

To calculate the underlying demand and transmission system demand, half-hourly (i.e. every settlement period) data from Elexon's *Balancing Mechanism Reports* [154] and National Grid ESO's *Data finder and explorer* [155] was collated for the years 2014–2019. From Elexon's *Balancing Mechanism Reports*, we acquired the average MW generated during each half-hour period for all the different types of transmission connected generation: CCGT, coal, nuclear, wind, PS, non-PS hydro, OCGT, and other/biomass. From National Grid ESO's *Data finder and explorer*, we acquired the average MW generated during each half-hour period for interconnector imports and exports, embedded wind, and embedded solar. Half-hourly data for other embedded generation fuel types (gas, non-PS hydro, and bioenergy) was not available. However, yearly energy totals were available from the UK government's *Digest of United Kingdom Energy Statistics* publication [156]. These yearly energy totals were converted to an estimated half-hourly profile by the following method. It was assumed that the amount of embedded generation during each half-hour settlement period for gas, non-PS hydro, and bioenergy (as a percentage of their respective yearly energy totals) was the same as their transmission connected counterparts CCGT+OCGT, non-PS hydro, and other/biomass, respectively. For example, in 2017 the energy total of embedded non-PS hydro was 1874 GWh, and the energy total for transmission connected non-PS hydro generation was 3962 GWh. In the half-hour time period 05:30–06:00 on 12th January 2017, there was an average of 588 MW of transmission connected non-PS hydro generation, which means the energy total for this half-hour was 294 MWh. The estimated level of embedded non-PS hydro generation in the same half-hour time period was therefore estimated to be

$$\begin{aligned} \text{Embedded non-PS hydro (Jan 12th 05:30–06:00)} &= 2 \times 1874 \times \frac{0.294}{3962} \\ &= 278\,\text{MW}\,. \end{aligned} \tag{3.2}$$

There were a few instances of clear errors in the generation data. For example, there were instances of all generation types having zero output for a small number of half-hour periods. The erroneous data was deleted and linear interpolation used to replace the

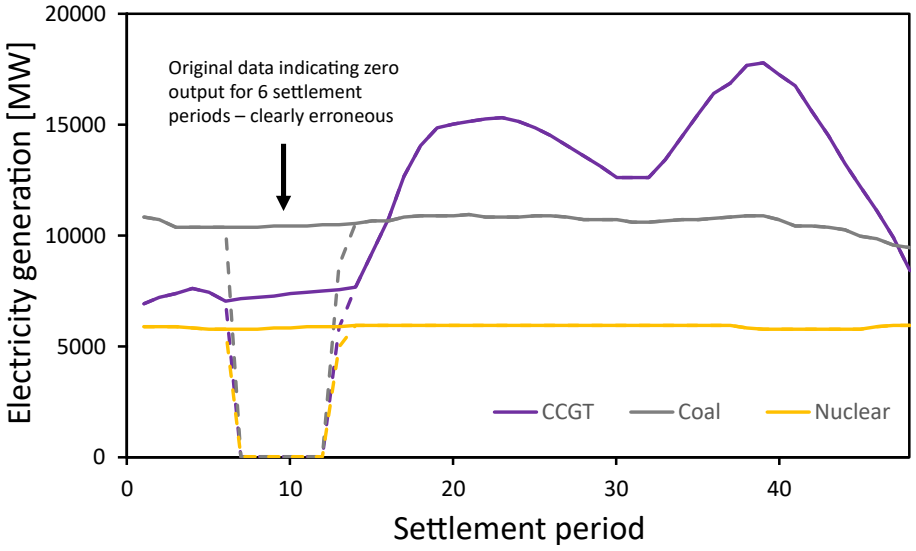

Figure 3.1: Half-hourly generation data on 11th Oct 2014. The dashed lines indicate the original, clearly erroneous, data. The solid lines indicate the corrected data using linear interpolation.

deleted data. Fig. 3.1 shows an example of some clearly erroneous data. On 11th Oct 2014, the original data from Elexon's *Balancing Mechanism Reports* indicated that all the transmission connected generation types had zero output between 03:00 and 06:00 (settlement periods 7–12). In the figure, only CCGT, coal, and nuclear are shown for clarity. Also shown in the figure is the corrected data, which has linearly interpolated values between 03:00 and 06:30 (settlement periods 7–13). The original data for settlement period 13 was still obviously an error, so also needed correcting. In total, there were 134 settlement periods (0.13%) that had data that needed correcting in this way over the six year period, the vast majority from Elexon's *Balancing Mechanism Reports* dataset.

3.2.2 Decentralisation and decarbonisation

Fig. 3.2 shows duration curves for transmission system demand and underlying demand for each year in the period 2014–2019. Transmission system demand decreased over the six year period: the median in 2014 was 34.4 GW and in 2019 it was 29.9 GW. The decrease in underlying demand across the six years is less pronounced. The median in 2014 was 38.3 GW and in 2019 it was 36.4 GW. This slight decrease is likely due to energy efficiency improvements [157]. The difference between underlying demand and

	2014	2015	2016	2017	2018	2019
Underlying demand	333	331	324	324	322	316
Transmission system demand	302	289	284	278	275	268
Embedded generation	38	47	46	52	52	54

Table 3.1: Yearly energy totals (in TWh) for underlying demand, transmission system demand, and embedded generation.

transmission system demand, as established in Eq. (3.1), is due to embedded generation, interconnector exports, and PS pumping. Table 3.1 shows the yearly energy totals for underlying demand, transmission system demand, and embedded generation. This table makes it clear that transmission system demand decreased more rapidly than underlying demand in the six year period, and also highlights the reason why. In the time period 2014–2019, underlying demand stays fairly constant due to the fact that electricity users have not changed their consumption significantly (energy efficiency improvements are probably the cause of a slight decrease). However, the amount of embedded (decentralised/distributed) generation on the grid has risen from 12% of underlying demand in 2014 to 17% in 2019. This rise, and a fairly stable underlying demand, results in lower transmission system demand i.e. less generation required from transmission connected generators.

Fig. 3.3 shows electricity generation from CCGTs, coal, and wind + solar in GB for each month over the past six years. Wind is the sum of transmission connected wind generation and embedded wind generation. Together these generator types contributed 61% to the total underlying consumption. Nuclear provided a large contribution (19%), but is not shown in Fig. 3.3 due to the fact that generation levels did not significantly change in the time period (nuclear was between 4 and 6 TWh in almost every month). The level of coal generation declined dramatically from being the largest contributor in 2014 (29% of underlying demand) to being insignificant in 2019 (2% of underlying demand). This reduction in coal generation was largely driven by the UK's carbon price support and the increase in low-carbon generation on the system and will be permanent given the UK government's decision to phase out unabated coal generation by 2025 [158]. Throughout the decline of coal, there was strong seasonal periodicity: the level of coal generation

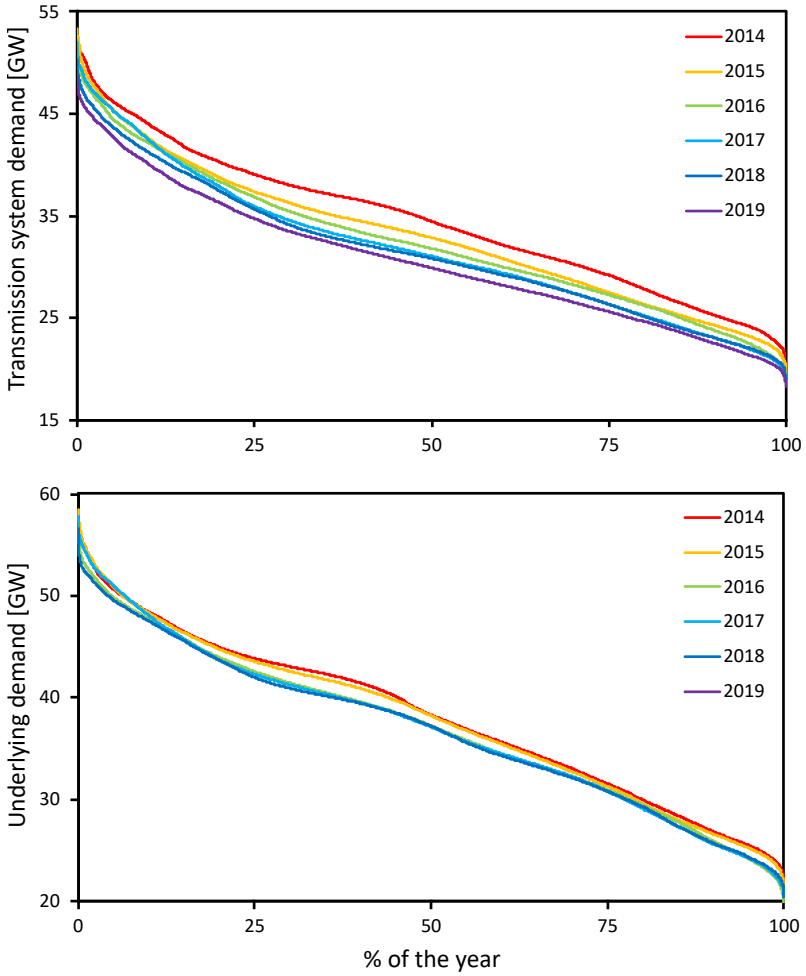

Figure 3.2: Duration curves of transmission system demand (top) and underlying demand (bottom) each year.

remained significant in the winter up to 2019 but from 2016 onwards was very low in the summer. The first two years of coal reduction was met with a 50% increase in CCGT generation levels. From 2015 onwards, in every year, CCGTs were the largest contributors to underlying demand: 25% in 2015 then between 35% and 40% in 2016–2019. The level of wind + solar generation steadily increased from 10% of underlying demand in 2014 to 22% in 2019.

2019 was a record year for solar and wind generation in GB with 11.67 TWh of electricity generated from solar and 58.52 TWh generated from wind (transmission connected + embedded). Fig. 3.4 shows heatmaps of the average solar and wind power generation each calendar month and hour of the day in 2019. Average solar power generation follows the

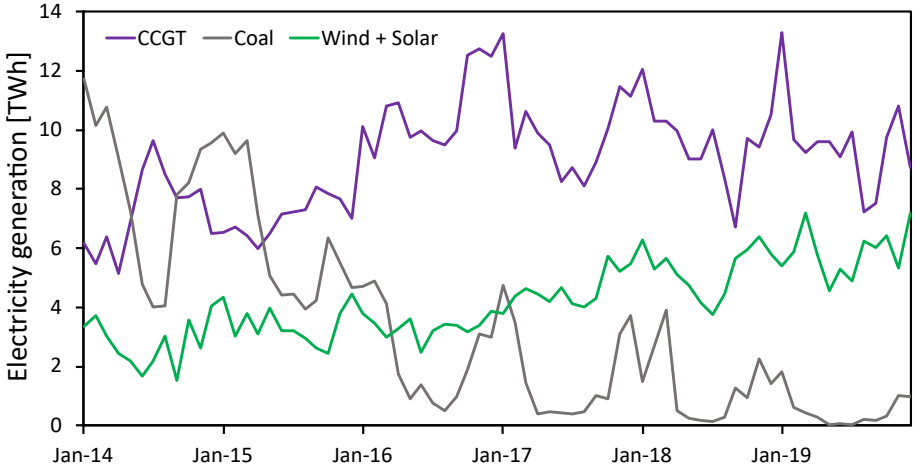

Figure 3.3: Electricity generation from CCGTs, coal, and wind + solar for each calendar month over the past six years.

obvious pattern of being greater in the summer compared to the winter and either zero or negligible at night throughout the year. Solar power generation averaged over 5000 MW between the hours of 12:00 and 14:00 in the period April–September. April 13:00–14:00 had the highest average at 6050 MW, but the maximum half hour of solar generation occurred on 14th May 13:00-13:30, where it reached 9550 MW. In each month, the average wind power generation throughout the day does not vary that significantly, with only a slight rise in the evening. Far more significant is the variation between different months of the year. Across all the six years in the period 2014–2019, the general pattern is less wind generation from April–September compared to the other six months of the year. Interestingly, this is exactly the period in the year when solar generation is at its peak, albeit only in the middle of the day. In 2019, this pattern is roughly the one seen: the three lowest wind generation months were May, June, and July. December 11:00–12:00 had the highest average at 9780 MW, but the maximum half hour of wind generation occurred on 10th December 16:30-17:00, where it reached 16 886 MW. It should be noted that the heatmaps in Fig. 3.4 show average power generation and therefore do not reflect the intermittency of wind and solar.

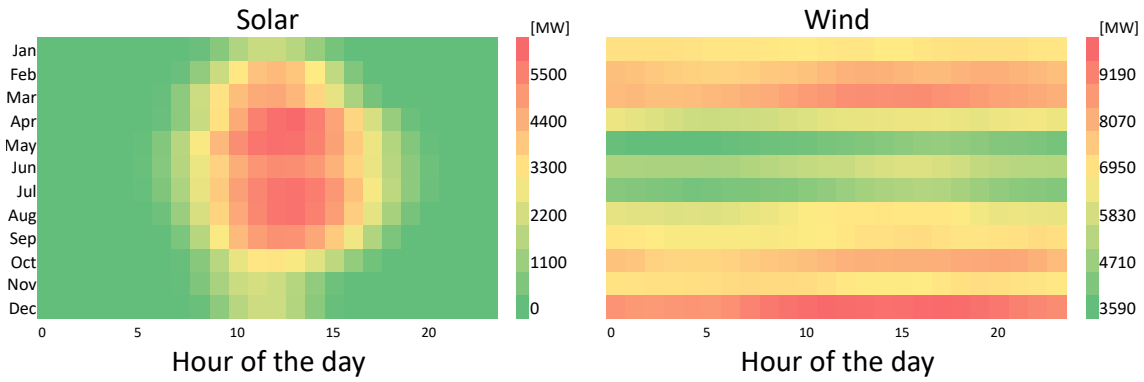

Figure 3.4: Average solar (left) and wind power (right) generation each calendar month and hour of the day in 2019.

3.2.3 Hourly and monthly variation in demand

The heatmap on the left of Fig. 3.5 shows the average underlying demand each calendar month and hour of the day in 2019. The heatmap can be roughly split into five different areas. The lowest tier of underlying demand (23 GW–29 GW) occurred in the early hours at night between April and October. The second tier (29 GW–35 GW) occurred in the early hours at night between November and March and in the late evenings all year round. The third tier (35 GW–41 GW) occurred mainly throughout the day between April and October. The fourth tier 41 GW–47 GW) occurred throughout the day between November and March except for certain times where there is exceptionally high demand, which is the next tier. The highest tier 47 GW–53 GW) occurred during the November, December, and February early evening and between 10:00 and 20:00 in January. The patterns of underlying demand described here are very similar for every year in the 2014–2019 time period.

In the previous section we established that the median transmission connected demand has decreased from 2014 to 2019 by about 4.5 GW. The decrease for underlying demand is less pronounced at about 2 GW. This means that the difference between underlying demand and transmission connected demand ($UD - TSD$) increased between 2014 and 2019. The heatmap on the right of Fig. 3.5 shows the average difference between underlying demand and transmission connected demand each calendar month and hour of the day in 2019. This tells us clearly that it is in the middle of the day in non-winter months that the

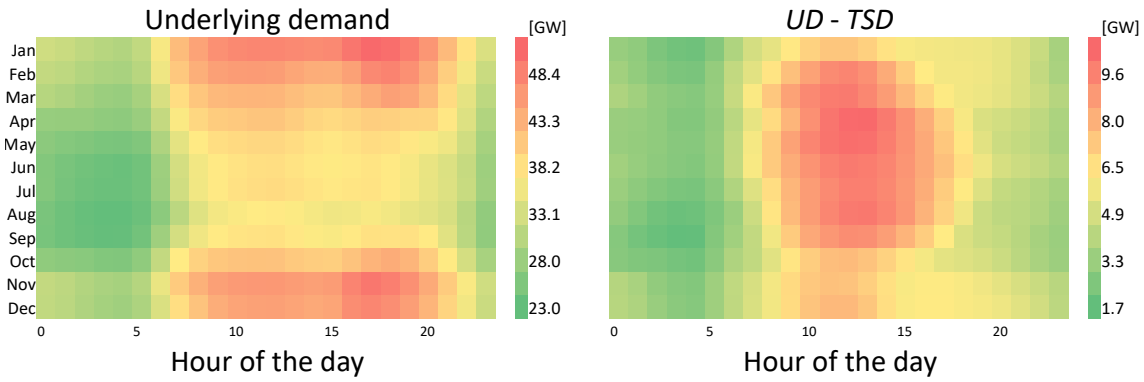

Figure 3.5: Average underlying demand (left) and the average difference between underlying demand and transmission connected demand (right) each calendar month and hour of the day in 2019.

difference between the two types of demand is greatest, which matches the solar generation (which is embedded generation) pattern seen in Fig. 3.4. The average difference was 10 GW between the hours of 11:00 and 14:00 in April and May. April 13:00–14:00 had the highest average difference at 10.4 GW, but the maximum half hour difference occurred on 15th April 12:00-12:30, where it reached 14.0 GW. This temporal pattern in the difference between underlying demand and transmission connected demand is similar across the 2014–2019 years with the change being the magnitude of the difference increasing from 2014 to 2019.

Now we have a heatmap for underlying demand, we can return to Fig. 3.4 and discuss the solar and wind penetration in 2019. I define solar and wind penetration as the sum of solar and wind generation as a percentage of the underlying demand. In 2019, throughout spring, summer, and autumn there was high penetration around midday, which corresponds to the time of year and time of day that solar generation is highest. The largest penetrations (35%) were reached in the early-afternoon of August. Wind and solar penetrations were high at night in the autumn and winter months, which was due to windy conditions and low demand levels. Throughout the year, wind and solar penetration was low during the evening. This was due to there being a large amount of dispatchable generation online at this time to cover the demand rise in the evening.

3.3 Grid inertia

3.3.1 Grid inertia calculation method

The inertia of the grid is calculated using the same data sources as mentioned in Section 3.2.1. The total inertia of the grid (E_{n}) is the sum of contributions from the generation side ($E_{\mathrm{n,gen}}$) and demand side ($E_{\mathrm{n,dem}}$), which is estimated to provide 20% of the total in GB [20, 27]. Multiplying the transmission system demand by 1.75 is a simple calculation for estimating the demand inertia (and the contribution from embedded generation) [27]. Inertia from the generation side (excluding embedded generation) is calculated in a similar way to the method described in Ref. [13], using inertia constants, generation output, and estimated capacity factors. The total inertia is therefore given by

$$\begin{aligned} E_{\mathrm{n}} &= E_{\mathrm{n,dem}} + E_{\mathrm{n,gen}} \\ &= 1.75 \times TSD + \sum_i H_i S_i \\ &= 1.75 \times TSD + \sum_i \frac{H_i P_i}{\beta_i u_i} \end{aligned} \tag{3.3}$$

where H_i is the inertia constant of each generation type (i), S_i is the rated capacity in MVA.s, P_i is the power generation at each half-hour, u_i is the power factor, and β_i is the capacity factor. It is assumed that the power factor of all generation types that contribute inertia is 0.85. Table 3.2 shows the assumed inertia constants and capacity factors for each major generation type. Wind, solar, and interconnectors do not offer inertia to the grid, due to being non-synchronous, so their inertia constants are zero. This means their capacity factors are irrelevant for the purposes of calculating inertia. Nuclear has the highest capacity factor, given its use as baseload generation.

Justification of assumptions

Table 3.3 shows National Grid ESO's estimate of inertia on 9th August (when a large frequency deviation occurred resulting in demand disconnection) at two different times. I estimated the inertia using generation data for those specific times and the method

Generation type	Inertia constant, H [s]	Capacity factor, β
Combined-cycle gas turbine (CCGT)	8	0.75
Nuclear	5	0.9
Coal, biomass, and PS	4	0.75
Non-PS hydro	3	0.75
Wind, solar, and interconnectors	0	–

Table 3.2: Inertia constants and average capacity factors for different generation types [13].

Time	National Grid ESO inertia estimate [159]	Inertia estimate (using Section 3.3.1 method)
11:00	201353	203808
16:52	219632	214512

Table 3.3: Comparison of National Grid ESO's inertia estimate and the inertia calculated using the method described in Section 3.3.1 on 9th August at two different times (both in MVA.s).

described in Section 3.3.1. At 11:00 and 16:52 the difference between the National Grid ESO's estimate and ours is +1.2% and -2.3%, respectively.

Our method of calculating inertia assumes a constant capacity factor. The capacity factor in this case is the ratio of actual power output to total possible power output. In other words, the power output divided by the capacity of all the generators (of that type) online at the particular point in time. Clearly, the capacity factor will not be constant at each point in time. However, calculating this capacity factor at each point in time would require knowledge of the capacities of each power generator online at each half-hourly period. This is data we did not have, so I was required to use constant capacity factors. The capacity factors chosen were made based on discussions with industrial partners.

By subtracting $\sum_i H_i P_i$ from $E_{\text{n,gen}}$, we get a rough idea of the inertia contribution from partially-loaded generation (as a percentage of the total generation inertia contribution). This contribution ranged from 29% to 35% for the years 2014–2019, with an average of 33.6%. Bian *et al.* [27] found that the contribution from partial-loading varied between 25% and 43% with an average of 30% (see Section 2.3).

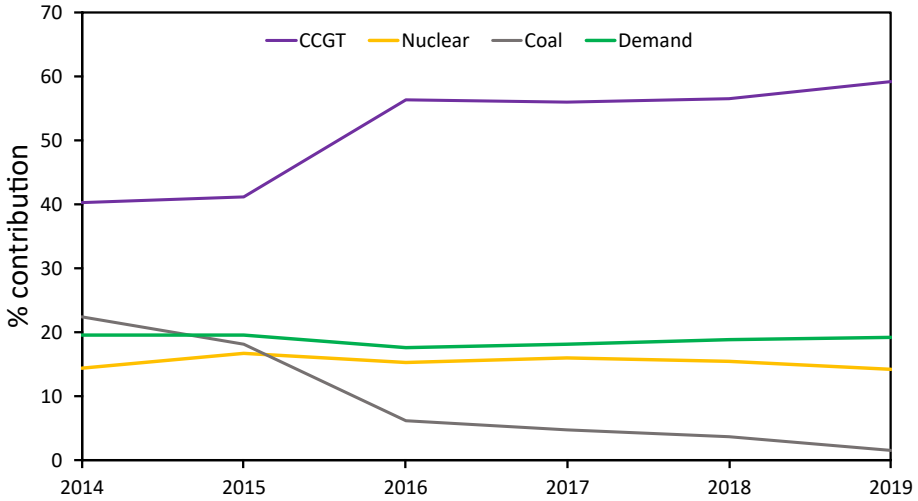

Figure 3.6: Average contributions to grid inertia each year from different generation types and demand.

3.3.2 Contributions to grid inertia

Fig. 3.6 shows the average contributions to grid inertia (as a percentage of the total) from different generation types in the time period 2014–2019. CCGTs provided the largest contribution every year because they were the largest source of electricity generation in the time period (see Fig. 3.3) and because of their high inertia constant ($H = 8$). In 2014, coal power stations used to contribute significantly to the total grid inertia, but this contribution dropped to almost zero in 2019 due to their phase out. To make up for the shortfall in inertia provided by coal, CCGTs increased their share from 40% in 2014 to 60% in 2019. The contribution from nuclear has been consistent at roughly 15%. The contribution from demand has also been consistent at 20%.

3.3.3 Decreasing grid inertia

An estimate of the inertia of the grid at each half-hour period in the years 2014–2019 was calculated using the method described in Section 3.3.1. Fig. 3.7 shows duration curves of grid inertia in GB each year. The 25th percentile ranges from 337 GVA.s to 379 GVA.s, the 50th percentile (median) ranges from 270 GVA.s to 320 GVA.s, and the 75th percentile ranges from 210 GVA.s to 257 GVA.s. In the last few years there is a trend of decreasing inertia, which can be seen more clearly in Table 3.4. 2016 is the year of highest inertia,

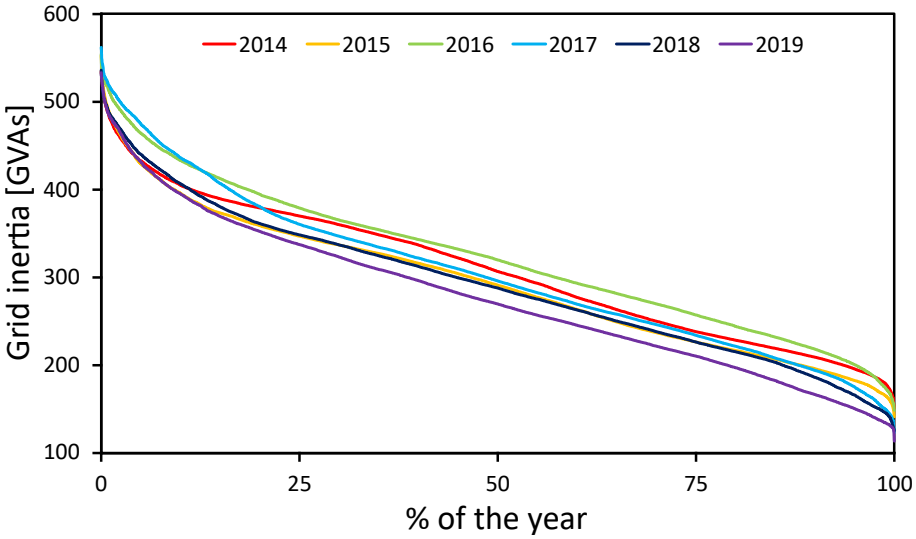

Figure 3.7: Duration curves of grid inertia each year.

	2014	2015	2016	2017	2018	2019
Median	307	291	320	296	288	270
Max	535	553	554	562	536	533
Min	150	141	149	123	125	114

Table 3.4: The median, maximum, and minimum of grid inertia (in GVA.s).

but the median inertia decreased by 16% between 2016 and 2019.

The difference between particularly low inertia days in 2014 and 2019 is perhaps of greater significance than the trend in Fig. 3.7. Fig. 3.8 shows the inertia profile on the day in 2014 and 2019 in which the minimum inertia of the year was reached. This also corresponded to the day where the average inertia of the day was lowest. It just so happens that in 2014 and 2019 this occurred on the same day: 17th August. In 2014, the minimum inertia was 150 GVA.s and occurred at 02:45 whereas in 2019 the minimum inertia was 114 GVA.s and occurred at 15:15. The reasons for the minimum inertia in the two cases are different. In 2014, it was the combination of windy conditions and low demand at night. In 2019 it was the combination of windy and extremely sunny conditions resulting in a very high penetration of wind and solar, which do not offer inertia to the grid. Note how the minimum inertia profile in 2019 is almost always below the absolute minimum of the minimum inertia profile in 2014.

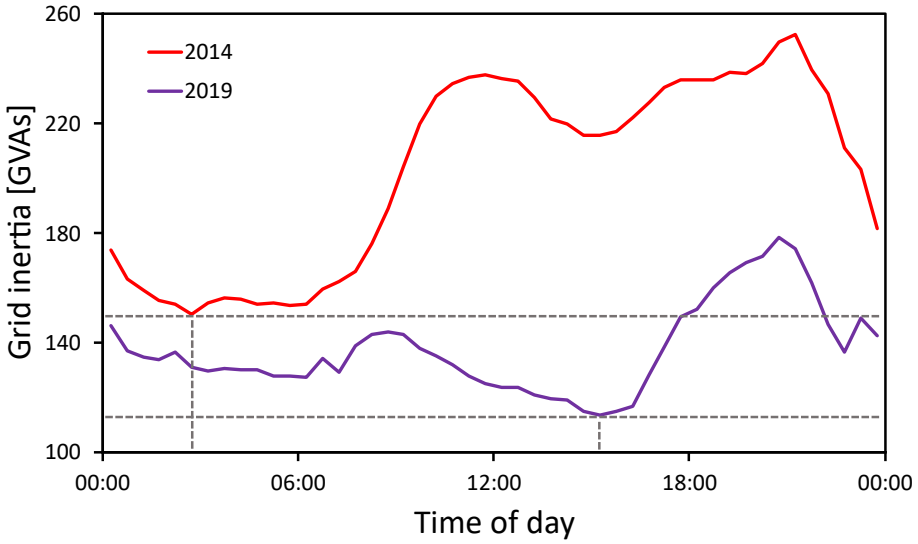

Figure 3.8: Inertia profiles of the entire day in which the minimum inertia of the year was reached in 2014 and 2019 (the day was August 17th in both years).

3.3.4 Hourly and monthly variation in grid inertia

The hourly and monthly variation of inertia is very similar to the hourly and monthly variation of underlying demand and transmission system demand. The reasoning for this is two-fold. Firstly, load-following generation, primarily CCGTs in Great Britain, offer lots of inertia to the grid. As the demand rises in the morning and evening, load-following generation capacity that is online increases. Secondly, there is also a contribution to inertia from demand. Using the simple method of multiplying transmission system demand by 1.75 to estimate demand inertia means that demand inertia and transmission system demand are perfectly correlated, which in turn means that demand inertia and underlying demand are also very highly correlated. The correlation coefficient between total inertia and underlying demand is $r = 0.93$ in 2014 and $r = 0.86$ in 2019, so a slight decrease. It is likely that this decrease in correlation will continue as the penetration of wind and solar generation increases in the future.

3.4 Frequency response

Here we use National Grid ESO data [160] on frequency response holding volumes to determine how the levels of frequency response in the GB grid have varied in recent years. The holding volume is the energy that the electricity system operator can rely on to supply a frequency response service. It is the procured capacity of response multiplied by the time that the service would need to be provided. The two types of frequency response that the data related to were Mandatory Frequency Response (MFR) and Firm Frequency Response (FFR). MFR, as the name implies, is mandatory for large generators and FFR is type of frequency response procured on a commercial market. The data for MFR and FFR was recorded separately so they needed to be collated. The frequency response holding volume data contains a list of every Balancing Mechanism unit and the amount of frequency response holding volume provided by that unit for each day. The data was sorted into monthly totals and the Balancing Mechanism unit ID used to categorise the units by generation type with the help of online resources [161].

Fig. 3.9 shows the frequency response holding volume (MFR+FFR) for the primary, secondary, and high service each month 2014–2019. The average holding volume for primary, secondary, and high is 450 GWh, 420 GWh, and 446 GWh, respectively. Since 2016, the volumes for each service have been quite similar. There is a large spike in the primary holding volume in August 2016 for reasons unknown.

Fig. 3.10 shows the percentage contribution to the primary holding volume from different generation types. CCGTs and PS have consistently provided a large amount. By 2016, the contribution from coal dropped below 10%, which makes sense considering its decline (Fig. 3.3). From 2016 to 2017, the contribution from DSF/BESS/Hybrid (DSF = demand side flexibility and BESS = battery energy storage system) increased by 270%, and from 2017 to 2018, by 160%. This does not include frequency response from batteries providing the EFR service, which started to come online in 2018. Almost no frequency response was provided by renewable generation in the 2014–2018 time period.

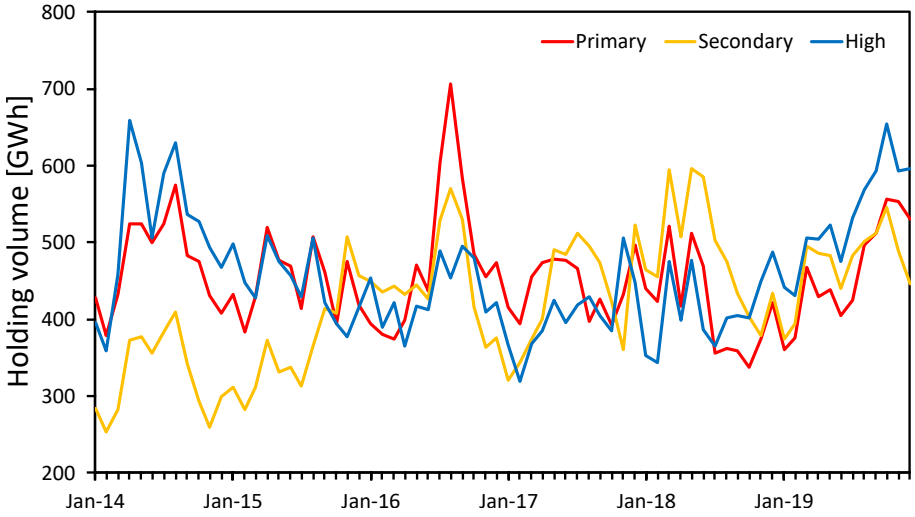

Figure 3.9: Frequency response holding volume each month for the primary, secondary, and high service.

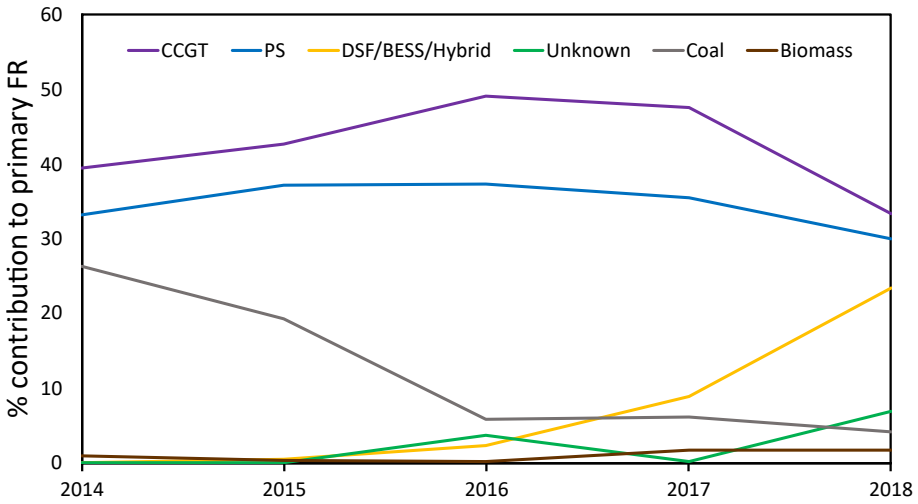

Figure 3.10: Contributions to the primary frequency response holding volume each year from different technologies (DSF = demand side flexibility and BESS = battery energy storage system).

3.5 Frequency volatility

The analysis of historic GB frequency data was conducted using 1 s resolution data at three decimal place precision from National Grid ESO's *Data finder and explorer* [155]. The data extracted ran from Jan 2014 to Dec 2019: 189 302 400 data points. The analysis in this section focuses on frequency volatility, and two ways of measuring this are used: the number of frequency events and the frequency standard deviation.

3.5.1 Frequency distribution

The nominal grid frequency in GB is 50 Hz. One of the electricity system operator's priorities is to maintain the frequency as close to that value as possible. Fig. 3.11 shows the distributions of grid frequency each year in the period 2014–2019. The bin width is 0.01 Hz and the counts are normalised by dividing by the total number of counts in each year (which is the same as the total number of seconds in each year). The distribution shown is limited to the range 49.8 Hz to 50.2 Hz. Beyond this range the normalised counts are below 10^{-3}.

Table 3.5 shows the distribution parameters for each year. Each year the mean of the distribution is within 0.001% of 50 Hz (every year it is slightly lower than 50 Hz). The standard deviation rises between 2014 and 2018 to a high of 0.066 Hz in 2018. It drops off a little in 2019, but 2019 still has the 2nd highest standard deviation out of all the years. The distributions are positively skewed, meaning that they are asymmetric around the nominal frequency. More time was spent lower than 50 Hz (51.9%) than higher (47.4%). Also, more time was spent outside the frequency response deadband ($|\Delta f| \geq 0.015$ Hz) on the low side (42.7%) than the high side (39.3%). The skewness has decreased in recent years to the point where the 2019 distribution is almost exactly symmetric. The highest skewness occurred in 2015.

Kurtosis is a measure of how heavy the tails are on a distribution i.e. how outlier-prone it is. The kurtosis of a normal distribution is 3. Distributions that have heavier tails (more outlier-prone) than the normal distribution have kurtosis greater than 3. Distributions

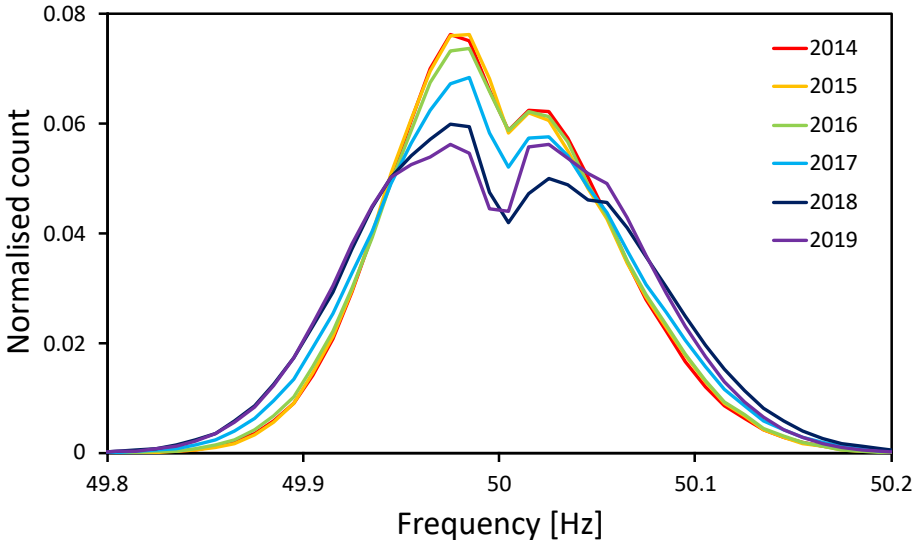

Figure 3.11: Distribution of grid frequency each year 2014–2019. Bin width: 0.01 Hz.

	2014	2015	2016	2017	2018	2019
Standard deviation [Hz]	0.054	0.054	0.055	0.060	0.066	0.064
Skewness	0.23	0.26	0.19	0.17	0.14	0.03
Kurtosis	3.02	2.91	2.93	2.87	2.62	2.80

Table 3.5: Grid frequency distribution parameters for each year. The mean was within 0.001% of 50 Hz for each year.

that have lighter tails (less outlier-prone) than the normal distribution have kurtosis less than 3. The kurtosis of GB frequency data is quite close to that of a normal distribution, but in general slightly lower. It is lowest in 2018 at 2.62 and highest in 2014 at 3.02.

Another interesting point about the distributions is that there are spikes either side of 50 Hz in the range 49.97 Hz–49.99 Hz and 50.01 Hz–50.03 Hz. The spike is higher on the lower side in all distributions apart from in 2019 where it is almost exactly equal with the spike on the higher side. These spikes are a result of having a frequency response deadband set to ±0.015 Hz. Table 3.6 shows the amount of time the frequency spent in three areas: within the frequency response deadband, outside of the frequency response deadband but within ±0.1 Hz, and outside of ±0.1 Hz. This effectively means that frequency response was not needed to operate 18% of the time. The majority of time is spent outside of the frequency response deadband (so some frequency response will be utilised) but far away

Absolute frequency deviation from 50 Hz [Hz]	Proportion of time
$\lvert\Delta f\rvert \leq 0.015$ (within deadband)	18%
$0.015 > \lvert\Delta f\rvert \leq 0.1$	74%
$\lvert\Delta f\rvert > 0.1$	8%

Table 3.6: The proportion of time the grid frequency spent at different deviation ranges away from 50 Hz (2014–2019).

from operational limits (±0.2 Hz). In the next section we take a more detailed look at what is going on near and beyond the operational limits.

3.5.2 Frequency event definitions

Based on the operational and statutory frequency limits in GB, stipulated in the Grid Code [162], we define six types of frequency event:

- *High frequency event*: frequency deviations above 50.2 Hz (upper operational limit) for any length of time
- *Significant high frequency event*: frequency deviations above 50.3 Hz for any length of time or frequency deviations above 50.2 Hz that last longer than 5 min
- *Severe high frequency event*: frequency deviations above 50.5 Hz (upper statutory limit) for any length of time
- *Low frequency event*: frequency deviations below 49.8 Hz (lower operational limit) for any length of time
- *Significant low frequency event*: frequency deviations below 49.7 Hz for any length of time or frequency deviations below 49.8 Hz that last longer than 5 min
- *Severe low frequency event*: frequency deviations below 49.5 Hz (lower statutory limit) for any length of time

Fig. 3.12 presents an example of a low frequency event and the definitions of event start, event end, event duration, and event magnitude. The event duration is the time difference between the event start (when the frequency moves outside the 49.8 Hz lower

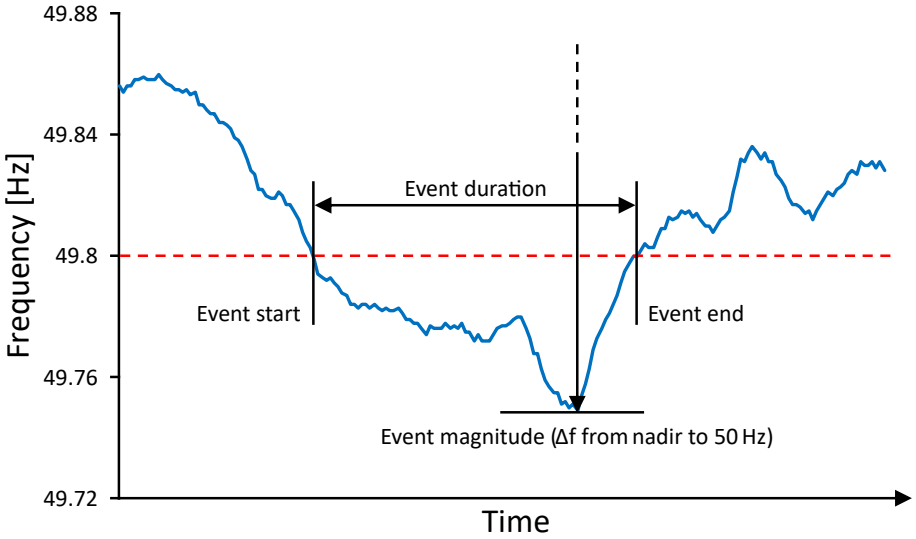

Figure 3.12: An example of a low frequency event, with event definitions.

operational limit) and the event end (when the frequency moves back within the 49.8 Hz lower operational limit). In the case of a high event, the start and end of an event are defined by the crossing of the 50.2 Hz limit. The event magnitude is the maximum absolute difference between 50 Hz and the frequency during an event.

3.5.3 Standard deviation and number of events

Fig. 3.13 shows the number of events (high and low) and standard deviation each month during the six year period (2014–2019). In total, there were 3317 high events and 1632 low events, which equates to an average of 1.5 high events per day and 0.7 low events per day. There were 97 significant events in the same time period (see Section 3.5.6) and only one severe event (9th August 2019 incident). The ratio of high events to low events is 2:1, and there are only 10 individual months where low events are more numerous than high events. However, seven of those months are in 2019. Between 2014 and 2018 the percentage of events that were low was never more than 36%, but in 2019 this increased to 51%.

There is a particularly noticeable spike in the number of events in October 2017 where there are 188 high events and 69 low events, the highest total of any month. The month with the highest standard deviation is November 2018 (0.070 Hz) and the month with

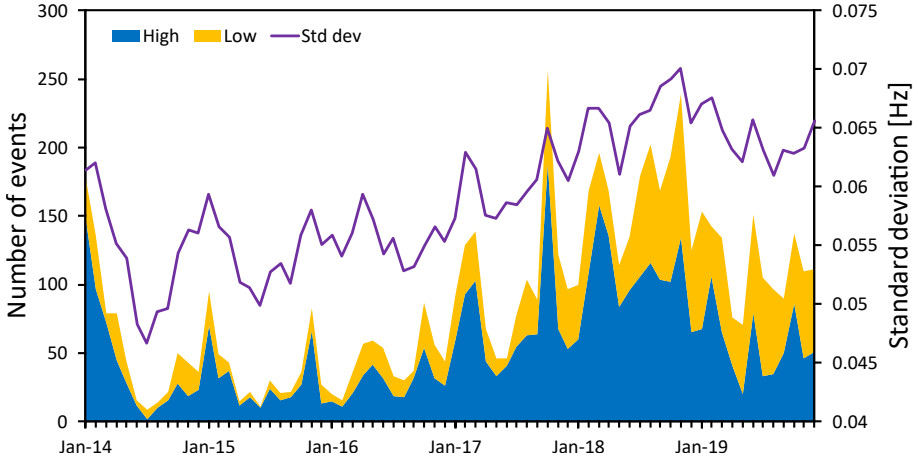

Figure 3.13: Number of frequency events and frequency standard deviation each month Jan 2014–Dec 2019.

the lowest is July 2014 (0.047 Hz). The summer of 2014 contains four of the five lowest standard deviation months and the autumn/winter of 2018–2019 contains all of the five highest standard deviation months. The standard deviation and number of events are, unsurprisingly, highly correlated ($r = 0.89$).

It is apparent from Fig. 3.13 that the number of events and standard deviation increased in the period 2017–2018. Fig. 3.14 makes it clearer by showing the number of events (high and low) and standard deviation each year during the six year period (2014–2019). The number of events (high + low) in 2014, 2015, and 2016 are fairly similar: 708, 454, and 529, respectively. However, in 2017, this increases to 1268, and then in 2018 it increases again to 1990. The number reduces down to 1378 in 2019, but this is still significantly higher than in the first three years. The yearly standard deviation follows a similar trajectory: level during 2014–2016, increasing in 2017 and 2018, then slightly reducing in 2019.

Over the six year time period, the frequency was outside of operational limits on the high side for 0.044% of the time, which averages to 38 s per day. The frequency was outside of operational limits on the low side for 0.017% of the time, which averages to 15 s per day.

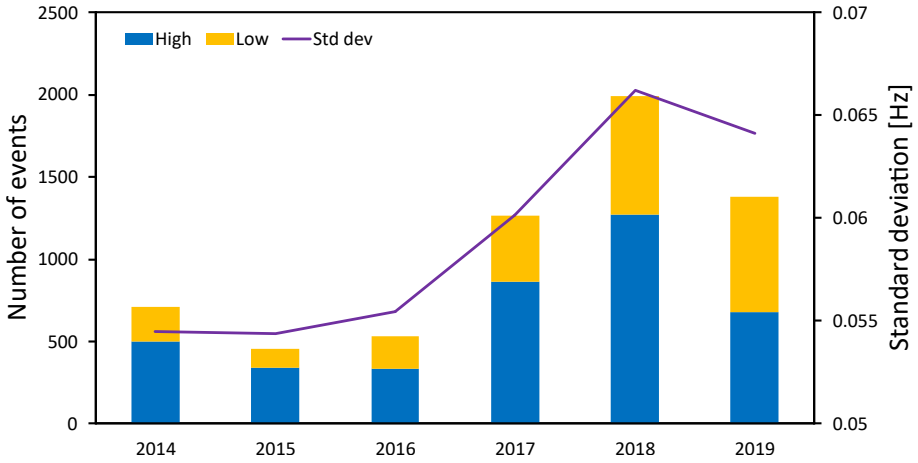

Figure 3.14: Number of frequency events and frequency standard deviation each year 2014–2019.

3.5.4 Temporal nature of standard deviation and events

Fig. 3.15 presents a heatmap of the number of events for individual months of the year and hours of the day during the six year period. There were more events in the late autumn, winter (excluding December), and early spring with fewer events in the summer. High events occurred most often in the evenings (all year round) whereas low events occurred most often in the mornings and autumn/winter evenings. October 19:00–20:00 had the most high events (64) and both October 06:00-07:00 and November 16:00-17:00 had the most low events (29) over the six years. These patterns suggest that one of the causes of frequency events is a high rate of change of demand, since mornings and evenings are when the rate of change of demand is at its highest. The number of events also follow a weekday/weekend pattern: the total number of events on weekdays ranged from 925 to 1092, compared to 648 on Saturdays and 668 on Sundays (about a third less).

Fig. 3.16 presents a heatmap of the average standard deviation for individual months of the year and hours of the day during the six year period. For example, the value for January 13:00–14:00 is the average of the standard deviation of that particular hour for all days in January and for all years. The standard deviation was highest in the mornings and evenings in the spring, autumn, and winter. November 16:00–17:00 had the highest average standard deviation at 0.0608 Hz. Between April and October and between the

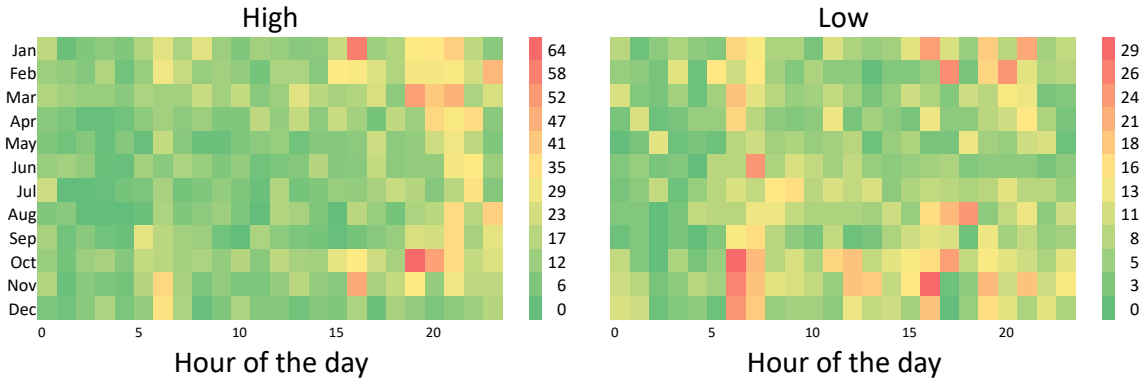

Figure 3.15: Number of frequency events each month of the year and hour of the day (2014–2019).

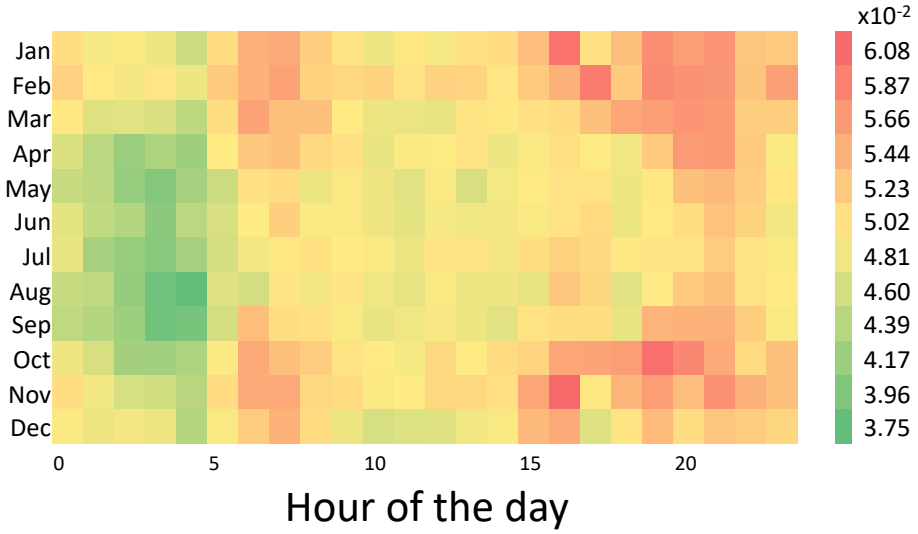

Figure 3.16: Average frequency standard deviation (in Hz) each month of the year and hour of the day (2014–2019).

hours of 01:00 and 05:00 is a region of low standard deviation: August 04:00–05:00 had the lowest average standard deviation at 0.0375 Hz.

Fig. 3.17 shows in which minute of the hour all the events in the six year period started. 34% of events occurred in the first and last 5 min of the hour. However, the distribution for high and low events is a bit different. Low events occurred most often at the start of the hour, and for the rest of the hour remain at fairly constant levels. The number of high events has spikes at the start and end, and also slightly smaller spikes at 8 min, 27 min, and 38 min.

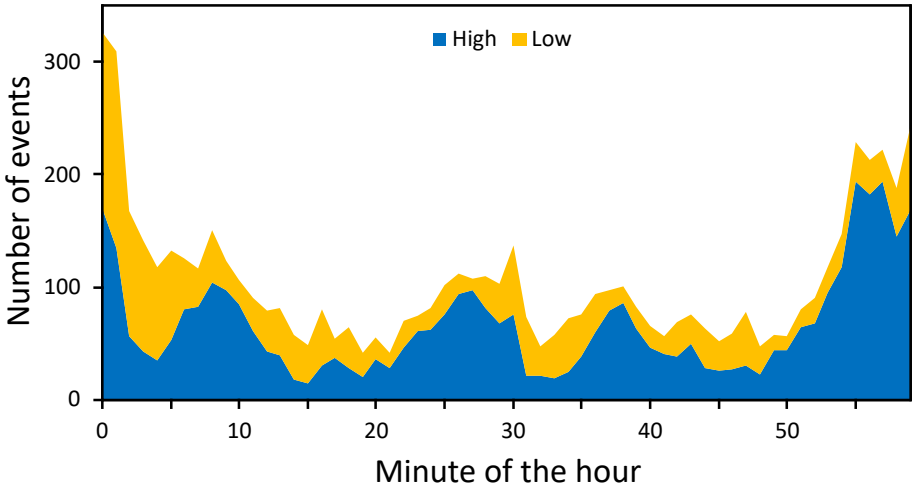

Figure 3.17: Number of frequency events each minute of the hour (2014–2019).

3.5.5 Severity of events

In this section, the difference in severity between high and low events and change in severity over the six years is analysed. This is done by looking at event duration and magnitude, defined in Section 3.5.2. Perhaps the most important point to make is that frequency events are overwhelmingly short in duration and small in magnitude. From Table 3.7, we can observe that the median of event duration and magnitude both do not change significantly from year to year. However, there is quite a change in low event duration from 2018 to 2019. In other words, event severity has remained fairly constant, which is not the case in terms of the number of events, as shown in Section 3.5.3. Across all years, high and low events have a similar median magnitude, but high events generally have a slightly longer duration. The average event duration over the whole time period is 21.0 s for high events and 13.7 s for low events, both significantly higher than the median duration.

Fig. 3.18 shows the event duration and magnitude distributions up to a duration of 60 s and 0.25 Hz, respectively. 91% of high events and 96% of low events are below 60 s in duration. 96% of high events and 91% of low events are below 0.25 Hz in magnitude. The frequency went outside ±0.3 Hz 93 times and there were five events of duration longer than 5 min. These *significant* events are discussed in more detail in Section 3.5.6. The greatest deviations from 50 Hz during the six year period were −1.213 Hz and 0.410 Hz.

	2014	2015	2016	2017	2018	2019	All
Duration [s]							
High	8	8	10	10	9.5	9	9
Low	7	5	6	5	5	8.5	6
Magnitude [Hz]							
High	0.206	0.206	0.208	0.207	0.208	0.208	0.208
Low	0.212	0.209	0.209	0.208	0.207	0.210	0.209

Table 3.7: The median values of frequency event duration and magnitude each year.

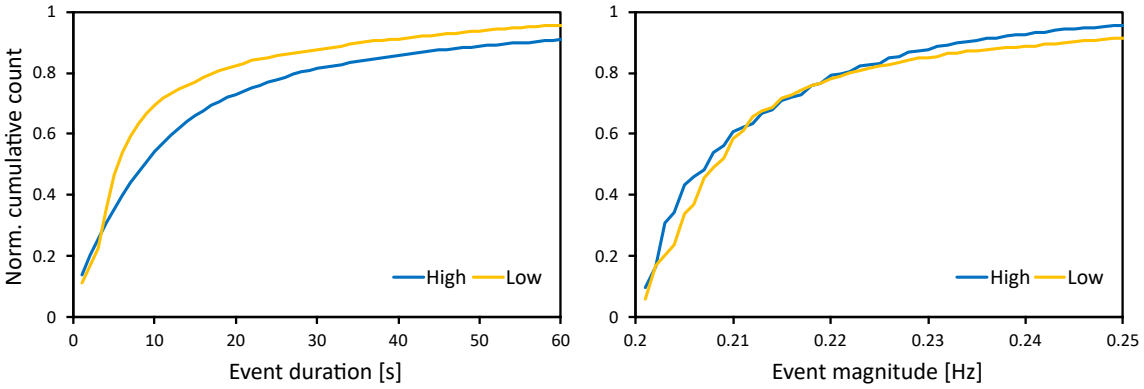

Figure 3.18: Frequency event duration and event magnitude distribution (2014–2019).

3.5.6 Significant events

It is important to focus a little deeper on significant frequency events because these are events of concern for the electricity system operator and usually caused by something going wrong. Between 2014–2019 there were 97 significant events (as defined in Section 3.5.2). As previously mentioned, 93 of these were events where $|\Delta f| > 0.3$ Hz and five were events of duration longer than 5 min. One event, a high event on 27th September 2018, had a magnitude of 0.342 Hz and a duration of 332 s.

Fig. 3.19 shows the number of significant events (high and low) each year. In total, there were 24 significant high events and 73 significant low events, which equates to one every three months and one every month, respectively. The 1:3 significant high events to significant low events ratio contrasts with the 2:1 ratio for high events to low events in Section 3.5.3. There is a large increase in the number of significant events in 2019, a 60% increase on the next highest year, 2017. A third of significant events occurred in the first

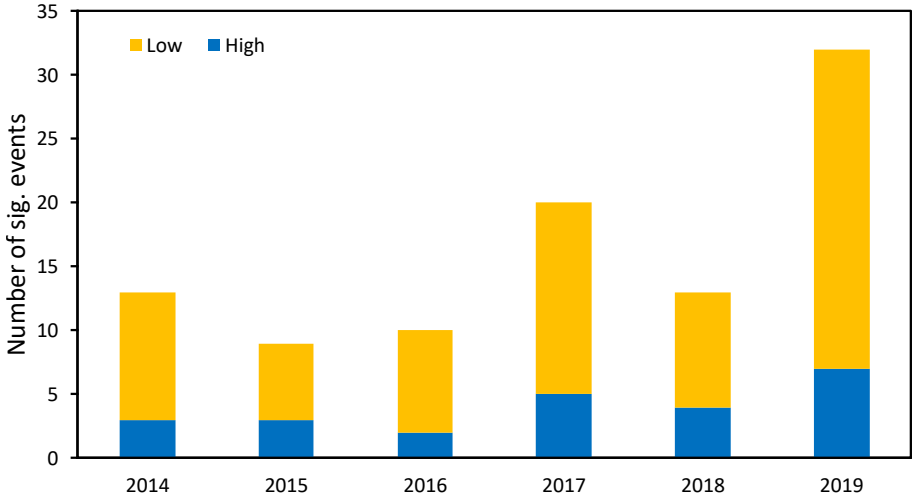

Figure 3.19: Number of significant frequency events each year.

Time period	High	Low	Total
00:00–06:00	6	6	12
06:00–12:00	5	29	34
12:00–18:00	5	26	31
18:00–00:00	8	12	20

Table 3.8: Number of significant frequency events in each 6 h time period (2014–2019).

three years and two-thirds in the last three years.

Table 3.8 shows when the significant events occur during the day. The high events are fairly evenly spread, but low events occur mostly in daylight hours.

A recent report by National Grid ESO [163] listed 33 significant frequency events that occurred in 2018 and 10 months of 2019. The list also includes the size of generation/demand loss that caused the event and the generator that experienced the fault. Their definition of *significant event* is the same as in Section 3.5.2 but with the additional possibility of being defined based on the size of the generation loss being over 1000 MW. By categorising the generators into generation types, we can compare the number of events caused by each type, see Fig. 3.20. Interconnector failures were responsible for 17 significant events, over half the total.

CCGTs were responsible for nine events. It is not surprising that CCGTs are responsible for quite a few events because as Fig. 3.3 shows, they are the biggest provider of

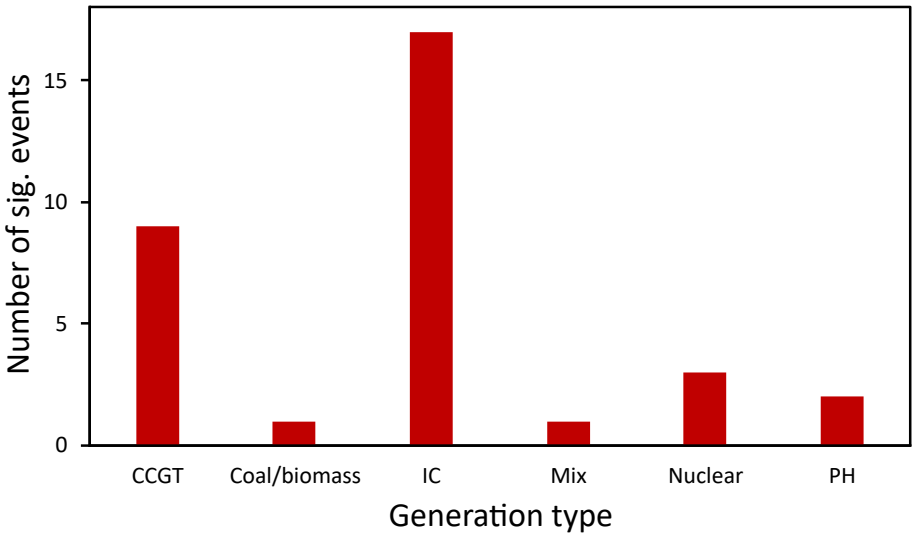

Figure 3.20: Number of significant frequency events caused by the failure/trip of different generator types (2018–2019).

electricity generation, so a fair number of units are often online and many of the units are large enough to cause significant events if they trip.

The only frequency event that was severe (based on the definitions in Section 3.5.2) in 2014–2019 was the event that occurred on 9th August 2019. The generation loss was a combination of a wind farm, CCGT units, and embedded generation (categorised as *Mix* in Fig. 3.20). The magnitude of the loss reached a high of 2058 MW and the frequency reached a low of 48.79 Hz. This event will be discussed more in Section 5.3.

3.5.7 Frequency volatility in Continental Europe

So far in Section 3.5 we have focussed on frequency volatility in Great Britain. In this section, we will conduct a brief analysis of frequency volatility in the Continental European electricity grid.

Frequency data at 10 s resolution for the years 2015–2018 was used. This data was from the French electricity system operator (Réseau de Transport d'Électricité). This data was chosen as it was the longest period of continuous complete data available at a resolution that made it possible for an in-depth analysis.

In Section 3.5.2, we defined six types of frequency events based on the operational and statutory frequency limits in GB, stipulated in the GB Grid Code. ENTSO-E do not offer

such guidelines and so we have chosen $|\Delta f| > 0.1$ to be the definition of a frequency event. This is the same definition used by Schäfer *et al.* [134] when they counted the number of frequency events on the Continental European grid in 2011 and 2017 each minute of the hour (see Fig. 2.20). The justification of this choice is given below.

The lowest frequency in the data was 49.849 Hz (February 2018) and the highest frequency was 50.148 Hz (June 2018). Also, the standard deviation of all the data was 0.02 Hz. For the GB grid in the years 2014–2019, the lowest frequency was 48.787 Hz, the highest frequency was 50.410 Hz, and the standard deviation was 0.06 Hz. Firstly, it tells us that the frequency volatility of the Continental European grid is much lower than the GB grid. This makes sense because the Continental European grid is much larger with a higher demand (about ten times greater [164]) and higher inertia, which means a greater imbalance is required in the Continental European grid for an equivalent frequency deviation. Secondly, it tells us that using the GB grid frequency event definitions in Fig. 3.12 for the Continental European grid frequency data does not make sense because there would not be any events in the whole time period. Choosing $|\Delta f| > 0.1$ Hz as the definition of a frequency event in the Continental European grid implies that there were 573 high events and 741 low events in the 2015–2018 time period. In the same time period for the GB grid, with the $|\Delta f| > 0.2$ Hz frequency event definition (Section 3.5.2), there were 2814 high events and 1427 low events. The numbers of events are of a similar order of magnitude so $|\Delta f| > 0.1$ Hz seemed a sensible frequency event definition for the Continental European grid.

Fig. 3.21 shows the monthly standard deviation of the Continental European grid frequency from Jan 2015 to Dec 2018. The month with the lowest standard deviation was August 2015 at 0.017 Hz and the month with the highest standard deviation was May 2018 at 0.024 Hz. There is not a clear trend in the standard deviation apart from a very slight seasonal trend, which is discussed later. Fig. 3.21 also shows the monthly number of high and low events of the Continental European grid. The month with the highest number of high events was October 2018 with 46 and the month with the highest number of low events was February 2018 with 46. There were no high events in April 2015 and

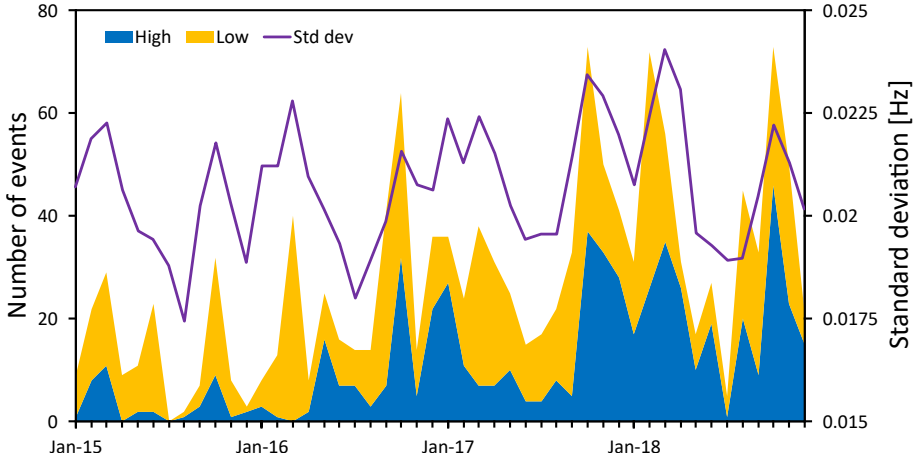

Figure 3.21: Number of frequency events and frequency standard deviation ($|\Delta f| > 0.1$ Hz) in the Continental European grid each month Jan 2015–Dec 2018.

March 2016 and no events at all in July 2015. In 2015 there were 155 events, in 2016 there were 293, in 2017 there were 405, and in 2018 there were 461. This indicates an increasing trend over the years, which is similar to the trend seen in the GB frequency data. The correlation between standard deviation and number of frequency events is less in the Continental European grid ($r = 0.66$) compared to the GB grid ($r = 0.89$). In total there were 741 low events and 573 high events. This differs to the GB grid where there were two high events for every low event.

In terms of seasonal trends, the standard deviation peaks in March and October with a trough in the summer. This is similar to the GB grid, except the peaks were in February and November instead. The number of low events has peaks in March and October with a trough in the summer, but also a trough in January and December at the same level as the summer months. The number of high events does not have a very clear seasonal trend, but the month of October stands out as a significant spike with almost twice the amount of high events as any other month. These seasonal trends differ somewhat from the trends seen in the GB grid.

3.6 Discussion

Over the six year period analysed, two thirds of frequency events in the GB grid were high events. The capacity of frequency response that the GB ESO procures for specific times of the day is based on the level of inertia, demand, and size of the largest loss. The size of the largest loss is greater on the generation side than the demand side [165], so it follows that more dynamic primary response is procured than dynamic high response [74]. This means that when the frequency drops below 50 Hz, there is more frequency response delivered for a given Δf than when it goes above 50 Hz. A greater imbalance is therefore required to cause a low event than a high event, which might explain why there are fewer low events.

In GB, the electricity market is split into settlement periods. There are 48 settlement periods in a day, each lasting half an hour. Before the start of each settlement period, National Grid ESO is aware of the expected generation levels and has an estimate for the demand. During the settlement period, generation and demand do not exactly match, so National Grid ESO use the Balancing Mechanism (as well as frequency response in real-time) to increase or decrease generation or demand to ensure they are in balance. Fig. 3.22 shows the ensemble averaged frequency profile over 24 hours (2014–2019). There is a large change in the ensemble frequency on the every hour throughout the day (more pronounced at night and early morning). There is also a slightly smaller, but still significant, change every half hour. Fig. 3.22 and Fig. 3.17 are both evidence for how the settlement period boundaries are likely causes of frequency events.

As mentioned before, Fig. 3.15 suggests that frequency events are correlated with rate of change of demand. Fig. 3.23 (left) shows the total number of events at each hour of the day and also the average rate of change of demand at each hour of the day over the 5 year period. The frequency event profile over the day has three spikes: one in the morning, one in the early evening, and one in the late evening. These spikes correspond to periods of high rate of change of demand: the morning ramp up in demand, the early evening ramp up, and the late evening ramp down. The correlation coefficient is $r = 0.72$. Fig. 3.23

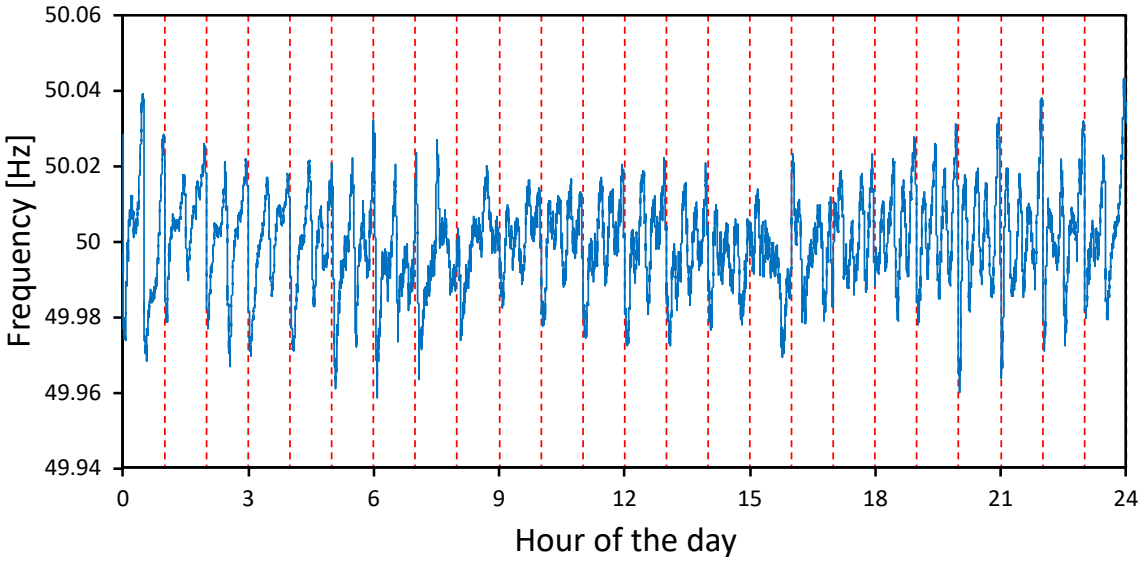

Figure 3.22: Ensemble averaged GB frequency profile over 24 hours (2014–2019).

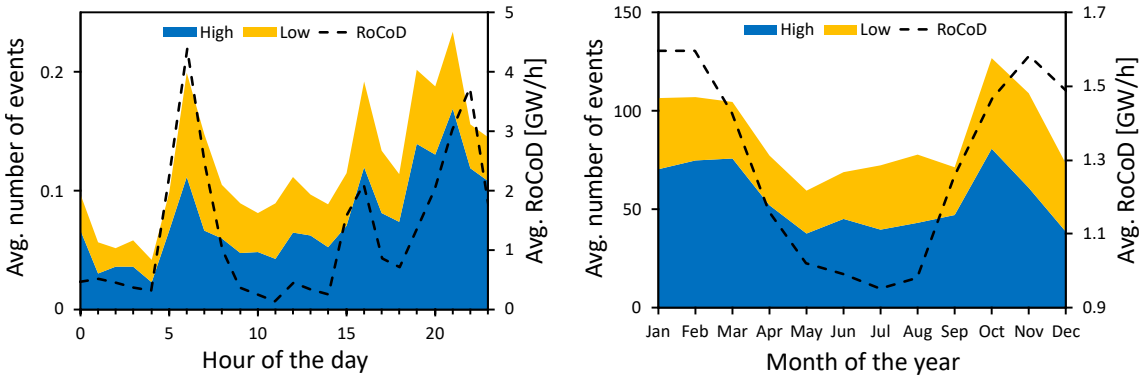

Figure 3.23: Average number of frequency events and rate of change of demand (RoCoD) each hour of the day and month of the year (2014–2019).

(right) shows the total number of events at each month of the year and also the average rate of change of demand over each month of the year over the six year period. There are clearly fewer events in the summer months, which is also when the average rate of change of demand over a month is at its lowest. The same is observed when it comes to number of events each day of the week: there are fewer events on the weekend days (average of two per day), where the average rate of change of demand over the day is lower, compared to the weekdays (average of three per day).

Settlement period boundaries and rate of change of demand are likely causes of frequency events. However, this does not explain the increase in the number of events during

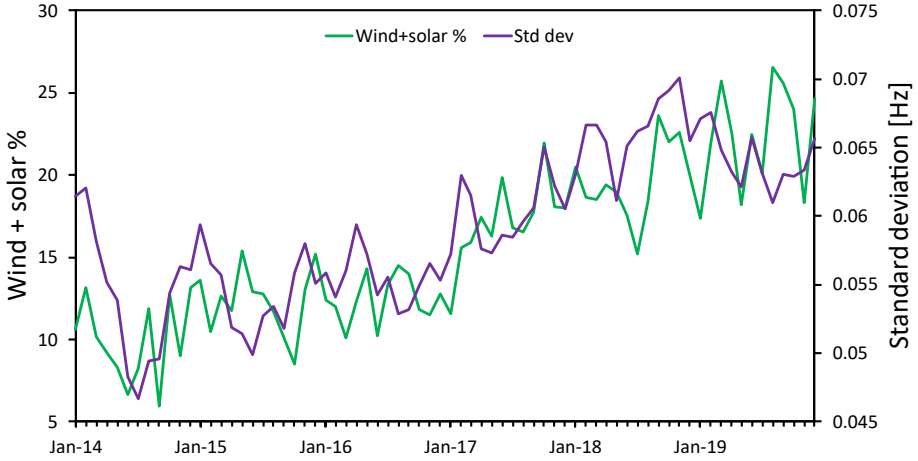

Figure 3.24: Wind and solar penetration and frequency standard deviation each month.

2017 and 2018, seen in Fig. 3.13. Settlement periods exist in the same way in 2017 and 2018 as they did in earlier years, and the average rate of change of demand each month has a slight downwards trend from 2014 to 2018 (although a seasonal pattern each year). Fig. 3.24 shows the penetration of wind and solar generation (as a percentage of underlying demand) and the frequency standard deviation each month during the five year period. While the correlation is fairly high ($r = 0.79$), it is impossible to say conclusively whether there is a causal relationship, though it is clear it has not been due to the lack of inertia provided by wind and solar. The inertia levels are not low enough in the 2014–2018 period to be a cause in the increase of frequency standard deviation and number of events. There is no correlation between total inertia and frequency standard deviation ($r = 0.07$) during the six year period. Also, between 2014 and 2018, the amount of inertia in the grid does not change by a significant amount, as can be seen in Fig. 3.7. The correlation between the penetration of wind and solar generation and the frequency standard deviation each day during the six year period is $r = 0.49$, much lower than the monthly correlation.

3.7 Conclusions

In this section, I first return to the research questions set out in the introduction to this chapter and discuss the extent to which each have been answered. Then, in Section 3.7.1, I present the highlights of the results of the chapter. Key findings of this chapter are

discussed within a wider context in Chapter 6.

What is the recent trend in grid parameters such as demand, generation, inertia, and frequency response holding volumes and what is their monthly and hourly variation?

In terms of generation and demand, the decline of coal generation (from contributing 29% of underlying demand to 2%) is the most significant change over recent years. This decline has been mirrored by an increase in wind and solar generation (10% to 22%) and CCGT generation. CCGTs provide the largest contribution to grid inertia and primary frequency response holding volume, which will need to be replaced by another technology in the future because CCGTs are not compatible with net-zero ambitions (unless carbon capture and storage is used). Average inertia levels decreased slightly over recent years, and the drop is more dramatic when looking at the minimum levels reached during each year.

What is the current state of frequency volatility and have there been significant changes in recent years?

Between 2014 and 2019, the grid only suffered one severe frequency event, suggesting a high level of stability. The number of frequency events and standard deviation increased from 2016 to 2017 and peaked in 2018, reducing slightly in 2019 (but still remaining higher than in 2014–2016).

What are the underlying drivers behind frequency volatility?

This has been more difficult to answer. The underlying drivers behind frequency volatility are likely numerous and it's very hard to pin down with certainty what they are. Settlement period boundaries and high rate of change of demand are likely the main drivers and the increasing penetration of wind and solar generation probably does play a small role as well.

3.7.1 Highlights of the results

The highlights of the results from this chapter are listed below (all relate to the GB grid in the time period 2014–2019 unless otherwise explicitly stated):

- Transmission system demand decreased more than underlying demand due to an increase in embedded generation
- Coal generation declined dramatically while CCGT, wind, and solar generation increased
- On average, inertia has fallen slightly. However, this reduction in inertia is much more significant when comparing the levels on particularly low inertia days.
- CCGTs provide a lot of inertia and a lot of frequency response to the grid, so they are very important for stability
- Demand side flexibility and batteries are providing increasing amounts of fast frequency response to the grid
- Frequency volatility increased in 2017 and 2018, but levelled off in 2019
- The number of significant events is highest in 2019. Also, interconnectors were responsible for over half of the significant frequency events in the years 2018–2019.
- Rate of change of demand and settlement period boundaries are the main drivers behind frequency volatility
- Increasing wind and solar penetration probably played a small role in Great Britain's recent increase in frequency volatility

Chapter 4

Frequency dynamics after a large infeed loss: an analytical approach

4.1 Introduction

A large infeed loss is a rapid loss of generation of a large magnitude. They are caused by generator trips, which in turn could be caused by generator faults, natural disasters, sabotage, etc. Large infeed losses cause the grid frequency to suddenly dip, often falling outside the normal operating range. The electricity system operator must protect the grid against large infeed losses so that unacceptable frequency conditions do not occur, since they can lead to equipment failure and blackouts.

To counter frequency dips caused by large infeed losses, electricity system operators use frequency response. Electricity system operators need the appropriate amount of capacity and speed of frequency response to secure the grid against the largest infeed loss that could reasonably occur in the grid at each point in time. This calculation is also dependent on the demand level and volume of inertia in the grid.

There are many studies in the literature that investigate the dynamics of the grid frequency after a large infeed loss using generic grid models, which have drawn attention to the importance of fast frequency response in combatting the difficulties raised by low inertia scenarios. However, an understanding of the mathematical relationship between

grid parameters (e.g. inertia, demand, frequency response capacity) in the context of a maintaining acceptable frequency conditions after a large infeed loss is less well understood. To fill this gap in knowledge and to further existing work, this chapter addresses the following research questions:

- **What are the future frequency response requirements of the GB grid, in terms of capacity and speed, to secure the grid against a large infeed loss in different inertia and demand scenarios?**

- **With the constraint of maintaining acceptable frequency conditions after a large infeed loss, is there a simple mathematical relationship between the grid parameters (e.g. inertia and frequency response speed)?**

Both of these research questions are addressed through solving the swing equation analytically. This was achieved by approximating frequency response as a linear ramp. We use three frequency requirements (these are requirements on different stages of the frequency evolution) to then derive constraints on grid parameters. Answering the first research question requires estimates for future grid parameters in GB. This is achieved by using analysis presented in Chapter 3 and predictions by National Grid ESO. The second research question is answered by using mathematical analysis and reasonable approximations.

The rest of this chapter is outlined as follows. In Section 4.2 I present the swing equation and give a detailed explanation of the terms within it. I then proceed to solve the swing equation analytically in Section 4.3: Section 4.3.1 describes my approximation of frequency response and Section 4.3.2 introduces general frequency requirements that lead to constraints on certain grid parameters. In Section 4.4, I look at the GB grid specifically and assign values to current and future grid parameters. I use these values to produce results presented in Section 4.5, which focus on inertia and frequency response capacity and speed. Section 4.6 concludes the chapter and includes a list of the highlights of the results.

4.2 The swing equation

The swing equation (derived in Appendix A) governs the relationship between the grid frequency and power imbalances of the grid [6, 18]:

$$\begin{aligned}\frac{\mathrm{d}f}{\mathrm{d}t} &= \frac{f_{\mathrm{n}}^2}{2E_{\mathrm{n}}f}(R + I - kD_{\mathrm{n}}\Delta f) \\ &= \frac{f_{\mathrm{n}}^2}{2E_{\mathrm{n}}f}\Delta P\,. \end{aligned} \tag{4.1}$$

The definitions of each term are given in Section 2.2 with a more in depth discussion of demand damping (the $kD_{\mathrm{n}}\Delta f$ term) given in Section 2.2.1.

When $\Delta P = R + I - kD_{\mathrm{n}}\Delta f = 0$, the right hand side of Eq. (4.1) is zero, so the RoCoF is zero and the frequency of the grid is constant. At this point, if a large negative imbalance occurs on the grid (e.g. the loss of a large generator), then I has a step change reduction. ΔP becomes negative and so does the RoCoF (i.e. the frequency falls). After some time delay, power is injected into the grid via frequency response units and the demand of the grid slightly falls due to the grid operating at a lower frequency (demand damping). Frequency response and demand damping raise ΔP back to zero again. The minimum frequency occurs when $\Delta P = R + I - kD_{\mathrm{n}}\Delta f = 0$ again. This is part of the frequency containment stage. To recover the frequency back to the nominal level, the RoCoF needs to be positive for a period of time, which requires ΔP to be positive. For this to happen, more power needs to be injected into the grid, which can come from additional frequency response or other actions.

4.3 Solving the swing equation analytically in the case of a large infeed loss

The setup is as follows. At $t < 0$, the grid frequency is at the nominal value, f_{n}, and the RoCoF is zero. The RoCoF is zero because Δf, I, and R are all zero making the net power imbalance zero ($\Delta P = 0$). At $t = 0$, a large infeed loss occurs in the grid. The imbalance, I, step changes to a negative value and has a magnitude equal to the size of the loss. At

the moment of the loss, the grid has a certain amount of demand, D_{n}, inertia, E_{n}, and demand damping, k. For the purposes of investigating frequency dynamics after a large infeed loss, the parameters mentioned so far (f_{n}, I, D_{n}, E_{n}, and k) remain constant for all time after $t = 0$. The frequency response, $R(t)$, and grid frequency, $f(t)$, evolve with time.

To solve the swing equation analytically, it first needs to be linearised. We can linearise Eq. (4.1) by using the fact that $f \approx f_{\mathrm{n}}$. In other words, the frequency deviations are very small compared to the magnitude of the nominal frequency ($\Delta f \ll f_{\mathrm{n}}$). From Section 3.5.1 we know that the frequency spends the vast majority of time within ± 0.1 Hz of 50 Hz, which is just $\pm 0.2\%$. However, in this chapter we are considering frequency dynamics after a large infeed loss where the frequency deviations are much larger. It turns out that $f \approx f_{\mathrm{n}}$ is still a good approximation in this case. As evidence for this fact, in GB the largest frequency deviation in recent years was 1.21 Hz below 50 Hz [130], which is still only a percentage deviation of 2.4%. By putting $f = f_{\mathrm{n}}$ into the denominator of the right hand side of Eq. (4.1), we get the linearised swing equation:

$$\begin{aligned} \frac{\mathrm{d}f}{\mathrm{d}t} &= \frac{f_{\mathrm{n}}}{2E_{\mathrm{n}}}(R + I - kD_{\mathrm{n}}\Delta f) \\ &= \frac{f_{\mathrm{n}}}{2E_{\mathrm{n}}}\Delta P\,. \end{aligned} \tag{4.2}$$

Eq. (4.2) tells us that the RoCoF of a grid is proportional to the net power imbalance and inversely proportional to the amount of inertia in the system. If demand is greater than generation (e.g. a sudden loss of generation incident) then the frequency will fall. If demand is less than generation (e.g. a sudden loss of demand incident or maybe a rapid, unexpected increase in wind generation) then the frequency will rise.

4.3.1 Frequency response approximated as a linear ramp

Within the swing equation, the term R represents the frequency response of the grid. This is the sum of the response from all generators and demand units offering frequency response. The electricity system operator procures different frequency response services

with different response characteristics. Even units providing the same service will have slightly different response curves. Therefore, we have to make some approximations to define R analytically, which is necessary to be able to solve Eq. (4.2) analytically.

After a large infeed loss, the frequency will quickly drop. Frequency response will either be dynamic (output proportional to frequency deviation) or static (full output triggered at a certain frequency deviation). If the frequency drop is fast enough, then we can ignore these details and assume that the frequency response approaches full output as fast as possible. We approximate frequency response as a linear ramp to full capacity after a delay as soon as the large infeed loss occurs. This approximation also ignores the frequency response deadband, which is justified because the frequency will be outside the deadband almost immediately after the loss.

Frequency response approximated as a linear ramp to full capacity after a delay has three stages:

$$R(t) = \begin{cases} 0 & \text{when } t \leq t_\mathrm{d}\,, \\ R_\mathrm{cap}\left(\frac{t-t_\mathrm{d}}{t_\mathrm{r}}\right) & \text{when } t_\mathrm{d} \leq t \leq t_\mathrm{d} + t_\mathrm{r}\,, \\ R_\mathrm{cap} & \text{when } t \geq t_\mathrm{d} + t_\mathrm{r}\,, \end{cases} \tag{4.3}$$

where t_d is the delay time between the large infeed loss and the start of the linear ramp and t_r is the time it takes for the frequency response to ramp from zero to full capacity, R_cap. Fig. 4.1 illustrates the frequency response of the grid after a large infeed loss with this approximation. The imbalance caused by the large infeed loss drives the frequency down but the fall is arrested by the ramping frequency response and demand damping.

4.3.2 Frequency requirements and associated grid constraints

With our linearisation of the swing equation and approximation of frequency response as linear ramp to full capacity after a delay, we can now proceed to solve the swing equation analytically to investigate the frequency dynamics after a large infeed loss. Eq. (4.2) with R approximated as a linear ramp is a first-order linear ordinary differential equation.

As mentioned in Section 4.1, electricity system operators must ensure that unaccept-

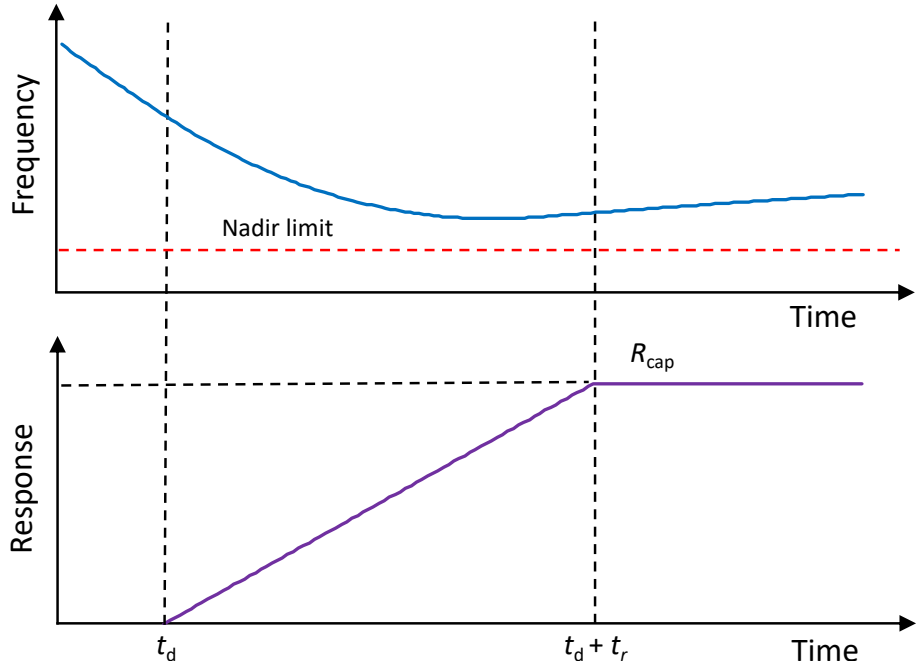

Figure 4.1: An example frequency profile after a large infeed loss (top) and the frequency response approximated as a linear ramp after a delay (bottom).

able frequency conditions do not occur after a large infeed loss. Two examples of unacceptable frequency conditions are a RoCoF with a magnitude that is too high and a frequency outside of the safe operating range. These are unacceptable for the following reasons: a RoCoF that is too high may cause the tripping of embedded generation off the system due to RoCoF protection relays being triggered, and a frequency outside of the safe operating range can cause damage to machinery connected to the grid. Unacceptable frequency conditions have the potential to lead to widescale blackouts, which are costly and put lives at risk.

Following a large infeed loss, we define three frequency requirements: the RoCoF requirement, the steady-state requirement, and the nadir requirement. The RoCoF requirement is that the magnitude of the RoCoF must be below the RoCoF limit, L_{rf}, at all times. The RoCoF limit is dependent on the loss of main protection settings of embedded generation. The nadir requirement is that the frequency must never go below the nadir limit, L_{nad}. This is dependent on the value of grid frequency that is deemed unacceptable by the electricity system operator. The steady-state frequency, f_{ss}, is the frequency after

the transient period is over ($t \gg t_\mathrm{d} + t_\mathrm{r}$), and $\mathrm{d}f/\mathrm{d}t = 0$. The steady-state requirement is that the steady-state frequency must not be below the steady-state limit. In the setup, the RoCoF requirement is mathematically expressed as

$$\left|\frac{\mathrm{d}f}{\mathrm{d}t}\right| \leq L_\mathrm{rf} \quad \text{when } t \geq 0\,, \tag{4.4}$$

the nadir requirement is mathematically expressed as

$$f \geq L_\mathrm{nad} \quad \text{when } t \geq 0\,, \tag{4.5}$$

and the steady-state requirement is mathematically expressed as

$$f_\mathrm{ss} \geq L_\mathrm{ss}\,. \tag{4.6}$$

We now use the linearised swing equation (Eq. (4.2)) to determine how these requirements are met after a large infeed loss and what constraints this might impose on the system. The setup for these derivations is described at the start of Section 4.3.

The RoCoF, $\mathrm{d}f/\mathrm{d}t$, is proportional to ΔP, so will be at maximum magnitude when ΔP is at maximum magnitude. In the setup, this occurs at the moment of the large infeed loss ($t = 0$) because at this moment the overall imbalance of the grid is equal to the entire infeed loss because frequency response and demand damping are at zero output. For the RoCoF requirement to be satisfied at all times, the magnitude of the RoCoF at $t = 0$ cannot be greater than L_rf. Using Eq. (4.2) and Eq. (4.4), we get the RoCoF requirement constraint on inertia:

$$E_\mathrm{n} \geq \left|\frac{f_\mathrm{n} I}{2 L_\mathrm{rf}}\right|\,. \tag{4.7}$$

If the inertia does not meet this constraint, then the RoCoF at the moment of the large infeed loss will be too high and above the RoCoF limit. The minimum inertia is equal to the right-hand side of Eq. (4.7) and would result in a RoCoF equal to the RoCoF limit.

As discussed previously, the steady-state frequency occurs when the loss is contained and $\mathrm{d}f/\mathrm{d}t = 0$ and $t \gg t_\mathrm{d} + t_\mathrm{r}$. Substituting $\mathrm{d}f/\mathrm{d}t = 0$ into Eq. (4.2), we get that the

steady-state frequency deviation is $\Delta f_{\mathrm{ss}} = f_{\mathrm{ss}} - f_{\mathrm{n}} = (R_{\mathrm{cap}} + I)/kD_{\mathrm{n}}$. Using Eq. (4.6), we then get the steady-state requirement constraint on frequency response capacity:

$$R_{\mathrm{cap}} \geq kD_{\mathrm{n}}(L_{\mathrm{ss}} - f_{\mathrm{n}}) - I\,. \tag{4.8}$$

If the frequency response capacity does not meet this constraint, then the steady-state frequency will be too low and below the steady-state limit. The minimum frequency response capacity is equal to the right-hand side of Eq. (4.8) and would result in a steady-state frequency equal to the steady-state limit.

The solution to Eq. (4.2) when $t \leq t_{\mathrm{d}}$ (no frequency response yet, $R = 0$) with the initial condition $f(t = 0) = f_{\mathrm{n}}$ is

$$f = \frac{I}{kD_{\mathrm{n}}}\left(1 - \exp\left(-\frac{A}{E_{\mathrm{n}}}t\right)\right) + f_{\mathrm{n}} \quad \text{when } t \leq t_{\mathrm{d}}\,, \tag{4.9}$$

where $A = kD_{\mathrm{n}}f_{\mathrm{n}}/2$. $t \leq t_{\mathrm{d}}$ is the time period before frequency response has started ramping. Therefore, during this period, the RoCoF is always negative (i.e. the frequency keeps falling) so the minimum frequency during the period is at $t = t_{\mathrm{d}}$. This frequency must be above the nadir limit to satisfy the nadir requirement, so using Eq. (4.9) with $t = t_{\mathrm{d}}$ and Eq. (4.5), we get the nadir requirement constraint on inertia:

$$E_{\mathrm{n}} \geq \frac{-At_{\mathrm{d}}}{\ln\left(1 - kD_{\mathrm{n}}(L_{\mathrm{nad}} - f_{\mathrm{n}})/I\right)}\,. \tag{4.10}$$

If the inertia does not meet this constraint, then the frequency will be too low and below the nadir limit before the frequency response has started ramping. The minimum inertia is equal to the right-hand side of Eq. (4.10) and would result in the frequency reaching the nadir limit at $t = t_{\mathrm{d}}$.

The previous constraint must be satisfied to ensure the frequency has any chance of fulfilling the nadir requirement after a large infeed loss. However, Eq. (4.10) only ensures that the nadir limit is not breached before the frequency response starts ramping at $t = t_{\mathrm{d}}$. With only this constraint, there is still the possibility of the nadir limit being breached at

some point during the ramping time period ($t_\mathrm{d} \leq t \leq t_\mathrm{d} + t_\mathrm{r}$). Avoiding this possibility gives us the nadir requirement constraint on frequency response parameters:

$$R_\mathrm{cap} \exp\left(\frac{At_\mathrm{r}\big(kD_\mathrm{n}(L_\mathrm{nad} - f_\mathrm{n}) - I\big)}{E_\mathrm{n}R_\mathrm{cap}}\right) = R_\mathrm{cap} - \frac{At_\mathrm{r}I}{E_\mathrm{n}} \exp\left(-\frac{At_\mathrm{d}}{E_\mathrm{n}}\right). \tag{4.11}$$

Eq. (4.11) can be solved for one of the frequency response parameters (R_cap, t_r, or t_d). Eq. (4.11) is a transcendental equation for R_cap and t_r, so cannot be solved analytically for these parameters. Instead, numerical methods for finding the solution have to be deployed. I used the *fzero* function in MATLAB, which is built for finding roots of non-linear functions. The solution results in the frequency reaching, but not breaching, the nadir limit. There are a few additional points to make. If the inertia, E_n, is low enough, then Eq. (4.11) does not have a solution. This is because, in this case, there is no delay time that can prevent the nadir limit being breached before the frequency response has started ramping. The nadir requirement constraint on inertia, Eq. (4.10), prevents this situation. Also, we need to remember the steady-state requirement constraint on frequency response capacity, Eq. (4.8). Assuming that the solution of Eq. (4.11) is above the minimum R_cap determined from Eq. (4.8), then the solution to Eq. (4.11) is the absolute limit (i.e. minimum frequency response capacity, maximum delay time, and maximum ramp time) for the particular frequency response parameter being solved for. If the solution of Eq. (4.11) is below the minimum R_cap determined from Eq. (4.8), then the minimum frequency response capacity is determined by Eq. (4.8) rather than Eq. (4.11). Eq. (4.11) is derived fully in Appendix B.2.

Table 4.1 summarises the frequency requirements we have defined in this section along with the constraints (on grid parameters) associated with them. The RoCoF requirement constrains only the inertia, the steady-state requirement constrains only the frequency response capacity, and the nadir requirement constrains inertia and multiple frequency response parameters: capacity, delay time, and ramp time. There is a minimum inertia associated with the RoCoF requirement and a minimum inertia associated with the nadir requirement. The ultimate minimum inertia to maintain acceptable frequency conditions is the higher of the two minimums. It is the same with frequency response capacity: there

	Description	Mathematical description	Associated grid constraint
RoCoF requirement	The magnitude of the RoCoF must never be above the RoCoF limit, L_{rf}.	$\left\lvert \frac{\mathrm{d}f}{\mathrm{d}t} \right\rvert \leq L_{\mathrm{rf}}$	Eq. (4.7)
Nadir requirement	The frequency must never go below the nadir limit, L_{nad}.	$f \geq L_{\mathrm{nad}}$	Eq. (4.10) and Eq. (4.11)
Steady-state requirement	After the transient period is over, the steady-state frequency must not be below the steady-state limit, L_{ss}.	$f_{\mathrm{ss}} \geq L_{\mathrm{ss}}$	Eq. (4.8)

Table 4.1: Frequency requirements and associated grid constraints after a large infeed loss.

is a minimum associated with the steady-state requirement and a minimum associated with the nadir requirement. The ultimate minimum frequency response capacity is the higher of the two.

I decided that grid inertia and the frequency response parameters should be the grid parameters that are constrained, rather than demand or demand damping. This is because the electricity system operator has more control over these parameters. The demand of the grid is a parameter that the electricity system operator must plan for and react to rather than constrain.

4.4 Current and future grid parameters in Great Britain

The previous section described frequency requirements and their associated constraints in a general sense, which would be applicable to most grids around the world. Here we present actual values (or range of values) for some current and future grid parameters in Great Britain. We have used our own analysis from Chapter 3 to acquire current values for the parameters and National Grid ESO's Future Energy Scenarios and System Operability Frameworks to acquire future values for the parameters. The parameters we are referring to are the nominal grid frequency, f_{n}, demand, D_{n}, demand damping, k, inertia, E_{n}, frequency response capacity (that acts when the frequency falls below 50 Hz),

R_{cap}, frequency response delay time, t_{d}, frequency response ramp time, t_{r}, imbalance, I, RoCoF limit, L_{rf}, steady-state limit, L_{ss}, and nadir limit, L_{nad}. The aim of this section is to help frame the discussion of the results presented in Section 4.5.

The nominal frequency in Great Britain is 50 Hz, and National Grid ESO aim to keep the real-time frequency as close to this nominal value as possible. The frequency requirements of Great Britain are explained in more detail in Section 4.4.1.

The demand damping constant is a parameter that cannot be accurately known in real-time since this would require detailed knowledge of every single demand unit connected to the grid. However, the demand damping constant is possible to infer by analysing frequency dynamics after real infeed losses on the grid. In the 2016 SOF [11], it was stated that the demand damping constant is 2.5 %MW/Hz based on the method of inferring from past infeed loss events. From our own analysis of the 9th August 2019 low frequency event (presented in the next chapter in Section 5.3), a demand damping constant of 1.65 %MW/Hz gives the best match between a simulated frequency trace and the real frequency during that event. A value of $k = 2$ %MW/Hz was chosen for the results in Section 4.5. It is very hard to predict what the demand damping constant will be in the future, and no prediction is made in any National Grid ESO publication. There has been an increasing trend in non-synchronous generation (converter connected) on the generation side in recent years, and if this occurs on the demand side as well, then the demand damping constant will reduce in the future. The percentage of demand that is frequency sensitive is directly proportional to the demand damping constant: if it halves in the future, then the demand damping constant will likely be less than 0.01 Hz in the future. Another important point to make is that demand and the demand damping constant are multiplied together (kD_{n}) in the linearised swing equation (Eq. (4.2)), which is used for the results in Section 4.5. This means that observing the effect that varying demand has on the results is equivalent to observing the effect that a varying demand damping constant has on the results. For example, if a particular quantity calculated, such as minimum inertia, was found to increase by a factor of 1.3 if demand reduces by a factor of 3, then we know that the same 1.3x increase would occur if demand stayed the

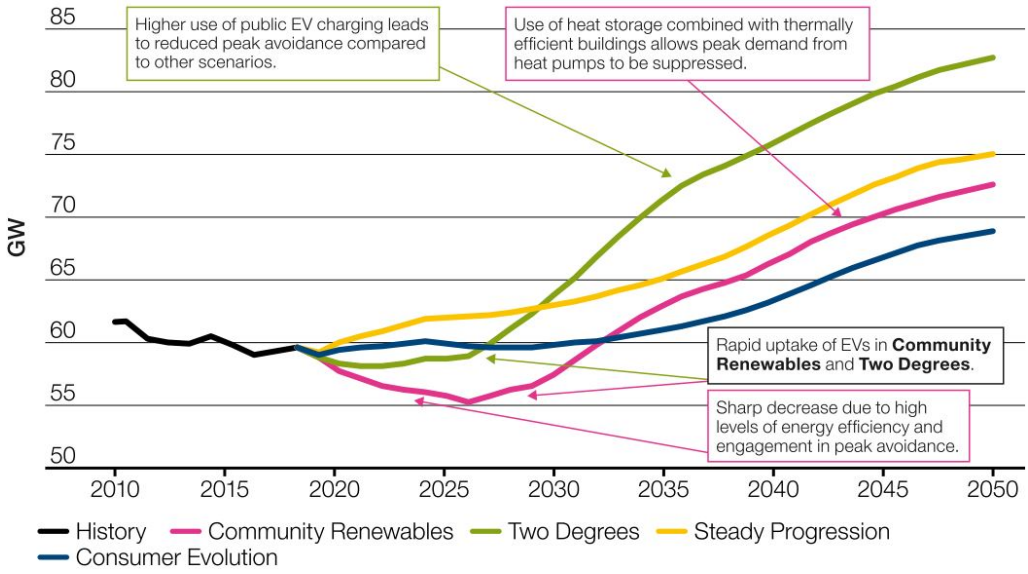

Figure 4.2: Underlying peak demand in future scenarios (and historic). Reproduced from Ref. [166].

same but the demand damping constant reduced by a factor of three.

The demand in Eq. (4.2), D_{n}, is the demand that is relevant for calculating the magnitude of the demand damping contribution to the net power imbalance. Out of the transmission system demand and the underlying demand, the relevant one is the underlying demand. We can use our analysis conducted in Section 3.2 to present current values of underlying demand. The minimum underlying demand between the years 2014–2019 was 19.5 GW, the maximum was 58.5 GW, and the median for each year ranged from 36.4 GW to 38.3 GW. In National Grid ESO's Future Energy Scenarios 2019 [166] predictions are given for both peak and minimum demand. Fig. 4.2 shows the underlying peak demand in different future scenarios (and historic). Beyond 2030, the peak demand rises in every scenario due to the electrification of heat and EV charging. By 2050, there is a possibility of a peak demand of 80 GW. In terms of minimum underlying demand, in all future scenarios this remains relatively static at around 20 GW.

We can use our analysis conducted in Section 3.3 to present current values of inertia. The minimum inertia between the years 2014–2019 was 114 GVA.s, the maximum was 562 GVA.s, and the median for each year ranged from 270 GVA.s to 320 GVA.s. In the SOF of 2016, predictions were given for inertia distributions in 2025/26, shown in

Fig. 2.13. The minimum inertia in this future scenario is around 70 GVA.s and the maximum around 270 GVA.s. There is a possibility of inertia occasionally reaching even lower levels than 70 GVA.s past 2025/26 due to the expected extremely high levels of wind and solar generation capacity. In fact, the limiting factor for how low the inertia might go in the future is likely to be grid stability.

Given the subject of this chapter, here the interest is in obtaining a value for the frequency response capacity that acts quickly when the frequency falls below 50 Hz. The frequency response capacity is a parameter that will vary day-to-day depending on the grid conditions. However, we can still estimate the current frequency response holding capacity range in a few different ways. From Section 3.4, we know that the average holding volume for primary response (ignoring secondary and high response) is 450 GWh per month between the years 2014–2019. This averages to a constant 625 MW. However, the frequency response requirements are higher at certain times of the day than others so the peak will be higher. Also, the 450 GWh primary response holding volume only includes mandatory frequency response and firm frequency response. Additional response through other markets was likely procured. From the technical report into the low frequency event of 9th August 2019 [130], we know that just under 1000 MW of frequency response was outputting power within 10 s of the infeed loss. In terms of future frequency response capacity, this was discussed in the SOF of 2015 [119] and can be seen in Fig. 2.12. The prediction is the requirement of roughly 2500 MW of traditional response by 2030. Traditional response refers to response from traditional synchronous generators and of the timescale of 2 s to 10 s. The amount of response capacity might vary depending on the speed of the response, and this is something investigated in Section 4.5.

The GB grid code [162] stipulates that generating units in frequency sensitive mode must start delivering response within 2 s with their response capacity fully delivered by 10 s. This implies a delay time of 2 s and a ramp time of 8 s. This type of response is delivered by synchronous generators such as CCGTs. Recently, a new service, EFR, has been introduced in the GB grid. The delay and ramp time for this service are both 0.5 s. Another even more recent service, Dynamic Containment, has the same delay and

ramp time stipulations. It is difficult to make predictions on future delay and ramp times, but the trend is definitely in the direction of faster response. It is clear there is now viable technology (e.g. batteries) that can deliver power into the grid on the timescale of milliseconds rather than seconds.

Although demand and inertia are treated separately in this section, in reality, as was shown in Section 3.3.4, there is a degree of connection between the two parameters. In other words, periods of high inertia are likely to correlate with periods of high demand due to the increased amount of generation capacity online and the contribution to inertia from demand itself and vice versa. From historic data, the highest inertia reached in the GB grid in the period 2014–2019 at a demand lower than 25 GW was 195 GVA.s, which is significantly lower than the median value for all demand levels. Although in the future demand and inertia may be more decoupled, this is a fact to bear in mind in the results section.

Table 4.2 provides a summary of the parameters discussed in this section and the current and future values of these parameters in the GB grid. These parameter values are used in the results section: Section 4.5. The values vary from being exact (e.g. nominal frequency) to very approximate (e.g. frequency response capacity). An additional note to make is that the minimum future inertia in the table is 0 GVA.s. Although this is an almost impossible scenario, it opens up the results to explore the absolute minimum levels of inertia required for stability rather than only exploring likely scenarios.

4.4.1 Frequency requirements in Great Britain

As mentioned previously, a RoCoF that is too high may cause the inadvertent tripping of embedded generation off the system due to RoCoF protection relays being triggered. As described in detail in Section 2.7.2, the RoCoF magnitude that triggers the RoCoF relays has changed in the GB grid due to concerns of excessive spurious tripping in the future under regular low inertia conditions. The RoCoF trigger has increased from $0.125\,\mathrm{Hz\,s^{-1}}$ to $1\,\mathrm{Hz\,s^{-1}}$ in recent years (some generation units are still in the process of updating their settings). The RoCoF must be measured to be continuously in excess of $1\,\mathrm{Hz\,s^{-1}}$ over

Parameter	Current value	Predicted future value
Nominal frequency, f_n	50 Hz	50 Hz
Demand, D_n	20 GW–60 GW	20 GW–80 GW
Demand damping constant, k	2 %MW/Hz	Likely to be less than 2 %MW/Hz
Inertia, E_n	114 GVA.s–562 GVA.s	0 GVA.s–270 GVA.s
Frequency response capacity, R_{cap}	1000 MW	2500 MW[1]
Frequency response delay time, t_d	Maximum 2 s. Some response capacity as low as 0.5 s.[2]	As low as milliseconds
Frequency response ramp time, t_r	Maximum 8 s. Some response capacity as low as 0.5 s.[2]	As low as milliseconds

[1] Amount of traditional response (response between 2 s and 10 s)
[2] EFR and Dynamic Containment

Table 4.2: Current and future grid parameters in Great Britain (used in Section 4.5).

500 ms for the relays to be triggered. The electricity system operator manages the grid so that the RoCoF should never have a greater magnitude than the trigger setting to avoid a large infeed loss from multiple small embedded generation trips. Therefore, the RoCoF limit in GB is now $1\,\mathrm{Hz\,s^{-1}}$, and in the past was $0.125\,\mathrm{Hz\,s^{-1}}$.

National Grid ESO publish a document, the System Security and Quality of Supply Standard [165], that sets out a coordinated set of criteria that the electricity grid (and therefore the electricity system operator) and generators with a transmission license (and therefore companies operating generators) have to meet. Within this document are the definitions of unacceptable frequency conditions. In order to avoid the occurrence of unacceptable frequency conditions the following frequency requirements are stipulated:

- The frequency must not deviate below 49.5 Hz or above 50.5 Hz (either transiently or in steady-state) after a *normal* infeed loss, defined as a sudden loss of up to 1320 MW.

- The frequency must not deviate below 49.5 Hz or above 50.5 Hz for more than 60 s after an *infrequent* infeed loss, defined as a sudden loss between 1320 MW and 1800 MW.

	Normal infeed loss	*Infrequent* infeed loss
Imbalance	$I = -1320\,\text{MW}$	$I^* = -1800\,\text{MW}$
RoCoF limit	$L_{\text{rf}} = 1\,\text{Hz}\,\text{s}^{-1}$	$L^*_{\text{rf}} = 1\,\text{Hz}\,\text{s}^{-1}$
Steady-state limit	$L_{\text{ss}} = 49.5\,\text{Hz}$	$L^*_{\text{ss}} = ?$
Nadir limit	$L_{\text{nad}} = 49.5\,\text{Hz}$	$L^*_{\text{nad}} = ?$

Table 4.3: Imbalance and frequency limits for a *normal* infeed loss and *infrequent* infeed loss in Great Britain.

Note, unless explicitly stated otherwise, hereafter the upper value of the respective infeed loss definitions (1320 MW for *normal* infeed loss and 1800 MW for *infrequent* infeed loss) is used because securing the grid against these upper values guarantees security for all infeed losses of smaller magnitude. From these stipulations it is clear that the steady-state limit and nadir limit for a *normal* infeed loss are $L_{\text{ss}} = 49.5\,\text{Hz}$ and $L_{\text{nad}} = 49.5\,\text{Hz}$, respectively. However, it is unclear what these limits should be for an *infrequent* infeed loss. In fact, this is explicitly mentioned in the System Security and Quality of Supply Standard document: "*It is not possible to be prescriptive with regard to the type of secured event which could lead to transient deviations since this will depend on the extant frequency response characteristics of the system which National Grid ESO adjust from time to time to meet the security and quality requirements of this Standard*" [165]. The frequency must return above 49.5 Hz within 60 s, which is long enough for additional manual response/reserve to come online and raise the steady-state frequency from a slightly lower level. Part of Section 4.5 will investigate what are appropriate steady-state and nadir limits for an *infrequent* infeed loss.

Table 4.3 is a summary of the frequency limits for a *normal* infeed loss and *infrequent* infeed loss in GB. The * superscript indicates a value associated with an *infrequent* infeed loss. As mentioned above, the steady-state limit and nadir limit for an *infrequent* infeed loss are not strictly defined. Another important frequency limit worth mentioning is the point at which demand starts being disconnected. This starts at 48.8 Hz [162] (5% of demand gets disconnected) and continues in stages until 47.8 Hz, at which point 60% of demand has been disconnected.

4.5 Inertia and frequency response considerations in the case of a large infeed loss

In this section, I investigate how much inertia and frequency response is needed after a large infeed loss to prevent unacceptable frequency conditions. I use the frequency requirements and associated grid constraints explained and derived in Section 4.3.2 along with parameter values given in Section 4.4. Therefore, the results in this section apply to the GB grid specifically, but also can be applied to other similar sized grids. As mentioned in Section 4.4, the parameter values chosen represent current and future scenarios.

4.5.1 Rate of change of frequency and steady-state frequency

Eq. (4.7) tell us that the minimum inertia needed to ensure the RoCoF requirement is met is

- proportional to the infeed loss magnitude
- and inversely proportional to the RoCoF limit.

It also tells us that once the RoCoF limit is set, the only controllable grid parameter is inertia. For a RoCoF limit of $L_{\text{rf}} = 1\,\text{Hz}\,\text{s}^{-1}$, for a *normal* infeed loss the minimum inertia given by Eq. (4.7) is 33 GVA.s, and for an *infrequent* infeed loss the minimum inertia is 45 GVA.s. In Section 3.3.3 we estimate that the lowest inertia in the GB grid up to 2019 was 114 GVA.s, which is far higher. The RoCoF magnitude after an *infrequent* infeed loss at this level of inertia is $0.395\,\text{Hz}\,\text{s}^{-1}$. The minimum inertia with a RoCoF limit of $L_{\text{rf}} = 0.125\,\text{Hz}\,\text{s}^{-1}$ (the old limit) for a *normal* infeed loss is 264 GVA.s and for an *infrequent* infeed loss it is 360 GVA.s. This is why the RoCoF limit was increased in 2014 (see Section 2.7.2). In the time period 2014–2019, the inertia was lower than 264 GVA.s 38.1% of the time and lower than 360 GVA.s 75.8% of the time. In other words, quite often. Keeping the RoCoF limit at $0.125\,\text{Hz}\,\text{s}^{-1}$ would have exposed the system to the regular risk of a cascade event where a large infeed loss causes a high RoCoF which in turn causes embedded generation to trip offline due to their relay settings.

The RoCoF requirement constraint on inertia, Eq. (4.7), is actually stricter than it needs to be given that the RoCoF relays on the new setting will only trip if the RoCoF magnitude continuously exceeds $1\,\mathrm{Hz\,s^{-1}}$ over 500 ms. Within the setup we defined at the start of Section 4.3, this requirement is effectively that the RoCoF magnitude must not exceed $1\,\mathrm{Hz\,s^{-1}}$ at $t = 500\,\mathrm{ms}$. We will refer to the RoCoF magnitude at $t = 0$ as the instantaneous RoCoF magnitude and the RoCoF magnitude at 500 ms as the delayed RoCoF magnitude. Fig. 4.3 shows the instantaneous and delayed RoCoF magnitude against inertia for a *normal* infeed loss and an *infrequent* infeed loss at a demand of 80 GW. The demand level does not affect the instantaneous RoCoF magnitude (notice the absence of D_n from Eq. (4.7)). However, it does affect the delayed RoCoF magnitude. After 500 ms the frequency has had time to drop, so there is a reduction in the net power imbalance, ΔP, because demand damping is no longer zero. Demand damping contributes more to reducing the net power imbalance when the demand level is higher. Therefore, delayed RoCoF magnitudes are lower at higher demand. The demand of 80 GW was chosen in Fig. 4.3 because, as discussed in Section 4.4, this is the highest predicted future demand so will result in the largest difference between the instantaneous RoCoF and delayed RoCoF.

From Fig. 4.3 we can indeed see that the RoCoF requirement constraint on inertia, Eq. (4.7), is stricter than necessary if the RoCoF relays only trip if they measure a RoCoF magnitude over $1\,\mathrm{Hz\,s^{-1}}$ continuously over 500 ms. The delayed RoCoF magnitude curve is always lower than the respective instantaneous RoCoF magnitude curve. However, at an inertia of 180 GVA.s, the difference is only approximately 10%. The highest delayed RoCoF magnitude for a *normal* infeed loss is $0.607\,\mathrm{Hz\,s^{-1}}$, and for a *infrequent* infeed loss it is $0.828\,\mathrm{Hz\,s^{-1}}$. Both occur at 20 GVA.s. At lower inertia, while the instantaneous RoCoF magnitude gets ever larger, the delayed RoCoF magnitude decreases because the frequency gets so low by $t = 500\,\mathrm{ms}$ that demand damping is offering a huge contribution to counter the infeed loss (note: this does not make this a stable grid situation).

So, if the electricity system operator operates the grid to keep the instantaneous RoCoF magnitude below the $L_\mathrm{rf} = 1\,\mathrm{Hz\,s^{-1}}$ limit, then a minimum inertia of 45 GVA.s is required. However, if the inertia gets lower than this and a large infeed loss occurs the RoCoF relays

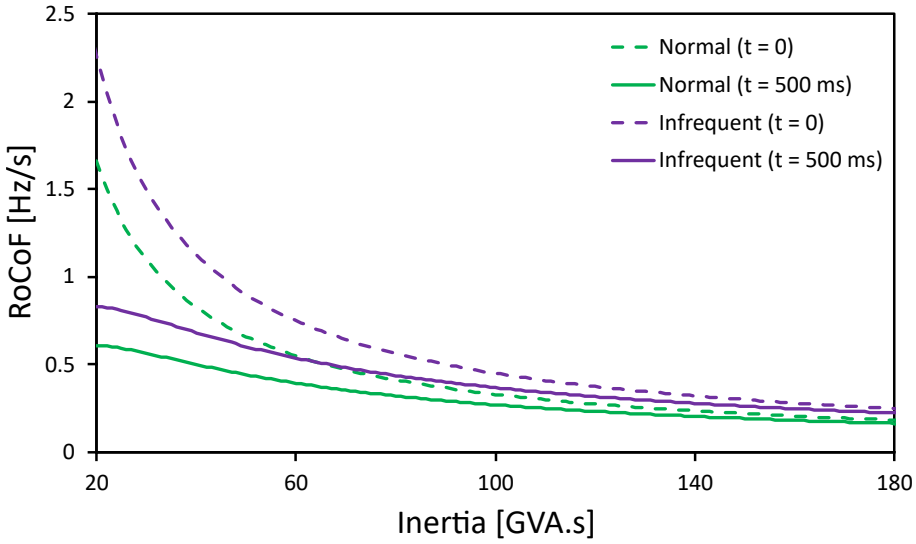

Figure 4.3: Instantaneous RoCoF magnitude at $t = 0$ and delayed RoCoF magnitude at $t = 500\,\text{ms}$ after a *normal* infeed loss and an *infrequent* infeed loss against inertia. The $t = 0$ plots are the same for all demand levels. The $t = 500\,\text{ms}$ plots are for a demand of 80 GW.

might not trip due to the $t = 500\,\text{ms}$ measurement delay. Going forward, it is assumed that the minimum inertia based on the RoCoF requirement is 45 GVA.s. Between 2014 and 2019 we estimate the minimum inertia contribution from demand to be 32 GVA.s and the median to be 55 GVA.s. The demand inertia was less than 45 GVA.s for 20% of the time. From National Grid ESO's Future Energy Scenarios 2019 [166], the minimum predicted nuclear capacity from the 2030s onwards is around half of the current capacity, so around 4 GW. Using the calculation method in Section 3.3.1, the minimum inertia provided by nuclear from the 2030s onwards is roughly 26 GVA.s. If we consider a future scenario where only demand and nuclear generation are providing inertia to the grid, then it is still unlikely that the RoCoF requirement constraint on inertia will be the limiting constraint in the future. The change from $L_{\text{rf}} = 0.125\,\text{Hz}\,\text{s}^{-1}$ to $L_{\text{rf}} = 1\,\text{Hz}\,\text{s}^{-1}$ has future-proofed the system.

Eq. (4.8) tell us that the minimum frequency response capacity needed to ensure the steady-state frequency requirement is met increases

- linearly with decreasing demand,
- linearly with increasing infeed loss magnitude,

- and increases linearly as the steady-state limit gets closer to the nominal frequency.

From Eq. (4.8), it can be seen that if the demand, demand damping level, and steady-state frequency limit remain unchanged, then the difference between the minimum frequency response capacities for a *normal* infeed loss and an *infrequent* infeed loss is equal to the difference in the infeed loss magnitudes. In other words, the grid needs an extra 480 MW of frequency response when an *infrequent* infeed loss occurs compared to when a *normal* infeed loss occurs to reach the same steady-state limit. For example, in the case of a *normal* infeed loss, at a demand of 20 GW, $R_{\text{cap}} \geq 1120\,\text{MW}$ to ensure that the steady-state frequency is not below 49.5 Hz. Whereas for an *infrequent* infeed loss, $R_{\text{cap}} \geq 1600\,\text{MW}$.

As explained in Section 4.4.1, there is not a strict steady-state frequency limit in the case of an *infrequent* infeed loss. To have the same minimum frequency response capacity as the *normal* infeed loss case requires the *infrequent* infeed loss steady-state limit to be

$$\begin{aligned} L^*_{\text{ss}} &= L_{\text{ss}} - \frac{I - I^*}{kD_{\text{n}}} \\ &= 49.5\,\text{Hz} - \frac{480\,\text{MW}}{kD_{\text{n}}}\,. \end{aligned} \tag{4.12}$$

So, for a 20 GW demand, $L^*_{\text{ss}} = 48.3\,\text{Hz}$. This is not acceptable because it is lower than the level at which demand disconnection begins (48.8 Hz). It is also 1.2 Hz below 49.5 Hz, so returning above this frequency level within 60 s would be difficult. For these reasons, based on the steady-state frequency alone, an *infrequent* infeed loss requires more frequency response capacity than a *normal* infeed loss for acceptable frequency conditions to be maintained. From this point on in our investigations, we will set the steady-state limit for an *infrequent* infeed loss to be the same as it is for a *normal* infeed loss $L^*_{\text{ss}} = 49.5\,\text{Hz}$. The frequency must return above 49.5 Hz within 60 s anyway, as stipulated in Ref. [165].

4.5.2 Frequency nadir

Eq. (4.10) tells us that the minimum inertia needed to ensure the nadir requirement is met in the time period before the frequency response starts ramping is proportional to

the frequency response delay time, t_{d}. It is not so obvious what the relationship is with demand and infeed loss magnitude. By using the power series expansion

$$\frac{1}{\ln(1-x)} = -\frac{1}{x} + \frac{1}{2} + \frac{x}{12} + \frac{x^2}{24} + \dots , \tag{4.13}$$

we can write Eq. (4.10) as

$$\mathrm{Min}\, E_{\mathrm{n}} = \frac{-kD_{\mathrm{n}} f_{\mathrm{n}} t_{\mathrm{d}}}{2} \left(-\frac{1}{x} + \frac{1}{2} + \frac{x}{12} + \frac{x^2}{24} + \dots \right), \tag{4.14}$$

where $x = kD_{\mathrm{n}}(L_{\mathrm{nad}} - f_{\mathrm{n}})/I$. Using typical values for the grid parameters (median underlying demand in 2019 = 36.4 GW) we get an order of magnitude estimate for x:

$$\begin{aligned} x &= \frac{kD_{\mathrm{n}}(L_{\mathrm{nad}} - f_{\mathrm{n}})}{I} \\ &\sim \frac{0.02 \times 36400 \times -0.5}{-1320} \\ &\sim 10^{-1} . \end{aligned} \tag{4.15}$$

Due to the fact that x is small, we can ignore higher terms in the power series expansion to get an approximation for the minimum inertia:

$$\mathrm{Min}\, E_{\mathrm{n}} \simeq \frac{f_{\mathrm{n}} t_{\mathrm{d}} I}{2(L_{\mathrm{nad}} - f_{\mathrm{n}})} - \frac{kD_{\mathrm{n}} f_{\mathrm{n}} t_{\mathrm{d}}}{4} . \tag{4.16}$$

Eq. (4.16) tells us that the minimum inertia needed to ensure the nadir requirement is met in the time period before the frequency response starts ramping approximately linearly decreases with demand and approximately linearly increases with infeed loss magnitude.

Table 4.4 shows the minimum inertia for a frequency response delay time of 2 s at a low demand level and a high demand level for a *normal* and *infrequent* infeed loss. At an inertia below 122 GVA.s, the frequency drops below the nadir limit at 2 s after a *normal* infeed loss at a demand level of 20 GW. For example, at 100 GVA.s the frequency reaches 49.402 Hz at $t = 2$ s. The minimum inertia for demand levels between 20 GW and 80 GW can be linearly interpolated given what we know from Eq. (4.16). Also, the

	Normal infeed loss	*Infrequent* infeed loss	
		$L^*_{\text{nad}} = 49.5\,\text{Hz}$	$L^*_{\text{nad}} = 49.2\,\text{Hz}$
20 GW demand	122	170	102
80 GW demand	85.9	136	64.4

Table 4.4: Minimum inertia (in GVA.s) that ensures the frequency stays above the nadir limit (in the time period before the frequency response starts ramping). The values in the table are for a frequency response delay time of 2 s.

minimum inertia for other frequency response delay times can be easily calculated given the proportionality between delay time and minimum inertia (e.g. a delay time of 1 s, would half all the values in Table 4.4).

For a delay time of 2 s, if the nadir limit for an *infrequent* infeed loss is 49.5 Hz (i.e. the same as the *normal* infeed loss nadir limit), then the minimum inertia is higher by roughly 50 GVA.s compared to its value for a *normal* infeed loss (all other parameters being equal). For a delay time of 2 s, if the nadir limit for an *infrequent* infeed loss is 49.2 Hz, then the minimum inertia is lower by roughly 20 GVA.s compared to its value for a *normal* infeed loss (all other parameters being equal).

From Table 4.4 we can see that for the minimum inertia to be the same for a *normal* and *infrequent* infeed loss, the nadir limit for an infrequent infeed loss must be between 49.5 Hz and 49.2 Hz. The exact value is

$$\begin{aligned} L^*_{\text{nad}} &= \frac{I^*(L_{\text{nad}} - f_{\text{n}})}{I} + f_{\text{n}} \\ &= \frac{-1800\,\text{MW}(49.5\,\text{Hz} - 50\,\text{Hz})}{-1320\,\text{MW}} + 50\,\text{Hz} \\ &= 49.318\,\text{Hz}\,. \end{aligned} \tag{4.17}$$

This result holds for all demand levels and frequency response delay times.

Additionally, it is possible to rearrange Eq. (4.10) and consider it a nadir requirement constraint on frequency response delay time. At a certain inertia level, there will be a maximum delay time. If the delay time is higher than this maximum, then the nadir limit will be reached before the frequency response has started ramping. Let us consider the

minimum inertia based on the RoCoF requirement: 45 GVA.s. At 20 GW, the maximum frequency response delay time is 0.74 s after a *normal* infeed loss (or an *infrequent* infeed loss with the nadir limit at 49.318 Hz). At 80 GW, the maximum frequency response delay time is 1.05 s.

Let us now consider the time period during which the frequency response ramps from zero to full capacity. Eq. (4.11), the nadir requirement constraint on frequency response parameters, allows us to calculate the values of the frequency response parameters that ensure the frequency reaches, but does not breach, the frequency nadir in the ramping time period. As mentioned before, assuming that the solution of Eq. (4.11) is above the minimum R_{cap} determined from Eq. (4.8), then the solution to Eq. (4.11) is the absolute limit (i.e. minimum frequency response capacity, maximum delay time, and maximum ramp time) for the particular frequency response parameter being solved for.

We begin by calculating the ramp times and delay times necessary to ensure the nadir requirement is met with a fixed frequency response capacity. The frequency response capacity chosen is the minimum determined by the steady-state requirement constraint on frequency response capacity, Eq. (4.8). This choice was made because it represents a grid that is utilising higher speeds of response rather than just simply adding capacity. Another way of putting it is that it represents a grid that has changed from a relatively slow frequency response provider (CCGT) to a fast frequency response provider (batteries), but has not added extra capacity. It will give us a good idea of just how low the delay time and ramp time may need to go in the future as inertia levels decrease. Earlier in Section 4.5.1 it was determined that at 20 GW and with $L_{\text{ss}} = L^*_{\text{ss}} = 49.5$ Hz, $\min R_{\text{cap}} = 1120$ MW for a *normal* infeed loss and $\min R_{\text{cap}} = 1600$ MW for an *infrequent* infeed loss. At 80 GW, $\min R_{\text{cap}}$ is 520 MW and 1000 MW for a *normal* and *infrequent* loss, respectively.

Fig. 4.4 shows the ramp time necessary to ensure the nadir requirement is met after a *normal* and *infrequent* infeed loss at 20 GW and 80 GW against inertia. The frequency response capacities are given at the end of the previous paragraph. On the left of Fig. 4.4 are the ramp times when the delay time is 0.5 s, and on the right are the ramp times when the delay time is as long as it can possibly be, 2 s, according to the Grid Code [162]. 0.5 s

was chosen because this is currently the speed for the fastest acting response in GB: EFR and Dynamic Containment. Marked on the graphs is the minimum inertia based on the RoCoF requirement, which is 45 GVA.s. It should be noted that in Fig. 4.4 the nadir limit for a *normal* infeed loss is $L_{\text{nad}} = 49.5\,\text{Hz}$, as given in Table 4.3, whereas the nadir limit for an *infrequent* infeed loss is $L^*_{\text{nad}} = 49.318\,\text{Hz}$. This nadir limit for an *infrequent* infeed loss was chosen based on the discussion leading up to Eq. (4.17).

The first thing to note is that the frequency response ramp times seem to be linear with inertia (at least between $t_{\text{r}} = 0$ and $t_{\text{r}} = 8$). This will be further explored later and in Appendix B.3. The ramp times are very similar for both magnitudes of infeed loss at 20 GW, but not at 80 GW (where the ramp times are higher for an *infrequent* loss). This is due to the choice of setting the nadir limit lower for an *infrequent* infeed loss. If the nadir limit was the same for both magnitudes of loss, then the ramp times would need to be quicker for an *infrequent* infeed loss. The ramp times are much shorter at 20 GW than 80 GW because there is less of a contribution from demand damping. With the frequency at 49.5 Hz, at 20 GW demand damping offers 200 MW of response contribution, whereas at 80 GW it offers 800 MW.

We can see from Fig. 4.4 that the ramp times need to be much shorter when the delay time is 2 s compared to when it is 0.5 s. In fact, when the delay time is 2 s the minimum inertia that can be reached is 122 GVA.s and 86 GVA.s for 20 GW and 80 GW, respectively. At these values the ramp time is almost zero. Below these values, the nadir limit would be breached before the frequency response has started ramping. In contrast, with a delay time of 0.5 s the ramp time ranges between 0.47 s and 1.44 s at an inertia equal to the minimum (45 GVA.s) based on the RoCoF requirement. These ramp times are similar to the ramp times required for the EFR and Dynamic Containment service and are definitely achievable with many technologies (e.g. batteries).

As mentioned above, I now move on to explore the linear relationship between delay time, ramp time, and inertia. This is discussed here and in more detail in Appendix B.3.

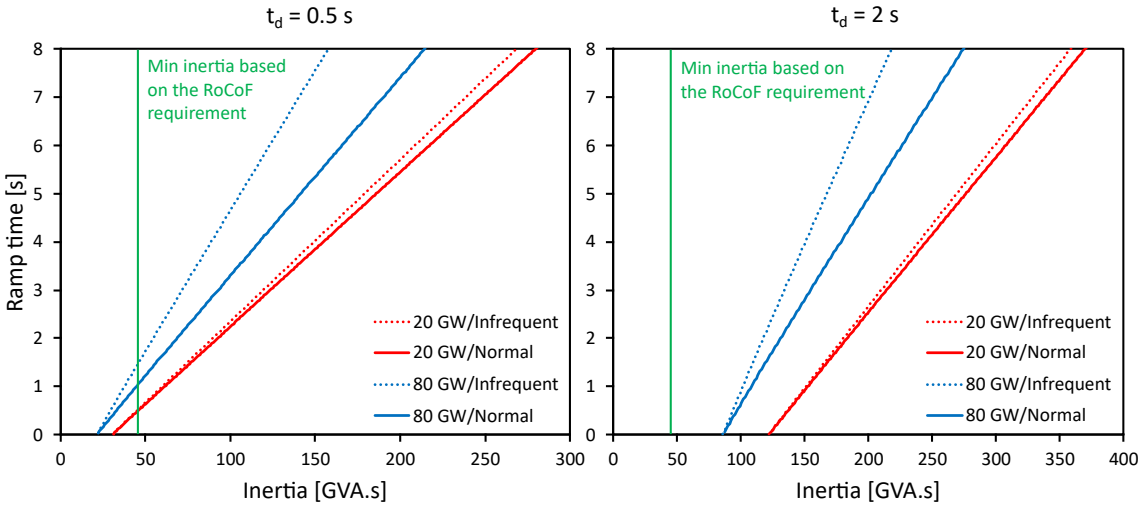

Figure 4.4: Ramp time necessary to ensure the nadir requirement is met after a large infeed loss against inertia for different delay times, demand, and loss magnitudes. On the left is the case where the response delay time is 0.5 s, and on the right is the case where the response delay time is 2 s.

Applying a linear fit to the ramp time for a *normal* infeed loss at 20 GW we get

$$\begin{aligned} t_\mathrm{r} &= \alpha_1 + \beta_1 E_\mathrm{n} \quad \text{for } t_\mathrm{d} = 0.5\,\mathrm{s}\,, \\ t_\mathrm{r} &= \alpha_2 + \beta_2 E_\mathrm{n} \quad \text{for } t_\mathrm{d} = 2\,\mathrm{s}\,, \end{aligned} \tag{4.18}$$

where $\alpha_1 = -0.96\,\mathrm{s}$, $\alpha_2 = -3.90\,\mathrm{s}$, $\beta_1 = 0.032\,\mathrm{GVA}^{-1}$, and $\beta_2 = 0.032\,\mathrm{GVA}^{-1}$. This suggests that $t_\mathrm{r} = -2t_\mathrm{d} + 0.032E_\mathrm{n}$ at 20 GW (with the appropriate units). This equation approximately holds for an *infrequent* infeed loss as well because at 20 GW, t_r is the same for both magnitudes of infeed loss except for a factor of 1.05. In Appendix B.3 we prove the linear relationship for a demand of 20 GW. The situation is more complicated at 80 GW, as explained in Appendix B.3.

The frequency response capacity was fixed in Fig. 4.4 at the minimum determined by the steady-state requirement constraint on frequency response capacity. At 20 GW and with $L_\mathrm{ss} = L^*_\mathrm{ss} = 49.5\,\mathrm{Hz}$, $\min R_\mathrm{cap} = 1120\,\mathrm{MW}$ for a *normal* infeed loss and $\min R_\mathrm{cap} = 1600\,\mathrm{MW}$ for an *infrequent* infeed loss. At 80 GW, $\min R_\mathrm{cap}$ is 520 MW and 1000 MW for a *normal* and *infrequent* loss, respectively. We now investigate how delay and ramp times can be relaxed by allowing the frequency response capacity to increase (the minimum is

still set by the steady-state requirement constraint). Fig. 4.5 shows the frequency response capacity necessary to ensure the nadir requirement is met after a *normal* and *infrequent* infeed loss ($L^*_{\text{nad}} = 49.318\,\text{Hz}$) at 20 GW and 80 GW against inertia. On the left of Fig. 4.5 is the case where the delay and ramp time are both 0.5 s (EFR and Dynamic Containment), and on the right is the case where the delay time is 1 s and the ramp time is 4 s. This response speed is representative of the fastest response possible from traditional forms of generation (e.g. CCGTs, coal).

At the minimum inertia based on the RoCoF requirement (45 GVA.s), with a 0.5 s/0.5 s delay/ramp time the frequency response capacity does not need to increase beyond the minimum (based on the steady-state requirement constraint) at a demand of 80 GW. It is almost the same case at a demand of 20 GW: at 45 GVA.s, only 60 MW and 8 MW of extra capacity are needed for a *normal* and *infrequent* infeed loss, respectively. Note, past 45 GVA.s (for *normal* loss) and 30 GVA.s (for *infrequent* loss), the required response capacity increases very rapidly.

The case is very different with a 1 s/4 s delay/ramp time. Using Eq. (4.10) we know that the minimum inertia for a delay time of 1 s is 61 GVA.s at a demand of 20 GW and 43 GVA.s at a demand of 80 GW. This is the same for a *normal* and *infrequent* infeed loss because we have chosen $L^*_{\text{nad}} = 49.318\,\text{Hz}$. Fig. 4.5 shows us that the practical inertia limit at 1 s/4 s delay/ramp time is even higher. $R_{\text{cap}} = 5000\,\text{MW}$ is considered to be the practical limit because this is five times greater than current frequency response capacity levels. At 20 GW, the minimum inertia is around 100 GVA.s and at 80 GW it is around 55 GVA.s. The level of inertia at which the frequency response capacity starts being greater than the minimum (based on the steady-state requirement constraint) is approximately 180 GVA.s at 20 GW, 140 GVA.s at 80 GW (*normal* loss), and 110 GVA.s at 80 GW (*infrequent* loss).

Fig. 4.6 shows the frequency evolution after an *infrequent* infeed loss at an inertia of 70 GVA.s and a demand of 80 GW. The two different frequency evolutions are due to different types of frequency response. One is *fast response*, where $R_{\text{cap}} = 1000\,\text{MW}$, the lowest it can be. To fulfil the nadir requirement, this response must be fast: $t_{\text{d}} = 0.5\,\text{s}$

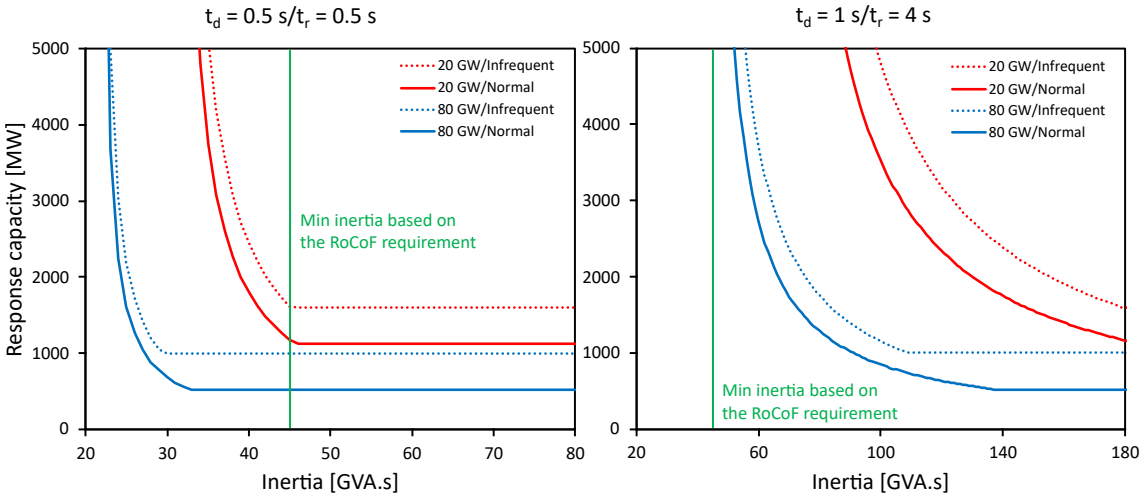

Figure 4.5: Frequency response capacity necessary to ensure the nadir requirement is met after a large infeed loss against inertia for different delay and ramp times, demand, and loss magnitudes. On the left is the case where the response delay time is 0.5 s and the ramp time is 0.5 s, and on the right is the case where the response delay time is 1 s and the ramp time is 4 s.

and $t_r = 2.9$ s. The second is *increased response capacity*, where $R_{cap} = 2374$ MW. This increase in response capacity relaxes the speed requirements of the response: $t_d = 1$ s and $t_r = 4$ s. However, an issue with having a large amount of response capacity is that the frequency overshoots in recovery. This issue can be mitigated by having a large proportion of the response capacity as dynamic response: response that is proportional to the frequency deviation. In the *fast response* case, after the nadir the frequency rises to the steady-state limit (49.5 Hz). For a full recovery back to 50 Hz, additional response would be required (e.g. manually instructed reserve).

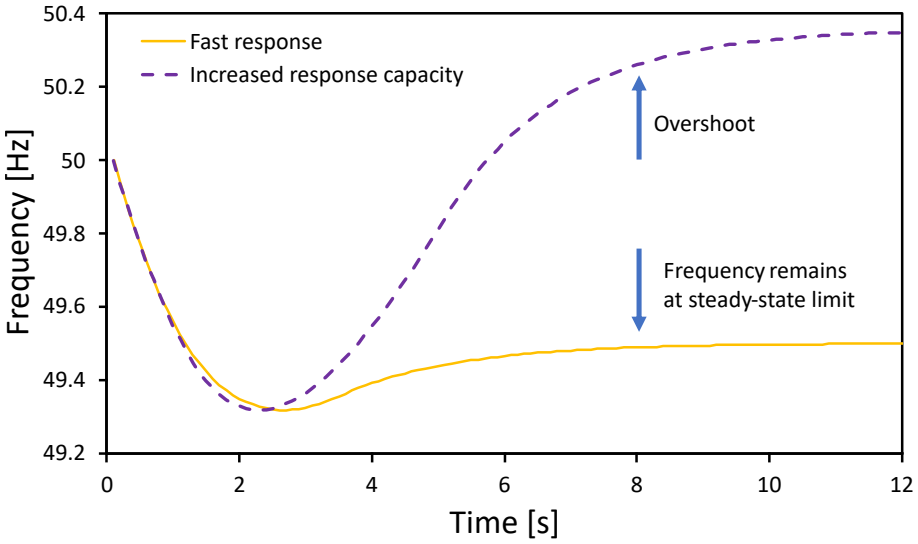

Figure 4.6: Frequency evolution after an *infrequent* infeed loss at 70 GVA.s and 80 GW. *Fast response*: $R_{\text{cap}} = 1000\,\text{MW}$, $t_{\text{d}} = 0.5\,\text{s}$, and $t_{\text{r}} = 2.9\,\text{s}$. *Increased response capacity*: $R_{\text{cap}} = 2374\,\text{MW}$, $t_{\text{d}} = 1\,\text{s}$, and $t_{\text{r}} = 4\,\text{s}$.

4.6 Conclusions

In this section, I first return to the research questions set out in the introduction to this chapter and discuss the extent to which each have been answered. Then, in Section 4.6.1, I present the highlights of the results of the chapter. Key findings of this chapter will be discussed within a wider context in Chapter 6.

What are the future frequency response requirements of the GB grid, in terms of capacity and speed, to secure the grid against a large infeed loss in different inertia and demand scenarios?

To secure the GB grid in the future, for all potential infeed loss, demand, and inertia scenarios, 1600 MW of frequency response at a delay/ramp time of 0.5 s/0.5 s is needed. There is already some capacity of this response speed on the GB grid (EFR and Dynamic Containment), but far less than 1600 MW. At certain times, when the inertia and demand levels are more favourable, slower response speeds are possible. However, as a general rule, the slower the response speed, the more capacity required. 1600 MW of frequency response at a delay/ramp time of 0.5 s/0.5 s would secure the grid against large infeed losses occurring if the inertia profile was the same as the CR30H0-75% profile from Chapter 5

(inertia only around 20% of current levels and only provided by nuclear and demand). For the above to hold, the nadir limit for an infrequent infeed loss would need to be set at 49.318 Hz, which is well above the 48.8 Hz demand disconnection level.

With the constraint of maintaining acceptable frequency conditions after a large infeed loss, is there a simple mathematical relationship between the grid parameters (e.g. inertia and frequency response speed)?

I have derived simple linear relationships between minimum inertia and other grid parameters in certain cases. The minimum inertia needed to ensure the nadir requirement is met in the time period before the frequency response starts ramping approximately linearly decreases with demand and approximately linearly increases with infeed loss magnitude. Also, at a fixed frequency response capacity and at a low demand, the frequency response ramp time required to ensure the nadir requirement is met is linear with inertia (and delay time).

4.6.1 Highlights of the results

The highlights of the results from this chapter are listed below. The specific values relate to the GB grid:

- At a RoCoF limit of $L_{\text{rf}} = 1\,\text{Hz}\,\text{s}^{-1}$, the minimum inertia based on the RoCoF requirement is 45 GVA.s. It is unlikely that the inertia level of the GB grid will be lower than this in the future, so the change in RoCoF relay limits from $0.125\,\text{Hz}\,\text{s}^{-1}$ to $1\,\text{Hz}\,\text{s}^{-1}$ has future-proofed the system.
- At 45 GVA.s, to prevent unacceptable frequency conditions, the maximum frequency response delay time is less than 1 s
- Based on our results, it is suggested that the steady-state limit for an *infrequent* infeed loss should be 49.5 Hz and the nadir limit should be 49.318 Hz.
- At a given frequency response capacity, low demand level, and imbalance magnitude, the frequency response ramp time and delay time which ensure the nadir limit is not breached is linear with inertia

- At frequency response delay/ramp times of 0.5 s/0.5 s, frequency response capacities do not need to increase beyond 1600 MW even at minimum inertia (45 GVA.s) and low demand (20 GW).

Chapter 5

Case studies into frequency volatility

5.1 Introduction

In the previous chapter the focus was on frequency dynamics after a large infeed loss. In this chapter the scope of my analysis is broadened with three case studies of frequency volatility, two of which are focused on much longer timescales. By building on the frequency response modelling to make it more accurate, I am able to simulate more than just a single isolated large infeed loss.

The aims of this chapter are to further the understanding of large infeed loss events, analyse the effect of inertia and frequency response characteristics on long-term frequency volatility, and analyse the efficacy of new frequency response services. The first aim of this chapter utilises the case study of the 9th August 2019 low frequency event in Great Britain to better understand real large infeed loss events. The second aim is to use data from November 2018 to calculate the underlying grid imbalance of that month and then use that imbalance in simulations where inertia and frequency response are varied. Estimates of reduced inertia profiles in future scenarios (i.e. November 2030) are provided. Similar methods are used in the third case study, which discusses the newly proposed frequency response services in Great Britain.

This chapter addresses the following research questions within the three case studies:

- 9th August 2019 low frequency event
  - **If the frequency response was faster or RoCoF relays were not triggered, could demand disconnection have been prevented?**
  - **What effect would a different inertia, demand, and demand damping have had on the frequency profile?**
- Frequency volatility over a month in current and future scenarios
  - **How do frequency response characteristics (capacity and speed) affect normal day-to-day frequency volatility?**
  - **In which future scenarios does the normal day-to-day frequency volatility become unacceptable and what needs to change in frequency response provision to mitigate this?**
- New frequency response services
  - **What is the efficacy of the proposed new frequency response services compared with the existing frequency response services in current and future scenarios?**

Section 5.2 explains the method used for modelling frequency response and provides justifications for the assumptions and approximations made in this chapter. The frequency response model is part of a grid model that is used throughout the chapter in all three case studies. Section 5.3 utilises the grid model (with a few additions) to answer the two research questions related to the 9th August 2019 low frequency event. Section 5.4 explains the method for calculating the underlying grid imbalance profile over a month-long period. The method for producing future reduced inertia scenarios is also explained. Section 5.5 presents the results of month-long simulations in current and future scenarios, which address the two associated research questions. Section 5.6, explains the modelling of the new services and similar month-long simulations as in Section 5.5 are performed

to address the research question related to new frequency response services. Section 5.7 concludes the chapter and includes a list of the highlights of the results.

5.2 Modelling frequency response

In GB, there are four main types of frequency response service. Their exact nature and aims are presented in Table 5.1. Primary, secondary, and high frequency response are either dynamic or static: dynamic frequency response is the continuous provision of proportional response as the frequency changes, and static frequency response is a discrete service activated when the frequency passes a defined value. EFR is a relatively new dynamic service, which is much faster acting than the other dynamic services. In 2016, National Grid ESO procured 200 MW of EFR via a tender exercise [69], and all of the contracts were awarded to batteries. By summer 2018, all contracts were delivering their contracted volume.

In the GB grid model developed here, frequency response is modelled continuously and more accurately compared to the one-off linear ramp used in the previous chapter (Fig. 4.1). The GB grid model was created in MATLAB Simulink, and screenshots of the model can be found in Appendix C. In the model, there are three frequency response services: EFR, low frequency response (LFR), and high frequency response (HFR). Static frequency response is ignored, so all response is dynamic. LFR acts when the frequency

Frequency response service	Speed and duration	Aim
Primary	Delivered within 10 s and sustained for a further 20 s	To contain a falling frequency when $f < 50$ Hz
Secondary	Delivered within 30 s and sustained for a further 30 min	To restore frequency back to 50 Hz when $f < 50$ Hz
High	Delivered within 10 s and sustained indefinitely	To contain and restore frequency back to 50 Hz when $f > 50$ Hz
Enhanced	Delivered within 1 s and sustained for 15 min	To provide fast response either side of 50 Hz (symmetric service)

Table 5.1: GB frequency response services [69, 162].

goes below 50 Hz and HFR acts when the frequency goes above 50 Hz. LFR is the combination of the primary and secondary frequency response service.

EFR, LFR, and HFR have the following characteristics: deadband, delay time (t_{d}), response profile, ramp rate, and capacity (EFR_{cap}, LFR_{cap}, and HFR_{cap}). The process of calculating the frequency response output at each time step is shown in Fig. 5.1. The frequency deviation is the input into the process each time step. The frequency deviation input is delayed by the frequency response delay time. This is because, in reality, every response technology has a delay due to the time taken to process the measurement of the frequency deviation (although in the case of some technologies this is very short indeed e.g. batteries [97]). If the frequency deviation is within the deadband then there is no frequency response output. However, if the frequency deviation is outside of the deadband then the response is calculated based on the response profile. The deadband for every service is set to 0.015 Hz. For each magnitude of deviation there is a required frequency response power output. The response profiles for EFR, LFR, and HFR are linear, with the maximum frequency response output at a ± 0.5 Hz deviation. This is to match the definition of primary, secondary, and high frequency response capability values found in the GB Grid Code [162] and to match the EFR delivery envelope [69]. The EFR profile is symmetrical whereas the LFR and HFR profiles are asymmetrical. The required frequency response output calculated from the response profile is not necessarily the actual output. Response technologies are also limited by how quickly they can ramp up or down. The required output calculated from the response profile becomes the target to aim for in a particular time step. The response endeavours to meet it but is limited by the ramp rate. The ramp rate limit applies to both upwards and downwards ramps. The total frequency response output of a grid, R, is the sum of the three types of response: EFR, LFR, and HFR.

Frequency response is modelled as described above to match the minimum requirements for frequency response as set out in the GB grid code [162] and the EFR delivery envelope [69]. Modelling frequency response in this way produces results for a worst-case scenario. In reality, some frequency response is delivered via governor action, which might act quicker than the frequency response modelled here and have slightly different dynam-

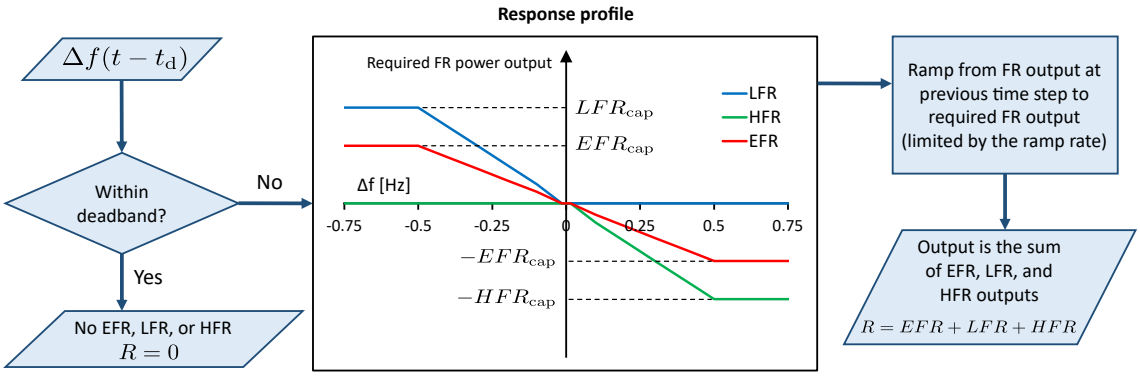

Figure 5.1: Process for calculating frequency response output in the GB grid model.

ics (see Section 2.5.3). Also, frequency response from governor action will vary slightly between different generators across the grid depending on their individual droop control settings.

In the grid model described above, primary and secondary frequency response have been combined into a single service, LFR, that acts when the frequency goes below 50 Hz. Secondary frequency response is only required for 30 min but it is unclear how the units providing this service ramp down. Therefore, the LFR service in my model acts indefinitely, as long as the frequency is on the low side of 50 Hz and outside of the deadband. This approximation is justified because frequency deviations outside of the low frequency deadband have a median duration of 11 s in the time period 2014–2019 and excursions lasting over 30 min were extremely rare (0.2% of deadband excursions on the low side). With the 2014–2019 frequency data as an input, the modelled LFR service would act for the same length of time as the real secondary frequency response service would in the overwhelming majority of cases.

Synthetic inertia is considered in this grid model and is based on the definition in Ref. [57]: *synthetic inertia is defined as the controlled contribution of electrical torque from a unit that is proportional to the RoCoF at the terminals of the unit.* Synthetic inertia is a symmetric service and has a delay time of 0.2 s and ramp time of 0.2 s and is proportional to RoCoF rather than frequency deviation. The response profile for synthetic inertia is similar to that presented in Fig. 5.1 but with $\mathrm{Hz\,s^{-1}}$ on the x axis (instead of Hz) and maximum capacity reached when RoCoF $= \pm 0.05\,\mathrm{Hz\,s^{-1}}$.

5.2.1 Comparison with linear approximations

Here, the grid model presented in Section 5.2 and the simple linear ramp model of frequency response described in Fig. 4.1 are compared. Fig. 5.2 shows the frequency after a *normal* infeed loss (−1320 MW) with the demand at 20 MW and the inertia at 140 GVA.s. The delay time is 1 s for both the linear and dynamic response. The ramp time is 4 s for the linear response and the ramp rate is $LFR_{\text{cap}}/4$ for the dynamic response i.e. they are equivalent. Using our analysis in the previous chapter (Fig. 4.5), we know that $R_{\text{cap}} = 1771$ MW for the frequency nadir to be 49.5 Hz. We set $LFR_{\text{cap}} = 1771$ MW as well to have a direct comparison of the two ways of modelling frequency response (it should be noted that the deadband has been removed from the LFR model to simply compare the dynamic nature of the response vs linear ramping). Fig. 5.2 shows that the two frequency profiles are identical until the frequency starts to recover from the nadir. This is because LFR is dynamic and therefore the response power reduces as the frequency recovers. This can be seen in Fig. 5.2 because the frequency response power output is also plotted. What this shows is that for large infeed loss analysis, a simple linear ramping model of frequency response is as accurate as a more realistic model. However, when modelling long-term frequency volatility, the grid model described in Section 5.2 and Fig. 5.1 is necessary.

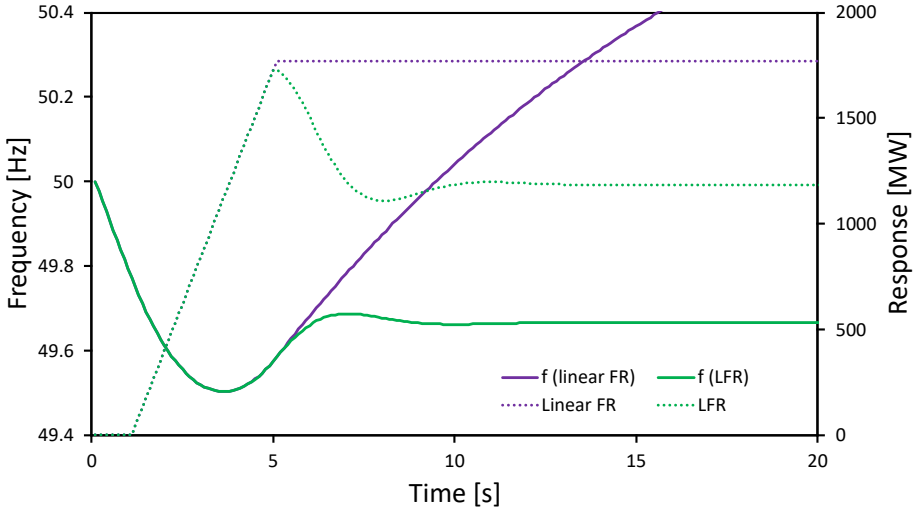

Figure 5.2: A comparison of the frequency profile after a *normal* infeed loss with the frequency modelled as in Fig. 4.1 (linear ramp) and modelled as described in Section 5.2 (dynamic response). Also shown, in dashed lines, is the response power output.

5.3 9th August 2019 low frequency event

5.3.1 Background

At 16:52 on 9th August 2019, a series of events led to a large frequency disturbance on the GB grid and resulted in one million users losing power plus significant rail travel disruption. Lightning strikes caused the unexpected simultaneous loss of Hornsea offshore wind farm, some embedded generation on vector shift protection, and a steam turbine at Little Barford CCGT plant. The cumulative loss of generation caused the frequency to rapidly fall and this triggered further embedded generation losses due to RoCoF protection. Frequency response arrested the fall and the frequency briefly stabilised until one of the gas turbines at Little Barford tripped and the frequency fell again and eventually reached 48.8 Hz: the point at which some demand is disconnected to protect the grid. This demand disconnection coupled with the activation of further reserves ensured the frequency recovered to 50 Hz within 5 min of the event start.

Most of the specific details about the event are from National Grid ESO's report on the event [130] and the appendices to that report [159].

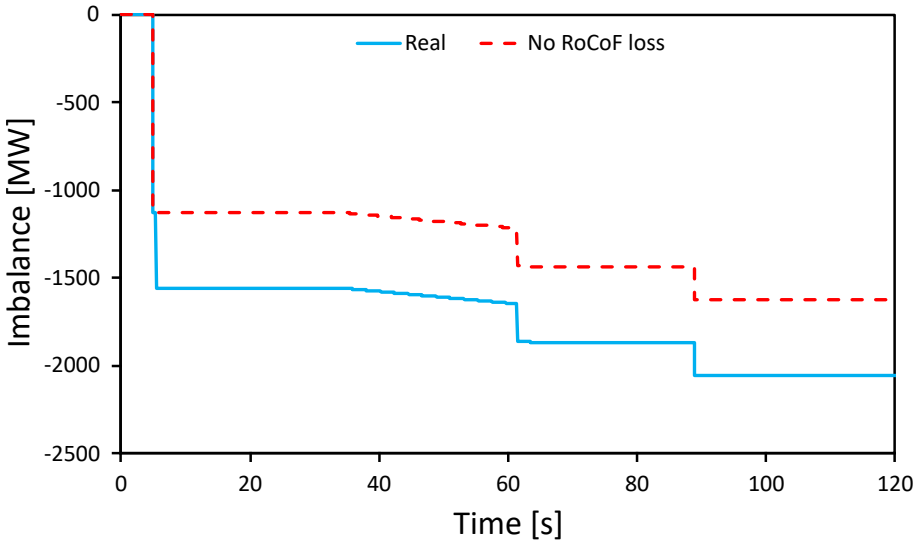

Figure 5.3: Imbalance profile of the 9th August event (for the first 2 min). Shown in the figure is the real profile (blue) and also the profile that would have occurred had no embedded generation been lost due to RoCoF protection relays (red dashed).

5.3.2 Modelling the event

Fig. 5.3 shows the imbalance profile of the event (for the first 2 min) and the profile that would have occurred had no embedded generation been lost due to RoCoF protection relays. At 16:52 ($t = 5$ s in the figure), a sudden imbalance of -1131 MW occurred. This was made up of losses at Hornsea wind farm (737 MW), Little Barford steam turbine (244 MW), and embedded generation losses due to vector shift protection (150 MW). Half a second later, 430 MW was lost due to RoCoF protection on embedded generation. This is why the *No RoCoF loss* profile in Fig. 5.3 is the same as the *Real* profile but just translated upwards by 430 MW after 0.5 s. Between 30 s and 60 s after the start of the event, there was a 100 MW ramp down (estimated linear) of generation. 56.5 s after the start of the event, one of the gas turbines at Little Barford tripped and 210 MW was lost. The other gas turbine tripped roughly 30 s later resulting in a 187 MW loss and a total cumulative imbalance of -2058 MW.

The two imbalance profiles in Fig. 5.3 are used for simulations of the event. The grid model described in Section 5.2 is used for the event simulations with the following additions for this specific event:

- Additional imbalances that were frequency dependent: at 49 Hz, 200 MW of generation was lost due to protection settings, and at 48.8 Hz, 350 MW of demand was disconnected under the low frequency demand disconnection scheme. These imbalances are triggered at those frequencies within the model.

- Static response is activated at 49.6 Hz. Static response is modelled as a linear ramp with no delay and a 1 s ramp time.

- Additional secondary frequency response modelled as a linear ramp from 10 s to 30 s

- Recovery actions modelled as a linear ramp 80 s after the start of the event

To accurately simulate the event, the values used for various parameters were chosen to match reality. Table 5.2 shows the values used for different frequency response capacities and other power flow parameters at the time of the event. Fig. 5.4 shows the contributions from different technologies delivering frequency response during the first 10 s of the 9th August event. This was estimated using Mandatory Frequency Response and Firm Frequency Response holding volumes [160] and then discerning the technology types by using the Balancing Mechanism Unit ID [161]. This was the same method as was used in Section 3.4. Note the high percentage of batteries and demand side flexibility. Had the event occurred 10 years ago, these two technologies would not have featured at all. This is good evidence that new technologies are positively assisting the grid.

Table 5.3 shows the values used for the underlying demand and inertia. The demand value was calculated using the same method as in Section 3.2.1 and the inertia value was from the appendices of National Grid ESO's report into the event [159]. The three highest generation types supplying the 35.9 GW of demand were wind (11 056 MW), CCGTs (8399 MW), and nuclear (6154 MW).

Now there are only two unknown parameters left to estimate for the modelling: the value of the demand damping constant (k), and the ramp rate of the recovery actions. Fig. 5.5 shows the real frequency trace and the simulated trace with $k = 1.65\,\%\text{MW/Hz}$ and the recovery action ramp rate at $8\,\text{MW}\,\text{s}^{-1}$. This value of k was chosen so that the first nadir of the simulation was as close as possible to reality and the ramp rate was chosen so

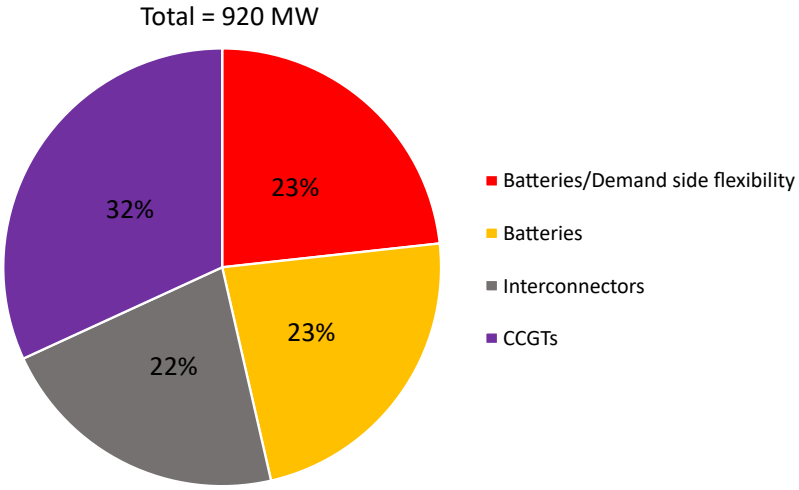

Figure 5.4: The contributions from different technologies delivering frequency response during the first 10 s of the 9th August event (estimated).

Parameter	Value [MW]
EFR	213
Dynamic LFR	484
Static frequency response	222
Extra SFR	241
Generation loss at 49.0 Hz	-200
Demand disconnection at 48.8 Hz	350
Recovery actions	1240

Table 5.2: Frequency response capacities and other parameters in the *real sim* simulation of the 9th August event [130].

that the simulation trace after ~ 100 s was as close as possible to reality. Table 5.4 shows the key properties of the real and simulated frequency trace. The initial RoCoF magnitude is the average RoCoF magnitude over the first 0.5 s after the start of the event. The initial RoCoF of the simulation is a bit lower than the real initial RoCoF. However, both are greater in magnitude than 0.125 Hz s^{-1}, which is the limit of some RoCoF protection relays in embedded generation. This is why 430 MW of embedded generation was lost at the start of the event.

Parameter	Value
Underlying demand	35.9 GW
Grid inertia	217 GVA.s

Table 5.3: Underlying demand and inertia values in the *real sim* simulation of the 9th August event.

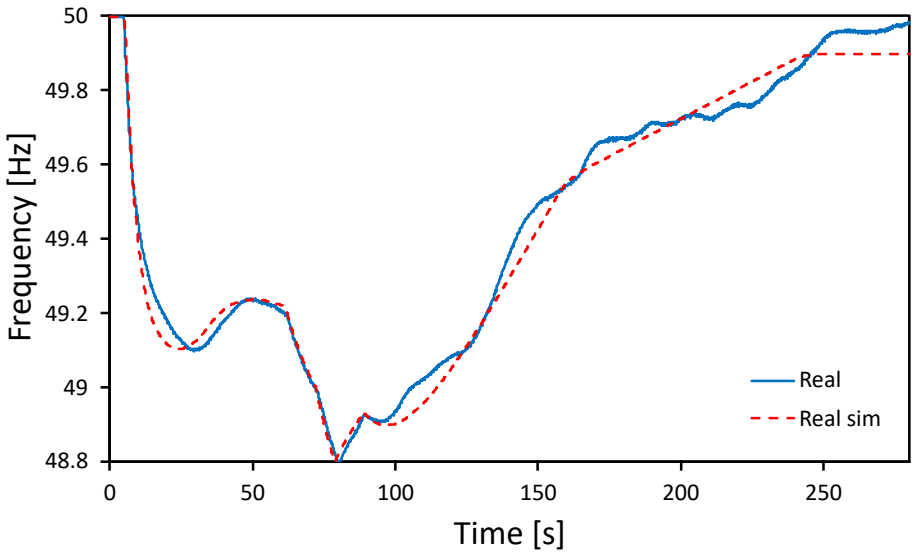

Figure 5.5: The real and simulated (*real sim*) frequency trace of the 9th August event.

5.3.3 Investigations

In this section, the grid model is used to investigate the event in more detail in order to help answer some of the research questions posed in the introduction to this chapter. The parameters used are exactly the same as the previous section unless otherwise mentioned.

Fig. 5.6 shows the frequency with the two different imbalance profiles from Fig. 5.3 and three different inertia levels: 100 GVA.s, 217 GVA.s, and 350 GVA.s. The reason for choosing these three levels is explained as follows. The frequency trace at 217 GVA.s and full imbalance is the same as the *real sim* trace. 217 GVA.s is the amount of inertia on

	Initial RoCoF [Hz s^{-1}]	First nadir [Hz]	Lowest nadir [Hz]
Real	-0.235	49.104	48.790
Real sim	-0.128	49.103	48.798

Table 5.4: Key properties of the real and simulated frequency trace.

the grid at the time of the real event. In 2018, the inertia was higher than this amount for 80% of the time, and in 2018, for 75% of the time, the inertia was lower than 350 GVA.s. 100 GVA.s is a level of inertia that is lower than has ever been reached so far on the grid but could become the norm in the future as the penetration of wind and solar increases.

As mentioned before, 430 MW of embedded generation was lost due to RoCoF protection relays being triggered with an initial RoCoF higher than their $0.125\,\mathrm{Hz\,s^{-1}}$ setting. At an inertia of 223 GVA.s, just 2.8% higher than the real inertia at the start of the event, the initial RoCoF is $0.1246\,\mathrm{Hz\,s^{-1}}$. This means that the inertia on the 9th August at 16:52 was very close to being high enough to prevent embedded generation loss from RoCoF protection relays. We can see from Fig. 5.6 that without this RoCoF loss, the frequency does not reach levels low enough to cause demand disconnection (this occurs when $f < 48.8\,\mathrm{Hz}$). The lowest frequency reached is the first nadir with the inertia at 100 GVA.s: 49.303 Hz. The initial RoCoF at this inertia is $0.273\,\mathrm{Hz\,s^{-1}}$, which is over the $0.125\,\mathrm{Hz\,s^{-1}}$ limit, so without a change to the RoCoF limits this would, in reality, result in embedded generation losses. Referring back to Section 2.7.2, this RoCoF magnitude would not trigger relays on the new setting of $1\,\mathrm{Hz\,s^{-1}}$.

The difference between the frequency traces in Fig. 5.6 at different inertia levels is quite pronounced with the full imbalance. The higher inertia (350 GVA.s) does not prevent demand disconnection with the frequency reaching 48.8 Hz about 10 s later than in *real sim.* At 100 GVA.s, the frequency falls so fast (initial RoCoF is $0.273\,\mathrm{Hz\,s^{-1}}$) at the start that the frequency response cannot prevent 48.8 Hz being breached within 10 s of the start of the event. The lower inertia speeds up the recovery after the first nadir and the final recovery at the end. Even at 100 GVA.s, the frequency does not fall lower than 48.794 Hz, so although the lower inertia hastens the sequence of negative consequences of the event, it does not increase their severity.

On the left of Fig. 5.7 are three frequency traces for different simulations in which the composition and capacity of frequency response is varied. In the *100% EFR* simulation, all of the frequency response (1160 MW) has the characteristics of EFR. Basically this is investigating the effect of having much faster frequency response. In the *more FR capacity*

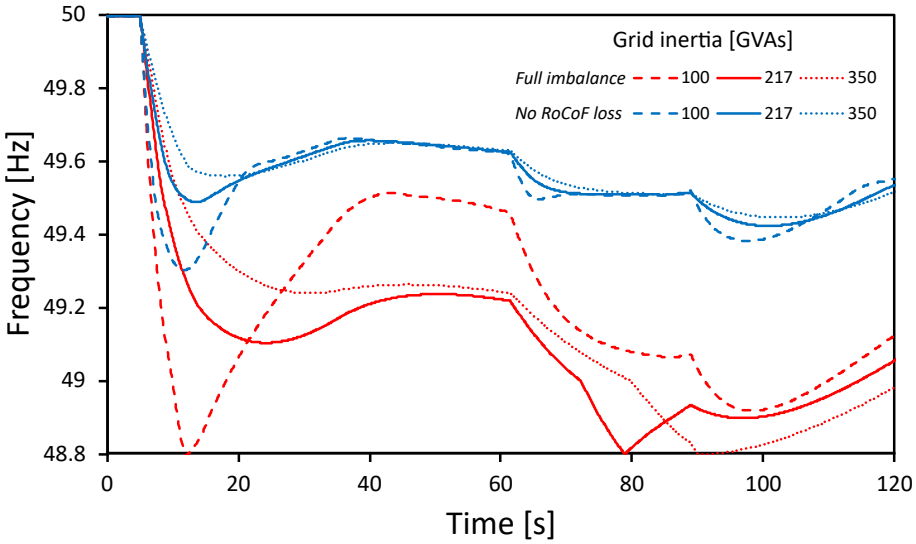

Figure 5.6: The effect of different inertia levels on the frequency with the full imbalance and an imbalance profile without the 430 MW loss of embedded generation from RoCoF protection. Note: 217 GVA.s with the full imbalance is the same as *real sim*.

simulation, the capacity of dynamic LFR is increased from 484 MW to 635 MW. On the right hand side of Fig. 5.7 is the frequency response power output profile of these three simulations.

The initial RoCoF is the same for each simulation because frequency response does not respond within 0.5 s in any of them. In the *100% EFR* simulation, the RoCoF magnitude reduces quicker than in the other two simulations due to the high amount of fast-acting response. No nadir is reached, but instead the frequency gradually falls to the same level (just over 49.2 Hz) as in *real sim* around 55 s after the start of the event. After this point and onwards, *real sim* and *100% EFR* follow the same path because the frequency response is at the same maximum capacity in both simulations. The first nadir reached in the *more FR capacity* simulation is at 49.230 Hz and the frequency recovers to 49.47 Hz at around 55 s after the start of the event due to the increased capacity. The further imbalances cause the frequency to fall until it recovers just before breaching 48.8 Hz. The increase of dynamic LFR from 484 MW to 635 MW is the minimum required to ensure there is no demand disconnection. This increase of about 150 MW is the same whichever type of frequency response it applies to. The amount of frequency response delivered before the recovery actions kick in at 80 s after the start of the event vary from 23.3 MWh (*real sim*)

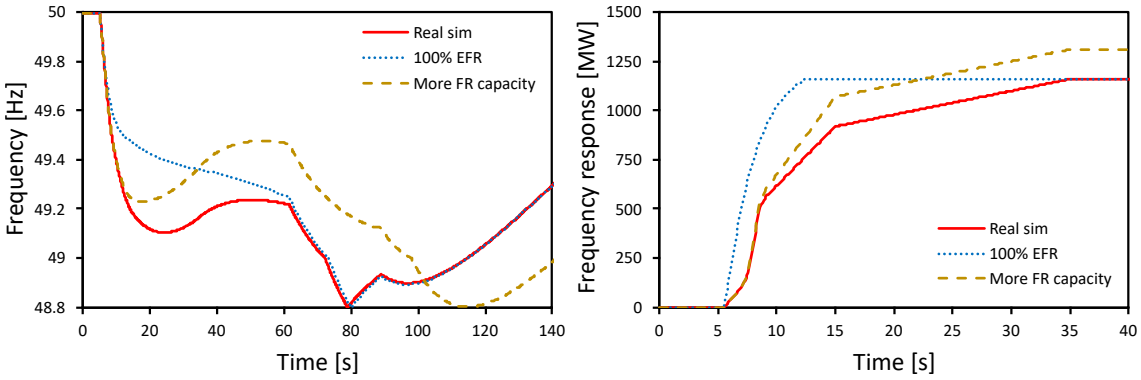

Figure 5.7: The effect of different frequency response characteristics on the frequency evolution (left) and the different response profiles for each simulation (right).

to 26.4 MWh (*more FR capacity*).

Fig. 5.8 shows the frequency with three different values of the demand damping constant. At $k = 1.1\,\%\text{MW/Hz}$, 48.8 Hz is reached at the first nadir within 20 s of the start of the event. Further imbalances later on cause a frequency minimum of 48.546 Hz. Under the low frequency demand disconnection scheme, this would have resulted in an extra 20% of demand disconnection. At $k = 2.1\,\%\text{MW/Hz}$, the first nadir is at 49.23 Hz and the frequency just avoids 48.8 Hz. It should be noted that the same frequency traces would have resulted from a fixed demand damping constant of $k = 1.65\,\%\text{MW/Hz}$ but underlying demands of 23.9 GW ($k = 1.1\,\%\text{MW/Hz}$), 35.9 GW (*real sim*), and 45.7 GW ($k = 2.1\,\%\text{MW/Hz}$).

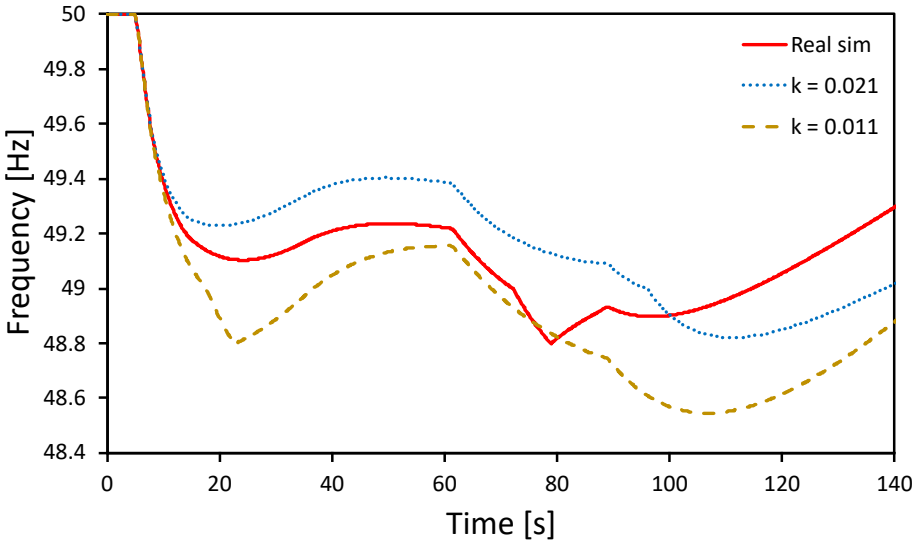

Figure 5.8: The effect of different demand damping constants on the frequency evolution.

5.4 Frequency volatility over a month in current and future scenarios: method

In Chapter 4 and Section 5.3 the focus was on single large infeed loss events. This section explains the method for looking at long-term frequency volatility. To start, in Section 5.4.1 it is explained how the estimate of the underlying power imbalance of the grid over a month is calculated, using November 2018 as a case study month. In Section 5.4.2, the method for estimating future inertia profiles is explained.

5.4.1 Imbalance profile of the grid over a month

The GB grid model can be used to produce a historic imbalance profile by rearranging Eq. (4.1) so that I is the subject, as long as the other grid variables and parameters are accurately known for the time period of the simulation. I chose to study a month-long period: long enough to capture the daily and weekly patterns of the grid but still giving sensible simulation times (~ 30 min). November 2018 was selected as the case study month because in the 2014–2018 time period it has the highest frequency standard deviation of any month (0.0701 Hz) and the second highest number of frequency events (134 high, 105 low), see Fig. 3.13. Also, the November 2018 frequency profile never breaches 49.7 Hz or

50.3 Hz, so it is likely that no static frequency response was called upon during the month (these are the tightest trigger frequencies for static frequency response). This means that the ignoring of static frequency response in Section 5.2 does not affect the accuracy of the November 2018 imbalance calculation.

To calculate the imbalance profile for the whole month of November 2018, 1 s resolution frequency data [155] is used and the demand and inertia profiles are obtained via the methods in Section 3.2.1 and Section 3.3.1. In the previous section, after fitting the GB grid model against the recent 9th August low frequency event, I estimated the demand damping constant to be $k = 0.0165$, which is the value used for November 2018. Frequency response parameter values used in the imbalance calculation are shown in Table 5.5. The frequency response capacities for November 2018 are estimated using a November 2018 frequency response market report produced by National Grid ESO [74]. EFR_{cap} and HFR_{cap} are constant, but LFR_{cap} varies throughout the day between three values. LFR_{cap} is based on the primary dynamic frequency response capacity in the report, not secondary. The secondary dynamic frequency response capacity in November 2018 is similar to primary, but differs slightly throughout the day. Therefore, LFR in the model accurately captures primary dynamic frequency response and is a reasonable estimate for secondary dynamic frequency response. With the delay time and ramp rates shown in Table 5.5, if a sudden $\Delta f = \pm 0.5$ Hz deviation occurred, LFR and HFR would start responding after 2 s and be at full capacity at 10 s, which matches the minimum acceptable response in November 2018 [162]. The time step of the grid model is 0.1 s, so all the variables mentioned are linearly interpolated during the November 2018 imbalance calculation. Fig. 5.9 provides a simple summary of the method discussed above.

The November 2018 imbalance profile is used as an input in simulations of the GB grid model where frequency is the output. To represent future (2030) grid scenarios, simulations with the November 2018 imbalance are run with different inertia profiles (predicting a future imbalance profile is beyond the scope of this work). The method behind the creation of these profiles is explained in the next section.

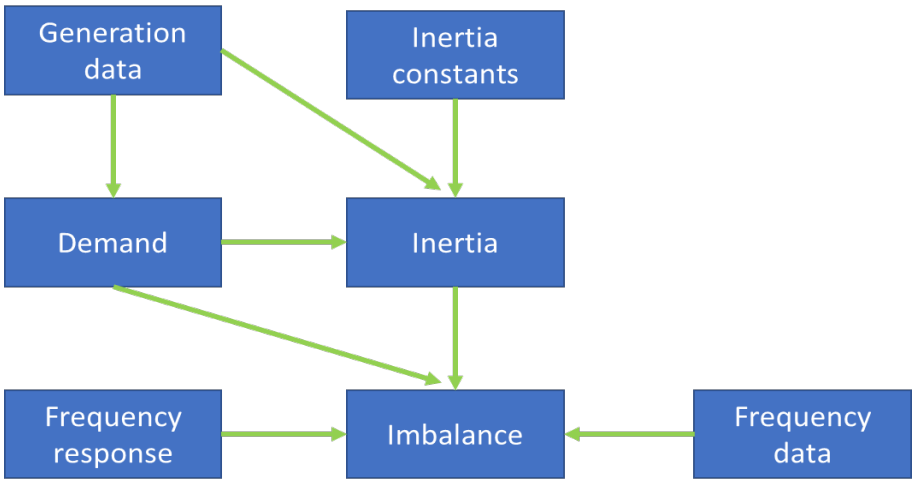

Figure 5.9: The method for calculating the imbalance profile of the grid from frequency and generation data, estimates of inertia constants, and frequency response capacity, speed, and type.

FR service	Capacity [MW]	Delay time [s]	Ramp rate [MW s^{-1}]
EFR	200	0.5	$2EFR_{\text{cap}}$
HFR	200	2	$\frac{1}{8}HFR_{\text{cap}}$
LFR	800 (00:00–07:00) 600 (07:00–15:00) 500 (15:00–00:00)	2	$\frac{1}{8}LFR_{\text{cap}}$

Table 5.5: November 2018 frequency response parameter values [74, 162].

5.4.2 Future (November 2030) inertia profiles

The annual level of electricity demand in GB is predicted to be fairly similar in 2030 as it is now [166]. Industrial and commercial demand is expected to reduce, but this is balanced by an increase in electricity demand in the transport sector (electric vehicles) and heating (domestic heat pumps). Given this, and the difficulty in predicting an accurate demand profile for 10 years in the future, the underlying demand in November 2030 is assumed to have the same profile as the underlying demand in November 2018.

To acquire inertia profiles for November 2030, the first step is estimating a future generation mix, which is based on a publication by National Grid ESO: Future Energy Scenarios [166]. Table 5.6 shows the 2018 capacities of wind, solar, and nuclear and the predicted 2030 capacities in the Community Renewables (CR) scenario. This scenario is

Generation type	2018 capacity [GW]	2030 (CR) capacity [GW]	Ratio
Wind (transmission)	14.7	42.2	2.87
Wind (distributed)	6.3	11.2	1.78
Solar	12.7	29.7	2.34
Nuclear	9.2	4.6	0.49

Table 5.6: Generation capacities in 2018 and in 2030 for the Community Renewables scenario in Future Energy Scenarios [166].

chosen because it is the scenario in which wind and solar capacity increases the most. The November 2018 half-hourly generation for these generation types is multiplied by the capacity ratio in the table. Then, the difference (Q) between the sum of this generation and the November 2018 underlying demand is calculated:

$$Q = UD - \sum_i r_i P_i \,, \tag{5.1}$$

where i, in this case, is only wind (transmission and distribution), solar, and nuclear. r_i is the 2030/2018 capacity ratio in Table 5.6. When $Q > 0$, additional generation is required to meet the underlying demand. It is beyond the scope of this study to predict what type of generation this might be, and for our purposes we are only interested in the inertia this additional generation can provide. When $Q \leq 0$, the assumption is that curtailment occurs to satisfy underlying demand. The penetration of wind and solar (as a percentage of underlying demand) is 23% in November 2018. The November 2030 generation mix, estimated using the method in this section, gives a wind and solar penetration of 58% (as a percentage of underlying demand and excluding curtailed generation).

The inertia from the generation side in November 2030 is given by

$$E_{\text{n,gen}} = \begin{cases} E_{\text{n,nuclear}} + \frac{QH_{\text{Q}}}{\beta_{\text{Q}} u_{\text{Q}}} & \text{when } Q > 0 \,, \\ E_{\text{n,nuclear}} & \text{when } Q \leq 0 \,. \end{cases} \tag{5.2}$$

H_{Q} is the inertia constant of the additional generation, $u_{\text{Q}} = 0.85$ is the power factor, and $\beta_{\text{Q}} = 0.75$ is the capacity factor. $E_{\text{n,nuclear}}$ is the inertia that the November 2030 nuclear

Profile name	Demand inertia ratio	H_Q [s]	Example generation mix for Q
CR30H8	1	8	100% CCGT
CR30H4	1	4	Similar mix to current grid
CR30H2	1	2	Mostly hydro, interconnectors, batteries, and a small amount of CCGTs.
CR30H0	1	0	All interconnectors and batteries
CR30H0-75%	0.75	0	All interconnectors and batteries

Table 5.7: Properties of the November 2030 inertia profiles representing future scenarios.

generation provides, which is calculated in the exact same way as in Section 3.3.1 but multiplied by 0.49, the capacity ratio (r) for nuclear.

Table 5.7 shows the names of the November 2030 inertia profiles created, their demand inertia compared to November 2018 demand inertia as a ratio, their H_Q values, and an example generation mix for Q given the H_Q value. The inertia from the demand side in November 2030 is considered to be the same as November 2018 apart from in the CR30H0-75% profile, where it is reduced to 75% of the November 2018 level. Fig. 5.10 shows the cumulative distributions of the November 2018 and November 2030 inertia profiles. At $H_Q \leq 2$, for the majority of the time the inertia is lower than the lowest level reached in November 2018. At $H_Q = 0$, the inertia is always below 105 GVA.s. The median value in the lowest inertia profile, CRH30H0-75%, is 52 GVA.s. This is roughly 20% of the median of inertia in 2014–2018. In November 2018, demand inertia contributes 20% to total inertia. As H_Q reduces, this contribution increases: in the CR30H2 profile, demand and generation contribute inertia in equal amounts, and in the CR30H0 profile demand is contributing 75% to the total.

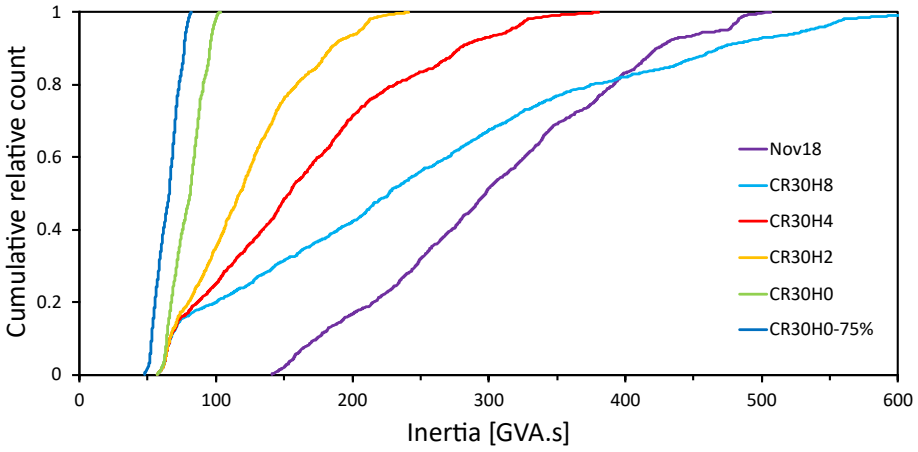

Figure 5.10: Cumulative distributions of the November 2030 inertia profiles in Table 5.7 and the November 2018 inertia profile.

5.5 Frequency volatility over a month in current and future scenarios: results

Here the results of analysing the frequency volatility over a month in current and future scenarios using the method described above are presented. In Section 5.5.1 I discuss the imbalance of November 2018. In Section 5.5.2 I look at how varying frequency response capacity and speed affects the frequency volatility over a month. In Section 5.5.3, I look at future scenarios with different inertia profiles and again see how this affects the frequency volatility over a month.

5.5.1 November 2018 imbalance

Fig. 5.11 shows the imbalance distribution for November 2018 (the bin width is 40 MW). The distribution has a peak at −80 MW and another peak at 40 MW. There is a longer tail on the negative imbalance side: at any imbalance magnitude above roughly 140 MW, there are more counts in the negative bin than the corresponding positive bin. The normalised count at either end, −700 MW and 500 MW, is $\approx 10^{-5}$.

The imbalance reaches a low of −766 MW and a high of 563 MW during the month. The −766 MW low is reached during a sudden drop from 64 MW ($\Delta I = -830$ MW), which causes a frequency drop from 50.052 Hz to the minimum frequency of the month,

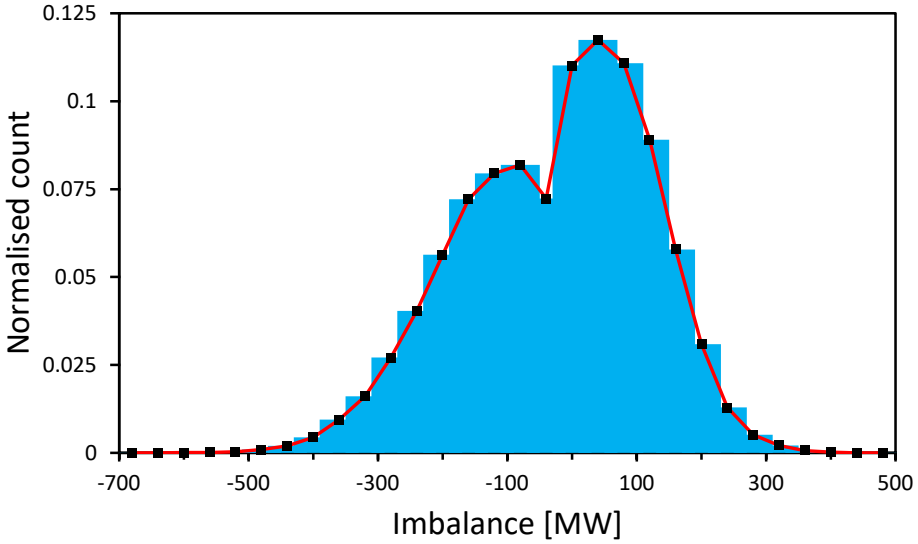

Figure 5.11: Imbalance distribution in November 2018. Bin width: 40 MW.

49.701 Hz. The 563 MW high causes a frequency of 50.243 Hz, which is almost as high as the maximum frequency of the month, 50.291 Hz.

5.5.2 Frequency response capacity and speed

In these results, Nov18 refers to November 2018 values for LFR and HFR capacity, delay time, and ramp rate. These are found in Table 5.5. Refer back to Section 3.5.2 for definitions of low and high events and low and high severe events.

Table 5.8 shows the results of five month-long frequency simulations where the frequency response capacity is varied in different ways. With all the variables and parameters the same as they were during the November 2018 imbalance calculation, the frequency standard deviation is 0.0701 Hz, and there are 134 high events and 105 low events. This matches reality (see Fig. 3.13), as expected. With 200 MW of extra LFR and HFR capacity, the number of high and low events decreases to 14 and 18, respectively, and the standard deviation reduces to 0.0582 Hz, a pre-2018 level (see Fig. 3.13). Removing EFR and adding this capacity onto LFR and HFR has very little effect. The standard deviation remains the same (0.0701 Hz) and the number of events only increases by a small amount. With 200 MW less LFR and HFR capacity, the standard deviation increases to 0.0889 Hz, which is greater than the maximum of any day during 2014–2018 (0.0827 Hz). The number

Capacity [MW]		Std dev [Hz]	Events		Severe events	
LFR/HFR	EFR		High	Low	High	Low
Nov18	200	0.0701	137	109	0	0
Nov18 + 200	200	0.0582	14	18	0	0
Nov18 + 200	0	0.0701	143	115	0	0
Nov18 − 200	200	0.0889	839	471	0	0
0	0	0.1879	2837	3972	7	482

Table 5.8: The effect of changing frequency response capacity on frequency volatility over a month.

of events increases by a factor of 5, but there are still no severe events. With no frequency response at all, as expected, the frequency volatility is completely unacceptable with an average of almost 10 events per hour throughout the month. Also, severe frequency events occur (with a lot more on the low side due to the asymmetry of the imbalance profile). The only thing stabilising the grid with no frequency response is demand damping.

Table 5.9 shows the results of four month-long frequency simulations where the LFR and HFR delay time is varied. In these simulations there is no EFR, but LFR_{cap} and HFR_{cap} are 200 MW higher than their November 2018 value so the overall frequency response capacity is the same as November 2018. The results show that a delay time of 5 s causes no significant effect. However, 10 s is clearly too long, with numerous severe events occurring. The total frequency response delivery volume over the month is roughly the same for delay times equal to and less than 5 s: 51 GWh. At 10 s, this increases to 61 GWh, but this volume is being delivered too late and often at detrimental times due to the delay. With an average November 2018 demand and inertia of 40 GW and 300 GVA.s, and an imbalance of ±350 MW, $\Delta f = \pm 0.2$ Hz is reached at 9.2 s, which is before frequency response has even started responding if the delay time is 10 s. As can be seen in Fig. 5.11, an imbalance of −350 MW is not that uncommon.

We find that even without EFR, it is not necessary for the ramp rate of LFR and HFR to be any higher than the values given in Table 5.5. The ramp rate has no significant effect on the frequency volatility, even at half the November 2018 value. This is because of the RoCoF during Nov18: it is never high enough to require a faster frequency response

LFR/HFR delay [s]	Std dev [Hz]	Events		Severe events	
		High	Low	High	Low
0.5	0.0700	136	101	0	0
2	0.0701	143	115	0	0
5	0.0706	163	165	0	0
10	0.0995	3914	4813	1155	911

Table 5.9: The effect of changing frequency response delay time on frequency volatility over a month.

ramp rate.

5.5.3 Future scenarios: November 2030

Again, Nov18 refers to November 2018 values for LFR and HFR capacity, delay time, and ramp rate. These are found in Table 5.5.

Fig. 5.12 shows the frequency standard deviation and number of events for five month-long frequency simulations with the different November 2030 inertia profiles in Fig. 5.10 and Table 5.7 (and November 2018 for comparison). In these five simulations there is no EFR, but LFR_{cap} and HFR_{cap} are 200 MW higher than their November 2018 value so the overall frequency response capacity is the same. As H_{Q} reduces, the standard deviation and number of events increase steadily. At no point are there any severe frequency events. However, with the CR30H0-75% profile, the frequency minimum and maximum are 49.536 Hz and 50.469 Hz, respectively. There is a large difference between the CR30H0 and CR30H0-75% profiles. At this level of inertia, where only nuclear (on the generation side) and demand (at 75% of the November 2018 level) are contributing, the number of frequency events is around 10 times higher than November 2018 levels and three times higher than CR30H0 levels. The low inertia is causing the frequency to change faster than the frequency response can effectively keep up with. One thing to note is that at a demand inertia of 75% of the November 2018 level, fewer synchronous demand units are likely to be connected to the grid (or smaller in size). This would almost certainly have a detrimental effect on the demand damping of the grid, a self-stabilising property, causing

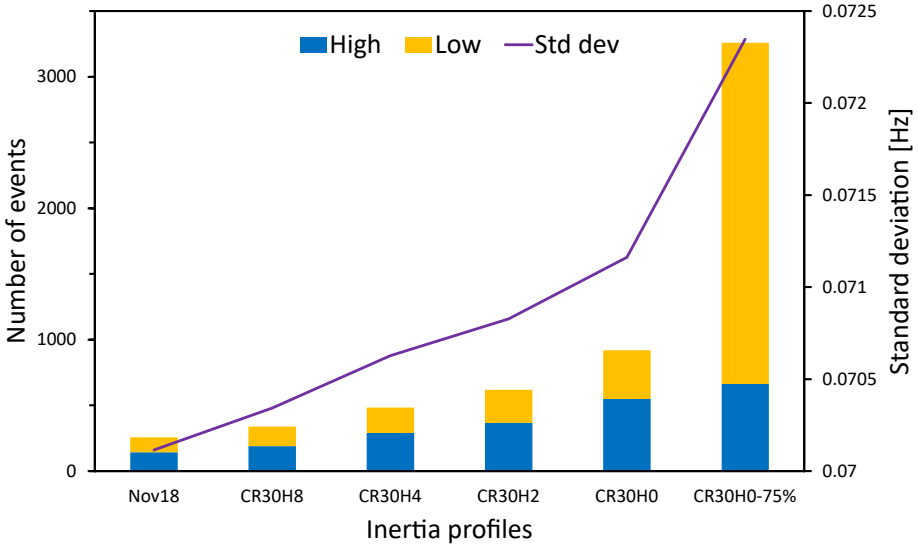

Figure 5.12: The effect of changing inertia (using November 2030 inertia profiles) on the number of frequency events and frequency standard deviation over a month.

far greater volatility in the frequency. Quantifying this detrimental effect is beyond the scope of this study.

Various low inertia mitigation methods are investigated to see which approach is able to bring the frequency volatility back into an acceptable range for the CR30H0-75% inertia profile. The results are shown in Table 5.10. The first method, *Increase LFR/HFR*, is simply increasing the LFR/HFR capacity by 200 MW, which results in a lower frequency standard deviation but a massive increase in the number of events, especially on the low side (also 20 severe low events). The increased frequency response capacity is not beneficial and is actually detrimental because there is now more response acting at occasionally unsuitable times. Fig. 5.13 shows approximately 25 min of frequency from the month-long simulation to illustrate the point about how more slow capacity, at a reduced inertia, is detrimental to frequency volatility. At around 700 s, the frequency starts oscillating rapidly with a large amplitude and then again at 1200 s.

With the *Faster LFR/HFR* method, the delay time of LFR/HFR is halved to 1 s and the ramp rate of LFR and HFR doubled. This reduces both the standard deviation and number of events, especially on the low side. However, the standard deviation and the number of events are still a lot higher compared to what they were in November 2018.

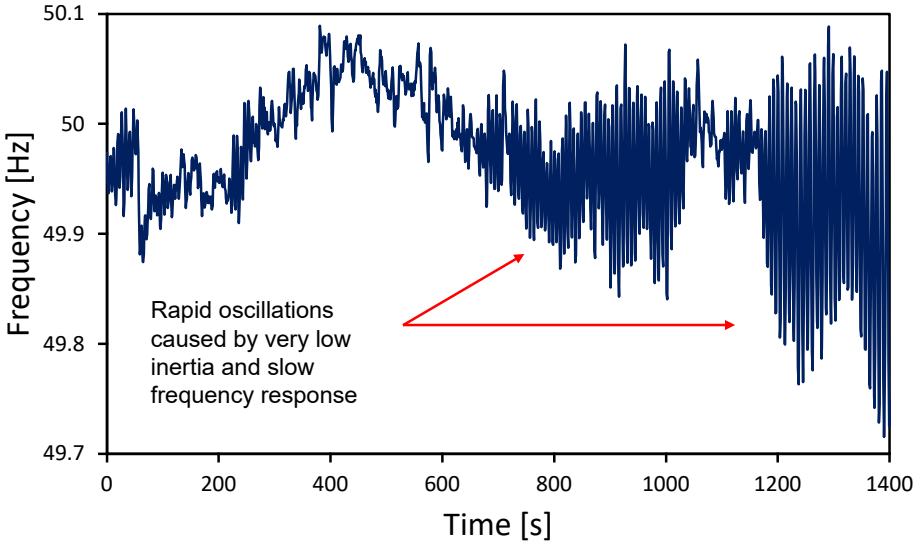

Figure 5.13: 25 min of frequency trace from the *Increase LFR/HFR* simulation.

For the *With SI* method, 200 MW of synthetic inertia replaces 200 MW of LFR/HFR (with the LFR/HFR delay time and ramp rates back at November 2018 values). The synthetic inertia does not act as a good substitute for frequency response and the frequency volatility is unacceptable.

The *With EFR* method is the same as the previous one but with 200 MW of EFR instead of synthetic inertia. Results are similar to the *Faster LFR/HFR* method, suggesting that only a portion of frequency response needs to be fast responding to see improvements.

The last mitigation method, *More EFR + SI*, is the same as the previous one but with an extra 100 MW of EFR and 100 MW of synthetic inertia. In this case, the synthetic inertia and extra frequency response capacity has a beneficial effect, unlike in *With SI* and *Increase LFR/HFR*, because there is fast acting frequency response (EFR) present. For the CR30H0-75% inertia profile, this mitigation method has brought the frequency volatility back into an acceptable range.

For all of the month-long simulations that produce acceptable frequency volatility, the minimum total frequency response delivery volume is 51 GWh, which equates to an average of 70 MW of frequency response being delivered at each point in time. This means that for the majority of time there is a lot of frequency response capacity that is not being used. If a frequency response service had a maximum output at smaller frequency deviations (e.g.

	Capacity [MW]				Events	
Mitigation method	LFR/HFR	EFR	SI	Std dev	High	Low
None	Nov18 + 200	0	0	0.0723	662	2597
Increase LFR/HFR	Nov18 + 400	0	0	0.0693	1220	12641
Faster LFR/HFR	Nov18 + 200	0	0	0.0710	619	415
With SI	Nov18	0	200	0.0895	2043	1036
With EFR	Nov18	200	0	0.0711	624	410
More EFR + SI	Nov18	300	100	0.0641	157	103

Table 5.10: Frequency volatility over a month with the CR30H0-75% (lowest) inertia profile with various low inertia mitigation methods.

0.2 Hz rather than 0.5 Hz) then all of the capacity would be utilised more often. Other frequency response services would be needed to manage the frequency for times when the deviations are larger e.g. post-fault. National Grid ESO have proposed such frequency response services and in the next section, I analyse their efficacy.

5.6 New frequency response services

In this section I use the methodology described in Section 5.4 to assess the efficacy of the new frequency response services mentioned in Section 5.1. I explain the characteristics of the new frequency response services and how they are modelled in Section 5.6.1. In Section 5.6.2 I run month-long simulations with the November 2018 imbalance and November 2018 inertia profile to analyse the new services and use the current frequency response services as a comparison. In Section 5.6.3 I do the same but with a reduced inertia profile: CR30H0-75% (see Section 5.4.2).

5.6.1 Additions to the grid model

The four new frequency response services proposed are called dynamic regulation (DR), dynamic moderation (DM), dynamic containment (DC), and static containment (SC), which we don't consider here. Dynamic regulation and dynamic moderation are symmetrical services, so providing 1 MW of the service means providing 1 MW of upwards (low) response and 1 MW of downwards (high) response. Dynamic containment is not a sym-

metrical service: a provider can choose to provide either upwards (DC low) or downwards (DC high) response or both.

The characteristics of the new frequency response services (except static containment) are detailed in a publication by National Grid ESO [71] and can be seen in Fig. 5.14. On the left of Fig. 5.14 is the relationship between required frequency response power output and frequency deviation for each service and on the right is the response and duration time required for each service. Dynamic regulation has a deadband of ±0.015 Hz and is at maximum output at ±0.1 Hz. Providers of this service must respond within 2 s of a frequency deviation outside the deadband and be able to ramp up to maximum output within 10 s. The provider must also be able to respond continuously, which in other words means having an infinite duration. Dynamic moderation starts at ±0.1 Hz and is at maximum output at ±0.2 Hz. Note the slight difference in response between dynamic regulation and dynamic moderation just outside their respective deadbands. Dynamic moderation has a maximum delay time of 0.5 s and full output must be reached within 1 s. The service must be sustained for at least 20 minutes. The purpose of dynamic moderation is to occasionally assist dynamic regulation by providing rapid response when frequency deviations start becoming slightly concerning. Dynamic containment (high and low) starts at ±0.2 Hz, the operational limits of frequency deviation in Great Britain. Dynamic containment has a maximum output at ±0.5 Hz and must have the same rapid response as dynamic moderation and the same duration. Dynamic containment is expected to be used very infrequently for large, unexpected frequency deviations to prevent the statutory limit of ±0.5 Hz being breached.

5.6.2 New frequency response products in a current inertia scenario

These definitions, along with the definitions of a high and low frequency event given in Section 3.5.2, are necessary for understanding the results that follow in this section and in Section 5.6.3.

- *Idle time*: the amount of time the frequency response service has zero output as a percentage of the total time

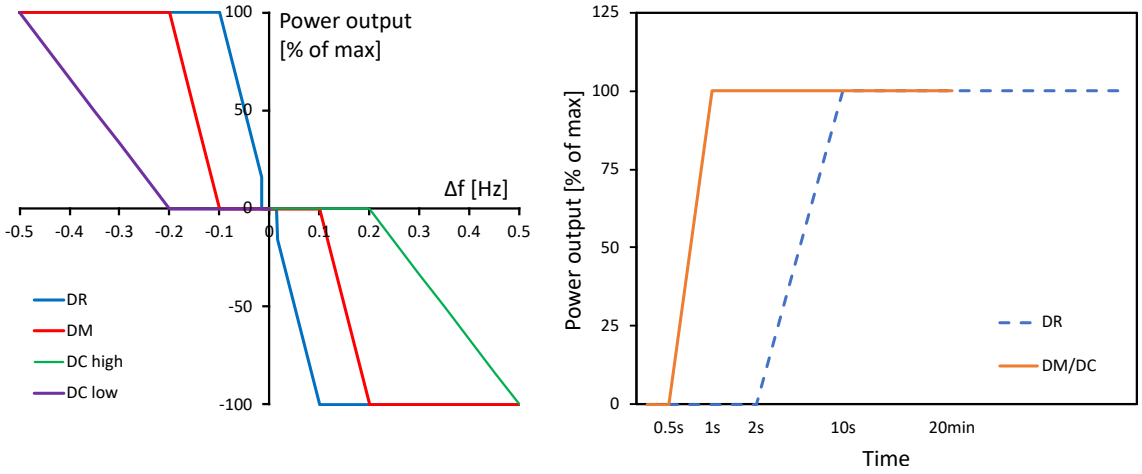

Figure 5.14: The characteristics of proposed new frequency response services: the power-frequency relationship (left) and delay, ramp, and duration times (right).

- *Utilisation*: the mean of the absolute output of the frequency response service (excluding idle time) as a percentage of the power capacity

- *Delivery volume*: the energy flow of the frequency response service (positive for output into grid and negative for the reverse)

I first run a month-long simulation with the November 2018 imbalance and the current frequency response services with parameter values given in Table 5.5. Obviously this just gives the real frequency volatility of November 2018: 0.0701 Hz standard deviation, 134 high events, and 105 low events. Table 5.11 shows the capacity, idle time, utilisation, and delivery volume of each current frequency response service in the same simulation. LFR and HFR spend more time being idle than EFR since they only respond in one direction. All services have the same utilisation because the frequency distribution is very close to symmetric and they all have the same power-frequency relationship. However, the frequency distribution is not exactly symmetric as evidenced by the fact that EFR outputs slightly more power than takes in.

Fig. 5.15 shows the results of simulations in which the proposed new frequency response services were providing the frequency response during the month. In all cases (in both the left and right plot) the total frequency response capacity is 450 MW on the high side and 550 MW on the low side. In the left plot, the capacity of the sum of dynamic moderation

Current FR service	Capacity [MW]	Idle time	Utilisation	Delivery volume [MWh]
Low	500/600/800	0.55	0.13	26000
High	200	0.57	0.13	-8100
Enhanced	200	0.13	0.13	8300/-8100

Table 5.11: Idle time, utilisation, and delivery volume of each current frequency response service during the November 2018 simulation.

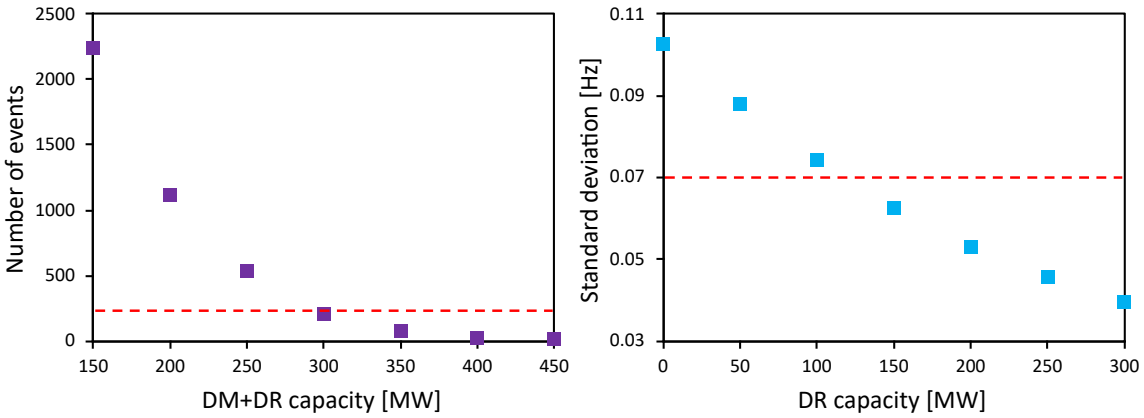

Figure 5.15: The number of frequency events (high + low) during the month for different combined capacities of dynamic regulation and dynamic moderation (left) and the standard deviation of frequency during the month for different dynamic regulation capacities (right). The red dashed lines indicate the real November 2018 values.

and dynamic regulation was varied (in every case dynamic moderation equals dynamic regulation). Dynamic containment fulfils the rest of the capacity up to 450 MW (high) and 550 MW (low). The number of events (high + low) decreases as DM + DR increases, as expected. Above DR = DM = 150 MW, the number of events is below the November 2018 value of 239. In the right plot, the capacity of dynamic regulation was varied and DM + DR kept constant at 300 MW, again dynamic containment fulfils the rest of the capacity up to 450 MW (high) and 550 MW (low). The standard deviation of frequency decreases as dynamic regulation capacity increases, improving on the November 2018 value at DR = 150 MW and above.

Table 5.12 shows the idle time, utilisation, and delivery volume of each proposed new frequency response service at a capacity mix that gives similar frequency volatility to November 2018. Dynamic regulation has a similar idle time to EFR, but a much higher

New FR service	Capacity [MW]	Idle time	Utilisation	Delivery volume [MWh]
DR	150	0.14	0.55	30000/-21000
DM	150	0.89	0.27	2900/-260
DC high	150	1.00	0.01	0
DC low	150	1.00	0.10	35

Table 5.12: Idle time, utilisation, and delivery volume of each proposed new frequency response service (at a specific capacity mix) during November 2018 simulation.

utilisation due to having maximum output at ±0.1 Hz rather than at ±0.5 Hz. Dynamic moderation is idle for 89% of the time and has a 27% utilisation. Dynamic containment (high and low) are both active for less than 0.5% of the time. As seen from the delivery volumes, dynamic regulation is doing the bulk of the work, with dynamic moderation offering occasional assistance and dynamic containment offering rare assistance. There is a large disparity in delivery volume between input and output for the dynamic moderation service. This service could be provided by batteries due to the fast response required. However, the battery would lose state-of-charge throughout the month and would need a state-of-charge balancing strategy to avoid needing a prohibitively large energy capacity.

To summarise, the dynamic regulation capacity alone is the main factor influencing standard deviation and the sum of dynamic regulation and dynamic moderation capacity is the main factor influencing the number of frequency events. The dynamic containment capacity has an insignificant influence on both of these measures of frequency volatility due to its large deadband of ±0.2 Hz. However, dynamic containment is extremely important to protect the grid when there are rare, large imbalances that dynamic regulation and dynamic moderation cannot contain alone.

5.6.3 New frequency response services in a future reduced inertia scenario

In this section I perform month-long simulations with the November 2018 imbalance and the CR30H0-75% inertia profile from Section 5.4.2. The inertia in this future scenario is provided by nuclear and demand only and has a median value five times smaller than

Inertia profile	Number of events	Standard deviation [Hz]	Maximum frequency [Hz]	Minimum frequency [Hz]
Nov 18	208	0.063	50.205	49.614
Nov 30	735	0.064	50.372	49.599

Table 5.13: Frequency volatility results for the proposed new frequency response services with a November 2018 inertia profile and a November 2030 reduced inertia profile (CR30H0-75%). The dynamic regulation, dynamic moderation, and dynamic containment capacities are the same as in Table 5.12.

current values. Table 5.13 shows the frequency volatility results, including the results from running the simulation with a November 2018 inertia profile for comparison. For both simulations, the dynamic regulation, dynamic moderation, and dynamic containment capacities are the same as in Table 5.12. The reduced inertia causes an increase in the number of events by a factor of 3.5 but only a small increase in the standard deviation. The maximum frequency deviation reached during the month increases quite a lot on the high side with the CR30HO-75% inertia profile but not so much on the low side. It was found that adding just 50 MW of extra capacity to dynamic regulation (to 200 MW in total), reduced the number of events to 266 and the standard deviation to 0.055 Hz (similar, if not better, frequency volatility to November 2018).

5.7 Conclusions

In this section, I first return to the research questions set out in the introduction to this chapter and discuss the extent to which each have been answered. Then, in Section 5.7.1, I present the highlights of the results of the chapter. Key findings of this chapter will be discussed within a wider context in Chapter 6.

Regarding the 9th August 2019 low frequency event, if the frequency response was faster or RoCoF relays were not triggered, could demand disconnection have been prevented?

I showed that if the RoCoF relays in embedded generation were not triggered, then demand disconnection could have been avoided. This is why the change in loss of mains protection settings, explained in more detail in Section 2.7.2, was/is so important. It is

unlikely faster frequency response would have prevented demand disconnection. However, based on my simulations, I found that an extra 150 MW of frequency response capacity was all that was needed to prevent demand disconnection. In other words, the grid was very close to not being talked about in the evening news.

Regarding the 9th August 2019 low frequency event, what effect would a different inertia, demand, and demand damping have had on the frequency profile?

In all inertia scenarios simulated, demand disconnection was not prevented. At a low inertia, 100 GVA.s, demand disconnection happens extremely quickly (within 10 s), but in general the severity of the event is similar across different inertia levels. Demand and demand damping have a larger effect. A demand of 45.7 GW (or a demand damping constant of $k = 2.1$ %MW/Hz) would have prevented there being any demand disconnection.

How do frequency response characteristics (capacity and speed) affect normal day-to-day frequency volatility?

When the capacity was increased by 200 MW, the standard deviation returned to levels seen in 2014–2016 (i.e. a lot lower than November 2018), as did the number of frequency events. When the capacity was decreased by 200 MW, the standard deviation over a month reached a level greater than any individual day in the 2014–2018 time period, and the number of frequency events increased by a factor of five. Swapping out fast EFR capacity with slow capacity had very little effect. In fact, increasing the delay time to 5 s rather than 2 s only had a very small negative impact on the frequency volatility. However, a delay time of 10 s was far too long and caused unacceptable volatility. At the November 2018 level of imbalances and inertia, a ramp rate of 8 s is more than quick enough to manage the frequency.

In which future scenarios does the normal day-to-day frequency volatility become unacceptable and what needs to change in frequency response provision to mitigate this?

In 2030, the grid is likely to have much lower levels of inertia than today, but we found that inertia needs to reach very low levels before it starts seriously affecting the

frequency volatility in normal day-to-day operation. In the most extreme low inertia scenario modelled (CR30H0-75%), inertia was only provided by nuclear generation and demand and was around 20% of current levels. In this extreme case, the frequency volatility was unacceptable, but it was found that a small total frequency response capacity increase together with substituting some slow acting frequency response with fast acting frequency response successfully mitigated this. The proportion of fast acting frequency response is roughly 50% of the total capacity in this scenario.

What is the efficacy of the proposed new frequency response services compared with the existing frequency response services in current and future scenarios?

It seems that the proposed new frequency response services have much more distinct roles than the current services. Dynamic regulation maintains an acceptable standard deviation, dynamic moderation works with dynamic regulation to prevent too many frequency excursions outside of ± 0.2 Hz, and dynamic containment is for protecting the grid against rare, large events. 150 MW of dynamic regulation and dynamic moderation keeps standard deviation to acceptable levels. The amount of dynamic containment capacity will depend on the future largest infeed loss. In a future very low inertia scenario (CR30H0-75%), an additional 50 MW of dynamic regulation capacity can maintain the frequency volatility at current levels.

5.7.1 Highlights of the results

The highlights of the results from this chapter are listed below. The specific values relate to the GB grid:

- 9th August 2019 low frequency event
  - Demand disconnection would not have occurred if there was an extra 150 MW of frequency response or there was not the extra loss of embedded generation from RoCoF protection relays
  - A higher demand level or a higher demand damping constant could have prevented demand disconnection, but a higher inertia could not

- Frequency volatility over a month in current and future scenarios
  - The volatility is not significantly negatively affected by reduced inertia until the point where the only inertia being provided is from nuclear and demand (at 75% of November 2018 levels). At this point, the volatility jumps to unacceptable levels.
  - Successful mitigation methods to reduced inertia are ones in which roughly 50% of frequency response capacity is fast-acting. Simply adding frequency response capacity (at standard speeds) is detrimental to frequency volatility.
- New frequency response services
  - Dynamic regulation capacity is the main factor influencing the frequency standard deviation and the sum of dynamic regulation and dynamic moderation capacity is the main factor influencing the number of frequency events
  - 150 MW of dynamic regulation and dynamic moderation keeps standard deviation and the number of frequency events to acceptable levels
  - The amount of dynamic containment capacity will depend on the future largest infeed loss. There must be enough DR+DM+DC to protect the grid against it.
  - In a future reduced inertia scenario, an additional 50 MW of dynamic regulation capacity can maintain the frequency volatility at current levels

Chapter 6

Conclusions and future work

6.1 Conclusions

The aim of this thesis was to further the understanding of future frequency response requirements in low inertia grids. I began in Chapter 2 by reviewing the literature on grid stability, frequency response, inertia, power grid modelling, the ESO's view on future grid stability, and historic frequency data analysis. This review helped inform my research questions. In Chapter 3, I analysed GB grid data on generation and demand, grid inertia, frequency response, and grid frequency. This was not only for the purpose of better understanding the current state of grid stability and drivers of frequency volatility but also for providing values for certain parameters to be used in subsequent chapters (e.g. inertia). In Chapter 4, I used an analytical approach to determine constraints on certain grid parameters (inertia, frequency response capacity, and frequency response speed) that would ensure that frequency requirements were met after a large infeed loss. In Chapter 5, I used three case studies to further my investigation into frequency response requirements. The three case studies were a real large infeed loss (a more complicated case than the setup in Chapter 4), month-long (November 2018) frequency volatility in current and future inertia scenarios, and National Grid ESO's newly proposed frequency response services. For the investigation into month-long frequency volatility, I developed a method for extracting the underlying imbalance of the grid, which is one of the main contributions

of this thesis alongside the results that helped to answer the research questions.

The research questions of this thesis were first stated in Section 1.3. In each results chapter (Chapter 3, Chapter 4, and Chapter 5), the relevant research questions were re-stated in the introduction and a discussion on the extent to which each had been answered in the conclusions. Here I will return to some of these discussions and review their implications.

It was found in Chapter 3 that the number of frequency events in Great Britain roughly doubled from 2016 to 2017 and then increased by about 50% from 2017 to 2018. The monthly standard deviation of the grid frequency also steadily rose from 2016 to 2018. The question is, is this cause for concern? The number of frequency events and standard deviation declined in 2019, so a continuous upwards trend is no longer occurring. However, when looking at the number of significant events (definitions of event types in Section 3.5.2), this is slightly concerning because of the big rise in 2019. In Chapter 3, I found that settlement period boundaries and high rate of change of demand are the main drivers behind frequency volatility. I also said that the increasing penetration of wind and solar generation may have played a role in the increasing frequency volatility seen between 2016 and 2018. The electrification of other energy sectors (e.g. heat and transport) will likely increase demand from the mid 2020s onwards. With no demand side flexibility, frequency volatility would likely increase due to the potential large increase in rate of change of demand in the mornings and evenings. However, it is also an opportunity to smooth out demand throughout the day if the extra demand connected is smart and flexible.

In Chapter 4, I found that 1600 MW of frequency response at a delay/ramp time of 0.5 s/0.5 s is needed to secure the GB grid in the future, for all potential infeed loss, demand, and inertia scenarios. That includes scenarios where the inertia is at 45 GVA.s and the demand is at 20 GW. Using the same conversion factor used in Section 3.3.1 for getting demand inertia from demand, implies that only 10 GVA.s would need to come from the generation side. Using Eq. (A.6), and assuming the inertia-providing generation has an inertia constant of $H = 4$ s, just over 2 GW of inertia-providing generation would deliver the 10 GVA.s needed. Obviously this generation would need to be nuclear, biomass, or hydro

for it to be low-carbon. 1600 MW of fast frequency response will have to be provided by batteries, demand side flexibility or interconnectors, since this response speed is beyond the capabilities of CCGTs and pumped storage. The prediction is for energy storage to exceed 6 GW capacity by 2026 and for there to be 10 GW of interconnection import capacity by 2023 [166]. If CCGTs and pumped storage remain part of the frequency response suite of services, then more capacity is required from them than a faster-responding technology for an equivalent level of security provision.

In this thesis I have made it clear that the increase in the RoCoF relay protection limits from $0.125\,\mathrm{Hz\,s^{-1}}$ to $1\,\mathrm{Hz\,s^{-1}}$ has future-proofed the system in regards to this aspect. It is highly unlikely that inertia levels and potential infeed loss magnitudes will reach levels where the RoCoF will trigger the relays spuriously. Furthermore, I showed that had all embedded generation been switched to the new setting by the time of the August 2019 low frequency event, no demand disconnection would have taken place.

From the analysis into long-term frequency volatility in Chapter 5, I found that inertia needs to reach very low levels before it starts seriously affecting the frequency volatility in normal day-to-day operation. In the most extreme low inertia scenario modelled (inertia only provided by nuclear and demand), only a small capacity increase in frequency response (from November 2018 levels) is required to bring the frequency volatility back to acceptable levels. The additional capacity increase must be fast acting frequency response otherwise the increase is detrimental.

As the inertia of the grid decreases, the difference between the frequency response capacity needed to secure the grid against large infeed losses and what is needed during normal day-to-day operation will increase. In other words, as the inertia of the grid decreases, the utlisation factor of the frequency response decreases. If frequency requirements are relaxed or the large infeed is reduced in future, the difference will be less pronounced. The newly proposed frequency response products perhaps make more sense in a low inertia grid. Dynamic regulation and moderation will have a high utilisation factor with only a small capacity increase required as inertia lowers. Dynamic containment is the service that will need large capacity increases as inertia lowers, but will always be a service with a low

utilisation. A suggestion here is to use the battery capacity of the electric vehicle fleet in the future as dynamic containment to avoid over-sizing the frequency response capacity.

6.2 Summary of main contributions

Here is a summary of the main contributions of this thesis, split into two categories: *results* and *methods*.

Results

- Comprehensive review of historical grid frequency data finding that the number of significant events have increased recently and the standard deviation post-2017 is much higher than pre-2017 levels
- Evidence that the change in RoCoF loss of mains protection settings from $0.125\,\mathrm{Hz\,s^{-1}}$ to $1\,\mathrm{Hz\,s^{-1}}$ has future-proofed the system
- 1600 MW of frequency response at a delay/ramp time of 0.5 s/0.5 s is needed to secure the GB grid in the future (for all large infeed loss and low inertia scenarios)
- Low inertia is much less of an issue in normal day-to-day operation: only a small frequency response capacity increase is needed to maintain current levels of frequency volatility in an extreme low inertia scenario for normal day-to-day operation (i.e., no large infeed losses)
- The new frequency response services recently introduced by National Grid ESO have much more defined roles than the current suite of services

Methods

- Creating a GB demand dataset by combining the open datasets from Elexon and National Grid ESO on generation output. The datasets were cleaned for errors.
- Novel method to back-calculate a power imbalance profile to allow investigations into day-to-day frequency volatility in different scenarios
- Technology agnostic frequency response models

6.3 Further work

From the work carried out in this thesis, several opportunities for future work are brought to the attention of the reader. Listed here are the potential avenues for further work for each results chapter in turn.

Historic grid data analysis

- The frequency volatility analysis should continue for 2020 onwards. It will be interesting to see whether the introduction of dynamic containment in October 2020 had any effect on the frequency volatility in Great Britain. Also, further into the future when dynamic containment and dynamic moderation become live services, further analysis of frequency volatility would prove (or disprove) the claims made in this thesis about the role of both these services.

- In addition to the main focus on the GB grid, I briefly analysed frequency volatility in the Continental European grid. Analysis of other grid data around the world would be helpful for furthering understanding on the underlying drivers behind frequency volatility. The barrier to this further work is accessibility of the data.

- The method for estimating inertia was only at half-hourly resolution and relied on quite a few assumptions. Reactive Technologies are a company that can measure the inertia levels of the grid in real-time. Acquiring some of this data would greatly improve the accuracy of this study.

Frequency dynamics after a large infeed loss: an analytical approach

- The inertia was assumed constant for all time after the large infeed loss. Inertia is a grid property that slows down the frequency drop but also slows down the frequency recovery. Technologies offering synthetic inertia would be able to offer inertia during the frequency containment phase but lower their inertia contribution during the frequency recovery phase, allowing for a faster recovery. This would make

the expression for inertia time-dependent and the differential equation used in the analysis, Eq. (4.2), should change accordingly.

- The analysis of this chapter could be made more useful by including information on the daily and yearly variation of certain grid parameters (e.g. inertia). This would allow graphs to be produced that would show the frequency response requirements throughout the day and year.

Case studies into frequency volatility

- In Section 5.4, I used National Grid Future Energy Scenarios to produce month-long future inertia profiles for November 2030. This method only involved changing the inertia between current and future scenarios. It would be interesting to investigate future frequency volatility under a difference imbalance profile as well. A future imbalance profile could be generated by extracting the stochastic element of the November 2018 imbalance and scaling this for the future based on different predicited wind and solar capacities.

- The efficacy of the new frequency response services was investigated in Section 5.6 and one of the next steps could be to understand how a battery would maintain state of charge while providing each type of service, especially dynamic moderation. Dynamic moderation is a fast responding service (suited to batteries), but also must be symmetrical. The work in this thesis suggests that there is likely to be a lot more low dynamic moderation required than high dynamic moderation. Without adaquate state-of-charge strategies, batteries will be unable to provide the service for very long.

References

[1] EDW Technology, "Glossary: Transmission Network Use of System Charges." Available at: http://www.edwt.org/glossary. [Accessed: 12-Oct-18].

[2] International Renewable Energy Agency (IRENA), "Renewable Energy Statistics 2018," 2018.

[3] UK Parliament, "Climate Change Act 2008," 2008.

[4] National Grid, "Historic frequency data." Available at: https://www.nationalgrideso.com/balancing-services/frequency-response-services/historic-frequency-data. [Accessed: 09-Oct-18].

[5] I. Newton, *Philosophiae Naturalis Principia Mathematica*. 1687.

[6] P. Kundur, *Power System Stability and Control*. McGraw-Hill, 1994.

[7] Everoze, "Batteries: Beyond the Spin," 2017.

[8] P. Denholm, T. Mai, R. W. Kenyon, B. Kroposki, and M. O. Malley, "Inertia and the Power Grid : A Guide Without the Spin," 2020.

[9] J. W. Busby, K. Baker, M. D. Bazilian, A. Q. Gilbert, E. Grubert, V. Rai, J. D. Rhodes, S. Shidore, C. A. Smith, and M. E. Webber, "Cascading risks: Understanding the 2021 winter blackout in Texas," *Energy Research and Social Science*, vol. 77, p. 102106, 2021.

[10] National Grid, "Balancing Services." Available at: https://www.nationalgrideso.com/balancing-services. [Accessed: 12-Nov-18].

[11] National Grid, "System Operability Framework 2016," 2016.

[12] National Grid ESO, "Zero Carbon Operation 2025," 2019.

[13] R. Lee, S. Homan, N. Mac Dowell, and S. Brown, "A closed-loop analysis of grid scale battery systems providing frequency response and reserve services in a variable inertia grid," *Applied Energy*, vol. 236, no. December 2018, pp. 961–972, 2019.

[14] S. Homan and S. Brown, "An analysis of frequency events in Great Britain," *Energy Reports*, vol. 6, pp. 63–69, 2020.

[15] S. Homan, N. Mac Dowell, and S. Brown, "Grid frequency volatility in future low inertia scenarios: Challenges and mitigation options," *Applied Energy*, vol. 290, no. 116723, 2021.

[16] S. Homan and S. Brown, "The future of frequency response in Great Britain," *Energy Reports*, vol. 7, pp. 56–62, may 2021.

[17] P. Kundur, J. Paserba, V. Ajjarapu, G. Andersson, A. Bose, C. Canizares, N. Hatziargyriou, D. Hill, A. Stankovic, C. Taylor, T. Van Cursem, and V. Vittal, "Definition and classification of power system stability," *IEEE Transactions on Power Systems*, vol. 19, no. 3, pp. 1387–1401, 2004.

[18] A. Ulbig, T. S. Borsche, and G. Andersson, "Impact of low rotational inertia on power system stability and operation," in *19th IFAC World Congress*, (Cape Town, South Africa), 2014.

[19] F. Milano, F. Dorfler, G. Hug, D. J. Hill, and G. Verbič, "Foundations and challenges of low-inertia systems," in *20th Power Systems Computation Conference (PSCC)*, (Dublin, Ireland), 2018.

[20] P. M. Ashton, C. S. Saunders, G. A. Taylor, A. M. Carter, and M. E. Bradley, "Inertia estimation of the GB power system using synchrophasor measurements," *IEEE Transactions on Power Systems*, vol. 30, no. 2, pp. 701–709, 2015.

[21] National Grid ESO, "The Enhanced Frequency Control Capability (EFCC) project closing down report," 2019.

[22] R. Pearmine, Y. Song, T. Williams, and A. Chebbo, "Identification of a load–frequency characteristic for allocation of spinning reserves on the British electricity grid," in *IEE Proceedings - Generation, Transmission and Distribution*, vol. 153, pp. 633–638, 2006.

[23] J. W. Taylor and M. B. Roberts, "Forecasting Frequency-Corrected Electricity Demand to Support Frequency Control," *IEEE Transactions on Power Systems*, vol. 31, no. 3, pp. 1925–1932, 2016.

[24] M. Davies, F. Moran, and J. I. Bird, "Power/Frequency characteristics of the British grid system," *Proceedings of the IEE - Part A: Power Engineering*, vol. 106, no. 26, pp. 154–162, 1959.

[25] M. Kurth and E. Welfonder, *Importance of the selfregulating effect within power systems*. IFAC, 2006.

[26] ENTSO-E, "Nordic Report: Future System Inertia," 2015.

[27] Y. Bian, H. Wyman-Pain, F. Li, R. Bhakar, S. Mishra, and N. Prasad Padhy, "Demand Side Contributions for System Inertia in the GB Power System," *IEEE Transactions on Power Systems*, vol. 33, no. 4, pp. 3521–3530, 2018.

[28] A. Beláň, B. Cintula, M. Cenký, P. Janiga, J. Bendík, Ž. Eleschová, and A. Šimurka, "Measurement of static frequency characteristics of home appliances in smart grid systems," *Energies*, vol. 14, no. 6, 2021.

[29] IEEE Task Force on Load Representation for Dynamic Performance, "Load representation for dynamic performance analysis," *IEEE Transactions on Power Systems*, vol. 8, no. 2, pp. 472–482, 1993.

[30] B. Berry, "Inertia Estimation Methodologies vs Measurement Methodology: Impact on System Operations," in *Cigre Symposium*, (Aalborg, Denmark), 2019.

[31] DigSILENT, "PowerFactory." Available at: https://www.digsilent.de/en/powerfactory.html. [Accessed: 18-Sep-21].

[32] K. Tuttelberg, J. Kilter, D. Wilson, and K. Uhlen, "Estimation of power system inertia from ambient wide area measurements," *IEEE Transactions on Power Systems*, vol. 33, no. 6, pp. 7249–7257, 2018.

[33] Reactive Technologies, "Reactive Technologies and National Grid Deliver Grid Stability Measurement World First." Available at: https://www.reactive-technologies.com/news/reactive-technologies-and-national-grid-deliver-grid-stability-measurement-world-first/. [Accessed: 29-Aug-21].

[34] Reactive Technologies, "Reactive Technologies Signs Landmark Commercial Agreement with National Grid ESO Supporting its 2025 Zero Carbon Goals." Available at: https://www.reactive-technologies.com/news/reactive-technologies-signs-landmark-commercial-agreement-with-national-grid-eso-supporting-its-2025-zero-carbon-goals/. [Accessed: 29-Aug-21].

[35] National Grid and Reactive Technologies, "Project SIM: Inertia Measurement," 2017.

[36] P. Wall and V. Terzija, "Simultaneous estimation of the time of disturbance and inertia in power systems," *IEEE Transactions on Power Delivery*, vol. 29, no. 4, pp. 2018–2031, 2014.

[37] X. Cao, B. Stephen, I. F. Abdulhadi, C. D. Booth, and G. M. Burt, "Switching Markov Gaussian Models for Dynamic Power System Inertia Estimation," *IEEE Transactions on Power Systems*, vol. 31, no. 5, pp. 3394–3403, 2016.

[38] D. Wilson, J. Yu, N. Al-Ashwal, B. Heimisson, and V. Terzija, "Measuring effective area inertia to determine fast-acting frequency response requirements," *International Journal of Electrical Power and Energy Systems*, vol. 113, no. March 2019, pp. 1–8, 2019.

[39] General Electric, "GE introduces new analytics to advance electric grid operations.." Available at: https://www.ge.com/news/press-releases/ge-introduces-new-analytics-advance-electric-grid-operations. [Accessed: 04-Sep-21].

[40] P. Du and J. Matevosyan, "Forecast system inertia condition and its impact to integrate more renewables," *IEEE Transactions on Smart Grid*, vol. 9, no. 2, pp. 1531–1533, 2018.

[41] T. Inoue, H. Taniguchi, Y. Ikeguchi, and K. Yoshida, "Estimation of Power System Inertia Constant and Capacity of Spinning-reserve Support Generators Using Measured Frequency Transients," *IEEE Transactions on Power Systems*, vol. 12, no. 1, pp. 136–143, 1997.

[42] D. P. Chassin, Z. Huang, M. K. Donnelly, C. Hassler, E. Ramirez, and C. Ray, "Estimation of WECC system inertia using observed frequency transients," *IEEE Transactions on Power Systems*, vol. 20, no. 2, pp. 1190–1192, 2005.

[43] D. Zografos, M. Ghandhari, and R. Eriksson, "Power system inertia estimation: Utilization of frequency and voltage response after a disturbance," *Electric Power Systems Research*, vol. 161, pp. 52–60, 2018.

[44] W. Wang, W. Yao, C. Chen, X. Deng, and Y. Liu, "Fast and Accurate Frequency Response Estimation for Large Power System Disturbances Using Second Derivative of Frequency Data," *IEEE Transactions on Power Systems*, vol. 35, no. 3, pp. 2483–2486, 2020.

[45] B. Kroposki, B. Johnson, Y. Zhang, V. Gevorgian, P. Denholm, B. M. Hodge, and B. Hannegan, "Achieving a 100% Renewable Grid: Operating Electric Power Systems with Extremely High Levels of Variable Renewable Energy," *IEEE Power and Energy Magazine*, vol. 15, no. 2, pp. 61–73, 2017.

[46] The European Commission, "COMMISSION REGULATION (EU) 2017/1485 of 2 August 2017 establishing a guideline on electricity transmission system operation," 2017.

[47] Statnett, Fingrid, Energinet.dk., and Svenska Kraftnat, "Challenges and Opportunities for the Nordic Power System," 2016.

[48] ENTSO-E, "Nordic Report: Future System Inertia 2," 2017.

[49] EirGrid and SONI, "Delivering a secure, sustainable electricity system (DS3) - programme overview," 2015.

[50] S. C. Johnson, D. J. Papageorgiou, D. S. Mallapragada, T. A. Deetjen, J. D. Rhodes, and M. E. Webber, "Evaluating rotational inertia as a component of grid reliability with high penetrations of variable renewable energy," *Energy*, vol. 180, pp. 258–271, 2019.

[51] S. C. Johnson, J. D. Rhodes, and M. E. Webber, "Understanding the impact of non-synchronous wind and solar generation on grid stability and identifying mitigation pathways," *Applied Energy*, vol. 262, no. 114492, 2020.

[52] P. Tielens and D. Van Hertem, "The relevance of inertia in power systems," *Renewable and Sustainable Energy Reviews*, vol. 55, pp. 999–1009, 2016.

[53] L. Mehigan, D. Al Kez, S. Collins, A. Foley, B. Ó'Gallachóir, and P. Deane, "Renewables in the European power system and the impact on system rotational inertia," *Energy*, vol. 203, 2020.

[54] U. Tamrakar, D. Shrestha, M. Maharjan, B. Bhattarai, T. Hansen, and R. Tonkoski, "Virtual Inertia: Current Trends and Future Directions," *Applied Sciences*, vol. 7, no. 7, p. 654, 2017.

[55] J. O'Sullivan, A. Rogers, D. Flynn, P. Smith, A. Mullane, and M. O'Malley, "Studying the maximum instantaneous non-synchronous generation in an Island system-frequency stability challenges in Ireland," *IEEE Transactions on Power Systems*, vol. 29, no. 6, pp. 2943–2951, 2014.

[56] G. Delille, B. François, and G. Malarange, "Dynamic frequency control support by energy storage to reduce the impact of wind and solar generation on isolated power

system's inertia," *IEEE Transactions on Sustainable Energy*, vol. 3, no. 4, pp. 931–939, 2012.

[57] R. Eriksson, N. Modig, and K. Elkington, "Synthetic inertia versus fast frequency response: a definition," *IET Renewable Power Generation*, vol. 12, no. 5, pp. 507–514, 2018.

[58] Y. Liu, S. Yang, S. Zhang, and F. Z. Peng, "Comparison of Synchronous Condenser and STATCOM for Inertial Response Support," in *2014 IEEE Energy Conversion Congress and Exposition (ECCE)*, (Pittsburgh, USA), IEEE, 2014.

[59] M. Bahrman and P. E. Bjorklund, "The new black start: System restoration with help from voltage-sourced converters," *IEEE Power and Energy Magazine*, vol. 12, no. 1, pp. 44–53, 2014.

[60] ENTSO-E, "Technopedia techsheets: Synchronous Condenser." Available at: https://www.entsoe.eu/Technopedia/techsheets/synchronous-condenser. [Accessed: 18-Sep-21].

[61] S. Nakamura, T. Yamada, T. Nomura, M. Iwamoto, Y. Shindo, S. Nose, A. Ishihara, and H. Fujino, "30 mva superconducting synchronous condenser: Design and it's performance test results," *IEEE Transactions on Magnetics*, vol. 21, no. 2, pp. 783–790, 1985.

[62] J. A. Oliver, B. J. Ware, and R. C. Carruth, "345 mva fully water-cooled synchronous condenser for dumont station part i. application considerations," *IEEE Transactions on Power Apparatus and Systems*, vol. PAS-90, no. 6, pp. 2758–2764, 1971.

[63] H. T. Nguyen, G. Yang, A. H. Nielsen, and P. H. Jensen, "Frequency stability improvement of low inertia systems using synchronous condensers," in *IEEE International Conference on Smart Grid Communications (SmartGridComm)*, 2016.

[64] H. T. Nguyen, G. Yang, A. H. Nielsen, and P. H. Jensen, "Combination of synchronous condenser and synthetic inertia for frequency stability enhancement in low-inertia systems," *IEEE Transactions on Sustainable Energy*, vol. 10, no. 3, pp. 997–1005, 2019.

[65] M. Nedd, Q. Hong, K. Bell, C. Booth, and P. Mohapatra, "Application of Synchronous Compensators in the GB Transmission Network to Address Protection Challenges from Increasing Renewable Generation," in *Cigre B5 Colloquium*, (Auckland, New Zealand), 2017.

[66] M. Nedd, C. Booth, and K. Bell, "Potential Solutions to the Challenges of Low Inertia Power Systems with a Case Study Concerning Synchronous Condensers," in *52nd International Universities Power Engineering Conference (UPEC)*, (Heraklion, Greece), 2017.

[67] SP Energy Networks, "Project Phoenix Progress Update," 2018.

[68] current-news, "SPEN announces world first stability trial dubbed Project Phoenix." Available at: https://www.current-news.co.uk/news/spen-announces-world-first-stability-trial-dubbed-project-phoenix. [Accessed: 18-Sep-21].

[69] National Grid, "Enhanced frequency response: Invitation to tender for pre-qualified parties," 2016.

[70] National Grid, "Enhanced Frequency Response Market Information Report," 2016.

[71] National Grid ESO, "Future of Frequency Response: Industry Update," 2019.

[72] National Grid ESO, "Future Requirements for Balancing Services," 2016.

[73] National Grid ESO, "Monthly Balancing Services Summary (November 2018)," 2018.

[74] National Grid ESO, "Firm Frequency Response (FFR) Market Information Report for Nov-18," 2018.

[75] X. Luo, J. Wang, J. D. Wojcik, J. Wang, D. Li, M. Draganescu, Y. Li, and S. Miao, "Review of voltage and frequency grid code specifications for electrical energy storage applications," *Energies*, vol. 11, no. 5, 2018.

[76] C. Roberts, "Review of International Grid Codes," 2018.

[77] L. Meng, J. Zafar, S. K. Khadem, A. Collinson, K. C. Murchie, F. Coffele, and G. M. Burt, "Fast Frequency Response from Energy Storage Systems - A Review of Grid Standards, Projects and Technical Issues," *IEEE Transactions on Smart Grid*, vol. 11, no. 2, pp. 1566–1581, 2020.

[78] R. H. Byrne, R. J. Concepcion, and C. A. Silva-Monroy, "Estimating potential revenue from electrical energy storage in PJM," in *IEEE Power and Energy Society General Meeting (PESGM)*, (Boston, USA), 2016.

[79] P. J. Vogler-Finck and W. G. Früh, "Evolution of primary frequency control requirements in Great Britain with increasing wind generation," *International Journal of Electrical Power and Energy Systems*, vol. 73, pp. 377–388, 2015.

[80] The Electropaedia, "Watt Flyball Governor." Available at: https://www.mpoweruk.com. [Accessed: 14-Sep-21].

[81] G. Lalor, J. Ritchie, D. Flynn, and M. J. O'Malley, "The impact of combined-cycle gas turbine short-term dynamics on frequency control," *IEEE Transactions on Power Systems*, vol. 20, no. 3, pp. 1456–1464, 2005.

[82] H. Wyman-Pain, Y. Bian, C. Thomas, and F. Li, "The economics of different generation technologies for frequency response provision," *Applied Energy*, vol. 222, no. April, pp. 554–563, 2018.

[83] F. Teng, V. Trovato, and G. Strbac, "Stochastic Scheduling With Inertia-Dependent Fast Frequency Response Requirements," *IEEE Transactions on Power Systems*, vol. 31, no. 2, pp. 1557–1566, 2016.

[84] P. V. Brogan, R. J. Best, D. J. Morrow, K. McKinley, and M. L. Kubik, "Effect of BESS Response on Frequency and RoCoF During Underfrequency Transients," *IEEE Transactions on Power Systems*, vol. 34, no. 1, pp. 575–583, 2019.

[85] T. Athay, R. Podmore, and S. Virmani, "A practical method for the direct analysis of transient stability," *IEEE transactions on power apparatus and systems*, vol. PAS-98, no. 2, pp. 573–584, 1979.

[86] D. M. Greenwood, K. Y. Lim, C. Patsios, P. F. Lyons, Y. S. Lim, and P. C. Taylor, "Frequency response services designed for energy storage," *Applied Energy*, vol. 203, pp. 115–127, 2017.

[87] M. Nedd, J. Browell, K. Bell, and C. Booth, "Containing a Credible Loss to within Frequency Stability Limits in a Low-Inertia GB Power System," *IEEE Transactions on Industry Applications*, vol. 56, no. 2, pp. 1031–1039, 2020.

[88] K. Forkasiewicz, M. Coldwell, A. Cross, and D. Strickland, "Meeting frequency response requirements with uncertain system inertia - a UK perspective," in *IEEE International Conference on Renewable Energy Research and Applications (ICRERA)*, (Birmingham, UK), 2016.

[89] Q. Hong, M. Nedd, S. Norris, I. Abdulhadi, M. Karimi, V. Terzija, B. Marshall, K. Bell, and C. Booth, "Fast frequency response for effective frequency control in power systems with low inertia," *The Journal of Engineering*, vol. 2019, no. 16, pp. 1696–1702, 2019.

[90] M. R. Rapizza and S. M. Canevese, "Fast frequency regulation and synthetic inertia in a power system with high penetration of renewable energy sources: Optimal design of the required quantities," *Sustainable Energy, Grids and Networks*, vol. 24, p. 100407, 2020.

[91] P. Wall, N. Shams, V. Terzija, V. Hamidi, C. Grant, D. Wilson, S. Norris, K. Maleka, C. Booth, Q. Hong, and A. Roscoe, "Smart frequency control for the

future GB power system," *IEEE PES Innovative Smart Grid Technologies Conference Europe*, 2016.

[92] F. Milano and R. Zaŕate-Miñano, "A systematic method to model power systems as stochastic differential algebraic equations," *IEEE Transactions on Power Systems*, vol. 28, no. 4, pp. 4537–4544, 2013.

[93] C. Roberts, E. M. Stewart, and F. Milano, "Validation of the Ornstein-Uhlenbeck process for load modeling based on μPMU measurements," in *19th Power Systems Computation Conference (PSCC)*, (Genoa, Italy), pp. 1–7, Power Systems Computation Conference, 2016.

[94] K. Wang and M. L. Crow, "The Fokker-Planck equation for power system stability probability density function evolution," *IEEE Transactions on Power Systems*, vol. 28, no. 3, pp. 2994–3001, 2013.

[95] P. Vorobev, D. Greenwood, J. H. Bell, J. W. Bialek, P. C. Taylor, and K. Turitsyn, "Deadbands, Droop and Inertia Impact on Power System Frequency Distribution," *IEEE Transactions on Power Systems*, vol. 34, no. 4, pp. 3098–3108, 2019.

[96] D. del Giudice, A. Brambilla, S. Grillo, and F. Bizzarri, "Effects of inertia, load damping and dead-bands on frequency histograms and frequency control of power systems," *International Journal of Electrical Power and Energy Systems*, vol. 129, no. March, p. 106842, 2021.

[97] T. Feehally, A. Forsyth, R. Todd, M. Foster, D. Gladwin, D. Stone, and D. Strickland, "Battery energy storage systems for the electricity grid: UK research facilities," in *8th IET International Conference on Power Electronics, Machines and Drives (PEMD)*, (Glasgow, UK), 2016.

[98] P. V. Brogan, A. H. Alikhanzadeh, R. J. Best, D. J. Morrow, and M. L. Kubik, "Fast Frequency Response Requirements for Replacement of Observed Generator Response During Under Frequency Transients," in *Cigre Symposium*, (Dublin, Ireland), 2017.

[99] SP Energy Networks, "SP Manweb Future Energy Scenarios Key Findings," 2020.

[100] Y. Mu, J. Wu, J. Ekanayake, N. Jenkins, and H. Jia, "Primary Frequency Response From Electric Vehicles in the Great Britain Power System," *IEEE Transactions on Smart Grid*, vol. 4, no. 2, pp. 1142–1150, 2013.

[101] J. Meng, Y. Mu, H. Jia, J. Wu, X. Yu, and B. Qu, "Dynamic frequency response from electric vehicles considering travelling behavior in the Great Britain power system," *Applied Energy*, vol. 162, pp. 966–979, 2016.

[102] F. Teng, Y. Mu, H. Jia, J. Wu, P. Zeng, and G. Strbac, "Challenges on primary frequency control and potential solution from EVs in the future GB electricity system," *Applied Energy*, vol. 194, pp. 353–362, 2017.

[103] P. M. Almeida, F. J. Soares, and J. A. Lopes, "Electric vehicles contribution for frequency control with inertial emulation," *Electric Power Systems Research*, vol. 127, pp. 141–150, 2015.

[104] BEIS, "Clean Growth - Transforming Heating," 2018.

[105] UK Government, "The Ten Point Plan for a Green Industrial Revolution," 2020.

[106] M. T. Muhssin, L. M. Cipcigan, N. Jenkins, S. Slater, M. Cheng, and Z. A. Obaid, "Dynamic Frequency Response from Controlled Domestic Heat Pumps," *IEEE Transactions on Power Systems*, vol. 33, no. 5, pp. 4948–4957, 2018.

[107] Y. Wang, Y. Xu, and Y. Tang, "Distributed aggregation control of grid-interactive smart buildings for power system frequency support," *Applied Energy*, vol. 251, 2019.

[108] M. Cheng, J. Wu, S. J. Galsworthy, C. E. Ugalde-Loo, N. Gargov, W. W. Hung, and N. Jenkins, "Power system frequency response from the control of bitumen tanks," *IEEE Transactions on Power Systems*, vol. 31, no. 3, pp. 1769–1778, 2016.

[109] W. Wang, A. Abdolrashidi, N. Yu, and D. Wong, "Frequency regulation service provision in data center with computational flexibility," *Applied Energy*, vol. 251, 2019.

[110] A. Postnikov, I. M. Albayati, S. Pearson, C. Bingham, R. Bickerton, and A. Zolotas, "Facilitating static firm frequency response with aggregated networks of commercial food refrigeration systems," *Applied Energy*, vol. 251, 2019.

[111] M. Dreidy, H. Mokhlis, and S. Mekhilef, "Inertia response and frequency control techniques for renewable energy sources: A review," *Renewable and Sustainable Energy Reviews*, vol. 69, pp. 144–155, 2017.

[112] A. Fernández-Guillamón, E. Gómez-Lázaro, E. Muljadi, and Ángel Molina-García, "Power systems with high renewable energy sources: A review of inertia and frequency control strategies over time," *Renewable and Sustainable Energy Reviews*, vol. 115, p. 109369, 2019.

[113] J. Aho, A. Buckspan, J. Laks, P. Fleming, Y. Jeong, F. Dunne, M. Churchfield, L. Pao, and K. Johnson, "A tutorial of wind turbine control for supporting grid frequency through active power control," in *Proceedings of the American Control Conference*, (Montreal, Canada), pp. 3120–3131, IEEE, 2012.

[114] J. Morren, S. W. de Haan, W. L. Kling, and J. A. Ferreira, "Wind turbines emulating inertia and supporting primary frequency control," *IEEE Transactions on Power Systems*, vol. 21, no. 1, pp. 433–434, 2006.

[115] G. Ramtharan, J. Ekanayake, and N. Jenkins, "Frequency support from doubly fed induction generator wind turbines," *IET Renewable Power Generation*, vol. 1, no. 1, pp. 3–9, 2007.

[116] P. Moutis, S. A. Papathanassiou, and N. D. Hatziargyriou, "Improved load-frequency control contribution of variable speed variable pitch wind generators," *Renewable Energy*, vol. 48, pp. 514–523, 2012.

[117] NREL, "Demonstration of Essential Reliability Services by a 300-MW Solar Photovoltaic Power Plant," 2017.

[118] National Grid, "System Operability Framework 2014," 2014.

[119] National Grid, "System Operability Framework 2015," 2015.

[120] National Grid, "System Needs and Product Strategy," 2017.

[121] National Grid, "Product Roadmap for Frequency Response and Reserve," 2017.

[122] National Grid ESO, "National Grid ESO debuts Dynamic Containment frequency response service." Available at: https://www.nationalgrideso.com/news/national-grid-eso-debuts-dynamic-containment-frequency-response-service. [Accessed: 10-Mar-21].

[123] National Grid ESO, "Operating a Low Inertia System," 2020.

[124] Ofgem, "Changes to the Distribution Code and Engineering Recommendation G59: Frequency Changes during Large Disturbances and their Impact on the Total System," 2014.

[125] National Grid, "Frequency Changes during Large Disturbances and their Impact on the Total System (report to the authority)," 2014.

[126] Ofgem, "Distribution Code: DC0079 - Frecuency Changes during Large Disturbances and their Impact on the Total System," 2017.

[127] Ofgem, "Distribution Code: DC0079 - Frequency Changes during Large Disturbances and their Impact on the Total System (Phase 2)," 2018.

[128] Ofgem, "Distribution Code: DC0079 - Frequency Changes during Large Disturbances and their Impact on the Total System (Phase 4)," 2019.

[129] National Grid ESO and Energy Networks Association, "Accelerated Loss of Mains Change Programme (ALoMCP) - Window 5 Report," 2021.

[130] National Grid ESO, "Technical Report on the events of 9 August 2019," 2019.

[131] T. Weissbach and E. Welfonder, "Improvement of the Performance of Scheduled Stepwise Power Programme Changes within the European Power System," in *IFAC Proceedings Volumes*, (Seoul, South Korea), pp. 11972–11977, IFAC, 2008.

[132] T. Weissbach and E. Welfonder, "High frequency deviations within the European power system: Origins and proposals for improvement," in *2009 IEEE/PES Power Systems Conference and Exposition, PSCE*, (Seattle, USA), pp. 1–6, IEEE, 2009.

[133] B. Schäfer, C. Beck, K. Aihara, D. Witthaut, and M. Timme, "Non-Gaussian power grid frequency fluctuations characterized by Lévy-stable laws and superstatistics," *Nature Energy*, vol. 3, no. 2, pp. 119–126, 2018.

[134] B. Schäfer, M. Timme, and D. Witthaut, "Isolating the Impact of Trading on Grid Frequency Fluctuations," in *2018 IEEE PES Innovative Smart Grid Technologies Conference Europe, ISGT-Europe*, (Sarajevo, Bosnia-Herzegovina), 2018.

[135] M. Anvari, L. R. Gorjão, M. Timme, D. Witthaut, B. Schäfer, and H. Kantz, "Stochastic properties of the frequency dynamics in real and synthetic power grids," *Physical Review Research*, vol. 2, no. 1, p. 013339, 2020.

[136] M. Folgueras, E. Wenger, A. Florita, K. Clark, and V. Gevorgian, "Grid Frequency Extreme Event Analysis and Modeling," in *International Workshop on Large-Scale Integration of Wind Power into Power Systems as well as on Transmission Networks for Offshore Wind Power Plants (Wind Integration Workshop)*, (Berlin, Germany), 2017.

[137] H. Wyman-Pain, Y. Bian, and F. Li, "Changes in Frequency Events and the Frequency Response Markets in Great Britain," in *IEEE Power & Energy Society General Meeting*, (Portland, USA), IEEE, 2018.

[138] Eirgrid and SONI, "All-Island Transmission System Performance Report 2019," 2019.

[139] N. P. Nkosi and J. Dikgang, "Pricing electricity blackouts among south african households," *Journal of Commodity Markets*, vol. 11, pp. 37–47, 2018.

[140] Drax, "Black start: the most important back up plan you've never heard of." Available at: https://www.drax.com/power-generation/black-start-important-back-plan-youve-never-heard/. [Accessed: 11-Sep-21].

[141] G. Andersson, P. Donalek, R. Farmer, N. Hatziargyriou, I. Kamwa, P. Kundur, N. Martins, J. Paserba, P. Pourbeik, J. Sanchez-Gasca, R. Schulz, A. Stankovic, C. Taylor, and V. Vittal, "Causes of the 2003 Major Grid Blackouts in North America and Europe, and Recommended Means to Improve System Dynamic Performance," *IEEE Transactions on Power Systems*, vol. 20, no. 4, pp. 1922–1928, 2005.

[142] O. P. Veloza and R. H. Cespedes, "Vulnerability of the Colombian electric system to blackouts and possible remedial actions," in *2006 IEEE Power Engineering Society General Meeting*, IEEE, 2006.

[143] O. P. Veloza and F. Santamaria, "Analysis of major blackouts from 2003 to 2015: Classification of incidents and review of main causes," *Electricity Journal*, vol. 29, no. 7, pp. 42–49, 2016.

[144] S. Kamali and T. Amraee, "Blackout prediction in interconnected electric energy systems considering generation re-dispatch and energy curtailment," *Applied Energy*, vol. 187, pp. 50–61, 2017.

[145] E. Zio and T. Aven, "Uncertainties in smart grids behavior and modeling: What are the risks and vulnerabilities? How to analyze them?," *Energy Policy*, vol. 39, no. 10, pp. 6308–6320, 2011.

[146] Z. Bo, O. Shaojie, Z. Jianhua, S. Hui, W. Geng, and Z. Ming, "An analysis of previous blackouts in the world: Lessons for China's power industry," *Renewable and Sustainable Energy Reviews*, vol. 42, pp. 1151–1163, 2015.

[147] ENTSO-E, "Final report - System Disturbance on 4 November 2006," 2007.

[148] R. Price and National Grid, "System Events of 27th May 2008," 2008.

[149] L. L. Lai, H. T. Zhang, S. Mishra, D. Ramasubramanian, C. S. Lai, and F. Y. Xu, "Lessons learned from July 2012 Indian blackout," in *9th IET Int Conference on Advances in Power System Control, Operation and Management (APSCOM 2012)*, 2012.

[150] AEMO, "Black System South Australia," 2017.

[151] A. Abedi, L. Gaudard, and F. Romerio, "Review of major approaches to analyze vulnerability in power system," *Reliability Engineering and System Safety*, vol. 183, pp. 153–172, 2019.

[152] London Economics, "The Value of Lost Load (VoLL) for Electricity in Great Britain: Final report for OFGEM and DECC," *OFGEM and DECC*, no. July, pp. 1–225, 2013.

[153] Ofgem, "9 August 2019 power outage report," 2020.

[154] Elexon, "Balancing mechanism reports." Available at: https://www.bmreports.com/bmrs/?q=generation/fueltype. [Accessed: 11-Feb-20].

[155] National Grid ESO, "Data finder and explorer." Available at: https://www.nationalgrideso.com/balancing-data/data-finder-and-explorer. [Accessed: 11-Feb-20].

[156] UK Government (BEIS), "Digest of United Kingdom Energy Statistics 2018," 2018.

[157] BEIS, "National Energy Efficiency Data-Framework (NEED): Summary of Analysis, Great Britain," 2020.

[158] UK Government (BEIS), "Implementing the end of unabated coal by 2025," 2018.

[159] National Grid ESO, "Appendices to the Technical Report on the events of 9 August 2019," 2019.

[160] National Grid, "Frequency response holding volumes." Available at: https://www.nationalgrideso.com/balancing-data/data-explorer. [Accessed: 11-Feb-19].

[161] National Grid ESO, "BM Unit Information (Elexon BM Unit Data)." Available at: https://www.netareports.com/data/elexon.jsp. [Accessed: 11-Feb-19].

[162] National Grid, "The Grid Code," 2018.

[163] National Grid ESO, "Past Frequency Events," 2019.

[164] ENTSO-E, "Power statistics." Available at: https://www.entsoe.eu/data/power-stats/. [Accessed: 17-May-21].

[165] National Grid, "System Security and Quality of Supply Standard," 2019.

[166] National Grid ESO, "Future Energy Scenarios," 2019.

[167] P. Schavemaker and L. van der Sluis, *Electrical Power System Essentials*. Wiley, 2008.

Appendices

Appendix A

Swing equation derivation

In Section 2.2 we introduced the swing equation. This equation plays an important role in Chapter 4 and Chapter 5, so it is important to fully explain the derivation, which I will do here. Note, what I refer to as the *grid swing equation* in this appendix is referred to simply as the *swing equation* in the main text.

A.1 The swing equation for a single synchronous generator

A simplified diagram of a synchronous generator is given in Fig. A.1. Mechanical power, $P_{\mathrm{m},i}$, provided by a prime mover (PM in the figure) is converted into electrical power, $P_{\mathrm{e},i}$, in an electrical generator. An example of a prime mover is a steam turbine. We will

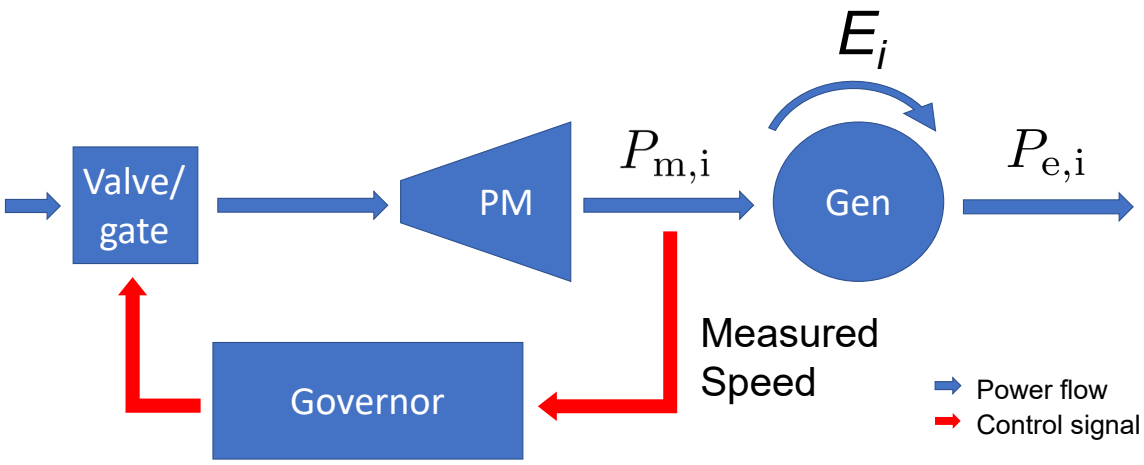

Figure A.1: Simplified diagram of a synchronous generator.

assume that the efficiency of this conversion is 100% (it is actually about 99% [167]). The synchronous generator has rotational kinetic energy, E_i, which has a rate of change given by

$$\frac{\mathrm{d}}{\mathrm{d}t}(E_i) = P_{\mathrm{m},i} - P_{\mathrm{e},i}\,, \tag{A.1}$$

where E_i is given by

$$E_i = \frac{1}{2} J_i (2\pi f_i)^2\,. \tag{A.2}$$

J_i is the moment of inertia (of all the rotating parts: fluids, prime mover, electric generator) and f_i is the frequency of the synchronous generator. The rotational kinetic energy of the synchronous generator at the nominal system frequency, f_n, is given by

$$E_{\mathrm{n},i} = \frac{1}{2} J_i (2\pi f_\mathrm{n})^2\,. \tag{A.3}$$

so E_i can be written as

$$E_i = E_{\mathrm{n},i} \left(\frac{f_i}{f_\mathrm{n}}\right)^2\,. \tag{A.4}$$

Substituting Eq. (A.4) into Eq. (A.1) gives

$$\frac{\mathrm{d}f_i}{\mathrm{d}t} = \frac{f_\mathrm{n}^2}{2E_{\mathrm{n},i} f_i}(P_{\mathrm{m},i} - P_{\mathrm{e},i})\,. \tag{A.5}$$

This is the swing equation for a single synchronous generator.

The inertia constant, H_i, for a synchronous generator is defined as

$$H_i = \frac{E_{\mathrm{n},i}}{S_i}\,. \tag{A.6}$$

S_i is the rated capacity of the synchronous generator. Different types of synchronous generators have different inertia constants: typical values are between $H_i = 2\,\mathrm{s}$ and $H_i = 13\,\mathrm{s}$ [6]. Using Eq. (A.6), the swing equation for a single synchronous generator Eq. (A.5) can be written as

$$\frac{\mathrm{d}f_i}{\mathrm{d}t} = \frac{f_\mathrm{n}^2}{2H_i S_i f_i}(P_{\mathrm{m},i} - P_{\mathrm{e},i})\,. \tag{A.7}$$

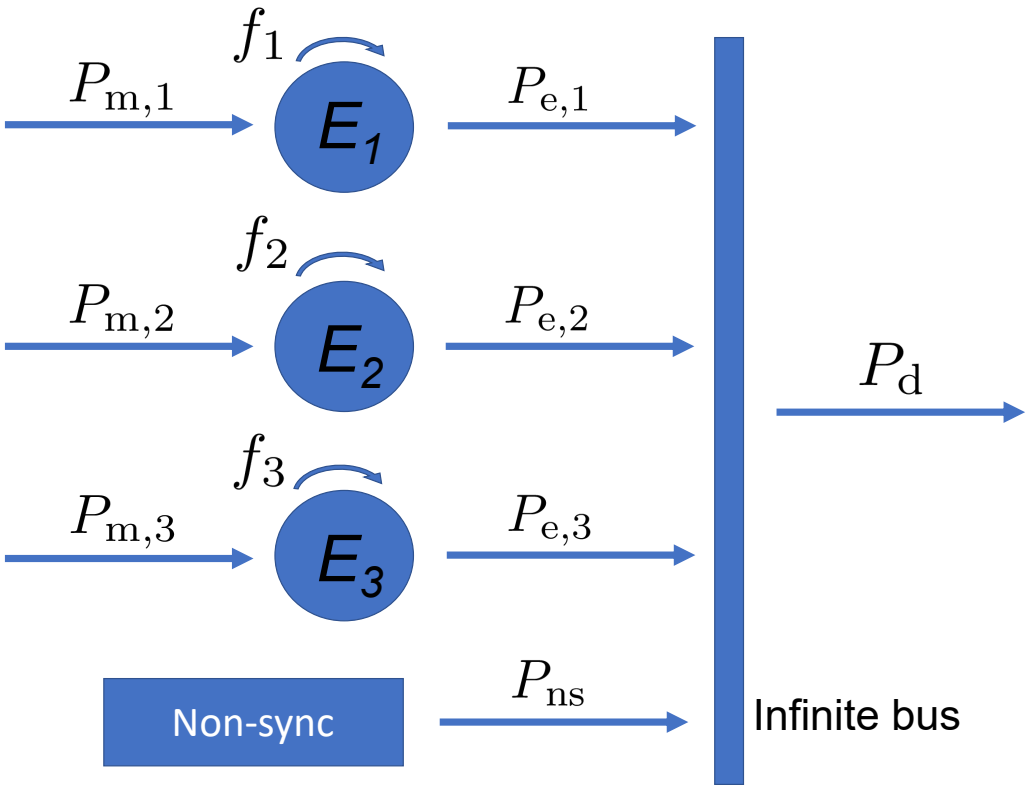

Figure A.2: Power flows on a simplified grid with the single infinite bus assumption.

A.2 Grid swing equation

Fig. A.2 represents a highly simplified grid with a single infinite bus assumption. Non-synchronous generation is represented by P_{ns}: examples include wind, solar, and interconnectors. It offers no inertia to the grid and the mechanical input power (if there is any) is decoupled from the electrical output power. All the electrical demand is represented by P_{d}, which is the sum of numerous and various sized loads. There are multiple synchronous generators on the grid. Each one has a mechanical input power, rotates at a certain frequency, offers rotational kinetic energy to the grid, and outputs electrical power. Eq. (A.1) is the conservation of energy equation for each synchronous generator on the grid. Adding all these equations together, in a grid with n synchronous generators, gives us

$$\frac{\mathrm{d}}{\mathrm{d}t}\left(\sum_i^n E_i\right) = \sum_i^n P_{\mathrm{m},i} - \sum_i^n P_{\mathrm{e},i}\,. \tag{A.8}$$

If losses on the system are ignored, conservation of energy dictates that the total electrical power generated is equal to the total system demand:

$$\underbrace{P_{\mathrm{d}}}_{\text{total electrical demand}} = \underbrace{\sum_{i}^{n} P_{\mathrm{e},i} + P_{\mathrm{ns}}}_{\text{total electrical generation}} . \tag{A.9}$$

Using Eq. (A.4) and Eq. (A.9), Eq. (A.8) becomes

$$\frac{\mathrm{d}}{\mathrm{d}t}\left(\sum_{i}^{n} E_{\mathrm{n},i} \left(\frac{f_i}{f_{\mathrm{n}}} \right)^2 \right) = \left(\sum_{i}^{n} P_{\mathrm{m},i} \right) + P_{\mathrm{ns}} - P_{\mathrm{d}} . \tag{A.10}$$

Using the single infinite bus approximation (all generation and demand connected to one infinite bus), frequency is the same throughout: $f_i = f$. The single infinite bus approximation is the same as the constant voltage approximation. This approximation gives us

$$\frac{\mathrm{d}}{\mathrm{d}t}\left(\left(\frac{f}{f_{\mathrm{n}}} \right)^2 \sum_{i}^{n} E_{\mathrm{n},i} \right) = \left(\sum_{i}^{n} P_{\mathrm{m},i} \right) + P_{\mathrm{ns}} - P_{\mathrm{d}} . \tag{A.11}$$

The sums can be defined as grid level quantities

$$\begin{aligned} E_{\mathrm{n}} &= \sum_{i}^{n} E_{\mathrm{n},i} , \\ P_{\mathrm{m}} &= \sum_{i}^{n} P_{\mathrm{m},i} . \end{aligned} \tag{A.12}$$

E_{n}, which is the sum of the rotational kinetic energy of all the synchronous generators at the nominal system frequency, f_{n}, will hereby be referred to as $E_{\mathrm{n,gen}}$. E_{n} is redefined as the sum of the inertia contribution from synchronous generators plus the contribution from synchronously connected demand (both at f_{n}): $E_{\mathrm{n}} = E_{\mathrm{n,gen}} + E_{\mathrm{n,dem}}$. This is the definition of system inertia. P_{m} is the sum of the mechanical input of all the synchronous generators. Eq. (A.11) can then be written as

$$\frac{\mathrm{d}}{\mathrm{d}t}\left(\left(\frac{f}{f_{\mathrm{n}}} \right)^2 E_{\mathrm{n}} \right) = P_{\mathrm{m}} + P_{\mathrm{ns}} - P_{\mathrm{d}} . \tag{A.13}$$

All the synchronous generators have, in effect, been combined into one generator with mechanical power input P_{m} and rotational kinetic energy E_{n}. The grid swing equation is

$$\frac{\mathrm{d}f}{\mathrm{d}t} = \frac{f_{\mathrm{n}}^2}{2E_{\mathrm{n}}f}(P_{\mathrm{m}} + P_{\mathrm{ns}} - P_{\mathrm{d}})\,. \tag{A.14}$$

Most of the time, $P_{\mathrm{m}} + P_{\mathrm{ns}} - P_{\mathrm{d}}$ will be very close to zero because the electricity system operator aims to keep generation and demand in perfect balance. The net power imbalance of the grid, ΔP, is equal to $P_{\mathrm{m}} + P_{\mathrm{ns}} - P_{\mathrm{d}}$ and is non-zero due to relatively small fluctuations in P_{m}, P_{ns}, and P_{d}. One of these fluctuations is the sudden, unexpected loss of generation or demand. I define this as the power imbalance of the grid, I, which is positive when there is a demand loss and negative when there is a generation loss.

Another fluctuation is as a result of the previous one. A proportion of generating and demand units respond to frequency changes by varying their power output, with the goal of keeping the grid in balance and maintaining a steady grid frequency. Synchronous generators provide frequency response to the grid using speed governors with droop control. When there is a frequency deviation, the speed governor makes sure there is a proportional change in the mechanical power output of the prime mover, which is then the input to the electrical generator. It is not just synchronous generators that provide frequency response to the grid. Response from batteries, interconnectors, and demand side flexibility are also contributors. I define the sum of the varying outputs of all the individual units as R (the total frequency response of the grid), which can be positive or negative.

The final fluctuation is due to a phenomenon known as demand damping, which is described in Section 2.2.1. Many loads on the grid have a power demand that is frequency dependent e.g. synchronous motors. If the relationship between frequency deviation and change in power demand (for frequency dependent loads) is approximated as linear then the total demand of the grid can be split into a frequency dependent part

and a frequency independent part

$$P_{\mathrm{d}} = D_{\mathrm{n}} + kD_{\mathrm{n}}\Delta f\,, \tag{A.15}$$

where Δf is the frequency deviation ($\Delta f = f - f_{\mathrm{n}}$), D_{n} is the demand of the grid at f_{n}, and k is the demand damping constant and is a measure of how 'damped' the system is.

The net power imbalance of the grid is the sum of these fluctuations ($\Delta P = R + I - kD_{\mathrm{n}}\Delta f$). Eq. (A.14) can therefore be written as

$$\begin{aligned}\frac{\mathrm{d}f}{\mathrm{d}t} &= \frac{f_{\mathrm{n}}^2}{2E_{\mathrm{n}}f}\Delta P \\ &= \frac{f_{\mathrm{n}}^2}{2E_{\mathrm{n}}f}(R + I - kD_{\mathrm{n}}\Delta f)\,,\end{aligned} \tag{A.16}$$

which is the swing equation used in the main text (Eq. (2.1)).

I define the inertia constant, H, for the whole grid as

$$H = \frac{E_{\mathrm{n,gen}}}{S} + H_{dem} = \frac{\sum_i^n H_i S_i}{\sum_i^n S_i} + H_{dem}\,, \tag{A.17}$$

where S is the sum of the rated capacities of the synchronous generators and H_{dem} is the inertia constant of demand. Using Eq. (A.17), the swing equation for the whole grid Eq. (A.16) can be written as

$$\frac{\mathrm{d}f}{\mathrm{d}t} = \frac{f_{\mathrm{n}}^2}{2HSf}(R + I - kD_{\mathrm{n}}\Delta f)\,. \tag{A.18}$$

Here is a recap of the main assumptions used in these derivations:

- Single infinite bus approximation (i.e. constant voltage approximation)
- The efficiency of an electric generator is 100%
- There are no transmission losses on the grid
- Demand reduction due to demand damping is linear with frequency deviation

Appendix B

Frequency dynamics after a large infeed loss

In Section 4.3.2 we determined what constraints were necessary on certain grid parameters to ensure frequency requirements are satisfied after a large infeed loss. These contraints were the RoCoF requirement constraint on inertia, Eq. (4.7), the steady-state requirement constraint on frequency response capacity, Eq. (4.8), the nadir requirement constraint on inertia Eq. (4.10), and the nadir requirement constraint on frequency response parameters. This appendix goes into further detail on the frequency evolution after a large infeed loss and gives a full derivation of Eq. (4.11).

B.1 Swing equation solutions

A reminder of the setup. At $t < 0$, the grid frequency is at the nominal value, f_{n}, and the RoCoF is zero. The RoCoF is zero because Δf, I, and R are all zero making the net power imbalance zero ($\Delta P = 0$). At $t = 0$, a large infeed loss occurs in the grid. The imbalance, I, step changes to a negative value and has a magnitude equal to the size of the loss. At the moment of the loss, the grid has a certain amount of demand, D_{n}, inertia, E_{n}, and demand damping, k. For the purposes of investigating frequency dynamics after a large infeed loss, the parameters mentioned so far (f_{n}, I, D_{n}, E_{n}, and k) remain constant for all time after $t = 0$. The frequency response, $R(t)$, and grid

frequency $f(t)$ evolve with time.

We start with the linearised swing equation,

$$\frac{\mathrm{d}f}{\mathrm{d}t} = \frac{f_\mathrm{n}}{2E_\mathrm{n}}(R + I - kD_\mathrm{n}\Delta f)\,, \tag{B.1}$$

and the approximation of frequency response as a linear ramp,

$$R(t) = \begin{cases} 0 & \text{when } t \leq t_\mathrm{d}\,, \\ R_\mathrm{cap}\left(\frac{t-t_\mathrm{d}}{t_\mathrm{r}}\right) & \text{when } t_\mathrm{d} \leq t \leq t_\mathrm{d} + t_\mathrm{r}\,, \\ R_\mathrm{cap} & \text{when } t \geq t_\mathrm{d} + t_\mathrm{r}\,. \end{cases} \tag{B.2}$$

We substitute Eq. (B.2) into Eq. (B.1) to get three linearised swing equations for each stage of the frequency response:

$$\frac{\mathrm{d}f}{\mathrm{d}t} = \begin{cases} \frac{f_\mathrm{n}}{2E_\mathrm{n}}(I - kD_\mathrm{n}\Delta f) & \text{when } t \leq t_\mathrm{d}\,, \\ \frac{f_\mathrm{n}}{2E_\mathrm{n}}\left(R_\mathrm{cap}\left(\frac{t-t_\mathrm{d}}{t_\mathrm{r}}\right) + I - kD_\mathrm{n}\Delta f\right) & \text{when } t_\mathrm{d} \leq t \leq t_\mathrm{d} + t_\mathrm{r}\,, \\ \frac{f_\mathrm{n}}{2E_\mathrm{n}}(R_\mathrm{cap} + I - kD_\mathrm{n}\Delta f) & \text{when } t \geq t_\mathrm{d} + t_\mathrm{r}\,, \end{cases} \tag{B.3}$$

where $\Delta f = f - f_\mathrm{n}$. The general solution for each differential equation is

$$f(t) = \begin{cases} c_1 \exp\left(-\frac{A}{E_\mathrm{n}}t\right) + \frac{I}{kD_\mathrm{n}} + f_\mathrm{n} & \text{when } t \leq t_\mathrm{d}\,, \\ c_2 \exp\left(-\frac{A}{E_\mathrm{n}}t\right) + \frac{R_\mathrm{cap}(t-t_\mathrm{d})}{kD_\mathrm{n}t_\mathrm{r}} - \frac{E_\mathrm{n}R_\mathrm{cap}}{kD_\mathrm{n}At_\mathrm{r}} + \frac{I}{kD_\mathrm{n}} + f_\mathrm{n} & \text{when } t_\mathrm{d} \leq t \leq t_\mathrm{d} + t_\mathrm{r}\,, \\ c_3 \exp\left(-\frac{A}{E_\mathrm{n}}t\right) + \frac{R_\mathrm{cap}+I}{kD_\mathrm{n}} + f_\mathrm{n} & \text{when } t \geq t_\mathrm{d} + t_\mathrm{r}\,, \end{cases} \tag{B.4}$$

where $A = kD_\mathrm{n}f_\mathrm{n}/2$.

Each differential equation in Eq. (B.3) is first-order, so one initial condition is needed for each for an exact solution. The setup described in the first paragraph of this section

imposes the initial condition for the first stage, $t \leq t_{\mathrm{d}}$:

$$f(t=0) = f_{\mathrm{n}}\,. \tag{B.5}$$

From this we get c_1, and the exact solution of the first stage is

$$f = \frac{I}{kD_{\mathrm{n}}}\left(1 - \exp\left(-\frac{A}{E_{\mathrm{n}}}t\right)\right) + f_{\mathrm{n}} \quad \text{when } t \leq t_{\mathrm{d}} \tag{B.6}$$

The initial condition for the second stage, $t_{\mathrm{d}} \leq t \leq t_{\mathrm{d}} + t_{\mathrm{r}}$, is the value of f at $t = t_{\mathrm{d}}$ given by the equation governing the evolution of the first stage:

$$f(t=t_{\mathrm{d}}) = \frac{I}{kD_{\mathrm{n}}}\left(1 - \exp\left(-\frac{A}{E_{\mathrm{n}}}t_{\mathrm{d}}\right)\right) + f_{\mathrm{n}} = K_1\,. \tag{B.7}$$

For simplicity, we have denoted $f(t=t_{\mathrm{d}})$ as K_1. From this we get c_2, and the exact solution of the second stage is

$$f = (K_1 - K_2)\exp\left(-\frac{A}{E_{\mathrm{n}}}(t-t_{\mathrm{d}})\right) + \frac{R_{\mathrm{cap}}(t-t_{\mathrm{d}})}{kD_{\mathrm{n}}t_{\mathrm{r}}} + K_2 \quad \text{when } t_{\mathrm{d}} \leq t \leq t_{\mathrm{d}} + t_{\mathrm{r}}\,, \tag{B.8}$$

where

$$K_2 = -\frac{E_{\mathrm{n}}R_{\mathrm{cap}}}{kD_{\mathrm{n}}At_{\mathrm{r}}} + \frac{I}{kD_{\mathrm{n}}} + f_{\mathrm{n}}\,. \tag{B.9}$$

The initial condition for the third stage, $t \geq t_{\mathrm{d}} + t_{\mathrm{r}}$, is the value of f at $t = t_{\mathrm{d}} + t_{\mathrm{r}}$ given by the equation governing the evolution of the second stage:

$$f(t=t_{\mathrm{d}}+t_{\mathrm{r}}) = (K_1 - K_2)\exp\left(-\frac{A}{E_{\mathrm{n}}}t_{\mathrm{r}}\right) + \frac{R_{\mathrm{cap}}}{kD_{\mathrm{n}}} + K_2 = K_3\,. \tag{B.10}$$

For simplicity, we have denoted $f(t=t_{\mathrm{d}}+t_{\mathrm{r}})$ as K_3. From this we get c_3, and the exact solution of the third stage is

$$f = (K_3 - f_{\mathrm{ss}})\exp\left(-\frac{A}{E_{\mathrm{n}}}(t-t_{\mathrm{d}}-t_{\mathrm{r}})\right) + f_{\mathrm{ss}} \quad \text{when } t \geq t_{\mathrm{d}} + t_{\mathrm{r}}\,, \tag{B.11}$$

where f_{ss} is the steady-state frequency and is given by $f_{\mathrm{ss}} = (R_{\mathrm{cap}} + I)/kD_{\mathrm{n}} + f_{\mathrm{n}}$.

In summary, the frequency evolution after a large infeed loss for each stage of the frequency response is

$$f(t) = \begin{cases} \frac{I}{kD_\mathrm{n}}\left(1 - \exp\left(-\frac{A}{E_\mathrm{n}}t\right)\right) + f_\mathrm{n} & \text{when } t \leq t_\mathrm{d}\,, \\ (K_1 - K_2)\exp\left(-\frac{A}{E_\mathrm{n}}(t - t_\mathrm{d})\right) + \frac{R_\mathrm{cap}(t-t_\mathrm{d})}{kD_\mathrm{n}t_\mathrm{r}} + K_2 & \text{when } t_\mathrm{d} \leq t \leq t_\mathrm{d} + t_\mathrm{r}\,, \\ (K_3 - f_\mathrm{ss})\exp\left(-\frac{A}{E_\mathrm{n}}(t - t_\mathrm{d} - t_\mathrm{r})\right) + f_\mathrm{ss} & \text{when } t \geq t_\mathrm{d} + t_\mathrm{r}\,, \end{cases} \tag{B.12}$$

where $A = kD_\mathrm{n}f_\mathrm{n}/2$, K_1 is defined in Eq. (B.7), K_2 is defined in Eq. (B.9), and K_3 is defined in Eq. (B.10).

B.2 Derivation of nadir requirement constraint on frequency response parameters

Differentiating Eq. (B.12) gives us

$$\frac{\mathrm{d}f}{\mathrm{d}t} = \begin{cases} \frac{IA}{kD_\mathrm{n}E_\mathrm{n}}\exp\left(-\frac{A}{E_\mathrm{n}}t\right) & \text{when } t \leq t_\mathrm{d}\,, \\ -\frac{A}{E_\mathrm{n}}(K_1 - K_2)\exp\left(-\frac{A}{E_\mathrm{n}}(t - t_\mathrm{d})\right) + \frac{R_\mathrm{cap}}{kD_\mathrm{n}t_\mathrm{r}} & \text{when } t_\mathrm{d} \leq t \leq t_\mathrm{d} + t_\mathrm{r}\,, \\ -\frac{A}{E_\mathrm{n}}(K_3 - f_\mathrm{ss})\exp\left(-\frac{A}{E_\mathrm{n}}(t - t_\mathrm{d} - t_\mathrm{r})\right) & \text{when } t \geq t_\mathrm{d} + t_\mathrm{r}\,. \end{cases} \tag{B.13}$$

$\mathrm{d}f/\mathrm{d}t \to 0$ as $t \to \infty$ in the first and third stage. From this we can see that a localised minimum in frequency, the frequency nadir, can only occur within the second stage: the time period where the frequency response is ramping.

The frequency nadir occurs when $\mathrm{d}f/\mathrm{d}t = 0$. Substituting this into Eq. (B.3) for the second stage gives us the time when the frequency nadir occurs:

$$t_\mathrm{nad} = \frac{t_\mathrm{r}}{R_\mathrm{cap}}\big(kD_\mathrm{n}(f_\mathrm{nad} - f) - I\big) + t_\mathrm{d}\,, \tag{B.14}$$

where f_{nad} is the value of the frequency nadir. Setting $\mathrm{d}f/\mathrm{d}t = 0$ and putting $t = t_{\text{nad}}$ into the second stage of Eq. (B.13) gives us, after some rearranging,

$$R_{\text{cap}} \exp\left(\frac{At_{\text{r}}\big(kD_{\text{n}}(f_{\text{nad}} - f_{\text{n}}) - I\big)}{E_{\text{n}}R_{\text{cap}}}\right) = R_{\text{cap}} - \frac{At_{\text{r}}I}{E_{\text{n}}} \exp\left(-\frac{At_{\text{d}}}{E_{\text{n}}}\right). \tag{B.15}$$

We want to know which frequency response parameters (R_{cap}, t_{r}, and t_{d}) result in a frequency nadir that is equal to the nadir limit. This will be the absolute limit (i.e. minimum frequency response capacity, maximum delay time, and maximum ramp time) for the particular frequency response parameter. We do this by setting $f_{\text{nad}} = L_{\text{nad}}$ in Eq. (B.15), which gives us Eq. (4.11).

B.3 Relationship between ramp time, delay time, and inertia with a fixed frequency response capacity

Rearranging Eq. (4.11) to make delay time the subject we get

$$t_{\text{d}} = -\frac{E_{\text{n}}}{A} \ln\left(\frac{E_{\text{n}}R_{\text{cap}}}{At_{\text{r}}I}\left(1 - \exp\left(\frac{At_{\text{r}}Y}{E_{\text{n}}R_{\text{cap}}}\right)\right)\right), \tag{B.16}$$

where $Y = kD_{\text{n}}(L_{\text{nad}} - f_{\text{n}}) - I$. Using the power series expansion of the exponential function ($e^x = 1 + x + x^2/2! + \dots$), and ignoring terms higher than the second power (we will explore the accuracy of this later), gives us

$$t_{\text{d}} = -\frac{E_{\text{n}}}{A} \ln\left(-\frac{Y}{I}\right) - \frac{E_{\text{n}}}{A} \ln\left(1 + \frac{At_{\text{r}}Y}{2E_{\text{n}}R_{\text{cap}}}\right). \tag{B.17}$$

Now we make use of the power series expansion of $\ln(1 + p) = p - p^2/2 + p^3/3 + \dots$. We ignore terms higher than the first power (again, accuracy explored later) to get

$$t_{\text{d}} = -\frac{E_{\text{n}}}{A} \ln\left(-\frac{Y}{I}\right) - \frac{Yt_{\text{r}}}{2R_{\text{cap}}}. \tag{B.18}$$

Rearranging for t_r we get

$$\begin{aligned} t_\mathrm{r} &= -\frac{2R_\mathrm{cap}}{Y}\left(t_\mathrm{d} + \frac{E_\mathrm{n}}{A}\ln\left(-\frac{Y}{I}\right)\right) \\ &= \alpha t_\mathrm{d} + \beta E_\mathrm{n}\,, \end{aligned} \tag{B.19}$$

where

$$\begin{aligned} \alpha &= -\frac{2R_\mathrm{cap}}{Y} \\ \beta &= -\frac{2R_\mathrm{cap}}{YA}\ln\left(-\frac{Y}{I}\right). \end{aligned} \tag{B.20}$$

A reminder that $A = kD_\mathrm{n}f_\mathrm{n}/2$ and $Y = kD_\mathrm{n}(L_\mathrm{nad} - f_\mathrm{n}) - I$. So, for a given frequency response capacity, demand level, and imbalance magnitude, the frequency response ramp time and delay time which ensure the nadir limit is not breached is linear with inertia, which explains what we see in Fig. 4.4. In Fig. 4.4, R_cap is set to the minimum it can be determined by the steady-state requirement constraint on frequency response capacity (Eq. (4.8)). So $R_\mathrm{cap} = \min R_\mathrm{cap} = kD_\mathrm{n}(L_\mathrm{ss} - f_\mathrm{n}) - I$.

The assumption made in this derivation is that $x = 2p = At_\mathrm{r}Y/E_\mathrm{n}R_\mathrm{cap} < 1$, so the higher powers in the power series expansions can be ignored. Effectively, this assumption is $At_\mathrm{r}/E_\mathrm{n} < 1$ since Y is always less than or equal to R_cap (because $L_\mathrm{ss} \geq L_\mathrm{nad}$).

$$\frac{At_\mathrm{r}}{E_\mathrm{n}} = \frac{kD_\mathrm{n}f_\mathrm{n}t_\mathrm{r}}{2E_\mathrm{n}}\,. \tag{B.21}$$

When $D_\mathrm{n} = 20\,\mathrm{GW}$, $k = 2\,\%\mathrm{MW/Hz}$, $f_\mathrm{n} = 50\,\mathrm{Hz}$

$$\frac{At_\mathrm{r}}{E_\mathrm{n}} = \frac{10t_\mathrm{r}}{E_\mathrm{n}}\,. \tag{B.22}$$

When $D_\mathrm{n} = 80\,\mathrm{GW}$, $k = 2\,\%\mathrm{MW/Hz}$, $f_\mathrm{n} = 50\,\mathrm{Hz}$

$$\frac{At_\mathrm{r}}{E_\mathrm{n}} = \frac{40t_\mathrm{r}}{E_\mathrm{n}}\,. \tag{B.23}$$

Using Fig. 4.4, we can see that $t_\mathrm{r}/E_\mathrm{n}$ is always less than 0.032 when $D_\mathrm{n} = 20\,\mathrm{GW}$. This

means that $At_\mathrm{r}/E_\mathrm{n} < 1$ in the range considered and Eq. (B.19) holds. However, when $D_\mathrm{n} = 80\,\mathrm{GW}$, $t_\mathrm{r}/E_\mathrm{n}$ goes above 0.025 so Eq. (B.19) is not accurate because the assumption that $At_\mathrm{r}/E_\mathrm{n} < 1$ does not hold. Interestingly, from Fig. 4.4, the relationship between ramp time and inertia still seems linear in the range considered for $D_\mathrm{n} = 80\,\mathrm{GW}$, but I am unable to offer a proof of why.

Appendix C

MATLAB Simulink model

Here are screenshots of the MATLAB Simulink model that was used in Chapter 5. Fig. C.1 shows the whole model and Fig. C.2 shows the EFR block in more detail (the HFR_d and LFR_d blocks have a similar process but with different parameters).

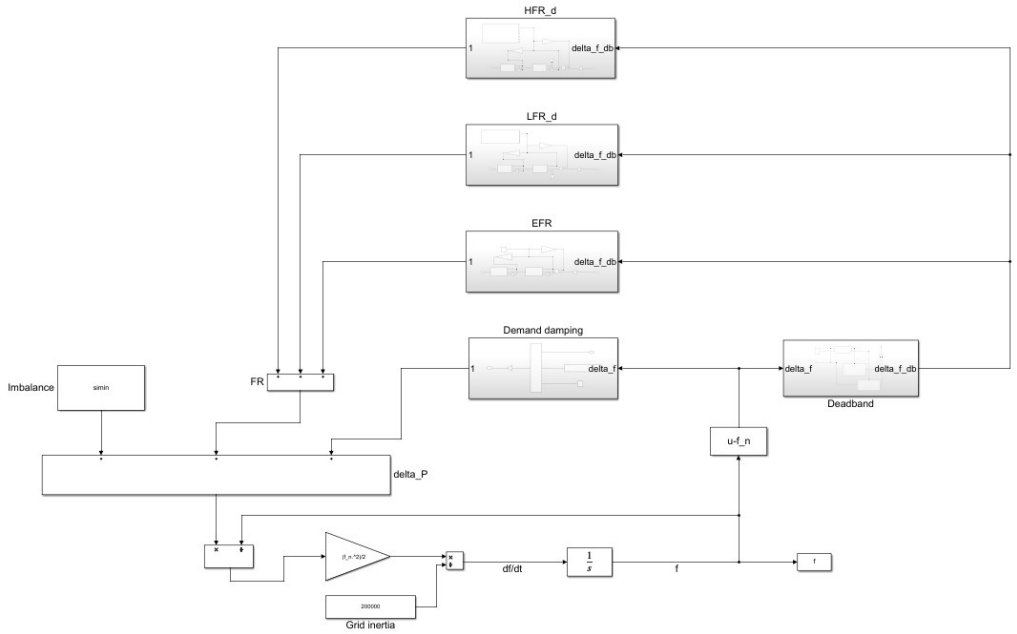

Figure C.1: A screenshot of the main Simulink model. HFR_d, LFR_d, EFR, Demand damping, and Deadband are all blocks that have further controls embedded within them.

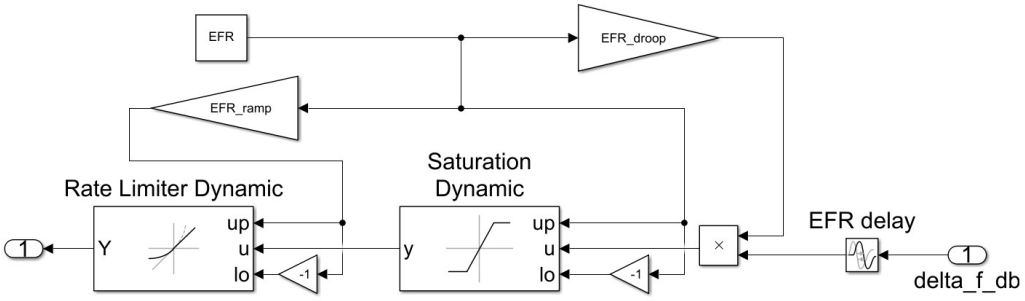

Figure C.2: A screenshot of the EFR block shown in Fig. C.1.